

**Institut für Geowissenschaften
Christian-Albrechts-Universität
zu Kiel**



Endbericht

FOUNDATION 3

Magmatische und hydrothermal Prozesse einer Spreizungsachse
im Einflußbereich eines Hotspots: der Pazifisch – Antarktische
Rücken und die Off-Axis Seamounts bei 37°S

Förderkennzeichen 03G0157

(01.05.2001 - 30.04.2003)

Projektleiter: Prof. Dr. Peter Stoffers

Inhaltsverzeichnis

Vorwort

Teilprojekt A: Magmatische Prozesse an einer Spreizungsachse im Einflussbereich eines Hotspots: Der Pazifisch-Antarktische Rücken und die Off-axis Seamounts bei 37°S

Teilprojekt B: Hydrothermale Prozesse an einer Spreizungsachse im Einflussbereich eines Hotspots: Der Pazifisch-Antarktische Rücken und die Off-axis Seamounts bei 37°S

Anhang

Publikationen

Kurzfassungen

Öffentlichkeitsarbeit

**Institut für Geowissenschaften
Christian-Albrechts-Universität
zu Kiel**



Endbericht

FOUNDATION 3

Magmatische und hydrothermal Prozesse einer Spreizungsachse
im Einflußbereich eines Hotspots: der Pazifisch – Antarktische
Rücken und die Off-Axis Seamounts bei 37°S

Förderkennzeichen 03G0157A

(01.05.2001 - 30.04.2003)

Projektleiter: Prof. Dr. Peter Stoffers

SO 157 – FOUNDATION 3

Magmatische und hydrothermale Prozesse einer Spreizungsachse im Einflußbereich eines Hotspots: der Pazifisch – Antarktische Rücken und die Off-Axis Seamounts bei 37°S

Vorwort

Während des Projektes mit dem Titel „Magmatische und Hydrothermale Prozesse einer Spreizungsachse im Einflußbereich eines Hotspots: der Pazifisch – Antarktische Rücken und die Off-Axis Seamounts bei 37°S“ wurde eine detaillierte Beprobung des Pazifisch-Antarktischen-Rückens (PAR) zwischen 36.5°S und 41.5°S, der Schnittstelle Foundation Seamount Kette – Pazifisch-Antarktischer Rücken (PAR), durchgeführt. Im Pazifik wurden bisher nur wenige Plume-Rücken-Systeme beobachtet. Untersuchungen haben jedoch gezeigt, daß geochemische Anomalien von Spreizungsachsen in der Nähe von Hotspots oft komplexer sind, als es in geophysikalischen Anomalien (z.B. Bathymetrie) zum Ausdruck kommt. Dies läßt vermuten, daß das Plumematerial komplexen Verteilungsmustern unterliegt. In diesem Zusammenhang stellt das System „Foundation Hotspots – PAR“ eine weitere Besonderheit dar, da es sich um ein Gebiet handelt, in dem ein Rücken auf einen Hotspot zuwandert. Aus diesen Zusammenhängen haben sich verschiedene Projektzielsetzungen ergeben. Die Untersuchungen der Kieler Arbeitsgruppe beziehen sich hierbei hauptsächlich (1) auf die Charakterisierung der Plume-Rücken Interaktionen und der ihnen zu Grunde liegenden Manteldynamik sowie (2) auf die Ermittlung der Prozesse, die für das Auftreten und die weite Verbreitung von hoch differenzierten Laven, wie Daziten, verantwortlich sind. Die Untersuchungen der Freiburger Arbeitsgruppe konzentrieren sich im Wesentlichen auf lagerstättenkundliche und petrologische Fragestellungen, die sich durch die Assoziation von Massivsulfiden mit höher differenzierten Laven (Andesiten bis Daziten) in diesem geotektonischen Milieu ergeben. Die entwickelten Gesteine des Pazifisch-Antarktischen Rückens werden als Produkt der Wechselwirkung des Mittelozeanischen Rückens mit dem Hotspot Vulkanismus der Foundation Seamount Kette angesehen. Die lagerstättenkundlichen Untersuchungen fokussieren dabei insbesondere auf eventuelle Auswirkungen der differenzierter Laven auf die hydrothermalen Mineralisationen.

Teilprojekt 03G0157A

Magmatische Prozesse einer Spreizungsachse im Einflußbereich eines Hotspots: der Pazifisch – Antarktische Rücken und die Off-Axis Seamounts bei 37°S

Das 2500 km lange, schnell spreizende (84-100 mm/a) Rückensystem des PAR, wird im Norden durch die Juan Fernandez Triple Junction und im Süden durch die Heezen Transformstörung begrenzt und bildet die südliche Fortsetzung des East-Pacific-Rise (EPR). Der PAR kann anhand von Transformstörungen und Overlapping Spreading Centers in sechs verschieden lange und verschieden differenzierte Segmente unterteilt werden, wobei das nördlichste Segment durch seine Lage in unmittelbarer Nähe des Foundation Hotspots von besonderem Interesse ist. Erste Untersuchungen dieses Segments während der Ausfahrten „SO100“ und „Atalante“ haben eine ausgeprägte bathymetrische Anomalie sowie das für ozeanische Spreizungsachse ungewöhnliche Vorkommen von hochdifferenzierten Laven in diesem Bereich gezeigt.

Während der Ausfahrt wurden an 60 verschiedenen Dredge- und TV-Greifer-Stationen insgesamt 230 Gesteinsproben genommen. Das Probenmaterial umfaßt glasige bis kristalline Proben, deren Zusammensetzung von Basalt über basaltischen Andesit und Andesit bis zu Dazit variiert, wobei Basalte, basaltische Andesite und Andesite innerhalb einer Probenlokation auftreten können. Dies legt den Schluß nahe, daß der Chemismus der eruptierten Laven häufig wechselt und ein Magmenkammersystem unter dem Rücken vorhanden sein muß. Hochdifferenzierte Laven treten hauptsächlich in dem Gebiet des PAR auf, der am stärksten vom Foundation Hotspot beeinflusst ist (36.5° bis 38.5°S). Diese differenzierten Laven stehen nicht im Zusammenhang mit propagierenden Riftsystemen. Im Gegensatz dazu sind die Dazite und Andesite bei 39.5° bis 40°S im Zusammenhang mit den bei 39.85°S und 40.14°S liegenden überlappenden Spreizungsachsen zu sehen. Haupt- und Spurenelementdaten sowie die Sr-, Nd-, und Pb-Isotopenzusammensetzung der Proben zeigen, daß die Magmen des nördlichen PAR (1) aus einer heterogenen Quelle stammen und (2) über verschiedene Differentiationstrends miteinander in Beziehung stehen.

Modellierungen der fraktionierenden Kristallisation zeigen, daß der Chemismus der Basalte durch die Fraktionierung von Olivin, Plagioklas, Klinopyroxen und Ti-Magnetit bei niedrigen Drücken kontrolliert wird, wobei zwei verschiedene Trends definiert werden können: (1) Basalte, die zwischen 37°S und 39.5°S eruptierten, sind durch die Kristallisation von Olivin → Olivin + Plagioklas → Olivin + Plagioklas + Klinopyroxen kontrolliert und Basalte, die zwischen 40°S und 41°S eruptierten, werden durch die Kristallisationssequenz Plagioklas → Plagioklas + Olivin → Plagioklas + Olivin + Klinopyroxen kontrolliert. Diese unterschiedlichen Differentiationstrends kommen durch einen höheren Kristallisationsdruck der Magmen im nördlichen Bereich zustande. Eine Erhöhung des Wassergehalts in den Magmen würde zur Verzögerung der Plagioklaskristallisation führen, kann aber als Ursache der Entwicklung verschiedener

Differentiationstrends ausgeschlossen werden, da die H₂O - Konzentration in den Proben entlang des Rückens nur wenig variiert.

Die Andesite und Dazite sind nicht durch simple fraktionierte Kristallisation bei niedrigen Drücken aus den Basalten entstanden. Klinopyroxenphänokristalle mit Mg# zwischen 40 und 87 und Plagioklasphänokristalle mit An-Gehalten zwischen 22 und 87 in den Andesiten legen den Schluß nahe, daß diese aus der Mischung basaltischer und dazitischer Schmelzen entstanden sind. Hohe Cl/K und ⁸⁷Sr/⁸⁶Sr Verhältnisse sind weiterhin ein Indiz dafür, daß die Assimilation alterierter ozeanischer Kruste eine Rolle bei der Bildung der Andesite und Dazite gespielt hat.

Pb-Isotope und La/Yb Verhältnisse korrelieren positiv mit ⁸⁷Sr/⁸⁶Sr Verhältnissen und zeigen, daß eine binäre Mischung zwischen einer angereicherten, radiogeneren Quelle (Plume-Quelle) und einer verarmten, weniger radiogenen Quelle (MORB Mantel) bei der Bildung der Magmen vorliegt. Ein südwärts gerichteter geochemischer Gradient ist in den Proben zu beobachten, wobei die am stärksten angereicherten und radiogensten Proben um 37.5°S (Position des Foundation Hotspot) zu finden sind und die verarmtesten bei 40°S. Ein nördlich gerichteter geochemischer Gradient tritt offenbar nicht auf, wobei allerdings hier auch nur wenige Proben vorliegen. Die Isotopentrends zeigen, daß mindestens vier verschiedene Mantelquellen die Magmen des PAR beeinflussen. Dabei kann eine Quelle, die vermutlich die Zusammensetzung des oberen Mantels reflektiert, aufgrund der linearen Trends genau definiert werden. Außerdem treten zwei verschiedene Mantelquellen im Foundation Hotspot auf, wobei eine an inkompatiblen Elementen angereichert ist und die andere verarmt ist. Die südlichsten Laven des PAR weisen wiederum den Einfluß einer weiteren Mantelquelle der Asthenosphäre auf.

Zusammenfassend läßt sich sagen, daß der Foundation Hotspot eine asymmetrische geochemische Anomalie verursacht, die die Entwicklung der Magmen dieses Segments des PAR (zwischen 37.5°S und 39.5°S) nachhaltig beeinflusst. Die durch den Hotspot verursachte Krustenverdickung führt zu einer polybarischen fraktionierenden Kristallisation der Schmelzen in einem komplexen Magmenkammersystem unter dem PAR.

Ar/Ar Altersdatierungen an Laven der Foundation Seamountkette, die während der So100 und Atalante Ausfahrten genommen wurden, zeigen, dass der Plume offenbar pulsierte und gleichaltrigen Vulkanismus an langgestreckten Rücken produzierte (siehe O`Connor et al., 2002). Das pulsierende Material wird dabei im Mantel fokussiert, so dass die Rückensysteme entstehen können.

Die aus diesem Projekt bisher hervorgegangenen Manuskripte und Abstracts befinden sich im Anhang. Eine Zusammenfassung der bisherigen geochemischen Ergebnisse findet sich in Tabelle 1.

Veröffentlichungen und geplante Veröffentlichungen

Neben den schon veröffentlichten Publikationen werden z.Zt. mehrere Manuskripte über die Bildung der silizischen Magmen sowie den Einfluss des Foundation Plume auf den Pazifisch-Antarktischen Rücken vorbereitet (siehe Anlage):

Stoffers, P., Worthington, T., Hekinian, R., Petersen, S., Hannington, M., Türkay, M., and the SO157 Shipboard Scientific Party (2002) Silicic volcanism and hydrothermal activity documented at Pacific-Antarctic Ridge. EOS, American Geophysical Union Transactions, 83(28): 303-304.

Stoffers, P., Worthington, T., Hekinian, R., Petersen, S., Hannington, M., Türkay, M., Ackermann, D., Borowski, C., Dankert, S., Fretzdorff, S., Haase, K., Hoppe, A., Jonasson, I., Kuhn, T., Lancaster, R., Monecke, T., Renno, A., Stecher, J., and Weiershäuser, L. (2002) Widespread silicic volcanism and hydrothermal activity on the Northern Pacific-Antarctic Ridge. InterRidge News, 11(1): 30-32.

O`Connor, J. A., Stoffers, P., and Wijbrans (2002) Pulsing of a focused mantle plume: Evidence from the distribution of Foundation Chain hotspot volcanism. Geophys. Res. Lett., 29 (9): 64.1-64.4

O`Connor, J. A., Stoffers, P., and Wijbrans (in press) The Foundation Chain: Inferring hotspot-plate interaction from a weak seamount trail. Oceanic Hotspots, Eds. Hekinian, R., Stoffers, P., and Cheminée, Springer

Stecher, J., Türkay, M., and Borowski, C. (2002) Faunal Assemblages on the Pacific-Antarctic Ridge near the Foundation Seamount Chain (37°30'S, 110°30'W). Cah. Biol. Mar, 43: 271-274

Haase, K. M., Stroncik, N. A.; and Stoffers, P. Bimodal volcanism along the Pacific-Antarctic-East-Pacific-Rise (PA-EPR) spreading axis. To be submitted to Nature

Stroncik, N. A., Haase, K. M., and Stoffers, P. Geochemical Case Study of a Ridge Approaching a Plume – Plume-Ridge Interaction between the Foundation Plume and the Pacific-Antarctic-East-Pacific Rise (PA-EPR). To be submitted to Earth and Planetary Sciences Letters

Die Untersuchungen der Kieler Arbeitsgruppe wurden im Rahmen der Chapman Konferenz 2002 in New Zealand, der DMG Tagung 2002 in Hamburg, der Herbsttagung der American Geophysical Union 2002 in San Francisco, der Penrose Konferenz 2003 in Island, der Herbsttagung der American Geophysical Union 2003 in San Francisco sowie des BMBF Statusseminars 2003 in Hamburg, vorgestellt (siehe Anlage):

Hekinian, R., Worthington, T., and Stoffers, P. (2002) Explosive and Silicic Magmatism in the Deep Ocean. Chapman Conference on Explosive Subaqueous Volcanism, 21th – 25th Jan. 2002, New Zealand

Stroncik, N. A., Haase, K. M., and Stoffers P. (2002) Petrogenesis of lavas from the Pacific-Antarctic-Ridge (PAR) – insights into magma generation processes at fast spreading ridges in proximity to hotspots. Beihefte zum European Journal of Mineralogy, 14: 163

Stroncik, N. A., Haase, K. M., and Stoffers P. (2002) Generation of highly silicic lavas along the Pacific-Antarctic-Ridge (PAR): Insights into magma chamber processes along a hotspot influenced ridge section. Eos. Trans. AGU, 83 (47), Fall Meet. Suppl., Abstract

O`Connor, J. A., Stoffers, P., and Wijbrans (2003) Distinguishing local from deep sources using high-resolution age-mapping of oceanic hotspot volcanism. Penrose Conference, 25th -29th Aug. 2003, Iceland

O`Connor, J. A., and Wijbrans (2003) Lithospheric and Melt Anomaly Control of Foundation Chain Volcanism. Eos. Trans. AGU, 84 (46), Fall Meet. Suppl., Abstract

Stroncik, N. A., Haase, K. M., and Stoffers (2003) Mantelplume-Einfluß und die Bildung von andesitischen Laven am Pazifisch-Antarktischen Rücken: Ergebnisse der Ausfahrt SO157. BMBF Statusseminar 2003, Hamburg

Erfolgskontrollbericht

Verwertung der Ergebnisse

Eine unmittelbare wirtschaftliche Verwertungsmöglichkeit der erzielten Ergebnisse ist nicht gegeben.

Fortschritt auf dem Gebiet des Vorhabens bei anderen Stellen

Für das Vorhaben relevante Ergebnisse von dritter Seite sind in der Zwischenzeit nicht bekannt geworden.

Beitrag zu den förderpolitischen Zielen

Die Untersuchungen dienen dem besseren Verständnis der Wechselwirkungen zwischen den Teilsystemen Erdmantel, Kruste, Hydrosphäre und Atmosphäre.

Wissenschaftlicher und technischer Erfolg

- (1) Erstbeschreibung der Mantelgeochemie sowie des tatsächlichen Einflusses des Foundation Plume auf die Genese der Magmatite entlang des Pazifisch-Antarktischen Rückens (PAR).

- (2) Beitrag zur generellen Charakterisierung von Plume-Rücken Interaktionen und der ihnen zu Grunde liegenden Manteldynamik

Erfindungen und Schutzrechtanmeldungen

Keine

Arbeiten, die zu keiner Lösung geführt haben

Keine

Einhaltung der Ausgaben- und Zeitplanung

Der Finanzierungs- und Zeitplan wurde eingehalten. Für die Beschaffung wurden die Richtlinien des Landes Schleswig-Holstein beachtet. Der Verwendungsnachweis und die Schlussrechnung sind dem Projektträger bereits zugegangen.

Institut für Mineralogie
Lehrstuhl für Lagerstättenlehre und Petrologie &
Leibniz-Labor für Angewandte Meeresforschung

Abschlußbericht

**" SO 157 FOUNDATION III:
Magmatische und hydrothermale Prozesse an einer
Spreizungsachse im Einflussbereich eines Hotspots:
Der Pazifisch-Antarktische Rücken und die Off-axis Seamounts bei 37°S "**

BMBF 03G0157B
(01.05.2001 - 30.04.2003)

Technische Universität Freiberg

Projektleiter: Prof. Dr. P. M. Herzig

Teilprojekt 03GO157B - Hydrothermale Prozesse an einer Spreizungsachse im Einflussbereich eines Hotspots: Der Pazifisch-Antarktische Rücken und die Off-axis Seamounts bei 37°S

Im Rahmen der Forschungsfahrt SO-157 (15. Juni - 14. Juli 2001) wurden von der Freiburger Arbeitsgruppe die Rückensegmente des Pazifisch-Antarktischen Rückens (PAR) in Bezug auf das Auftreten hydrothermal beeinflusster Gebiete im Kreuzungsbereich von PAR und der submarinen Foundation Vulkankette kartiert und beprobt. Die Ergebnisse der Kartierung und der Suche nach hydrothermalen Mineralisationen wurden in dem englisch-sprachigen Fahrtbericht zusammenfassend dargestellt. Darüber hinaus sind die ersten Ergebnisse der Freiburger Arbeitsgruppe in den Publikationen [InterRidge News vol.11(1) und EOS, Transactions of the American Geophysical Union vol. 83(28)] enthalten.

Die Untersuchungen der TU Bergakademie Freiberg konzentrierten sich im Wesentlichen auf lagerstättenkundliche und petrologische Fragestellungen, die sich durch die Assoziation von Massivsulfiden mit höher differenzierten Laven (Andesiten bis Daziten) in diesem geotektonischen Milieu ergeben. Die entwickelten Gesteine des Pazifisch-Antarktischen Rückens werden als Produkt der Wechselwirkung des Mittelozeanischen Rückens mit dem Hotspot Vulkanismus der Foundation Seamount Kette angesehen. Die lagerstättenkundlichen Untersuchungen fokussieren dabei insbesondere auf eventuelle Auswirkungen der differenzierter Laven auf die hydrothermalen Mineralisationen. Das Hauptinteresse liegt dabei auf der Charakterisierung der hydrothermalen Präzipitate, die sowohl entlang des Pazifisch-Antarktischen Rückens als auch an Off-axis Seamounts geborgen wurden. Die hydrothermalen Präzipitate beinhalten zum einen hochtemperiert gebildete Massivsulfide und zum anderen Fe- und Mn-Oxyhydroxide, die geochemisch, mineralogisch und isotopengeochemisch bearbeitet wurden. Alle Untersuchungsergebnisse sind in diesem Bericht zusammenfassend dargestellt und werden in Kürze in internationalen Fachzeitschriften mit Peer-Review-System publiziert (vgl. Anhang).

1.1 Polymetallische Mineralisationen im Bereich des Foundation Hotspot

Prof. Dr. Peter Herzig, Dr. Sven Petersen (Lehrstuhl für Lagerstättenlehre und Leibniz-Labor für Angewandte Meeresforschung, TU Bergakademie Freiberg)

Dr. Mark Hannington, Dr. Ian Jonasson (Geological Survey of Canada, Ottawa)

Im Rahmen der Forschungsfahrt SO-157 (Juni – Juli 2001) konnten am Pazifisch-Antarktische Rücken (PAR) hydrothermale Präzipitate geborgen werden, die zusammen mit angereicherten Vulkaniten, wie Andesiten und Daziten vorkommen. Das gemeinsame Auftreten von SiO₂-reichen Magmen und hydrothermalen Bildungen wurde bisher nur sehr selten an Mittelozeanischen Spreizungsachsen beobachtet^[1,2], obwohl aus fossilen

Funden bekannt ist, dass solche Vergesellschaftungen in Inselbögen und Back-Arc Bereichen durch große Massivsulfidkörper gekennzeichnet sein können. Die Untersuchung der Vorkommen am PAR bietet die Möglichkeit, die Bildung der Erze in einem neuen tektonischen Milieu systematisch in Hinblick auf die Abhängigkeit zwischen Krustengestein und Erzablagerung zu untersuchen. Dabei sollte insbesondere ein möglicher Einfluss des Foundation Manteldiapirs auf die Sulfidgenese untersucht werden. Unterschiede in der geochemischen Zusammensetzung der unterlagernden ozeanischen Kruste sollten sich u. a. in der chemischen Zusammensetzung der Sulfide bemerkbar machen. So weisen z.B. Sulfide, die mit sauren Laven in Back-Arc Becken assoziiert sind, oft Anreicherungen von Ba, Pb, As, Sb, Ag und Au auf.

Geologischer Rahmen

Der nördliche Teil des Pazifisch-Antarktischen Rückens befindet sich in der Nähe der Foundation Vulkankette, die sich aufgrund der Bewegung der Pazifischen Platte über den Foundation Manteldiapir gebildet hat. Der Pazifisch-Antarktische Rücken im Bereich von 37°38'S bis 37°49'S wird aus einer Reihe vulkanischer Rücken und Hügel aufgebaut, die teilweise einen ausgeprägten zentralen Graben aufweisen^[3]. Im Bereich des nördlichen PAR treten neben N-MOR Basalten auch angereicherte Basalte, Andesite und Dazite auf^[4,5]. Die Laven bestehen hauptsächlich aus älteren Pillow- und Schichtlaven, die entlang von rückenparallelen tektonischen Spalten ausgeflossen sind. Während der Forschungsfahrt SO-157 konnten nahe 37°40'S sehr frische, glasige Laven beobachtet werden, die auf einem Gebiet von ca. 3500 x 200 m den zentralen Graben teilweise ausfüllen und die älteren Laven überdecken (Abb. 1). Die frischen Laven konnten bei vorausgegangenen Forschungsfahrten 1995 und 1997 nicht beobachtet werden^[4,5], was auf ein Bildungsalter dieser Laven von weniger als 6 Jahren hindeutet. Die Flanken des zentralen Grabens sind zum größten Teil von älterem Talus bedeckt.

Hydrothermale Aktivität

Auf OFOS-Profilen konnten ausgedehnte Bereiche hydrothermalen Aktivität entlang der Riftachse (TVG-33; TVG-31) und im Krater eines zur Foundation Vulkankette gehörenden Off-ridge Vulkans gefunden werden (TVG-08; TVG-09). Innerhalb dieses Kraters treten mehrere Meter hohe, schlotartige Strukturen auf, die aus porösen Fe-Oxyhydroxiden und Nontronit aufgebaut werden (Abb. 2a).

Hydrothermale Aktivität konnte in verschiedenen Arbeitsgebieten entlang des PAR durch Temperaturanomalien (bis 0,25°C) in der Wassersäule nachgewiesen werden. Sie ist jedoch überwiegend auf diffuse Lösungsaustritte in der Nähe von tektonischen Spalten, aber auch im Talusmaterial beschränkt. Zum Teil sind die Bereiche diffuser Lösungen durch das vermehrte Auftreten vent-spezifischer Fauna (Krebse und Krabben) gekennzeichnet. Hydrothermale Sedimente ("plume fallout") konnten ebenfalls beobachtet werden und weisen auf aktiven, hochtemperierten Lösungsaustritt in der Umgebung hin, der jedoch nicht direkt beobachtet werden konnte.

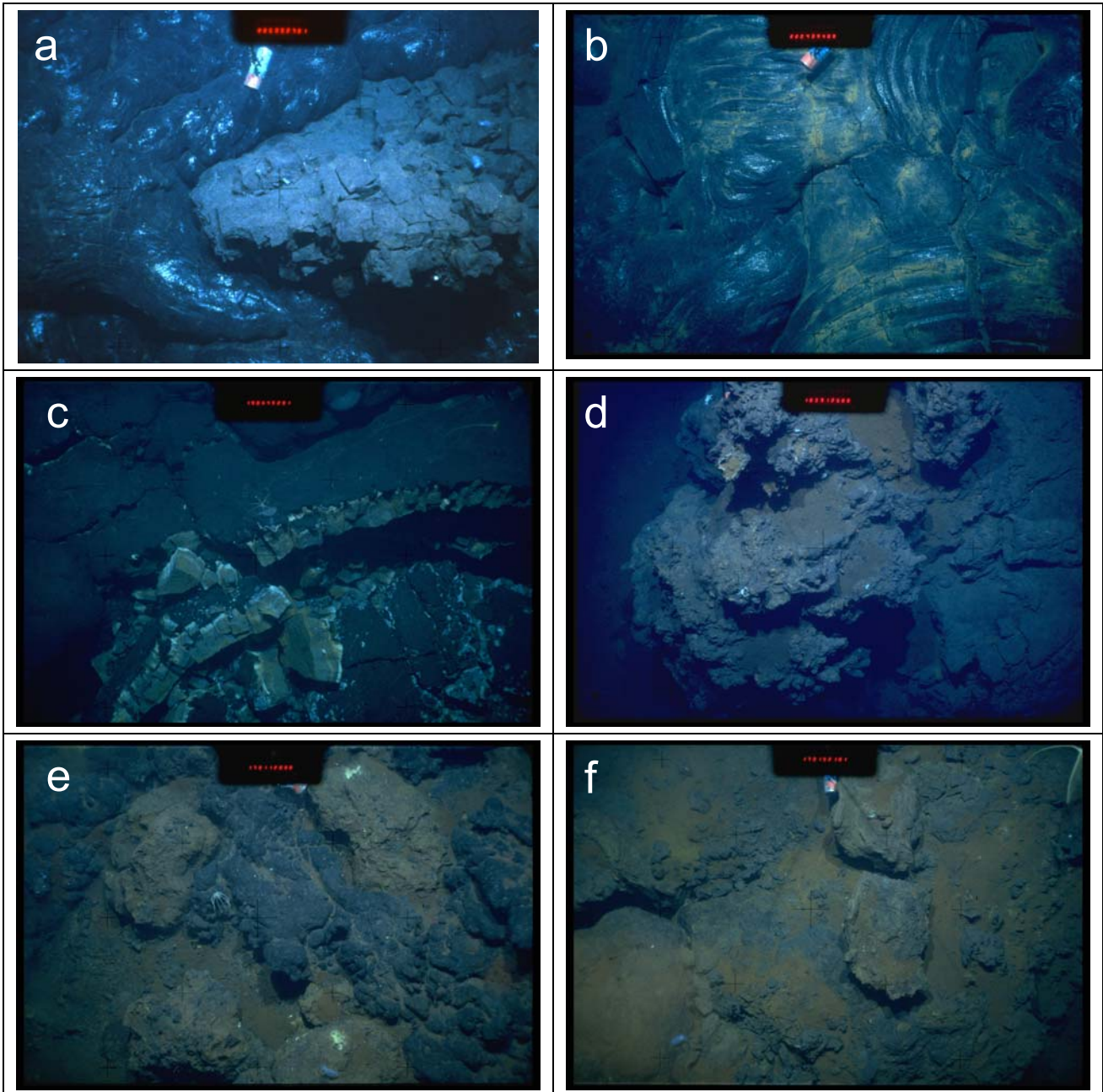


Abb. 1: Meeresbodenaufnahmen im Bereich des Pazifisch-Antarktischen Rückens. a-b) frische Pillow-, Tube-, und Sheetflow-Laven, die größere Bereiche des Meeresboden bedecken und vermutlich erst innerhalb der letzten 6 Jahre ausgeflossen sind. c) tektonische Zerstückelung relativ frischer Basalte. d-f) Massivsulfide und hydrothermale Präzipitate am Meeresboden. Obwohl Anzeichen für hydrothermale Aktivität in der Wassersäule festgestellt werden konnten, wurden sich rezent bildende Massivsulfide nicht beobachtet.

Inaktive, oxidierte Sulfidstrukturen konnten an mehreren Stellen im Talus an der Ostflanke des Grabens beobachtet werden und sind dabei oft von jüngeren Lavaströmen überdeckt. Im Bereich eines lokalen bathymetrischen Hochs bei 37°47'S wurden Schwarze Raucher und begleitende Muschelfelder entdeckt. Darüber hinaus konnten inaktive, teilweise von Lava überdeckte Massivsulfide mittels TV-Greifer aus einer Wassertiefe von 2219 m geborgen werden (Abb. 2b). Hierbei handelt es sich um poröses, teilweise oxidiertes

Material eines ehemaligen Sulfidschlotes, das überwiegend aus Pyrit und Markasit mit untergeordnet Chalkopyrit und Sphalerit besteht (Abb. 2c-e).

Erzmikroskopisch konnten noch Spuren von Galenit und Isokubanit nachgewiesen werden. Das Auftreten von Isokubanit und die Ausbildung des Chalkopyrits weisen auf hohe (>350°C) Bildungstemperaturen hin (Abb. 2f). Amorphe Kieselsäure ist beim Abklingen der hydrothermalen Aktivität entstanden und zementiert die primären Sulfide. Die Oxidation der Sulfide führte zur Bildung von Limonit, Na-Jarosit, Bornit, Digenit und Chrysokoll. Eine Besonderheit der Massivsulfide vom PAR sind hervorragend erhaltene Relikte hydrothermaler Fauna (Wurmrohren und Muschelschalen), die von Chalkopyrit und Sphalerit ausgefüllt werden. Der gute Erhaltungsgrad erlaubt eventuell eine Identifizierung der jeweiligen Gattung. Zu diesem Zweck wurden fossile, sulfidisierte Röhrenwurmreste und Muschelschalen zur weiteren Untersuchung an Dr. Crispin Little am Natural History Museum in London gesandt, die Ergebnisse stehen jedoch noch aus.

Die geochemischen Analysen der Massivsulfide wurden mittels ICP-MS, ICP-ES und Neutronenaktivierung durchgeführt (Tabelle 1). Die Variationen und durchschnittlichen Gehalte an Fe ($\bar{\text{Ø}}=34,2\%$ Fe; N=24) und den Buntmetallen ($\bar{\text{Ø}}=2,4\%$ Cu, 2,2 % Zn und 0,03 % Pb) spiegeln die Verteilung von Chalkopyrit, Sphalerit und Galenit in den einzelnen Proben wieder, wobei in Ausnahmefällen Gehalte bis zu 14,2 % Cu und 6,5 % Zn erreicht werden können (Tabelle 1). Auch die durchschnittlichen Spurenelementgehalte sind gering (z. B.: 325 ppm As, 257 ppm Co, 252 ppm Pb, 120 ppm Mo, 40 ppm Ag, 14 ppm Sb).

Es konnten Anreicherungen von Se (bis zu 350 ppm Se, $\bar{\text{Ø}}=96$ ppm) und Co (bis zu 637 ppm Co, $\bar{\text{Ø}}=257$ ppm) in bestimmten Proben festgestellt werden, die auf hohe Bildungstemperaturen der jeweiligen Massivsulfide hinweisen. Anreicherungen von Au, Ag, As, Bi, Hg, In, Pb, Sb und Te, wie sie in Massivsulfiden in Back-Arc Bereichen vorkommen, die mit angereicherten Gesteinen (Andesiten oder höher differenziert) assoziiert sind, konnten nicht beobachtet werden. Insbesondere die Gehalte an Bi und Te sind extrem gering und liegen unterhalb der Nachweisgrenzen von 0,2 ppm.

Die geochemischen Daten zeigen kaum Unterschiede zwischen den Sulfiden des Pazifisch-Antarktischen Rückens und denjenigen von typischen Massivsulfidvorkommen des Ostpazifischen Rückens, die an N-MORB gebunden sind (Tabelle 2). Auch die Spurenelementkonzentrationen entsprechen in etwa den Gehalten typischer Massivsulfidvorkommen, die an N-MORB Basalte gebunden sind. Nur der Gehalt an Gold und Arsen ist gegenüber Massivsulfiden entlang des East Pacific Rise leicht erhöht ($\bar{\text{Ø}}=0,8$ ppm Au gegenüber 0,3 ppm Au; 325 ppm As gegenüber 165 ppm As). Bei Vergleichen mit Massivsulfidvorkommen, die durch das Auftreten von angereicherten Gesteinen (z.B. E-MORB, Explorer Ridge und Endeavour Segment) oder durch den Einfluss des Azoren Hotspots gekennzeichnet sind, werden auffällige Unterschiede deutlich. So ist, auch bei geringen Anteilen angereicherter Gesteine im Untergrund, ein deutlicher Anstieg der Gehalte an Ba, Pb und Sb in diesen Vorkommen zu beobachten.

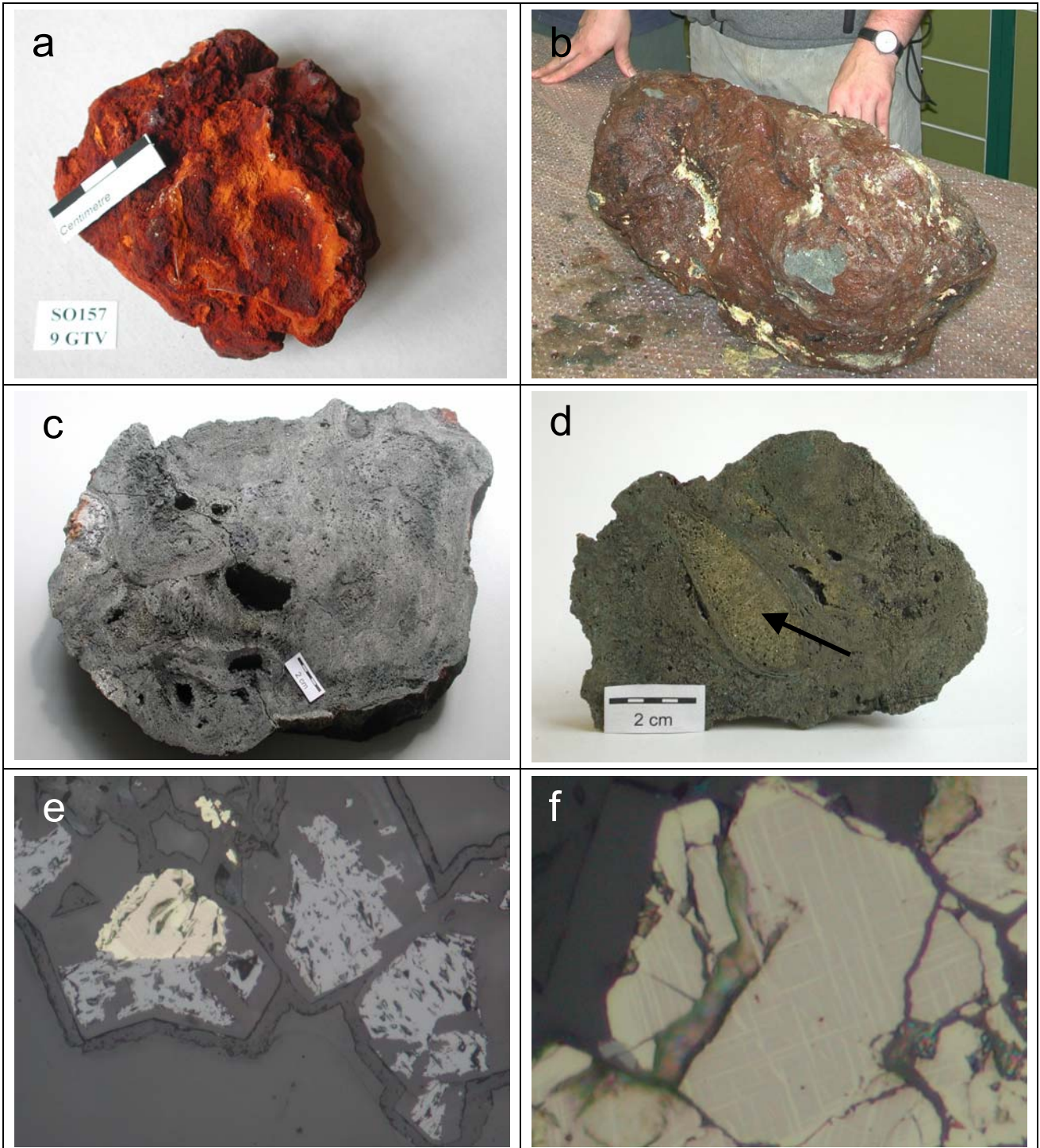


Abb. 2: Hydrothermale Präzipitate aus dem Kraterbereich eines Seamounts der Foundation Hotspot-Kette (a) bzw. vom Pazifisch-Antarktischen Rücken (b-d). a) Poröse Fe-Oxyhydroxidkruste. b) Inaktiver Massivsulfidblock mit Fe-oxidkruste sowie sekundärem, gelbem Jarosit. Probe 33GTVA-1. c) Schnitt durch die Probe 33GTVA-1. Deutlich wird die poröse Struktur mit einzelnen Fluidkanälen, die durch Chalkopyrit und Sphalerit ausgekleidet sind. d) Fossile Muschelschale, die vollständig mit Chalkopyrit gefüllt ist (Pfeil). e) Verwachsung von Sphalerit, Chalkopyrit und Isokubanit. Deutlich wird die starke Korrosion des Sphalerits. Die ursprünglichen Korngrenzen wurden von amorpher Kieselsäure ummantelt und bleiben daher sichtbar. Erzmikroskopische Aufnahme. Bildbreite 500 μm . f) Detailansicht einer Isokubanit-Chalkopyritverwachsung. Erzmikroskopische Aufnahme. Bildbreite 200 μm .

Tabelle 1. Repräsentative and mittlere geochemische Zusammensetzung von Massiv-sulfiden des Pazifisch-Antarktischen Rückens.

	Cu-reich			Zn-reich			Fe-reich			Mittelwert (N=24)
	33- 1BC	33- 1BF	33- 2B	33- 1BD	33- 3B2	33- 4B1	33- 1BH	33- 1GA3	33- 1GI3	
Fe %	32.9	28.1	28.7	30.8	37.4	37.8	36.5	38.3	28.2	34.2
Cu	10.4	9.7	14.2	0.5	0.7	0.1	0.1	1.5	0.2	2.4
Zn	2.5	6.2	0.3	6.5	5.0	5.5	2.5	0.6	0.7	2.2
S	37.2	34.2	31.6	37.6	44.0	48.6	41.0	47.7	33.1	40.6
SiO ₂	12.5	15.8	21.3	20.3	8.1	2.5	8.9	7.9	34.0	15.0
Au ppm	0.38	0.57	0.26	0.68	1.31	2.42	1.12	0.63	0.33	0.82
Ag	36	47	32	33	65	158	33	30	17	40
As	350	340	89	347	560	353	267	321	354	325
Ba	72	41	<20	40	54	653	508	23	<20	210
Bi	<0.2	<0.2	<0.2	<0.2	<0.2	<0.2	<0.2	<0.2	<0.2	<0.2
Cd	114	295	11	236	175	85	103	25	29	75
Co	313	310	220	168	47	233	31	487	637	257
Cr	36	31	31	33	40	41	38	42	31	37
Ga	15	34	5	27	20	7	9	4	6	9
Hg	5	10	8	5	5	15	4	2	5	5
In	4.6	7.7	2.3	0.6	1.7	0.2	0.3	0.7	0.4	1.2
Mo	150	120	220	110	69	44	49	170	190	120
Ni	<10	<10	<10	<10	<10	<10	<10	<10	<10	<10
Pb	98	164	69	223	268	702	415	211	92	252
Sb	24	36	3	27	20	27	11	8	10	14
Se	213	180	350	66	26	6	15	149	145	96
Sn	8.2	11.0	2.3	5.4	7.0	1.5	1.4	6.9	2.2	6.5
Te	<0.2	<0.2	<0.2	<0.2	<0.2	<0.2	<0.2	<0.2	<0.2	<0.2
Tl	8.6	8.7	3.2	24	57	85	37	22	4	25
U	<0.1	0.2	0.2	0.2	0.4	0.6	0.3	<0.1	<0.1	0.2

Methoden: Hauptelemente (Gew.%) mit ICP-ES; Schwefel durch LECO; Au, Ag, As, Co, Hg, Mo, Sb, und Se mittels INAA; Cd, Ga, Ni, Pb, Sn, Te, Tl und U durch ICP-ES; Bi und In mittels ICP-MS.

Tabelle 2: Mittlere geochemische Zusammensetzung von Massivsulfiden des Pazifisch-Antarktischen Rückens (N=24) im Vergleich zu Mittelwerten publizierter Analysen von anderen Vorkommen, die an sedimentfreie mittelozeanische Rücken gebunden sind.

	PAR (24)	EPR (275)	Lucky Strike (MAR) (83)	Menez Gwen (MAR) (11)	Explorer (JdFR) (51)	Endeavour (JdFR) (142)
Cu %	2,4	5,1	6,5	0,4	3,2	2,6
Zn	2,2	9,8	3,6	1,2	5,4	7,5
Fe	34,2	26,8	20,6	1,2	25,2	27,4
Ba	<0.1	0,3	9,2	27,8	7,9	3,1
SiO ₂	15,0	8,1	12,2	13,2	9,5	11,5
Au ppm	0,8	0,3	0,5	-	0,7	0,2
Ag	40	59	72	42	125	195
As	325	165	304	28	575	345
Co	257	659	85	6	485	55
Hg	5	8	-	-	11	10
In	1,2	9	-	-	-	14
Mo	120	90	100	19	162	112
Ni	<10	20	10	13	8	22
Pb	252	460	500	900	1095	4100
Sb	14	12	27	29	42	38
Se	96	180	97	28	100	80

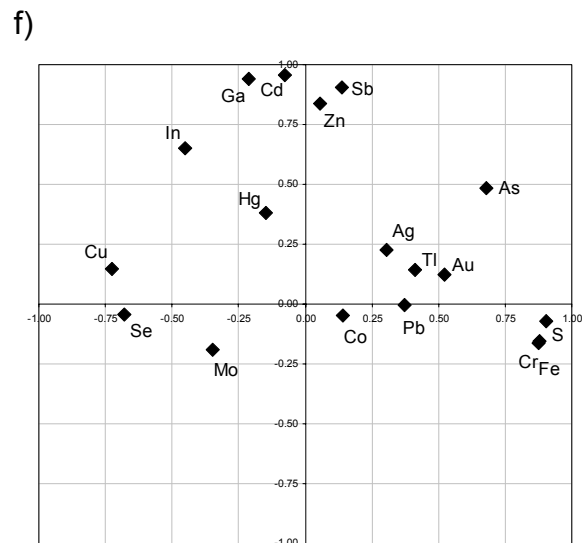
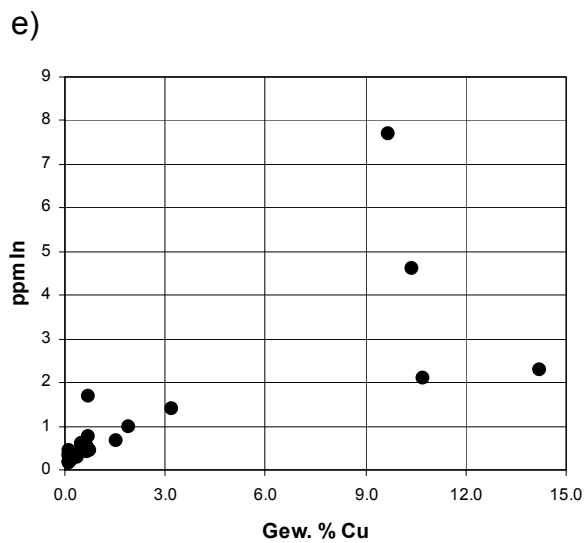
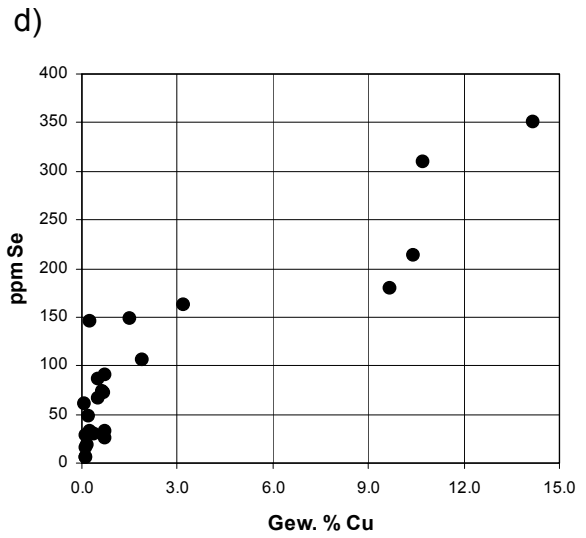
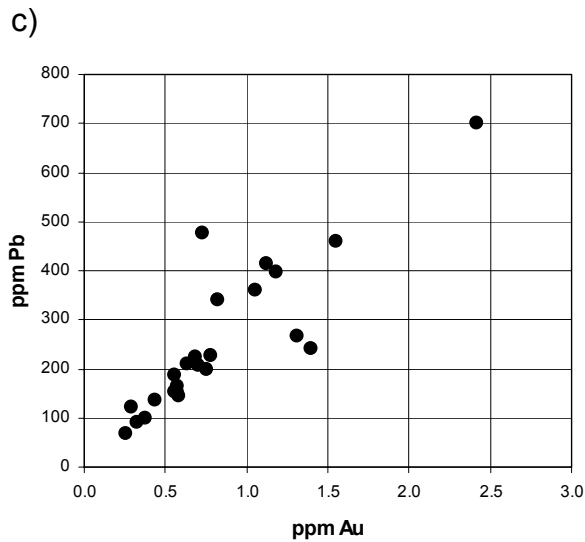
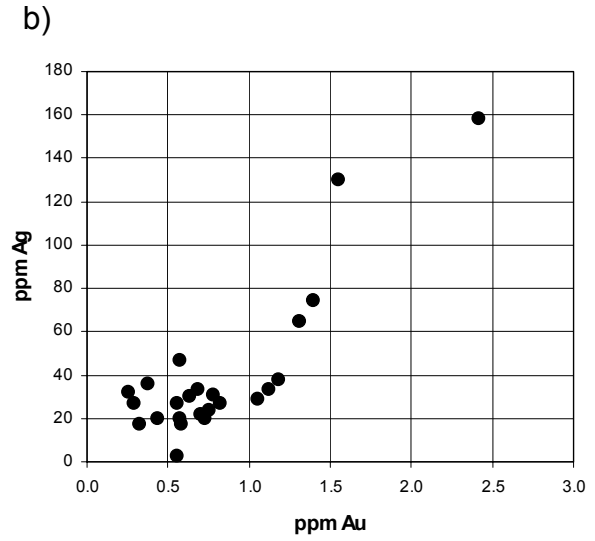
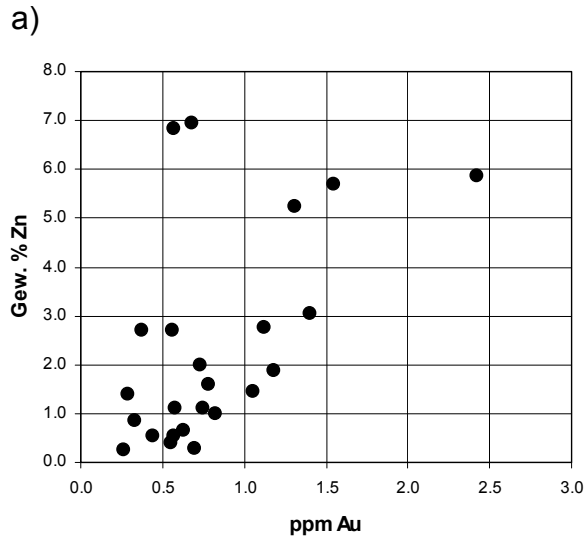


Abb. 3: a-e) Covarianz ausgewählter Elemente in Massivsulfidproben vom Pazifisch-Antarktischen Rücken (N=24). f) Graphische Darstellung der Ergebnisse einer Faktorenanalyse (siehe Text für Details).

Geochemische Korrelationen ergeben sich zwischen einer ganzen Reihe von Elementen (Abb. 3). Wie in anderen Vorkommen auch ergibt sich eine positive Korrelation zwischen Elementen, die normalerweise als niedriger temperiert gebildet angesehen werden. Dazu gehören z.B. Zn, Cd, Sb, As, Ag, Ga, Hg und Pb. Positive Korrelationen zwischen den Elementen Cu, Se, Mo und auch, in geringerem Maße In, zeigen den bevorzugten Einbau dieser Spurenelemente in Chalkopyrit an, während Cr überwiegend in den Pyrit eingebaut wird. Eine Faktorenanalyse wurde durchgeführt, um die geochemischen Korrelation zwischen den Elementen graphisch besser darstellen zu können (Abb. 3f). Hieraus wird ersichtlich, das eine Reihe von Elementen (Au, Ag, Pb, Tl), die normalerweise zusammen mit Zn, Cd, Ga und Sb in den zinkreichen Partien von Massivsulfiden abgesetzt werden, eine eigenständige Gruppe bilden. Vermutlich ist dies durch sekundäre Prozesse zu erklären, die nach dem Absatz der Sulfide zu Remobilisationen geführt haben. Solche Prozesse scheinen sich z.B. in den starken Korrosionserscheinungen der Sphaleritkristalle widerzuspiegeln (e.g. Abb. 2e). Eigenständige Gruppierungen werden durch die Elemente Fe+S+Cr und Cu+Se+Mo gebildet

Die **Schwefelisotopenzusammensetzung** der Sulfide wurde an ausgewählten Proben am Mineralogischen Institut in Freiberg bestimmt. Die Werten reichen von 2,8 bis 4,3 ‰ $\delta^{34}\text{S}$ (N=9, Tabelle 3) und liegen im Bereich von Werten typischer Massivsulfide des Ostpazifischen Rückens. Die Werte zeigen nur geringe Unterschiede in den einzelnen Mineralen, was ein deutlicher Hinweis auf isotopische Ungleichgewichte während der Präzipitation ist.

Table 3. Schwefelisotopenverhältnisse von Sulfidseparaten des Pazifisch-Antarktischen Rückens (N=9).

Sample	$\delta^{34}\text{S}$ (‰)			
	sl	cpy	mc	py
SO157/33GTVA-1B1	-	-	-	3.3
SO157/33GTVA-1B2	-	-	-	3.7
SO157/33GTVA-2A	3.1	-	-	-
SO157/33GTVA-2A2	3.7	4.3	-	-
SO157/33GTVA-2B	-	3.5	-	-
SO157/33GTVA-3A1	-	-	6.0	4.0
SO157/33GTVA-3B2	3.7	-	-	-

Insgesamt lässt sich feststellen, dass ein Einfluss der angereicherten Gesteine auf die Massivsulfide mineralogisch, geochemisch oder isotopengeochemisch kaum nachzuweisen ist. Dies deutet darauf hin, dass die hydrothermale Konvektionzelle in der die hydrothermalen Lösungen ihre finalen physiko-chemischen Charakteristika erhielt, überwiegend aus Basalten aufgebaut wird. Dies ergibt sich insbesondere durch Vergleiche mit Massivsulfiden an Mittelozeanischen Rücken, in denen leicht angereicherte Magmen

(E-MORB) in größerer Menge auftreten. So lassen sich deutliche Anreicherungen an Pb und Ba, aber auch an As und Sb in Massivsulfiden entlang des Juan de Fuca Rückens und insbesondere in den Massivsulfiden in der Nähe des Azoren Hotspots (Lucky Strike und Menez Gwen Hydrothermalfelder) nachweisen, die auf Wechselwirkungen mit den angereicherten Gesteinen zurückzuführen sind.

Die Ergebnisse zur Mineralogie, Isotopie und Geochemie der Massivsulfide werden zur Zeit für die Publikation in einem international anerkannten Journal vorbereitet.

Literatur

- [1] Thompson G, Bryan WB und Humphris S (1989) Axial volcanism on the East Pacific Rise, 10-12°N. In Saunders AD und Norry MJ, eds., Magmatism in the Ocean Basins, Geological Society Special Publication 42: 181-200.
- [2] Clague DA, Frey FA, Thompson G und Rindge S (1981) Minor and trace geochemistry of volcanic rocks dredged from the Galapagos Spreading center: role of crystal fractionation and mantle heterogeneity. Journal of Geophysical Research 86: 9469-9482.
- [3] Stoffers P, Worthington T, Hekinian R, Petersen S, Hannington M et al (2002) Silicic volcanism and hydrothermal activity documented at Pacific-Antarctic Ridge. EOS Trans Amer Geophys Union 83: 301-304.
- [4] Devey CW, Hekinian R, Ackermann D, Binard N, Francke B, Hemond C, Kapsimalis V, Lorenc S, Maia M, Möller H, Perrot K, Pracht J, Rogers T, Statteger K, Steinke S und Victor P (1997) The Foundation Seamount Chain: a first survey and sampling. Marine Geology 137: 191-200.
- [5] Hekinian R, Stoffers P, Ackermann D, Revillon S, Maia M und Bohn M (1999) Ridge-hot spot interaction: the Pacific-Antarctic Ridge and the Foundation seamounts. Marine Geology 160: 199-223.
- [6] Herzig PM, Hannington MD und Arribas A (1998) Sulfur isotopic composition of hydro-thermal precipitates from the Lau back-arc: implications for magmatic contributions to seafloor hydrothermal systems. Mineralium Deposita 33: 226-237.

1.2 Charakterisierung des hydrothermalen Potentials entlang des Pazifisch-Antarktischen Rückens

Dr. Thomas Kuhn & cand.-geol. Kerstin Schreiber (Lehrstuhl für Lagerstättenlehre und Leibniz-Labor für Angewandte Meeresforschung, TU Bergakademie Freiberg)

Während der Forschungsfahrt SO 157 wurden Fe-Mn-Überzüge in Form von dünnen Überzügen und Krusten (1-4 mm) auf vulkanischen Gesteinen geborgen. Im Rahmen einer Studienarbeit wurden 13 Fe-Mn-Überzüge von 9 verschiedenen Dredgepositionen entlang des Pazifisch-Antarktischen Rückens (PAR) geochemisch untersucht. Ziel der

Untersuchungen war die Charakterisierung des hydrothermalen Potentials des Pazifisch-Antarktischen Rückens zwischen 37°33'S und 41°43' S.

Da eine saubere mechanische Trennung der Fe-Mn-Präzipitate vom Nebengestein nicht möglich war, wurden die Proben selektiv gelaugt und infolge dessen nur die Mn-Oxide und amorphen Fe-Oxidhydroxidpartikel gelöst. Als Laugungsreagenz wurde ein Gemisch aus di-Ammoniumoxalat und Oxalsäure-Dihydrat eingesetzt.

Die Messungen der Elementkonzentrationen von Mn, Fe, Al, Cu, Co, Zn, Ba, Y und der SEE erfolgten mit Hilfe der AAS, ICP-AES und ICP-MS an den geochemischen Laboren der TU Bergakademie Freiberg und der FU-Berlin. Die Überprüfung der Laugungsmethode mittels einiger Doppelmessungen, „In-Haus-Standards“ und internationaler Standards (NOD-A-1) sowie einiger Gesamtaufschlüsse führte zu dem Ergebnis, dass die angewandte selektive Laugung eine geeignete Methode zur qualitativen Charakterisierung von Fe-Mn-Präzipitaten ist, die durch Nebengestein kontaminiert sind. Bei den SEE konnte eine Readsorption der mittleren und leichten SEE während des Laugungsvorganges festgestellt werden, jedoch bleiben die tonsteinnormierten Ce_{SN} - und Eu_{SN} -Anomalien weitestgehend erhalten.

Die untersuchten Fe-Mn-Überzüge des PAR sind durch negative Ce_{SN} -Anomalien sowie niedrige Co- und SEE-Konzentrationen gekennzeichnet, was auf eine hydrothermale Entstehung hinweist. Aufgrund der Mn/Fe-Verhältnisse (0,37 bis 1,02), den meist niedrigen Cu-, Zn- und Ba-Gehalten und den fehlenden positiven Eu_{SN} -Anomalien wird für den Großteil der Proben eine Entstehung aus distalen hydrothermalen Wolken (sog. „non-bouyant hydrothermal plume“) vermutet. Die Probe 24DS scheint dagegen direkt aus einem eisenreichen hydrothermalen Fluid präzipitiert zu sein. Drei Krusten von der Probenlokation 31GTV weisen außerdem außergewöhnlich hohe Cu- und Zn-Gehalte auf. Mineralogische Untersuchungen zeigen dabei, dass die beiden Elemente in diesen Proben keine eigenen Mineralphasen (wie z.B. Sulfide) bilden, sondern an die Mn- und Fe-Phasen adsorbiert sind. Letztere bilden amorphe (δ - MnO_2) bzw. kryptokristalline Phasen (δ -FeOOH), was ebenfalls auf die Präzipitation aus einer, in diesem Fall proximalen hydrothermalen Wolke hinweist (sog. „bouyant hydrothermal plume“).

Da alle untersuchten Fe-Mn-Präzipitate eine hydrothermale Signatur aufweisen, kann man auf ein großes hydrothermalen Potential für den PAR im untersuchten Bereich schließen. Für einen regionalen Vergleich wurden zusätzlich geochemische Daten von Fe-Mn-Krusten der Foundation-Seamount-Kette herangezogen, die im Vergleich zum PAR eine viel geringere hydrothermale Aktivität für die Foundation-Seamount-Kette anzeigen. Die Details der Studie können dem Anhang entnommen werden.

1.3 Gefügekundliche Untersuchungen an Klinopyroxensphärolithen

Dr. Axel Renno & Dr. Thomas Monecke (Lehrstuhl für Lagerstättenlehre und Leibniz-Labor für Angewandte Meeresforschung, TU Bergakademie Freiberg)

Neben den lagerstättenkundlichen Fragestellungen wurden gefügekundliche Untersuchungen an Klinopyroxensphärolithen durchgeführt, die in den basaltischen Andesiten auftreten. Dabei sollte geklärt werden, zu welchem Zeitpunkt während der Abkühlungsgeschichte dieser Laven es zur Bildung der Sphärolithe kam, da der mikroskopische Befund Hinweise darauf lieferte, dass diese Sphärolithe, entgegen der Lehrmeinung, nicht als Entglasungserscheinungen zu deuten sind.

Die petrographischen Untersuchungen der glasigen Lava zeigten, dass die räumliche Anordnung der Klinopyroxensphärolithe stark variiert. Neben isolierten kugelförmigen Körpern findet man perlschnurartige Aneinanderreihungen, in denen sich die Sphärolithe an den Rändern berühren. Darüber hinaus treten auch Gruppen eng beieinander liegender Sphärolithe auf. Größere Cluster bestehen im Inneren aus polygonal ausgebildeten Sphärolithen, die im Kontakt zur umgebenden Glasmatrix eine halbkugelförmige Ausbildung aufweisen. Die einzelnen Sphärolithe sind meist zonar aufgebaut. Der Kern besteht aus dicht gepackten Klinopyroxenfibern. In fast allen Fällen sind sie von einem 100 - 200 µm breiten, zweigeteilten Saum aus Pyroxennadeln umgeben. Die Pyroxenkristalle in dem inneren Saum sind auf den Kristallenden der in den Sphärolithen enthaltenen Fibern aufgewachsen und sind meist ähnlich wie die ursprünglichen Kristalle orientiert. Im Übergang zur äußeren Grenzzone lockert sich die Packungsdichte auf. Im Kontakt zum Glas findet man feinste Kristalle, die fächerartig in die glasige Matrix hinein gewachsen sind.

Die Sphärolithe umschließen häufig Gasblasen, die nur zum Teil rundlich sind. Viele Gasblasen besitzen längliche Formen oder sind ausgelängt. Die Auslängung der Gasblasen erfolgt dabei immer parallel zur Wachstumsrichtung der Pyroxennadeln. Das Auftreten ausgelängter Gasblasen belegt, dass diese Sphärolithe direkt aus der viskoelastischen, unterkühlten Schmelze oberhalb der Glasübergangstemperatur gebildet wurden. Diese Schlussfolgerung steht im Widerspruch zu der häufig vertretenen Ansicht, dass Sphärolithe ausschließlich Entglasungserscheinungen darstellen, die sich bei Temperaturen unterhalb des Glasübergangs bilden.

Die gefügekundlichen Beobachtungen wurden in einem zur Veröffentlichung angenommenen Manuskript zusammengefasst (siehe Anlage).

Weiterführende Untersuchungen zur Kristallisationskinetik der Klinopyroxene in den Sphärolithen werden derzeit mit Hilfe transmissions-elektronenmikroskopischer Methoden durchgeführt. Die Aufklärung des dreidimensionalen Aufbaus der Sphärolithe soll mittels Mikroröntgentomographie erfolgen.

II.2 Verwertung der Ergebnisse

Eine unmittelbare wirtschaftliche Verwertungsmöglichkeit der erzielten Ergebnisse ist nicht gegeben.

II.3 Fortschritt auf dem Gebiet des Vorhabens bei anderen Stellen

Für das Vorhaben relevante Ergebnisse von dritter Seite sind in der Zwischenzeit nicht bekannt geworden.

II.4 Geplante Veröffentlichungen

Neben den unten angegebenen Publikationen wird z.Zt. ein Manuskript über das hydrothermale Potential des Pazifisch-Antarktischen Rückens vorbereitet, die auf den geochemischen Untersuchungen an den Manganoxiden basiert (siehe Anlage). Ein Manuskript zur Genese der Massivsulfide entlang des Pazifisch-Antarktischen Rückens ist ebenfalls in Vorbereitung.

Monecke, T., Renno, A.D., and Herzig, P.M. (in press) Primary clinopyroxene spherulites in basaltic lavas from the Pacific-Antarctic Ridge. *Journal of Volcanology and Geothermal Research*.

Stoffers, P., Worthington, T., Hekinian, R., Petersen, S., Hannington, M., Türkay, M., and the SO157 Shipboard Scientific Party (2002) Silicic volcanism and hydrothermal activity documented at Pacific-Antarctic Ridge. *EOS, American Geophysical Union Transactions*, 83(28):303-304.

Stoffers, P., Worthington, T., Hekinian, R., Petersen, S., Hannington, M., Türkay, M., Ackermann, D., Borowski, C., Dankert, S., Fretzdorff, S., Haase, K., Hoppe, A., Jonasson, I., Kuhn, T., Lancaster, R., Monecke, T., Renno, A., Stecher, J., and Weiershäuser, L., (2002) Widespread silicic volcanism and hydrothermal activity on the Northern Pacific-Antarctic Ridge. *InterRidge News*, 11(1):30-32.

Die Untersuchungen der Freiburger Arbeitsgruppe wurden im Rahmen des BMBF Statusseminars 2003 in Hamburg sowie auf der Jahrestagung der Geological Society of America 2003 in Seattle vorgestellt:

Petersen, S., Herzig, P.M., Hannington, M.D., Jonasson, I.R., and Stoffers, P. (2003) Hydrothermale Prozesse im Kreuzungsbereich einer Spreizungsachse und eines Manteldiapirs: Der Pazifisch-Antarktische Rücken und die Foundation Seamount Kette bei 37°45'S. BMBF Statusseminar, Meeresforschung mit FS Sonne: p.259-262.

Monecke, T., Renno, A.D., Stoffers, P., and Herzig, P.M. (2003) Gefügekundliche Untersuchungen an primären Klinopyroxensphärolithen in basaltischen Andesiten vom Pazifisch-Antarktischen Rücken. BMBF Statusseminar, Meeresforschung mit FS Sonne: p.267-270.

Petersen, S., Herzig, P.M., Hannington, M.D., and Kelley, D.S. (2003) Diversity of seafloor hydrothermal systems on sediment-free mid-ocean ridges. Geological Society of America Annual Meeting 2003, Seattle, Abstracts with Program, v.35(6), paper 1-2

III. Erfolgskontrollbericht

III.1 Beitrag zu den förderpolitischen Zielen

In den Programmen zur Meeresforschung der Bundesregierung ist das 'Meer als Ressourcenquelle' ausdrücklich hervorgehoben. Dabei wird insbesondere auf die Verbesserung der Grundlagenkenntnisse über die Meere und die Erforschung mineralischer Rohstoffe zur Ressourcensicherung hingewiesen. In diesem Zusammenhang ist die Untersuchung der Vielfalt hydrothermalen Mineralisation am Meeresboden von besonderer Bedeutung. Darüber hinaus dienen die Untersuchungen dem besseren Verständnis der Wechselwirkungen zwischen den Teilsystemen Erdmantel, Kruste, Hydrosphäre und Atmosphäre.

III.2 Wissenschaftlicher und technischer Erfolg

- Erstbeschreibung hydrothermalen Sulfide aus dem Bereich des Pazifisch-Antarktischen Rückens (PAR).
- Nachweis einer geringen Beteiligung angereicherter Hotspot Gesteine am Aufbau der ozeanischen Kruste in dem die Reaktionszone für das hydrothermale System liegt.
- Einschätzung der Häufigkeit hydrothermalen Quellen entlang des PAR.
- Nachweis einer primär magmatischen Entstehung von Sphärolithen, die im Gegensatz zur gängigen Lehrmeinung steht.

III.3 Erfindungen und Schutzrechtanmeldungen

Keine

III.4 Arbeiten, die zu keiner Lösung geführt haben

Keine

III.5 Einhaltung der Ausgaben- und Zeitplanung

Der Finanzierungs- und Zeitplan wurde eingehalten. Für die Beschaffung wurden die Richtlinien des Landes Sachsen beachtet. Der Verwendungsnachweis und die Schlussrechnung sind dem Projektträger bereits zugegangen.

Publikationen

Stoffers, P., Worthington, T., Hekinian, R., Petersen, S., Hannington, M., Türkay, M., and the SO157 Shipboard Scientific Party (2002) Silicic volcanism and hydrothermal activity documented at Pacific-Antarctic Ridge. EOS, American Geophysical Union Transactions, 83(28): 303-304.

SILICIC VOLCANISM AND HYDROTHERMAL ACTIVITY DOCUMENTED AT PACIFIC – ANTARCTIC RIDGE

How well do we know the composition of oceanic crust? Countless studies have described the occurrence of mid-ocean ridge basalt (MORB) at spreading centers, and few would argue that the bulk composition of oceanic crust is other than basaltic. Nevertheless, silicic volcanism (>55 wt.% SiO₂) does occur along part of the northern East Pacific Rise (10.5°N; *Thompson et al.* [1989]), on the 095° propagator of the Galápagos Spreading Center [*Clague et al.*, 1981], and was recently discovered on the Pacific–Antarctic Ridge (PAR) near its intersection with the Foundation seamount chain [*Hekinian et al.*, 1997, 1999]. Silicic lavas were recovered from a 290-km-long section of the northern PAR adjacent to the active Foundation plume (Figure 1) during cruise 157 of the F/S *Sonne*, which took place in June and July 2001. Furthermore, widespread hydrothermal activity indicates that the volcanogenic massive sulfide – silicic lava association is not only restricted to subduction and back arc settings.

The fast to super-fast spreading centers of the southeast Pacific form a complex and dynamic tectonic environment that features the active Easter and Juan Fernandez microplates; fossil microplates; and abandoned spreading ridge segments. The region also features two major mantle plumes, Foundation and Easter; in both cases, their distance from the spreading axis has varied with time. The F/S *Sonne* and the N/O *L'Atalante* visited the Foundation seamount chain during 1995 and 1997, respectively. Based on data acquired, the Foundation plume is presently 35 km west of the PAR near 37°25'S [*Maia et al.*, 2000, 2001].

Surprisingly, silicic lavas (up to 64 wt.% SiO₂) were recovered from the PAR crest in addition to N- and T-MORB [Hekinian *et al.*, 1997, 1999]. The F/S *Sonne* re-visited the PAR from 37.5–41.5°S in mid-2001 to determine the extent of the silicic lavas, their origin, and any associated hydrothermal activity.

The PAR at 37.5 – 41.5°S

The northern PAR consists of 6 large segments, two of which are separated by overlapping spreading centers (OSCs) and three by transform faults [Lonsdale, 1994]. A 630-km-long section centered on the second major segment was studied. It is bounded by large left-stepping OSCs near 36.5°S and 41.5°S (Figure 1). Detailed bathymetric data were collected using the newly-installed SIMRAD EM120 onboard the F/S *Sonne*, and 65 stations were devoted to recovering sea-floor samples in conjunction with video observations of hydrothermal activity and vent fauna. To the southeast of the Foundation plume, the PAR axis trends 011° and can be subdivided into 9 non-overlapping segments ~15 km long. Small, right-stepping, non-transform discontinuities offset each segment by ~1 km, although a more complex westward bending occurs around an off-axis seamount at 38°16'S. Each segment is dome-shaped, with the elevation decreasing gently along strike towards its ends (Figure 2). The domes are better developed north of the off-axis seamount, where they rise ~100 m above the segment ends. Graben-like clefts up to 200 m wide and 50 m deep cut through some of the domes.

The 37°40'S dome was selected for a detailed petrological and hydrothermal study. This dome rises to a depth of 2120 m and is cut by a cleft filled with fresh glassy lavas and talus from adjacent pillow mounds. Lavas from the summit and cleft include aphyric dacite and andesite and have glass crusts >5 mm thick. Conchoidal fractures, together with numerous strongly elongate and flow-aligned vesicles, characterize these silicic lavas. At least one lava

flow was emplaced since the area was video surveyed by the N/O *L'Atalante* in early 1997. The new lava covers an area of 3.5 km x 200 m, and was erupted from a series of partly-buried fissures whose location is marked by collapse pits. A more varied lava suite was recovered from the lower flanks of the dome, where the dominant lithologies were glass-encrusted, sparsely phyric pillow andesite and basalt. Light dustings of MnOx suggest that most of these lower lavas are older.

To the south of 38°16'S, the PAR axis continues at an almost constant depth of 2220–2250 m. Strongly elongated, flow-aligned vesicles and devitrification features also characterize the pillow and sheet flows of sparsely phyric andesite and basalt throughout this 120-km-long section. The sub-segment is terminated by two 120-m-high axial domes constructed near 39°20'S and 39°27'S (Figure 1). The crest of the southern dome at 2090 m depth is capped by a fresh 4-km-long tabular flow of glassy aphyric andesite with skeletal pyroxene and plagioclase crystals. Strongly elongated, flow-aligned vesicles often contained pyrite-cubanite crystals and released H₂S when they were cut.

Further south, an additional series of 5 ridge segments, each of which are 40–50 km long and trend 005°, are separated by left-stepping OSCs at 39°48', 40°09', 40°34', 40°55', and 41°19'S (Figure 1). The ridge axis is offset by 4–5 km at each of these discontinuities, and the overlap distance varies from 5–22 km. MORB-like pillow lavas were recovered from these segments. Our survey terminated at the large, left-stepping OSC near 41°27'S, where the ridge crest is offset by 18 km and the overlap extends for 10 km. An isolated 500-m-high seamount with a well-developed summit crater has been built in the overlap basin (Figure 1). Fresh aphyric basalt, older MnOx-stained sparsely phyric basalt, and dolerite were recovered from the summit crater.

Origin of the Silicic Lavas

Combining our data with those of the earlier F/S *Sonne* and N/O *L'Atalante* cruises, silicic lavas have now been recovered from the upper flanks and summits of PAR axial domes between 37°11'S and 39°48'S, a distance of 290 km. These lavas have 55–64 wt.% SiO₂ and Mg# <40 (Mg# = $100 \cdot \text{Mg}^{2+} / (\text{Mg}^{2+} + \text{Fe}^{2+})$). To investigate their origin, we modeled the co-variation of Mg# with SiO₂ content during fractional crystallization of a PAR MORB (Figure 3). The calculated trends are flat until ~65 % crystallization, but thereafter they are sensitive to the oxidation state of the melt. At high oxygen fugacity, Ti-magnetite is crystallized and the SiO₂ content of the magma increases at nearly constant Mg#. At low oxygen fugacity, little Ti-magnetite is removed and the SiO₂ content continues to increase with a slight decline in Mg#.

Silicic lavas from the PAR have a range of SiO₂ contents at a given Mg# (Figure 3). Some are consistent with fractionation of a parental basaltic magma at low oxygen fugacity – for example, the 37°11'S lavas – while some require high oxygen fugacity – for example, the 37°40'S lavas. Other silicic lavas are best explained by magma mixing between highly fractionated magmas formed at high oxygen fugacity and unevolved basaltic melts – for example, the 38°09'S lavas. We envisage crystal fractionation occurring in a solidification zone that surrounds the magma chamber [e.g., *Nielsen and DeLong, 1992*]. Relatively buoyant residual silicic magma can migrate upward along the margin of this solidification zone, potentially interacting with large volumes of altered wallrock and increasing its oxidation state.

Hydrothermal Activity and Vent Fauna

Active hydrothermal vents, together with abundant vent fauna and fossil sulfide deposits, were located during video sled and TV-controlled grab surveys. These surveys provided

comprehensive coverage of the 37°40'S and 37°48'S axial domes. The high-temperature sulfide deposits and vent fauna are the first reported occurrences from high latitudes on Southern Hemisphere spreading ridges. Widespread, diffuse venting with near-bottom water temperature anomalies up to 0.25°C is associated with the young silicic flows in the cleft of the 37°40'S dome. Both the cleft walls and recovered rocks were commonly stained with Fe-hydroxides. Two partly talus-covered sulfide outcrops occur along the eastern cleft wall. Both are 30 m in diameter, and comprise sulfide rubble with halos of metalliferous sediment and Fe-hydroxide staining. Free-standing sulfide spires were seen at the northernmost site. Three areas of dark, dusty hydrothermal sediment, interpreted as recent plume fallout, coincided with weak temperature anomalies. One was near a clam field seen during the 1995 F/S *Sonne* cruise, and another extended for 100 m over the post-1997 glassy silicic lava at the southern end of the cleft.

The 37°48'S axial dome consists of partly sediment-covered lavas buried by younger sediment-free flows and lacks a central cleft. Nevertheless, near-bottom water temperature anomalies of up to 0.25°C occur at deep fissures cutting the younger lavas on the southern dome flank. White hydrothermal fluid was observed near a sulfide outcrop 10 m across at one fissure. A 50-m-wide vesicomylid clam bed and abundant vent fauna surround the fissures (Figure 4). A fossil sulfide outcrop 30 m across occurs 1.7 km north of the clam field and includes two large sulfide spires up to 3 m high. There, an old sulfide mound has been partly buried and disrupted by young lavas. Abundant sulfide talus has been ramped onto the young lavas, and sulfide windows outcrop between pillows. The talus is strongly altered and stained with bright red Fe-hydroxides, yellow jarosite, and bright green atacamite. Sulfide blocks recovered consist of coalesced pyrite chimneys, massive recrystallized sphalerite and chalcopyrite, and they also include sulfide-pseudomorphed clams and large worm tubes up to 1.5 cm in diameter (Figure 4).

The faunal communities around the active hydrothermal vents are dominated by *Bathymodiolus* and *Neolepas*, and mobile animals include bythograeid crabs, *Munidopsis*, and zoarcid fish. Unlike *B. thermophilus* found near sulfide-rich vent fluids elsewhere, the gills of our recovered *Bathymodiolus* specimens were only moderately hypertrophic, and H₂S was not released when the shells were opened. Polychaete worms and snails were collected from the vent sites, and dense beds of dead vesicomid clams were seen in the peripheral zone. Filter-feeders at the active vents and in the peripheral zone were hexactinellid sponges and sessile crinoids, while the more distal zones were dominated by large assemblages of serpulid tubes, actinians, coryphaenid fish, and swimming crinoids. The abundance of swimming crinoids at the PAR is possibly unique, and they were a useful indicator of nearby hydrothermal venting.

Widespread hydrothermal activity and sulfide deposits are associated with these areas of silicic volcanism and may reflect the high heat flow available from the fractionating magma. Furthermore, these areas of silicic volcanism at spreading centers are characterized by nearby plume-ridge interactions. Thus, enhanced magma supply – mantle plume plus spreading ridge – appears to promote extensive magma fractionation in the crust.

Acknowledgements

We thank Captain Henning Papenhagen, his officers, and the crew onboard F/S *Sonne* cruise 157 for their expert help. The cruise, which involved a consortium of four German universities and two Canadian research groups, was funded by the Bundesministerium für Bildung und Forschung (BMBF).

Authors

P. Stoffers, T. Worthington, R. Hekinian, S. Petersen, M. Hannington, M. Türkay, and the SO 157 Shipboard Scientific Party.

For additional information, contact Peter Stoffers, Institut für Geowissenschaften, Universität Kiel, Germany.

References

- Clague, D.A., F.A. Frey, Thompson G., and Rindge S., Minor and trace geochemistry of volcanic rocks dredged from the Galápagos Spreading Center: role of crystal fractionation and mantle heterogeneity, *J. Geophys. Res.*, *86*, 9469–9482, 1981.
- Hekinian, R., et al., Intraplate versus ridge volcanism on the Pacific–Antarctic Ridge near 37°S - 111°W, *J. Geophys. Res.*, *102*, 12265–12286, 1997.
- Hekinian, R., P. Stoffers, D. Ackermann, S. Révillon, M. Maia, and M. Bohn, Ridge–hotspot interaction: the Pacific–Antarctic Ridge and the Foundation seamounts, *Mar. Geol.*, *160*, 199–223, 1999.
- Lonsdale, P., Geomorphology and structural segmentation of the crest of the southern (Pacific–Antarctic) East Pacific Rise, *J. Geophys. Res.*, *99*, 4683–4702, 1994.
- Maia, M., et al., The Pacific–Antarctic Ridge–Foundation hotspot interaction: a case study of a ridge approaching a hotspot, *Mar. Geol.*, *167*, 61–84, 2000.
- Maia, M., C. Hémond, and P. Gente, Contrasted interactions between plume, upper mantle, and lithosphere: Foundation chain case, *Geochem. Geophys. Geosyst.*, *2*, #2000GC000117, 2001.
- Nielsen, R.L., and S.E. DeLong, A numerical approach to boundary layer fractionation: application to differentiation in natural magma systems, *Contrib. Mineral. Petrol.*, *110*, 355–369, 1992.
- Thompson, G., W.B. Bryan, and S.E. Humphris, Axial volcanism on the East Pacific Rise, 10–12°N, in *Magmatism in the Ocean Basins*, Edited by A.D. Saunders and M.J. Norry, *Geol. Soc. Spec. Publ.*, *42*, 181–200, 1989.

Figure Captions

Fig. 1: The tectonic setting and bathymetry of the northern Pacific–Antarctic Ridge (PAR) are shown; (Left) location of the SO 157 area, Easter and Foundation seamount chains, Easter Microplate (EM) and Juan Fernandez Microplate (JFM) in the southeast Pacific. (Right) Detailed bathymetry of the PAR crest in the SO 157 area collected during the F/S *Sonne* (1995) and N/O *L'Atalante* (1997) cruises is superposed upon the Smith and Sandwell 2' data base (processed using GMT). The red circle marks the geoid anomaly associated with the Foundation mantle plume [Maia *et al.*, 2000, 2001], and black bars indicate the extent of silicic lavas along the PAR crest.

Fig. 2: This bathymetric profile of the northern Pacific–Antarctic Ridge (PAR) shows dredge stations. Silicic lavas predominate on the axial domes between 37°11'S and 39°48'S.

Fig. 3: Mg# versus SiO₂ is plotted for selected glasses from the Pacific–Antarctic Ridge (PAR). Microprobe analyses were completed at IFREMER. Solid lines are fractional crystallization trends at different oxygen fugacities calculated using the algorithms of Nielsen and DeLong [1992]. Also shown are silicic glass analyses from the Galápagos Spreading Center [Clague *et al.*, 1981], East Pacific Rise [Thompson *et al.*, 1989] and Iceland for comparison.

Fig. 4: a) Older talus is buried by fresh young lava in the cleft of the 37°40'S dome, b) a live clam field with associated vent crabs and lobsters on the 37°48'S dome, c) sulfide talus and hydrothermal dust at 37°47'S, d) massive pyrite containing a clam shell pseudomorphed by coarse-grained chalcopyrite at 37°47'S.

Figure 1: Stoffers et al., Eos

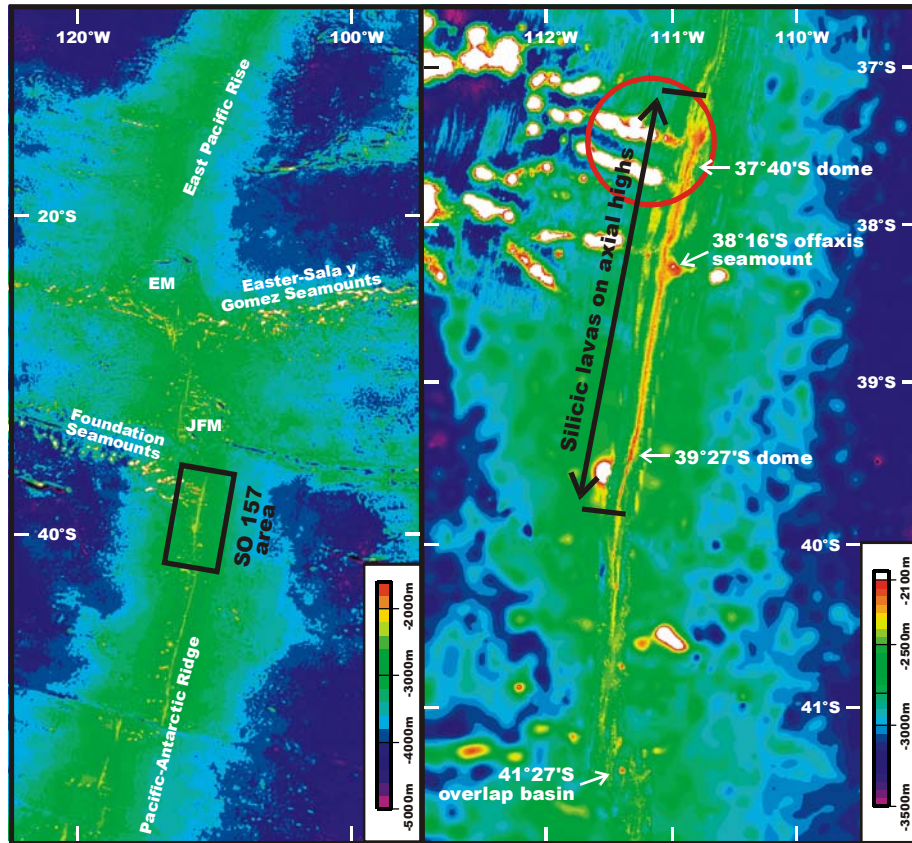


Figure 2: Stoffers et al., Eos

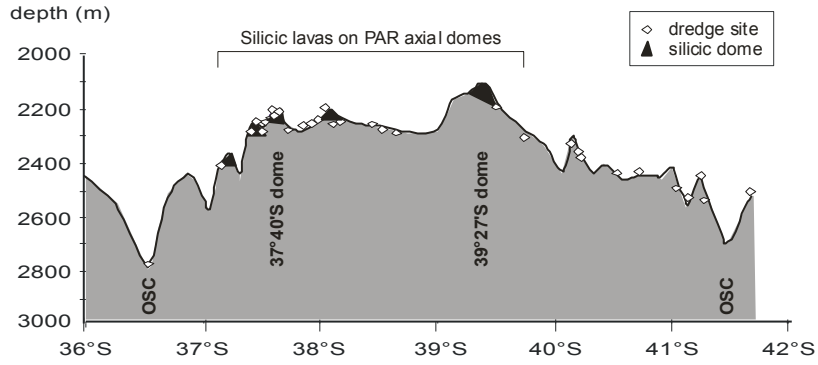


Figure 3: Stoffers et al., Eos

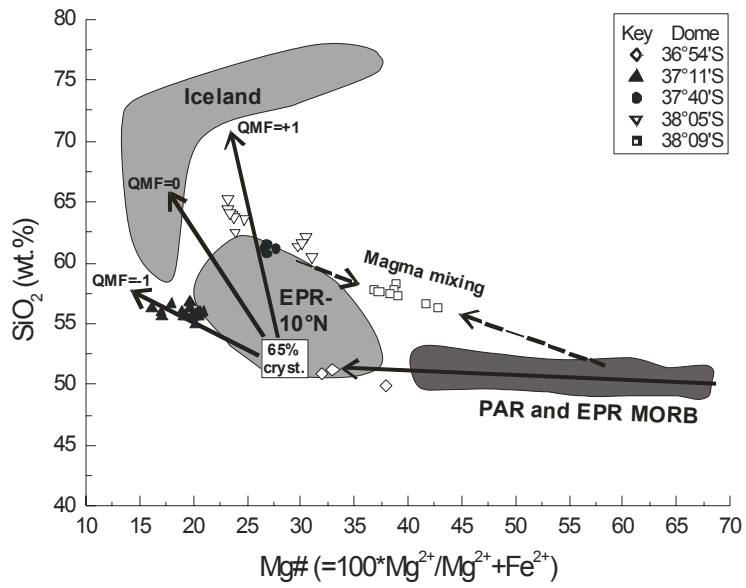
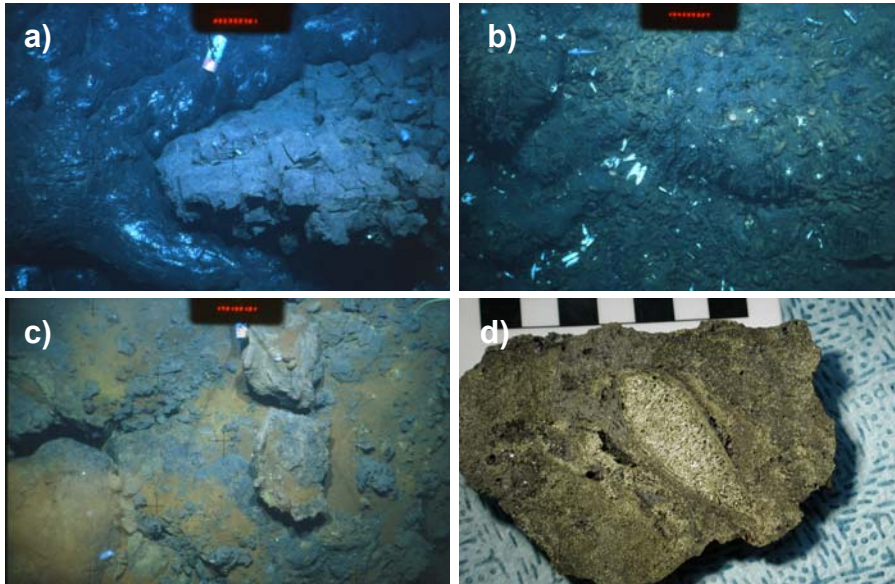


Figure 4: Stoffers et al., Eos



Stoffers, P., Worthington, T., Hekinian, R., Petersen, S., Hannington, M., Türkay, M., Ackermann, D., Borowski, C., Dankert, S., Fretzdorff, S., Haase, K., Hoppe, A., Jonasson, I., Kuhn, T., Lancaster, R., Monecke, T., Renno, A., Stecher, J., and Weiershäuser, L. (2002) Widespread silicic volcanism and hydrothermal activity on the Northern Pacific-Antarctic Ridge. *InterRidge News*, 11(1): 30-32.

P. Stoffers, T. Worthington, R. Hekinian, S. Petersen, M. Hannington, M. Türkay, D. Ackermann, C. Borowski, S. Dankert, S. Fretzdorff, K. Haase, A. Hoppe, I. Jonasson, T. Kuhn, R. Lancaster, T. Monecke, A. Renno, J. Stecher, L. Weiershäuser.

Widespread Silicic Volcanism and Hydrothermal Activity on the Northern Pacific – Antarctic Ridge

P. Stoffers¹, T. Worthington¹, R. Hekinian¹, S. Petersen², M. Hannington³, M. Türkay⁴, D. Ackermann¹, C. Borowski⁵, S. Dankert², S. Fretzdorff¹, K. Haase¹, A. Hoppe¹, I. Jonasson³, T. Kuhn², R. Lancaster³, T. Monecke², A. Renno², J. Stecher⁴, L. Weiershäuser⁶

¹ *Institut für Geowissenschaften, Universität Kiel, Germany*

² *Institut für Mineralogie, Technische Universität Bergakademie Freiberg, Germany*

³ *Natural Resources Canada, Ottawa, Canada*

⁴ *Forschungsinstitut Senckenberg, Frankfurt, Germany*

⁵ *Zoologisches Institut, Universität Hamburg, Germany*

⁶ *Department of Geology, University of Toronto, Canada*

The Foundation seamount chain was first visited during 1995 by the *R/V SONNE*, and subsequently in 1997 by the *R/V L'ATALANTE*. Geochemical and geophysical data from these cruises have shown that the Foundation seamounts formed during the passage of the Pacific Plate over a mantle plume, and that this plume is presently located 35 km west of the Pacific–Antarctic Ridge (PAR) near 37°25'S (Fig. 1; Maia *et al.*, 2000; 2001; O'Connor *et al.*, 2001). Surprisingly, silicic lavas (up to 64 wt.% SiO₂) were recovered from the PAR crest adjacent to the youngest Foundation seamounts (Hekinian *et al.*, 1997; 1999). Silicic volcanism (>55 wt.% SiO₂) on mid-ocean ridges is rare, but does occur on the northern East Pacific Rise (10.5°N; Thompson *et al.*, 1989) and the 095° propagator of the Galapagos Spreading Centre (Clague *et al.*, 1981).

The prime objectives of the FOUNDATION III cruise (*R/V SONNE*- SO 157) in mid-2001 were to determine the extent of the silicic lavas along the PAR and to investigate associated hydrothermal activity. We examined a 630 km-long segment of the northern PAR bounded by

large left-stepping overlapping spreading centres (OSCs) near 36.5°S and 41.5°S (Fig. 1). Detailed bathymetric data was collected using the newly installed SIMRAD EM120 onboard the *R/V SONNE*, and 65 stations were devoted to recovering seafloor samples in conjunction with video observations of hydrothermal activity and vent fauna.

The PAR at 37.5 – 41.5°S

In the northern part of the surveyed area, the PAR axis forms a series of short (~15 km-long) non-overlapping segments (Fig. 2). Small right-stepping non-transform discontinuities offset each segment by ~1 km, although a more complex westward bending occurs around an off-axis seamount near 38°15'S. Each segment is dome-shaped, with the elevation decreasing gently along strike towards its ends. The domes are better developed north of the off-axis seamount, where they rise ~100 m above the segment ends. Graben-like clefts up to 200 m-wide and 50 m-deep cut through some of the domes.

The 37°40'S dome was selected for a detailed petrological and hydrothermal study. This dome rises to 2120 m-depth, and is cut by a cleft filled with fresh glassy lavas and talus from adjacent pillow mounds. Lavas from the summit and cleft include aphyric dacite and andesite, and have glass crusts >5 mm thick. Conchoidal fractures, together with numerous strongly elongate and flow-aligned vesicles, characterise these silicic lavas. At least one lava flow was emplaced since the area was video surveyed by the *R/V L'ATALANTE* in early 1997. The new lava covers an area of 3.5 km x 200 m, and was erupted from a series of partly buried fissures whose location is marked by collapse pits. A more varied lava suite was recovered from the lower flanks of the dome, where the dominant lithologies were glass-encrusted sparsely phyrlic pillow andesite and basalt. Light dustings of MnOx suggest most of these lower lavas are older.

To the south of 38°15'S, the PAR axis continues at an almost constant depth of 2220–2250 m. Pillow and sheet flows of sparsely phyrlic andesite and basalt characterise this 120 km-long section. The section is terminated by two 120 m-high axial domes constructed near 39°20'S and 39°27'S (Fig. 1). The crest of the southern dome at 2090 m-depth is capped by a fresh 4 km-long tabular flow of glassy aphyric andesite with skeletal pyroxene and plagioclase crystals. Strongly elongated flow-aligned vesicles often contained pyrite-cubanite crystals, and released H₂S when cut.

Further south, a series of 40–50 km-long ridge segments (each 40–50 km-long) are separated by left-stepping OSCs at 39°48', 40°09', 40°34', 40°55', and 41°19'S (Fig. 1). The ridge axis is offset by 4–5 km at each of these discontinuities, and the overlap distance varies

from 5–22 km. MORB-like pillow lavas were recovered from these segments. Our survey terminated at the large left-stepping OSC near 41°22'S, where the ridge crest is offset by 18 km and the overlap extends for 10 km. An isolated 500 m-high seamount with a well-developed summit crater has been built in the overlap basin. Fresh aphyric basalt, older MnOx-stained sparsely phyrlic basalt and dolerite were recovered from the summit crater.

Hydrothermal activity and vent fauna

Active hydrothermal vents, together with abundant vent fauna and fossil sulfide deposits, were located during video sled and TV-controlled grab surveys. These surveys provided comprehensive coverage of the 37°40'S and 37°48'S axial domes. The high-temperature sulfide deposits and vent fauna are the first reported occurrences from high latitudes on southern hemisphere spreading ridges.

Widespread diffuse venting (near-bottom water temperature anomalies up to 0.25°C) is associated with the young silicic flows in the cleft of the 37°40'S dome. Both the cleft walls and recovered rocks were commonly stained with Fe-hydroxides. Two partly talus-covered sulfide outcrops occur along the eastern cleft wall. Both are 30 m in diameter, and comprise sulfide rubble with halos of metalliferous sediment and Fe-hydroxide staining. Free-standing sulfide spires were seen at the northernmost site. Three areas of dark, dusty hydrothermal sediment, interpreted as recent plume fallout, coincided with weak temperature anomalies. One was near a clam field seen during the 1995 *R/V SONNE* cruise, and another extended for 100 m over the post-1997 glassy silicic lava at the southern end of the cleft.

The 37°48'S axial dome consists of partly sediment-covered lavas buried by younger sediment-free flows, and lacks a central cleft. Nevertheless, near-bottom water temperature anomalies (up to 0.25°C) occur at deep fissures cutting the younger lavas on the southern dome flank. White hydrothermal fluid was observed near a sulfide outcrop 10 m across at one fissure, and the fissures are surrounded by a vesicomid clam bed 50 m in diameter and abundant vent fauna. A fossil sulfide outcrop 30 m across occurs 1.7 km north of the clam field, and includes two large sulfide spires up to 3 m high. There, an old sulfide mound has been partly buried and disrupted by young lavas. Abundant sulfide talus has been ramped onto the young lavas, and sulfide windows outcrop between pillows. The talus is strongly altered, and stained with bright red Fe-hydroxides, yellow jarosite, and bright green atacamite. Recovered sulfide blocks consisted of coalesced pyrite chimneys, massive recrystallised sphalerite and chalcopyrite, and included sulfide-pseudomorphed clams and large worm tubes up to 1.5 cm in diameter.

The faunal communities around the active hydrothermal vents are dominated by *Bathymodiolus* and *Neolepas*, and mobile animals include bythograeid crabs, *Munidopsis*, and zoarcid fish. Unlike *B. thermophilus* found near sulfide-rich vent fluids elsewhere, the gills of our recovered *Bathymodiolus* specimens were only moderately hypertrophic and H₂S was not released when the shells were opened. Polychaete worms and snails were collected from the vent sites, and dense beds of dead vesicomid clams were seen in the peripheral zone. Filter-feeders at the active vents and in the peripheral zone were hexactinellid sponges and sessile crinoids, whereas the more distal zones were dominated by large assemblages of serpulid tubes, actinians, coryphaenid fish and swimming crinoids. The abundance of swimming crinoids at the PAR is possibly unique, and they were a useful indicator of nearby hydrothermal venting.

Summary

Silicic lavas have now been recovered from the upper flanks of PAR axial domes between 37°11'S and 39°48'S, a distance of 290 km. These lavas outcrop on the upper flanks and summits of the axial domes, whereas less silicic lavas are found on the lower dome flanks (Fig. 3). Widespread hydrothermal activity and sulfide deposits are associated with the silicic volcanism, and may reflect the high heat flow available from fractionating magma.

Acknowledgements

We thank Captain Henning Papenhagen, his officers and the crew onboard *R/V SONNE* cruise 157 for their expert help. This project is funded by BMBF Grant 03G0157A.

References

- Clague, D.A., F.A. Frey, G. Thompson, and S. Rindge. Minor and trace geochemistry of volcanic rocks dredged from the Galapagos Spreading Center: role of crystal fractionation and mantle heterogeneity. *J. Geophys. Res.*, 86, 9469–9482, 1981.
- Hekinian, R., P. Stoffers, C. Devey, D. Ackermann, C. Hémond, J. O'Connor, N. Binard, and M. Maia. Intraplate versus ridge volcanism on the Pacific–Antarctic Ridge near 37°S - 111°W. *J. Geophys. Res.*, 102, 12265–12286, 1997.
- Hekinian, R., P. Stoffers, D. Ackermann, S. Révillon, M. Maia, and M. Bohn. Ridge–hotspot interaction: the Pacific–Antarctic Ridge and the Foundation seamounts. *Mar. Geol.*, 160, 199–223, 1999.

- Maia, M., D. Ackermann, G.A. Dehghani, P. Gente, R. Hekinian, D. Naar, J. O'Connor, K. Perrot, J. Phipps Morgan, G. Ramillien, S. Révillon, A. Sabetian, D. Sandwell, and P. Stoffers. The Pacific–Antarctic Ridge–Foundation hotspot interaction: a case study of a ridge approaching a hotspot. *Mar. Geol.*, 167, 61–84, 2000.
- Maia, M., C. Hémond, and P. Gente. Contrasted interactions between plume, upper mantle, and lithosphere: Foundation chain case. *Geochem. Geophys. Geosyst.*, 2, #2000GC000117, 2001.
- O'Connor, J.M., P. Stoffers, and J.R. Wijbrans. En echelon volcanic elongate ridges connecting intraplate Foundation Chain volcanism to the Pacific–Antarctic spreading center. *Earth Planet. Sci. Lett.*, 192, 633–648, 2001.
- Thompson, G., W.B. Bryan, and S.E. Humphris. Axial volcanism on the East Pacific Rise, 10–12°N, in: *Magmatism in the Ocean Basins*, eds. A.D. Saunders and M.J. Norry. *Geol. Soc. Spec. Publ.*, 42, 181–200, 1989.

Figure captions

- Fig. 1: Tectonic setting and bathymetry of the northern PAR. Left- location of the SO 157 work area and major tectonic features (EM = Easter Microplate, JFM = Juan Fernandez Microplate). Right- SO 157 station sites along the PAR crest and features referred to in the text. Black bars indicate the extent of silicic lavas along the PAR crest.
- Fig. 2: Detailed bathymetry and dredge stations in the northern part of the work area.
- Fig. 3: Bathymetric profile of the northern PAR. Silicic lavas predominate on the axial domes between 37°11'S and 39°48'S.

Figure 1: Stoffers et al., InterRidge News

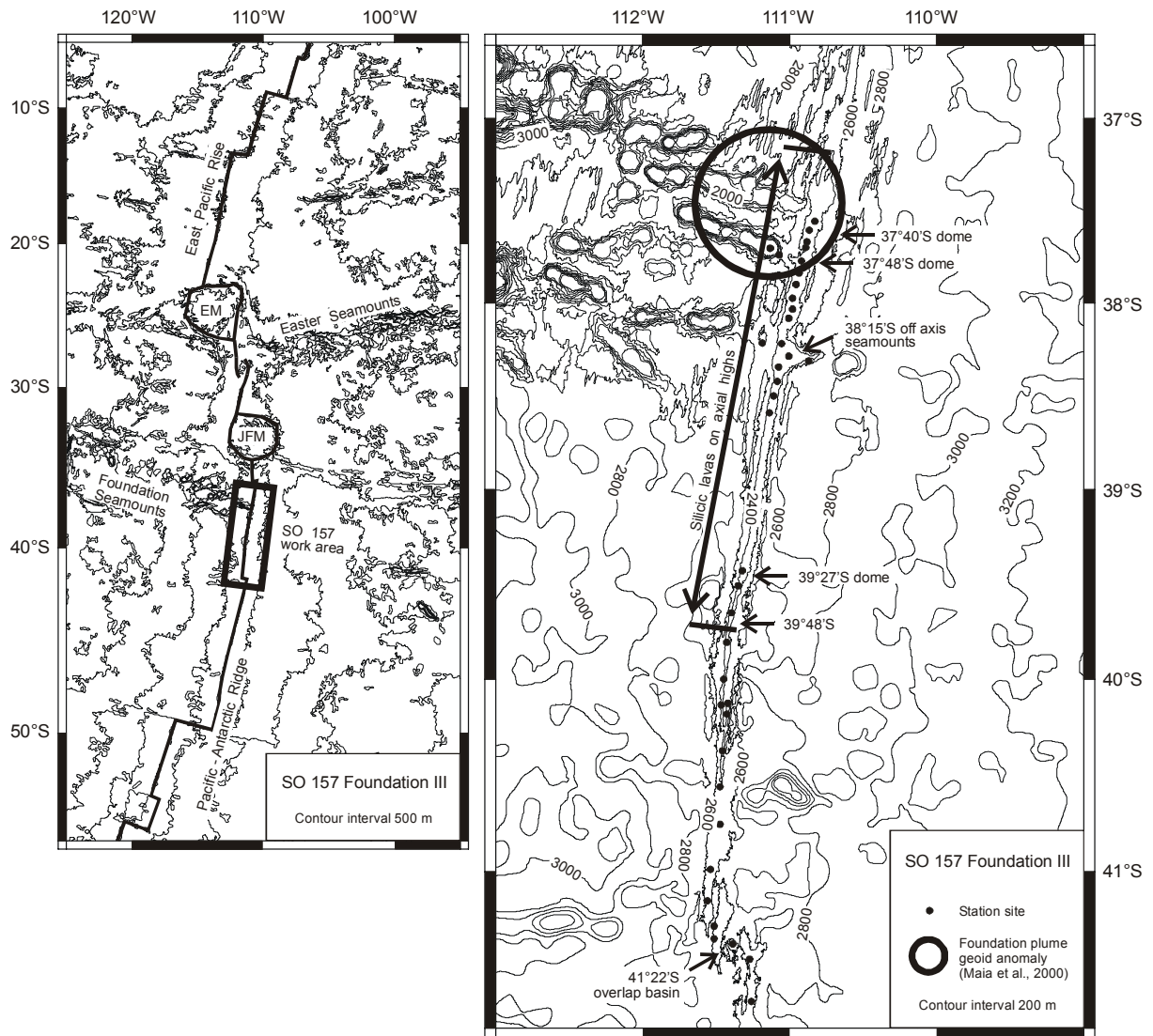


Figure 2: Stoffers et al., InterRidge News

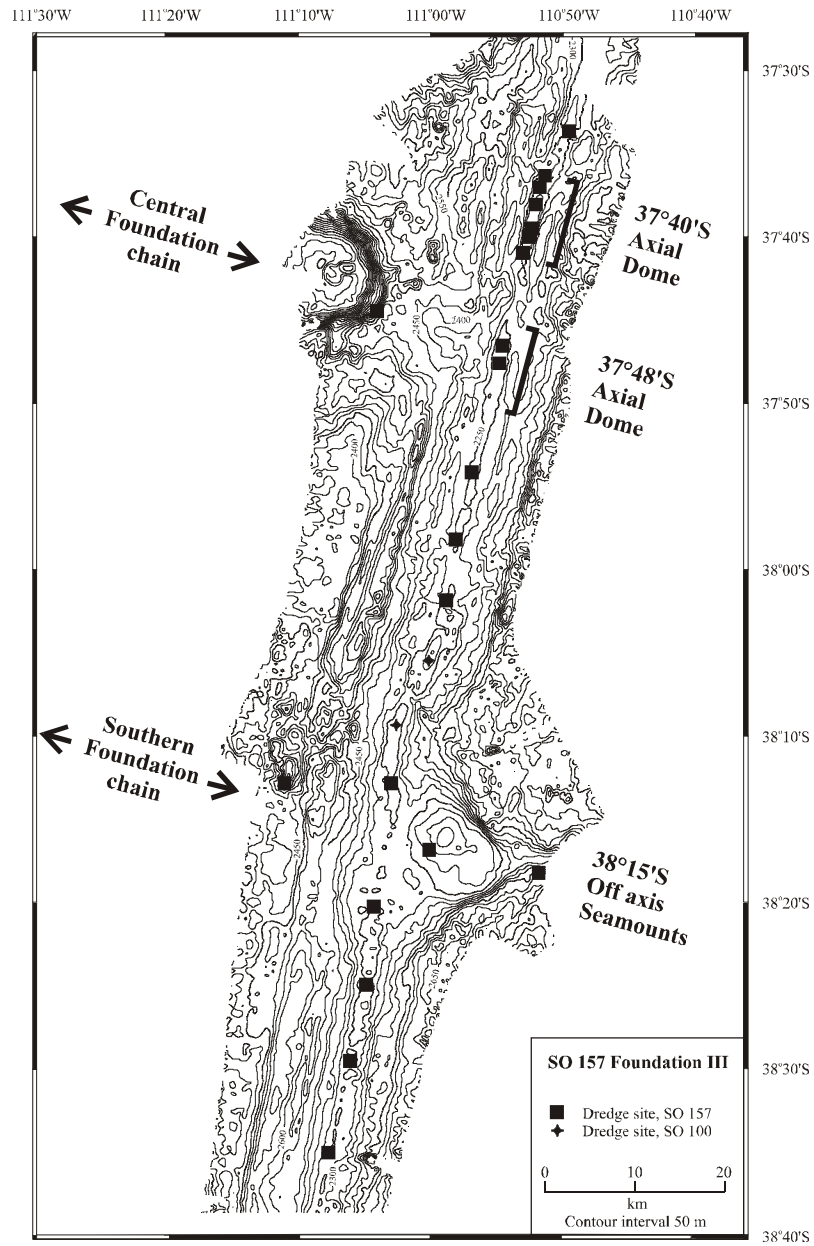
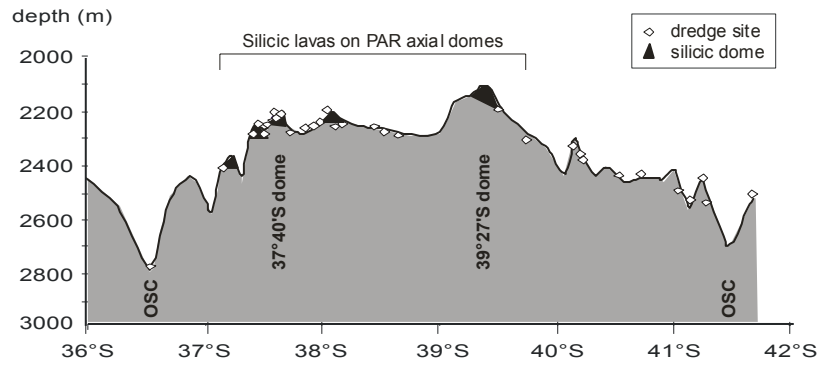


Figure 3: Stoffers et al., InterRidge News



**O`Connor, J. A., Stoffers, P., and Wijbrans (2002)
Pulsing of a focused mantle plume: Evidence from
the distribution of Foundation Chain hotspot
volcanism. Geophys. Res. Let., 29 (9): 64.1-64.4**

Pulsing of a focused mantle plume: Evidence from the distribution of Foundation Chain hotspot volcanism

John M. O'Connor

GEOMAR – Research Center for Marine Geosciences, Christian-Albrechts University, Kiel, Germany

Peter Stoffers

Institute for Geosciences, Christian-Albrechts University, Kiel, Germany

Jan R. Wijbrans

Department of Isotope Geochemistry, Vrije Universiteit, Amsterdam, The Netherlands

Received 7 January 2002; revised 27 March 2002; accepted 4 April 2002; published 16 May 2002.

[1] Using the rare case of a hotspot chain crossing a fossil microplate, we reveal fundamental mantle plume characteristics by comparing hotspot volcanism in a sequence of contrasting tectonic settings. Key new $^{40}\text{Ar}/^{39}\text{Ar}$ ages show that the Foundation mantle plume pulses hot masses from depth with an apparent periodicity of one Myr. Synchronous magmatism over large distances indicates that masses associated with individual pulses are focused initially into similarly sized zones under the Pacific plate. Since the plume, spreading on impact with the lithosphere, influences a very wide area, apparently unconnected hotspot volcanism can be produced simultaneously across wide swaths, often crosscutting seamount chains. Our model might explain in part much of the midplate volcanism scattered across the Pacific seafloor indicating the episodic addition of significantly greater masses of plume material into the upper mantle than suggested by the narrowness of major seamount chains. **INDEX TERMS:** 8121 Tectonophysics: Dynamics, convection currents and mantle plumes; 3040 Marine Geology and Geophysics: Plate tectonics (8150, 8155, 8157, 8158); 3035 Marine Geology and Geophysics: Midocean ridge processes; 1035 Geochemistry: Geochronology

1. Introduction

[2] We report here new $^{40}\text{Ar}/^{39}\text{Ar}$ ages for linear volcanic structures scattered to the south of the Foundation Seamount Chain (Figures 1 and 2). This 22 Myr old volcanic trail records the motion of the Pacific plate over the narrow locus of the upwelling Foundation mantle plume [O'Connor *et al.*, 1998, 2001, following Morgan, 1971]. Our ages (Table 1), supported by geochemical data [Hekinian *et al.*, 1997, 1999; Hemond *et al.*, 1999; Maia *et al.*, 2001], show that these linear, disconnected structures are coeval with Foundation Chain seamount magmatism to the north and reveal that a ~250 km wide swath of scattered, coeval hotspot volcanism was created at 17 Ma by an apparently single short lived event related to the activity of the Foundation mantle plume (Figure 2). This new information allows us to compare variations in the temporal and spatial distribution of midplate volcanism created in a series of very different tectonic settings that are linked, in this case, to the migration of a fossil microplate over the Foundation plume [e.g., O'Connor *et al.*, 1998, 2001]. We infer from this comparison that Foundation Chain development was controlled primarily by tectonic plate migration over broad zones of hot plume material of fundamentally constant size and orientation created with an apparent periodicity of about one Myr. This

modified plume theory might also explain the widespread scattered midplate volcanism revealed recently in satellite altimetry mapping [Smith and Sandwell, 1997], given that many other mantle plumes are similarly pulsing large masses of hot plume material (not necessarily with the same periodicity or mass) into broad regions impacting the base of the Pacific lithosphere.

2. Distribution of Foundation Hotspot Volcanism

[3] Inferring long-term mantle plume behavior from the ~17 Ma magmatic event reported here (cf. Table 1) is supported by the fact that for at least the past 5 Myr the Foundation Chain developed in a series of similarly sized elongate (~250 km × ~150 km) swaths of disconnected coeval hotspot volcanism created at intervals of approximately 1 Myr [O'Connor *et al.*, 2001]. Significantly, during the interval ~16 Ma to ~5 Ma the Foundation Chain formed as a narrow chain of seamounts, in contrast to the broad regions of scattered coeval magmatism created before and afterwards [O'Connor *et al.*, 1998]. We explain this major switch in morphology in terms of the age, and consequently thickness and strength, of the seafloor migrating over the Foundation plume acting as a threshold parameter controlling the mode of hotspot volcanism. This is suggested by the similarity in age (~6 Myr) of the oceanic plate drifting over the Foundation plume at the onset of both episodes of broadly distributed hotspot volcanism at ~22 Ma and again at ~5 Ma (Figure 3). Nonetheless, our current and previous dating [O'Connor *et al.*, 1998, 2001] demonstrates that the strict periodicity of Foundation Chain creation is not influenced by the changes in surface expression of hotspot magmatism.

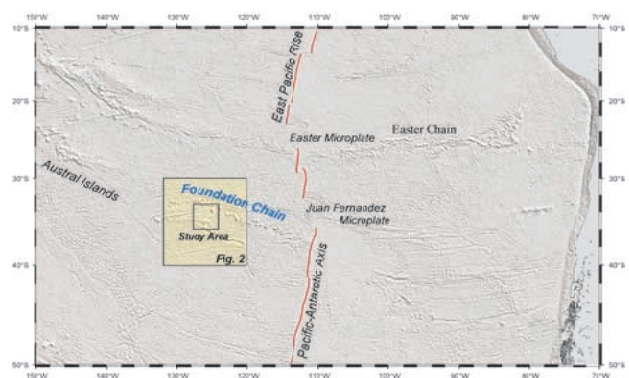


Figure 1. Predicted topography [Smith and Sandwell, 1997] of SE Pacific seafloor showing the location of the Foundation Chain and our study area.

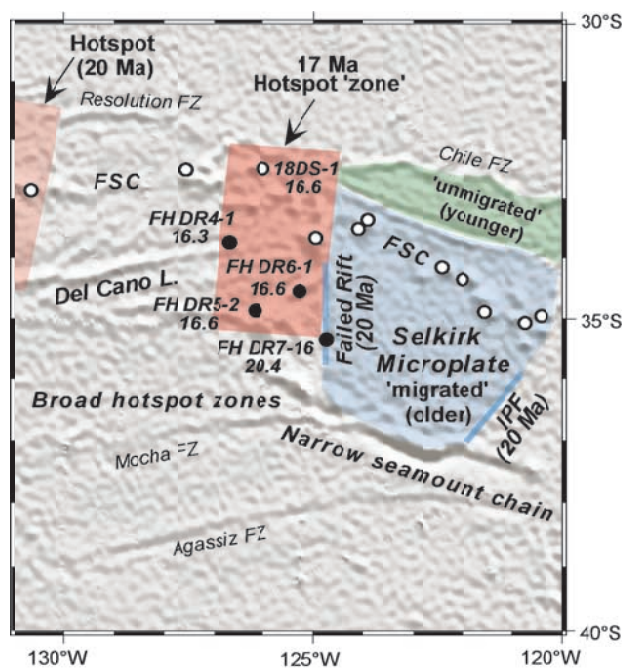


Figure 2. Red zones indicate the broad swath of scattered, structurally disconnected coeval Foundation hotspot magmatism produced during the ~ 17 Ma pulse (Table 1) of the Foundation mantle plume and the location of the hotspot at 20 Ma. The age of the seafloor labeled 'migrated' (older) was increased significantly by the creation of the Selkirk Microplate at 20 Ma (Table 1). This process involved an eastward jump of a spreading center located east of the Foundation plume ('failed') and initiation of a 'new rift' [Mammerickx, 1992; Tebbens and Cande, 1997]. Contrastingly, the significantly younger 'unmigrated' seafloor was generated by normal seafloor spreading at the spreading center segment extending north of the 'Failed Rift'. Variability in age of lithosphere drifting over, or close to, the Foundation plume is shown in Figure 3. Circles indicate dredge sites: black circles = $^{40}\text{Ar}/^{39}\text{Ar}$ ages reported in this study (Table 1 and Supplemental Material), open circles = $^{40}\text{Ar}/^{39}\text{Ar}$ ages reported in [O'Connor et al., 1998]. Measured ages are shown below dredge sample numbers. Rocks analyzed in this study were dredged from the Del Cano Lineament, a volcanic elongate ridge (VER) located further to the south, and the 'Failed Rift' of the Selkirk Microplate [Tebbens and Cande, 1997] during the 1997 N/O *Atalante* 'Hotline' cruise [Maia et al., 1997, 2001]. FSC = Foundation Seamount Chain; Bold blue lines = Failed Rift and IPF = Inner Pseudo Fault; FZ = Fracture Zone.

[4] Furthermore, we report here an $^{40}\text{Ar}/^{39}\text{Ar}$ age (Table 1) for a rock sample dredged from the 'failed' spreading center of the Selkirk Microplate (Figure 2) [Mammerickx, 1992; Tebbens and Cande, 1997] showing that it jumped eastward (failed) at 20.4 ± 0.3 Ma. This reveals that the process of Selkirk Microplate creation led to a large offset in the age of the seafloor that migrated later over the Foundation plume, resulting in the migration of seafloor ≤ 6 Myr only across the northern flank of the Foundation plume (Figure 3). Hotspot volcanism was restricted therefore to a narrow chain of seamounts between ~ 16 Ma and ~ 5 Ma, despite the inferred presence of much broader regions of Foundation plume material impacting periodically against the base of the Pacific plate. Another consideration is that seafloor in this region might also have been thermally reset to younger ages due to the

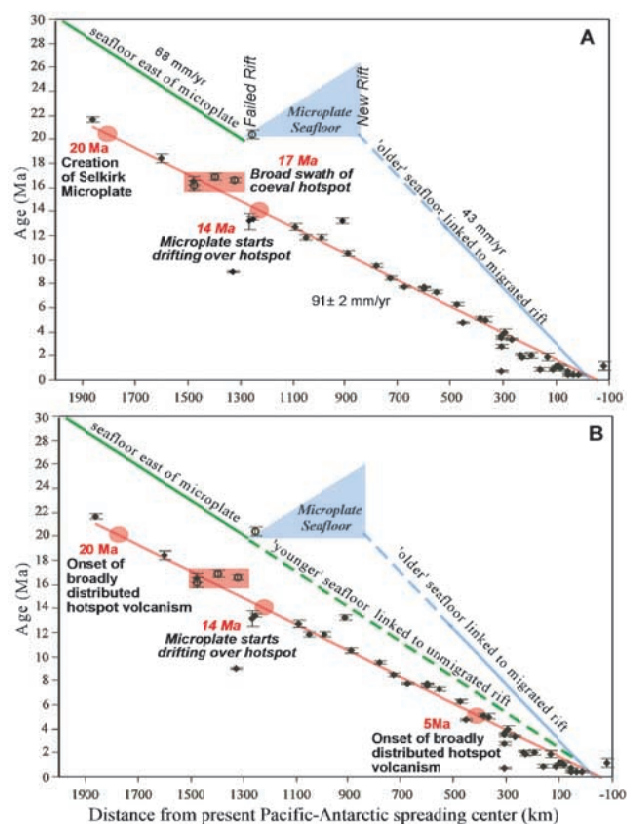


Figure 3. (a). Correlation between Foundation Chain dredge site $^{40}\text{Ar}/^{39}\text{Ar}$ ages and distance from the present Pacific-Antarctic spreading center. Also shown is the relationship between the Foundation Chain and the age of 'migrated' seafloor drifting directly over the hotspot (Figure 2). As the Selkirk Microplate reached the active hotspot region at about 14 Ma, increasingly older seafloor (≥ 6 Myr) began to cap the Foundation plume. This 'older' seafloor placed a sufficiently thick/strong lid over most of the region impacted by pulsed plume material to prevent the migration of plume melts to the seafloor during the interval ~ 14 Ma and ~ 5 Ma. The resulting transition from broad zones of hotspot volcanism to a narrow chain of seamounts is evident in Figure 2. Blue solid lines denote 'older' seafloor (unbroken lines indicate known seafloor ages [Mammerickx, 1992; Lonsdale, 1994]; blue dashed lines indicate extrapolated seafloor ages). The red swath indicates the broad zone of scattered coeval hotspot volcanism crosscutting the narrow Foundation Seamount Chain created by the 17 Ma pulse of the Foundation plume (Table 1). $^{40}\text{Ar}/^{39}\text{Ar}$ ages shown as open spheres are from this study (Table 1 and Supplemental Material) and [O'Connor et al., 1998, 2001]. The solid line is the York-2 linear regression fit to previously published data representing an average rate for the migration of volcanism along the chain of 91 ± 2 mm/yr [O'Connor et al., 1998]. Analytical error bars are $\pm 2\sigma$. (b). Relationship between Foundation Chain and younger, 'unmigrated' seafloor. The spreading center north of the 'Failed Rift' likely continued spreading normally such that 'younger' (≤ 6 Myr) seafloor was migrating over the northern flank of the Foundation plume. This younger, 'unmigrated' seafloor drifting by the northern flank of the Foundation plume was sufficiently thin to allow the passage of plume melts along a narrow strip leading to creation of a correspondingly narrow chain of Foundation seamounts (Figure 2). Long green dashed line indicates younger, 'unmigrated' seafloor created by the spreading center north of the 'Failed Rift' (extrapolation of known seafloor ages west of the Selkirk Microplate).

Table 1. $^{40}\text{Ar}/^{39}\text{Ar}$ ages for whole rock basalts^a

Sample ^b	Seamount/ Ridge	Latitude	Longitude	% ³⁹ Ar	Plateau (Ma)	2 σ	Inverse Isochron (Ma)	2 σ
FH DR4-1	<i>Del Cano Lineament</i>	33° 46.69' S	126° 43.83' W	44.5	16.1	0.4	16.3	0.7
FH DR5-2	<i>Volcanic Elongate Ridge</i>	34° 55.112' S	126° 13.798' W	99.7	16.8	0.3	16.6	1.0
FH DR6-1	<i>Volcanic Elongate Ridge</i>	34° 34.000' S	125° 16.400' W	32.3	16.6	0.2	16.1	0.6
18DS-1	<i>Seamount 5^c</i>	32° 28.871' S	126° 0.456' W	67.2	16.6	0.4	16.6	0.4
Weighted Average					16.6	0.1	16.4	0.3
FH DR7-16	<i>Failed Rift</i>	35° 20.849' S	124° 45.723' W	100	20.4	0.4	19.5	3.7
FH DR7-16	<i>Failed Rift</i>	35° 20.849' S	124° 45.723' W	22.5	20.3	0.6	18.5	3.7
Weighted Average					20.4	0.3	19.0	2.6

^aArgon isotopic data, age calculation from argon isotopic data, plateau and isochron plots available as Supplemental Material.

^bDetailed sample information available as Supplemental Material.

^cData from [O'Connor et al., 1998] recalculated in [O'Connor et al., 2001] using new TCR standard age of 28.34 Ma [Renne et al., 1998].

⁴⁰Ar/³⁹Ar ages were measured using the argon laser probe at Vrije University Amsterdam.

Details of sample preparation and analytical procedures are described in detail elsewhere [O'Connor et al., 1998].

$\lambda^{40}\text{K} = 5.543 \times 10^{-10}$ /yr; Correction factors: $^{40}\text{Ar}/^{39}\text{Ar}$ (K) = 0.00086; $^{36}\text{Ar}/^{37}\text{Ar}$ (Ca) = 0.00026; $^{39}\text{Ar}/^{37}\text{Ar}$ (Ca) = 0.00067.

preferential channeling of plume material [e.g., Morgan, 1978; Schilling, 1985, 1991] to the nearby spreading center responsible for this younger seafloor.

[5] If the previously proposed relationship between the Foundation plume and older seamounts in the Austral Island region [McNutt et al., 1997; O'Connor et al., 1998] is correct (Figure 1), then the Foundation plume was active for at least the past 34 Myr. As in the case of the Foundation Chain, the lack of significant hotspot volcanism between the Foundation Chain and the ≥ 34 Myr Ngatamoto and Taukina Seamounts [McNutt et al., 1997; Maia et al., 2001] can be explained by migration of seafloor that was too old and consequently too thick and strong (>6 Myr in the case of the Foundation plume) to allow Foundation plume magma to reach the lithospheric surface.

[6] We propose therefore that the development of broad swaths of coeval hotspot volcanism, with an apparent periodicity of approximately 1 Myr, is related primarily to the long-term dynamics of the Foundation plume since at least 34 Ma. This activity is characterized by periodic emplacement of large masses of hot plume material (pulsing) into broad, similarly sized and orientated zones (focused) (at least on initial impact at the base of the Pacific tectonic plate). The pattern of hotspot volcanism produced within each such 'zone' was controlled by localized factors such as lithospheric age and stress [McNutt et al., 1997; Hieronymus and Bercovici, 2000; Maia et al., 2001; O'Connor et al., 2001]. However, involvement of pre-existing lithospheric structures acting as 'weak zones' facilitating decompression melting of hot plume material is strongly indicated by the fact that volcanic lineaments south of the Foundation Chain parallel the local fracture zone (FZ) direction (Figure 2).

3. Implications for Plume Modeling

[7] We cannot resolve differences in age across individual, similarly sized and oriented, zones of Foundation midplate volcanism created at a rate of approximately once per Myr. A physical process is therefore required that periodically brings masses of hot plume material extremely fast from depth and is capable of focusing it into broadly elongate zones (~ 250 km \times ~ 150 km), at least on initial impact against the base of the drifting Pacific plate. Depth-dependent properties have been shown theoretically to play an important role in controlling plume dynamics [Hansen et al., 1993]. For example 'ultrafast' focused mantle plumes are theoretically possible in the upper mantle during thermal convection with a non-Newtonian temperature- and depth-dependent rheology operating at a reasonable effective Rayleigh number on the order of 10^6 [Larsen and Yuen, 1997; Larsen et al., 1999]. Such strong depth-dependence in viscosity also results in masses of

plume material pulsing at intervals ranging from a few Myr [Larsen et al., 1999] to about 10 Myr [Larsen and Yuen, 1997] with calm periods in between [Larsen et al., 1999]. These current models indicate that plumes can rise through the upper mantle in much less than one Myr [e.g., Larsen et al., 1999], so providing a mechanism by which hot plume material can be brought from the transition zone to the lithosphere extremely fast (m/yr) in an otherwise slowly convecting mantle (cm/yr). Following impact against the base of the lithosphere this material can flow laterally at rates as high as ~ 0.5 m/yr, so creating the potential of coeval magmatism scattered over large areas [Larsen and Yuen, 1997; Sleep, 1997; Larsen and Saunders, 1998; Larsen et al., 1999]. Our results suggest that SE Pacific mantle plumes are more tightly focused and faster pulsing than is presently incorporated into such numerical models indicating even greater viscosity stratification (or changes in the creep law) across the upper mantle compared to, for example, the region of the North Atlantic influenced by the Iceland plume [e.g., Larsen et al., 1999; O'Connor et al., 2000].

4. Discussion and Conclusions

[8] Prior to this study it was not possible to determine whether the elongate 'zones' of scattered coeval hotspot volcanism at the young end of the Foundation Chain [O'Connor et al., 2001] are the expression of the long-term dynamics of the Foundation mantle plume. We resolve this fundamental question by 1) showing that Foundation hotspot volcanism occurred within similarly sized elongate 'zones' prior to the migration of the fossil Selkirk Microplate over the Foundation plume hotspot, and 2) suggesting a possible mechanism to explain why only a narrow chain of seamounts developed across these elongate 'zones' during the interval between microplate migration over the plume hotspot at ~ 14 Ma and the onset of volcanic elongate ridge (VER) development ~ 5 Myr ago.

[9] We explain therefore the distribution of Foundation midplate volcanism in terms of a mantle plume pulsing hot masses with an apparent periodicity of approximately 1 Myr. Material associated with individual pulses is focused (at least on initial impact against the base of the lithosphere) into basically similarly sized and oriented elongate 'zones'. Variations in the age, structure and stress pattern of tectonic plates (e.g., migration of the Selkirk Microplate over the plume hotspot and plume-spreading-center interaction) drifting over pulsing mantle plumes control if and where hotspot volcanism develops on the Pacific plate.

[10] Our model proposed here for Foundation plume volcanism could have implications for Pacific midplate volcanism in general. Variations in the age, structure and stress patterns of tectonic plates drifting over pulsing mantle plumes might control if and where

hotspot volcanism develops on the Pacific plate, so leading to the development of broad swaths of scattered hotspot volcanism that often crosscut prominent seamount chains. Furthermore, this previously unknown, episodic/periodic emplacement of broad synchronous regions of hot plume material under Pacific tectonic plates, far larger than suggested by narrow seamount chains such as Hawaiian-Emperor, has important implications for measuring the activity of mantle plumes and for testing numerical models of plume dynamics and mantle circulation.

[11] **Acknowledgments.** We thank Captain J.-C. Gourmelon and crew of the N/O *Atalante* for fine ship operation and the scientific party for help with dredging and on board sample preparation. R. Hekinian is acknowledged for leading the dredge-sampling program. D. Ackerman, A. Dehghani, R. Hekinian, J. Phipps Morgan, D. Naar, and D. Sandwell are thanked for helpful discussions during the 'Foundation Hotline' cruise. We thank two anonymous reviewers for very helpful comments. This work was supported by BMBF projects 03G0100A0 and 03G0157A (P.S.) and INSU-CNRS. The contribution of JRW is covered by NSG #20020302.

References

- Hansen, U., D. A. Yuen, S. E. Kroening, and T. B. Larsen, Dynamical consequences of depth-dependent thermal expansivity and viscosity on mantle circulation and thermal structure, *Phys. Earth Planet. Inter.*, **77**, 205–223, 1993.
- Hekinian, R., et al., Intraplate versus oceanic ridge volcanism on the Pacific Antarctic Ridge near 37°S–111°W, *J. Geophys. Res.*, **102**, 12,265–12,286, 1997.
- Hekinian, R., et al., Ridge-hotspot interaction: The Pacific-Antarctic Ridge and the Foundation Seamounts, *Mar. Geol.*, **160**, 199–223, 1999.
- Hemond, C., M. Maia, and P. Gente, The Foundation Seamounts: Past and present ridge hotspot interactions?, *EOS Trans. Am. Geophys. Union*, *AGU*, **80**, 1056, 1999.
- Hieronimus, C. F., and D. Bercovici, Non-hotspot formation of volcanic chains: Control of tectonic and flexural stresses on magma transport, *Earth. Planet. Sci. Lett.*, **181**, 539–554, 2000.
- Larsen, T. B., and D. A. Yuen, Ultrafast upwelling bursting through the upper mantle, *Earth Planet. Sci. Lett.*, **146**, 393–399, 1997.
- Larsen, T. B., D. A. Yuen, and M. Storey, Ultrafast mantle plumes and implication for flood basalt volcanism in the Northern Atlantic Region, *Tectonophysics*, **311**, 31–43, 1999.
- Larsen, H. C., and A. D. Saunders, Tectonism and volcanism at the south-east Greenland rifted margin: A record of plume impact and later continental rupture, *Proc. ODP Sci. Res.*, **152**, 503–533, 1998.
- Lonsdale, P. J., Geomorphology and structural segmentation of the crest of the southern (Pacific-Antarctic) East Pacific Rise, *Geophys. Res.*, **99**, 4683–4702, 1994.
- Maia, M., et al., The Foundation Hotline cruise: Past and recent ridge-hotspot interaction zones in the South Pacific, *InterRidge News*, **6**, 36–39, 1997.
- Maia, M., C. Hemond, and P. Gente, Contrasted interactions between plume, upper mantle and lithosphere: Foundation chain case, *Geochem. Geophys. Geosyst.*, **1**, 2000GC000117, 2001.
- Mammerickx, J., The Foundation seamounts: Tectonic setting of a newly discovered seamount chain in the South Pacific, *Earth. Planet. Sci. Lett.*, **113**, 293–306, 1992.
- McNutt, M. K., D. W. Caress, J. Reynolds, K. A. Jordahl, and R. A. Duncan, Failure of plume theory to explain midplate volcanism in the southern Austral islands, *Nature*, **389**, 479–482, 1997.
- Morgan, W. J., Convection plumes in the lower mantle, *Nature*, **230**, 42–43, 1971.
- Morgan, W. J., Rodriguez, Darwin, Amsterdam, A second type of hotspot island, *J. Geophys. Res.*, **83**, 5355–5360, 1978.
- O'Connor, J. M., P. Stoffers, and J. R. Wijbrans, Migration rate of volcanism along the Foundation Chain, SE Pacific, *Earth Planet Sci. Lett.*, **164**, 41–59, 1998.
- O'Connor, J. M., P. Stoffers, and J. R. Wijbrans, En Echelon volcanic elongate ridges connecting intraplate Foundation Chain volcanism to the Pacific-Antarctic spreading center, *Earth Planet Sci. Lett.*, **189**, 93–102, 2001.
- O'Connor, J. M., P. Stoffers, and J. R. Wijbrans, Evidence from episodic seamount volcanism for pulsing of the Iceland plume in the past 70 Myr, *Nature*, **408**, 954–958, 2000.
- Schilling, J.-G., Upper mantle heterogeneities and dynamics, *Nature*, **314**, 62–67, 1985.
- Schilling, J.-G., Fluxes and excess temperatures of mantle plumes inferred from their interaction with migrating mid-ocean ridges, *Nature*, **352**, 397–403, 1991.
- Sleep, N. H., Lateral flow and ponding of starting plume material, *J. Geophys. Res.*, **102**, 10,001–10,012, 1997.
- Smith, W. H. F., and D. T. Sandwell, Global sea floor topography from satellite altimetry and ship depth soundings, *Eos*, **277**, 1956–1962, 1997.
- Tebbens, S. F., and S. C. Cande, Southeast Pacific tectonic evolution from early Oligocene to present, *J. Geophys. Res.*, **102**, 12,061–12,084, 1997.

J. M. O'Connor, GEOMAR-Research Center for Marine Geosciences, Christian-Albrechts University, Wischhofstr. Str. 1-3, Kiel, D-24148, Germany. (jocconnor@geomar.de)

P. Stoffers, Institute for Geosciences, Christian-Albrechts University, Kiel, D-24118, Germany.

J. R. Wijbrans, Department of Isotope Geochemistry, Vrije Universiteit, Amsterdam 1081 HV, The Netherlands.

O`Connor, J. A., Stoffers, P., and Wijbrans (in press) The Foundation Chain: Inferring hotspot-plate interaction from a weak seamount trail. Oceanic Hotspots, Eds. Hekinian, R., Stoffers, P., and Cheminée, Springer

The Foundation Chain: Inferring hotspot–plate interaction from a weak seamount trail

J.M. O'Connor^{a,b} P. Stoffers^b & J.R. Wijbrans^c

^a*GEOMAR, Christian-Albrechts University, Wischhofstrasse 1-3, D-24148 Kiel, Germany*
email: joconnor@gpi.uni-kiel.de

^b*Institute for Geosciences, Christian-Albrechts University, D-24118 Kiel, Germany*
email: pst@gpi.uni-kiel.de

^c*Department of Isotope Geochemistry, Vrije Universiteit, 1081 HV Amsterdam, The Netherlands*
email: Jan.Wijbrans@falw.vu.nl

1. Introduction

The Foundation Chain was first detected using a combination of satellite altimeter and conventional geophysical data (Sandwell, 1984; Mammerickx, 1992) and described initially as a ~1350 km-long chain of seamounts trending approximately in the direction of absolute motion of the Pacific plate (Mammerickx, 1992) (Fig. 1). A significant section of the Foundation Chain lies in a tectonic setting influenced by a change in the direction of seafloor spreading between 26 Ma and 11 Ma (Herron, 1972; Lonsdale, 1988; Mayes et al., 1990, Mammerickx, 1992). This motion change is reflected in the curvature of the Agassiz Fracture Zone (FZ) and its west-east shift in orientation between the Resolution/Del Cano and Chile FZs (Fig. 2). A segment of the Nazca plate was transferred to the Pacific plate during this period of reorganization to form the short-lived Selkirk Microplate (Fig. 2) (Mammerickx, 1992; Tebbens and Cande, 1997; Tebbens et al., 1997) via a spreading-ridge propagation event between Chron 6C (23.4–24 Ma) and Chron 6(o) (20.2 Ma) (Tebbens and Cande, 1997).

Predicted seafloor topography (Smith and Sandwell, 1997) reveals that the Foundation Chain changes ~450 km west of the present Pacific–Antarctic axis from a narrow line of individual or clustered seamounts to a much broader region of *en echelon* Volcanic Elongate Ridges (VERs) (Fig. 2). This morphology switch correlates broadly with a change in composition of Foundation lavas from enriched hotspot-like to a more depleted mixed type (Hemond and Devey, 1996; Hekinian et al., 1997; Devey et al., 1997). Such changing fabric and less hotspot-like composition have been explained by interaction between the inferred Foundation plume-hotspot and the Pacific–Antarctic spreading-axis (Hemond and Devey, 1996; Hekinian et al., 1997; Devey et al., 1997).

The Foundation Chain was extensively dredge-sampled (Fig. 2) during the *F/S Sonne* SO100 cruise in 1995 (Devey et al., 1995; Devey et al., 1997), followed by some additional sampling during the 1997 *N/O Atalante* 'Hotline' cruise (Maia et al., 2001). ⁴⁰Ar/³⁹Ar ages for Foundation rock samples (O'Connor et al., 1998, 2001, 2002) show a linear trend of decreasing Foundation Chain age between ~22 Ma (northwestern end) and ~2 Ma (southeastern end) at a rate of 91 ± 2 mm/yr (Fig. 3) (O'Connor et al., 1998). This rate corresponds well with estimates of the migration rate of volcanism along the Hawaiian Chain (O'Connor et al., 1998, Koppers et al., 2001) suggesting – together with the intraplate nature of the Foundation Seamounts (O'Connor et al., 1998) and their hotspot-like composition (Devey et al., 1997; Hekinian et al., 1997; Hekinian et al., 1999; Hemond and Devey, 1996; Hemond et al., 1999) – that Foundation Chain volcanism

documents an ~22 Myr history of Pacific plate motion over the narrow locus of an upwelling Foundation mantle plume (O'Connor et al., 1998, following Morgan, 1971). Furthermore, measured Foundation Chain ages suggest that volcanism erupted at a regular interval of ~1 Myr (O'Connor et al., 1998, 2001, 2002).

Mantle plumes appear to influence a significant part of the global spreading center system. Thus, to understand the global convection system it is important to determine the processes controlling plume-spreading center interactions. Foundation VERs present a valuable chance to directly investigate these processes. $^{40}\text{Ar}/^{39}\text{Ar}$ ages show that individual Foundation VERs can occasionally develop synchronously (i.e., coeval volcanism along one continuous ridge) (Fig. 4). But surprisingly the dominant trend in the new Foundation Chain age data is for structurally disconnected sections of different VERs to be coeval. These synchronously erupted, yet structurally unconnected VER sections define a series of NE-SW *en echelon* elongate zones of hotspot volcanism that cross-cut the overall NW-SE trend of the Foundation Chain (O'Connor et al., 2001) (Fig. 5). 'Zones' appear to have developed at intervals of ~1 Myr while maintaining a steady state size (~250 km by ~150 km) and orientation (NE-SW) as the Pacific-Antarctic spreading center migrated progressively closer to the Foundation hotspot.

Although such VER development was controlled in part by local factors (e.g. location of nearest spreading center segment, lithospheric stress), long-lived attributes of the Foundation plume hotspot (e.g. size, orientation, periodicity) appear to have played a significant role. The key to testing this notion is the fact that the Foundation Chain represents a rare, possibly unique, case of a hotspot trail crossing a fossil microplate. Prior to encountering the Selkirk Microplate the Foundation Chain formed as broad zones of scattered, synchronous Foundation volcanism – similar to those identified west of the present Pacific-Antarctic spreading center (Fig. 6). However, once the significantly older microplate lithosphere began capping the plume hotspot about 14 Myr ago (O'Connor et al., 2002), the chain narrowed abruptly into a line of discrete seamounts, only broadening again about 5 Myr ago when sufficiently young lithosphere once again drifted over the plume hotspot (Fig. 7). Foundation hotspot volcanism can therefore be prevented across elongate hotspot zones if the capping tectonic plate is too thick for plume melts to penetrate to the surface (O'Connor et al., 1998, 2002). We infer from this information that Foundation Chain development was controlled primarily by tectonic plate migration over broad zones of hot plume material of fundamentally constant size and orientation created with an apparent periodicity of about once per Myr (O'Connor et al., 2002).

2. Sample preparation and analytical procedure

2.1 Samples and preparation

Descriptions and locations of dredge samples are in O'Connor et al. (1998, 2001, 2002). Pieces of selected rock samples, following removal with a saw of outer surfaces and as much visible alteration as possible, were crushed and sieved. Altered whole rock samples (500–250 μm) were treated with 7 N HCl prior to treatment for 1 hour in 1.0 N HNO₃ (in an ultrasonic bath at 50°C) followed by rinsing in distilled water (Koppers, 1998). Plagioclase (250–125 μm) was separated from crushed whole rock using a magnetic separator. Separated plagioclase was treated in 7 N HCl for 30 min, 5–8% HF for 5 min, 1 N HNO₃ for 1 hour and then washed in distilled H₂O (Koppers, 1998). Complete removal of alteration products sometimes required the repetition of certain steps.

2.2 Dating technique

The theory of $^{40}\text{Ar}/^{39}\text{Ar}$ geochronology has previously been described (e.g., Faure, 1986, York, 1984; McDougall and Harrison, 1999). Sample ages are calculated using the standard age equation. The uncertainty in the age is calculated by partial differentiation of the age equation (Dalrymple and Lanphere, 1969; Dalrymple et al., 1981) and includes uncertainties in the determination of the flux monitor J , blank determination, the regression of the intensities of the individual isotope peaks, the correction factors for interfering isotopes, and the mass discrimination correction. The argon laserprobe facility at the Vrije Universiteit, Amsterdam, has previously been described in considerable detail (Wijbrans et al., 1985). It consists of a 24W argon ion laser, beam optics, a low volume UHV gas inlet system and a Mass Analyser Products Ltd. 215-50 noble gas mass spectrometer. The mass spectrometer is fitted with a modified Nier type electron bombardment source. During data collection the mass spectrometer is operated with an adapted version of the standard MAP software written in TurboPascal allowing data collection for all isotopes of argon using a secondary electron multiplier collector operated at a gain of 50,000. Modifications include variable dwell time on each peak during data collection, valve control, laser control and x-y stage control, allowing the data collection during data acquisition for this project in semi-automated mode. Data reduction is described in some detail in section 2.4. Mass fractionation was determined by measuring aliquots of air argon at regular intervals and at a later stage of the project by measuring aliquots of ^{38}Ar spiked air (Kuiper, 2003).

2.3 Irradiation and analysis

Plagioclase (250-125 μm) and whole rock chips (500-250 μm) were irradiated for either 7, or in the case of younger near axis seamounts, 1.5 hours with Cd-shielding in the CLICIT facility at the Oregon State University TRIGA reactor. Cd shielding significantly reduces the effects of slow neutrons leading to a major reduction in the ^{40}Ar produced without affecting the production of ^{39}Ar (e.g., McDougall and Harrison, 1999), which in turn reduces the impact of the $(^{40}\text{Ar}/^{39}\text{Ar})_{\text{K}}$ correction factor, particularly useful in the case of young and low potassium samples. The K and Ca correction factors for the Cd-shielded position at the OSU TRIGA reactor have previously been determined (Wijbrans et al., 1995). Between 50 and 100 mg of rock chips or plagioclase separate from each sample were wrapped in aluminum foil and stacked in 9 mm ID quartz tubes. Taylor Creek Rhyolite sanidine, TCR 85G003, (28.34 Ma; Renne et al., 1998) was used to measure the flux gradients. TCR was loaded between every four unknowns and also at the top and bottom of each vial. Between four and six replicate analyses of 4–6 sanidine crystals were made for each monitor position, typically giving uncertainties of 0.1 to 0.3% (s.e.m.). Using a best fit curve between all of the standards allowed determination of J factors with a similar precision.

High precision $^{40}\text{Ar}/^{39}\text{Ar}$ ages have been determined (plagioclase separates and whole rock chips) by incremental heating with the argon laser probe, using a defocused CW laser beam (e.g., York et al., 1981). We encountered difficulties initially in both heating samples with sufficient uniformity and in producing satisfactorily high peak intensities. Following some experimentation we solved these problems by using large (13 mm) custom-made Cu-sample pans, which allowed us to load significantly more sample in even, single-grain layers. Heating such thin layers of sample (under manual x-y stage control) allowed us to produce predictable analytical results: plagioclase consistently showed excellent plateaus, whereas the whole rock experiments for older samples typically showed elevated ages in the first ~20% of gas released, a good plateau, and anomalous young ages in the final ~10 to 20% when the sample was partially melting. However, due to the significantly younger sample ages involved in this study, combined with frequently low to very low % K_2O (Devey et al., 1997; Hekinian et al., 1997; Hekinian et al., 1999), we

conducted a significant number of multiple single fusion experiments in addition to incremental heating analyses whenever necessary in order to reduce analytical uncertainty to acceptable levels. The uncertainty in the system blank was shown to be the single most important factor contributing to the uncertainty in the ages, especially in cases where young, low-K samples were being analyzed. Blanks were run on average between every four blocks of unknown heating steps or fusions. The intensity and uncertainty for the ^{40}Ar , ^{39}Ar , ^{37}Ar and ^{36}Ar blanks for each day of analyses were calculated by regression of blank peak intensities versus time of measurement, allowing prediction of a blank for each experiment by interpolation (Koppers, 2002).

2.4 Data reduction

$^{40}\text{Ar}/^{39}\text{Ar}$ incremental heating data were reduced as both age spectra and isochrons using the freeware data reduction package ArArCALC developed at VU (Koppers, 2002). It allows the choice between a straight linear regression of peak intensities with respect to inlet time, asymptotic curve fitting minimizing standard deviation and sum of squared residuals as criteria for best fit, or an average of peak intensities. The asymptotic extrapolation was very often the most appropriate as the highest peak intensities often showed deviations from straight line behavior with time. A summary of the calculated ages is in Table 1. Calculated ages, analytical data as well as the plateau and isochron plots are in O'Connor et al. (1998, 2001, 2002). However, for consistency ages reported in O'Connor et al., 1998 have been recalculated (O'Connor et al., 2001) using the new TCR monitor age (28.34 Ma; Renne et al., 1998). Plateau ages are presented as weighted means over the steps contributing to the plateau. We have used the York-2 least-squared linear fit with correlated errors (York, 1969), and both the $^{40}\text{Ar}/^{36}\text{Ar}$ versus $^{39}\text{Ar}/^{36}\text{Ar}$ and $^{36}\text{Ar}/^{40}\text{Ar}$ versus $^{39}\text{Ar}/^{40}\text{Ar}$ correlated diagrams to calculate isochron ages. Mean squared weighted deviation values (MSWD) (York, 1969; Roddick, 1978) have been calculated for both the plateau and the isochron ages based on ($N-1$) and ($N-2$) degrees of freedom, respectively. If the scatter around the plateaus or isochrons was beyond analytical error at the 95% confidence level (i.e., MSWD >1), the reported analytical error was multiplied by the MSWD (York, 1969, Kullerud, 1991). Following Fleck et al. (1977), Lanphere and Dalrymple (1978), Dalrymple et al. (1980) and Pringle (1993), all of the Foundation Chain ages - with very rare exception - pass the following tests and so are accepted as reliable (Table 1):

- (1) A well-defined high temperature age spectrum plateau is created by three or more concordant (within 2σ), contiguous steps representing at least 50% of the ^{39}Ar released.
- (2) A well defined isochron exists for the plateau points, i.e., the mean squared weighted deviations (MSWD) (the ratio between the scatter about the line and the extent to which the scatter can be explained by analytical uncertainty) are not greater than the cut-off value of 2.5 (following Brooks et al., 1972 and McIntyre et al., 1966).
- (3) The $^{40}\text{Ar}/^{36}\text{Ar}$ intercepts found by regression analysis are not significantly different from the atmospheric level of 295.5, i.e. the plateau and isochron ages are concordant.

3. Results

3.1 Migration of volcanism along the Foundation Chain

- The 1900 km distribution of dredge sample $^{40}\text{Ar}/^{39}\text{Ar}$ ages shows that volcanism has migrated along the Foundation Seamount Chain at a constant rate of 91 ± 2 mm/yr for at least the past 22 Myr (Fig. 3).

- The distribution of $^{40}\text{Ar}/^{39}\text{Ar}$ dated seamounts predicts that the present Foundation hotspot (or at least its easternmost extent) is presently located under, or at least very close to, the Pacific–Antarctic spreading-axis (Fig. 3).
- Comparison between seamount and seafloor ages reveals that the Foundation Chain erupted primarily in the interior of tectonic plates (Fig. 7). Thus, linear migration of intraplate volcanism along the Foundation Chain is compatible with Pacific plate drifting over a stationary mantle plume-hotspot (Morgan, 1971).
- Foundation $^{40}\text{Ar}/^{39}\text{Ar}$ ages (Table 1) indicate that Foundation seamounts and VERs developed in a series of discrete magmatic episodes at intervals of ~ 1 Myr (Fig. 3). This apparent periodicity might, however, be an artifact of dredge-sampling of late stage volcanism coating seamount/ridge flanks. Nevertheless, we believe it more likely that the isolated Foundation Chain seamounts or seamount clusters erupted relatively rapidly (~ 1 Myr) considering 1) that episodicity is evident in both seamounts and VERs and 2) the significantly lower volumes of magma in individual Foundation chain seamounts and ridges compared to chains of larger seamounts such as Hawaii known to span at least 5 Myr of magmatism (e.g., Clague & Dalrymple, 1989).

3.2 *Plume-spreading center/microplate interaction*

- Between ~ 22 Ma and ~ 15 Ma the Foundation Chain was forming on the Pacific plate west of the ‘Failed Rift’ of the Selkirk Microplate (Fig. 7). The age of Pacific seafloor migrating over the plume decreased systematically during this interval (~ 7.5 Ma to ~ 5.5 Ma) (O'Connor et al., 1998, 2002).
- This tectonic configuration changed when the ‘Failed Rift’ representing the western boundary of the microplate migrated over the plume at ~ 14 Ma (Fig. 7). The arrival of the ‘Failed Rift’ marked the onset of microplate migration over the hotspot, which continued until about 11 Ma.
- A $^{40}\text{Ar}/^{39}\text{Ar}$ age for a rock sample dredged from the ‘failed’ spreading center of the Selkirk Microplate (Mammerickx, 1992; Tebbens and Cande, 1997) showed that it jumped eastward (failed) at 20.4 ± 0.3 Ma (O'Connor et al., 2002) (Table 1). However, the spreading center north of the ‘failed rift’ likely continued spreading normally after microplate development such that much ‘younger’ seafloor was migrating over the northern flank of the Foundation hotspot (O'Connor et al., 2002) (Figs. 6 & 7).
- East of the Selkirk Microplate, seafloor migrating over the Foundation plume decreased systematically in age from 11 Ma to 0 Ma at the present day Pacific–Antarctic spreading-axis (Fig. 7).
- Systematic changes in the age (i.e., thickness, strength, temperature) of Pacific lithosphere migrating over the Foundation plume-hotspot have been occurring since the start of Foundation Chain creation (Fig. 7) as local spreading boundaries (responsible for the formation of the seafloor on which the Foundation chain was later erupted) have migrated systematically towards the Foundation plume (i.e., ~ 23 mm/yr and ~ 48 mm/yr west and east of the failed rift of the Selkirk microplate, respectively) (Mammerickx, 1992; O'Connor et al., 1998).

3.3 *Volcanic Elongate Ridges (VERs)*

- Individual VERs, as defined on the basis of structural morphology (i.e., volcanism along one continuous ridge), may occasionally develop synchronously (Fig. 4).

- However, the dominant trend is for structurally disconnected sections of VERs to be coeval (Figs. 4 & 5). These synchronously erupted, yet structurally unconnected VER sections define a series of *en echelon* elongate zones of coeval volcanism at different stages of Foundation Chain development (Figs. 5 & 6). Elongate zones maintained a steady state size (~250 km by ~150 km) and NE-SW orientation, developing at intervals of approximately 1 Myr (Fig. 5).
- Overall, VER volcanism generated during each successive episode or zone of coeval volcanism was emplaced progressively onto younger seafloor and closer to the Pacific-Antarctic spreading center as it migrated steadily nearer to the Foundation hotspot (Fig. 4).
- The main direction of the somewhat sinuous VERs changed progressively with time from NE, to E-W, and most recently to SE. This change in direction correlates well with the location of the nearest spreading center segment to the plume hotspot (Fig. 4).
- VER structures tend to develop predominantly along the northern and southern ends of the elongate *en echelon* 'zones'. This resulted in the apparent bifurcation of the Foundation Chain into distinct 'North' and 'South' lines of volcanism, a distinction that had disappeared by ~1 Ma (Fig. 5). The NE-SW orientation of these zones resulted in the northern region of each elongated zone of coeval volcanism being emplaced closer to the Pacific-Antarctic spreading center than the corresponding southern region, i.e., the 'South' line developed systematically in a more unambiguously intraplate setting compared to the 'North' line (Fig. 4).
- The oldest Foundation Chain VER is possibly a minor NE trending 7.7 ± 0.1 Myr old volcanic ridge (Fig. 5). Volcanism erupted next at 6.3 ± 0.2 Ma in the form of a single large intraplate seamount without any associated VER (Figs. 4 & 5).
- In contrast, a prominent, somewhat sinuous, coeval ~200 km long VER formed at 5.0 ± 0.1 Ma, trending NE from a cluster of coeval intraplate seamounts as far as the Pacific-Antarctic spreading center (Fig. 4). The point of intersection was both the closest spreading boundary segment, and the active tip of a propagating spreading axis segment (Lonsdale, 1994).
- By 3.5 ± 0.1 Ma scattered coeval Foundation Chain volcanism was being emplaced in a basically NE-SW elongate zone that was equidistant from all local spreading boundaries (Fig. 4). Although the individual VER segments defining this zone were orientated to the NE, toward the spreading center, no volcanic connection was established. Subsequent VER development involved eruption of structurally disconnected coeval VER segments defining elongate zones of hotspot volcanism located successively closer to the Pacific-Antarctic spreading center (Fig. 4). Although the NE-SW orientation of the elongate zones remained unchanged between ~3.5 Ma and the present, the overall orientation of individual VER segments changed from NE to SE (Fig. 5).
- The most recent Foundation Chain volcanism developed in the form of three SE-orientated parallel VERs extending almost as far as the present Pacific-Antarctic spreading center (Fig. 4). The approximate midpoints of these three VERs are coeval (i.e., 0.5 ± 0.1 Ma) and formed on ~0.5 Myr old seafloor (Fig. 4). The 0.7 ± 0.1 Ma sample dredged at the western end of the central ridge is similar in age (within analytical uncertainty) indicating that these three ridges are probably also rapidly formed coeval VERs.
- Ages for five samples dredged from the most western dredge site located along the 'South' line indicate at least three different phases of volcanism, i.e., 3.5 ± 0.1 Ma, 2.8 ± 0.1 Ma, and 0.7 ± 0.1 Ma (Fig. 4) (O'Connor et al., 2001).
- A broad swath of scattered, structurally disconnected coeval Foundation hotspot magmatism was emplaced at ~17 Ma west of the Selkirk Microplate (Fig. 6).

4. Discussion

4.1 VERs and the Pacific-Antarctic spreading center

The main process responsible for VER development is continuation of the 91 ± 2 mm/yr lithospheric plate migration over the Foundation plume hotspot that began at least 22 Myr ago. We base this conclusion on the persistence during VER development of the linear trend of decreasing Foundation Chain age (O'Connor et al., 1998), their development in an intraplate setting (O'Connor et al., 1998), and hotspot-influenced geochemistry (Devey et al., 1997; Hekinian et al., 1997; Hekinian et al., 1999; Hemond & Devey, 1997; Hemond et al., 1999). However, other, second order processes are likely to have controlled the onset and development of the Foundation VERs. The most obvious notion is interaction between the Foundation plume hotspot and the Pacific-Antarctic spreading center (Devey et al., 1997; Hekinian et al., 1997; Hekinian et al., 1999; O'Connor et al., 1998; Maia et al., 2000; Hemond & Devey, 1996; Hemond et al., 1999).

Due to the long-standing Pacific-Antarctic spreading center migration toward the Foundation plume-hotspot, lithosphere migrating toward/over the plume-hotspot eventually became sufficiently young/thin/weak/hot to trigger the onset of VER development (e.g., O'Connor et al., 1998). The most unequivocal evidence is the synchronously developed ~200 km long NE-orientated 5 Myr old VER connecting Foundation intraplate volcanism with the Pacific-Antarctic spreading center (Fig. 4). This provides strong evidence that individual VERs can occasionally form synchronously (i.e., as lines of continuous volcanism) connecting intraplate volcanism with the Pacific-Antarctic spreading center. The correlation between changes in VER orientation and the minimum distance to the Pacific-Antarctic spreading center further supports plume-spreading center interaction (Fig. 4). Models envisioning plume-spreading center interaction in terms of sub-lithospheric channeling of plume material towards spreading centers (Schilling, 1985; Schilling et al., 1985, 1991) can draw support from these results.

However, other more dominant trends in VER chronology cannot be explained by current models of plume-spreading center interaction. The most prominent such trend is for coeval hotspot volcanism to erupt in a series of NE-SW elongate 'zones' cross-cutting the main NW-SE trend of the 22 Myr old Foundation Chain (O'Connor et al., 2001) (Fig. 5). The transition from isolated seamount chain to NE-SW elongate 'zones' of VER hotspot volcanism is marked by broadening of the Foundation Chain, *en echelon* VER distribution, and the significantly greater scatter of VER ages about the overall linear trend of decreasing Foundation Chain age. These zones are considerably larger in scale than individual VERs and maintained a steady state orientation and size, despite the fact that the Pacific-Antarctic spreading center was migrating progressively closer to the plume hotspot.

VER volcanism developed preferentially along the north and south sides of these elongate zones leading to the bifurcation of the Foundation Chain into seemingly continuous 'North' and 'South' lines of volcanism. Other such chains near to the East Pacific Rise have been attributed to thinner lithosphere and a more coherent stress field near spreading centers (Hieronymus & Bercovici, 2000). Straight and long lines of seamounts (e.g., 'North' and 'South' lines) might therefore be similarly explained by a strong and coherent near spreading center stress field with control of their alignments attributed to the direction of the most tensile principal tectonic stress (Hieronymus & Bercovici, 2000). Furthermore, control of the volume and location of intraplate volcanism by stress in the lithosphere has been shown in the case of the Ngatamoto Seamounts (McNutt et al., 1997). Compared to the 'South' line, the 'North' line has ~2-3 times greater seamount volume (Maia et al., 2001), a greater number of individual VERs showing more

pronounced changes in orientation (i.e., NE to SE), and possibly a less pronounced hotspot-like geochemistry (e.g., Hemond et al., 1999). These and other such compositional differences noted in Maia et al. (2001) can be explained therefore by the greater proximity of the 'North' line to the Pacific-Antarctic spreading center resulting in greater partial melting, more dilution of the plume geochemical signature, and greater perturbations to local stress control due to transform faults, overlapping spreading centers and propagators (Hieronymus & Bercovici, 2000). Thus, the pronounced shift 1 Myr ago from distinct 'North' and 'South' lines to an elongate zone of significantly more continuous volcanism can be explained by thinning/weakening of the lithosphere together with enhanced interaction between the Foundation plume hotspot and the encroaching Pacific-Antarctic spreading center. We infer further support for this notion from the three parallel, SE-orientated VERs that apparently developed synchronously at 0.5 ± 0.1 Ma between the 1 Myr old elongate 'zone' and the present Pacific-Antarctic spreading center (Fig. 4).

The second important trend in our age data not explicable by current VER and plume-spreading interaction models is the interval of approximately 1 Myr between development of successive elongate zones of hotspot volcanism (O'Connor et al., 2001). This trend has also been detected in measured ages for the Foundation seamounts, irrespective of tectonic setting (O'Connor et al., 1998). Persistence of this trend during transition in morphology from isolated seamounts to VERs suggests that it is an intrinsic characteristic of the Foundation hotspot and/or its hypothesized causal mantle plume. The ~3 Myr of volcanic activity at one dredge site can be explained by, for example, rejuvenation of the Foundation Chain triggered by local lithospheric weaknesses associated with the earlier loading of the Foundation Chain (McNutt et al., 1997). However, it could also point to a significantly greater (i.e., >300 km) distribution of Foundation plume material west of the Pacific-Antarctic spreading center than indicated by the inferred ~150 km wide elongated zones of hotspot volcanism. We speculate that this could reflect the second order flow of plume material under the lithosphere away from the elongate hotspot zones (e.g., Maia et al., 2000).

4.2 Foundation VERs and the Selkirk Microplate

A broad swath of ~17 Myr old scattered, structurally disconnected coeval Foundation seamounts and VERs was emplaced west of the Selkirk Microplate (Fig. 6) (O'Connor et al., 2002). This 'zone' is comparable in scale to the series of similarly sized elongate (~250 km by ~150 km) swaths of disconnected coeval hotspot volcanism created since at least 5 Ma at the young end of the chain (Fig. 5) (O'Connor et al., 2001). However, once the Selkirk Microplate began migrating over the Foundation hotspot at ~14 Ma, the Foundation Chain abruptly started forming as a narrow line of seamounts (O'Connor et al., 1998). We attribute this switch in morphology to differences in the age, and thus physical properties of the lithosphere migrating across the inferred broad Foundation hotspot 'zone'. A $^{40}\text{Ar}/^{39}\text{Ar}$ age for the 'failed rift' bounding the Selkirk Microplate to the west (Mammerickx, 1992; Tebbens and Cande, 1997) showed that it jumped eastward at 20.4 ± 0.3 Ma (O'Connor et al., 2002) (Fig. 6). This jump created a large offset in the age of the seafloor that subsequently migrated over the Foundation hotspot resulting in old/thick microplate (transferred Nazca plate) migrating over most of the hotspot and younger/thinner ('unmigrated') seafloor (≤ 6 Myr) across the northern flank (Fig. 6). We also consider it possible that younger/thinner seafloor flanking the hotspot to the north was thermally reset to younger ages due to preferential channeling of plume material (e.g., Morgan, 1978; Schilling et al., 1985; Schilling, 1985, 1991) to the much nearer 'unmigrated' younger spreading center. Hotspot magmatism between ~14 Ma and ~11 Ma was therefore likely restricted to a narrow region along the northern boundary of the Selkirk Microplate (Figs. 6 & 7).

Once the old/thick microplate lithosphere had drifted past the hotspot it was followed by seafloor formed at the spreading center segment that ‘jumped’ eastward at ~20 Ma to create the Selkirk Microplate (Fig. 7). This lithosphere was again too old/thick to allow passage of significant amounts of hotspot melt (Fig. 7). Nonetheless, narrow chain development continued because younger (‘unmigrated’) seafloor was migrating over the northern regions of the hotspot. This situation persisted until ~5 Ma when the Pacific-Antarctic spreading center had migrated sufficiently close such that younger/thinner lithosphere (≤ 6 Ma) reached the hotspot, so facilitating the onset of VER development/broadening of the Foundation Chain (Fig. 7). Thus, we explain broadening and narrowing of the Foundation Chain since at least 22 Ma in terms of the age, and consequently thickness and strength, of the seafloor migrating over the Foundation plume acting as a threshold parameter controlling the mode of hotspot volcanism.

4.3 Pacific plate motion

A linear velocity of 91 ± 2 mm/yr for plate motion over the Foundation mantle plume agrees with that predicted by selected Euler poles for Pacific plate motion over fixed hotspots (O’Connor et al., 1998; Koppers et al., 2001) (Figs. 3 & 6). The fact that single reconstruction poles can predict the plate velocities (and azimuths) derived from measured ages distributed along the Hawaiian and Foundation chains adds confidence to the assumption of fixed plume-hotspots (at least for the last 22 Myr of Pacific plate motion in the case of Hawaiian and Foundation).

Furthermore, if the previously proposed relationship between the Foundation plume and older Ngatamato Chain Seamounts (McNutt et al., 1997; O’Connor et al., 1998) is correct (Fig. 1), then the Foundation plume was active for at least the past ~34 Myr. Assuming that the stationary Foundation plume-hotspot is responsible for the formation of the Ngatamato–Foundation Chains, and that the plume has indeed been active for the last ~34 Ma, then the question arises as to why a more continuous chain of ~3000 km was not created? As in the case of the Foundation Chain, the lack of significant hotspot volcanism between the Foundation Chain and the Ngatamato and Taukina Seamounts (McNutt et al., 1997; Maia et al., 2001) can be explained by migration of seafloor that was too old and consequently too thick and strong (≥ 6 Myr in the case of the Foundation plume) to allow Foundation plume-hotspot magma to reach the lithospheric surface.

4.4 Implications for plume-hotspot theory

Key observations that need to be reconciled with standard plume-hotspot theory are 1) broadening and narrowing of the Foundation chain due to 2) the appearance and disappearance, respectively, of broad elongate ‘zones’ of scattered coeval volcanism, and 3) persistence of ~1 Myr episodicity/periodicity of Foundation Chain volcanism - irrespective of tectonic setting or chain mode of volcanism (VER or seamount). We propose that these observations are related primarily to the long-term dynamics of the Foundation plume for at least 22 Myr and possibly 34 Myr. In contrast, localized distribution of volcanism across each ‘zone’ linked to an ‘event’ or ‘pulse’ was controlled by localized factors as lithospheric age and stress (e.g., McNutt et al., 1997; Hieronymus and Bercovici, 2000; Maia et al., 2001; O’Connor et al., 2001, 2002). Likewise, involvement of pre-existing lithospheric structures acting as ‘weak zones’ facilitating decompression melting of hot plume material is strongly indicated by the fact that volcanic lineaments south of the Foundation Chain - e.g., Del Cano Lineament - parallel the local fracture zone direction (Fig. 6).

A physical process is therefore required that episodically/periodically brings masses of hot plume material extremely fast from depth and is capable of focusing it into broadly elongate

zones (~250 km by ~150 km) - at least on initial impact against the base of the drifting Pacific plate. Depth-dependent properties have been shown theoretically to play an important role in controlling plume dynamics (Hansen et al., 1993). For example 'ultrafast' focused mantle plumes are theoretically possible in the upper mantle during thermal convection with a non-Newtonian temperature- and depth-dependent rheology operating at a reasonable effective Rayleigh number on the order of 10^6 (Larsen and Yuen, 1997; Larsen et al., 1999). Such strong depth-dependence in viscosity also results in masses of plume material pulsing at intervals ranging from a few Myr (Larsen et al., 1999) to about 10 Myr (Larsen and Yuen, 1997) with calm periods in between (Larsen et al., 1999). These current models indicate that plumes can rise through the upper mantle in much less than one Myr (e.g., Larsen et al., 1999), so providing a mechanism by which hot plume material can be brought from the transition zone to the lithosphere extremely fast (m/yr) in an otherwise slowly convecting mantle (cm/yr). Following impact against the base of the lithosphere this material can flow laterally at rates as high as ~ 0.5 m/yr, so creating the potential of coeval magmatism scattered over large areas (Larsen and Yuen, 1997; Sleep, 1997; Larsen and Saunders, 1998; Larsen et al., 1999).

Thus, our observations about the temporal-spatial development of the Foundation Chain are compatible with non-Newtonian plume theory and indicate, furthermore, that SE Pacific mantle plumes are more tightly focused and faster-pulsing than incorporated presently into numerical models. This points in turn to even greater viscosity stratification (or changes in the creep law) across the upper mantle compared to, for example, the region of the North Atlantic influenced by the Iceland plume (Larsen et al., 1999; O'Connor et al., 2000).

5. Conclusions

Linear migration of intraplate - often geochemically enriched - volcanism at a rate of 91 ± 2 mm/yr along the Foundation Chain for at least the past 22 Myr is compatible with drifting of the Pacific plate over a narrow, stationary plume of hot mantle material upwelling from depth. Due to the isolated nature of the relatively small, likely rapidly created Foundation Chain seamounts, we have been able to distinguish second-order volcanism (using high precision ages) from that created via the first-order influence of a narrow, stationary Foundation mantle plume upwelling from depth under the drifting Pacific plate. Therefore, despite changes in morphology and geochemistry, the migration of volcanism along the Foundation Chain can be interpreted as a record of the absolute motion path of the Pacific plate (except for three seamount ages close to the outer edges of the Selkirk microplate - discussed in O'Connor et al., 1998). Similarity between rates of propagation of volcanism along the Hawaiian and Foundation chains supports a stationary Foundation versus Hawaiian mantle plume, at least for the past 22 Myr. On a more localized scale, the Foundation Chain developed as a line of relatively small, rapidly erupted (~1 Myr) individual seamounts or clusters at a rate of approximately one every Myr.

The transition from a narrow line of seamounts to a broad region of volcanic elongate ridges (VERs) about 5 Myr ago was assumed initially to be the result of interaction between the Foundation plume and the encroaching Pacific-Antarctic spreading-center. Some of our data support this notion by showing that volcanism along morphologically distinct VERs can develop occasionally as rapidly formed continuous lines of coeval volcanism extending from a region of intraplate volcanism to the Pacific-Antarctic spreading center. However, a significantly more dominant trend is for coeval, yet structurally disconnected, segments of Foundation Chain VERs to develop in a series of *en echelon*, NE-SW elongate 'zones' of coeval hotspot volcanism. These elongate zones developed at intervals of approximately 1 Myr while maintaining a basically

steady state orientation and size as the Pacific-Antarctic spreading center migrated continually closer to the Foundation plume hotspot.

Our age data indicate that Foundation Chain development between ~22 Ma and ~14 Ma was also in the form of broad zones of scattered, synchronous Foundation volcanism - very similar to those identified west of the present Pacific-Antarctic spreading center. But once the significantly older Selkirk Microplate lithosphere (Tebbens & Cande, 1997) began capping the plume hotspot about 14 Myr ago, the Foundation Chain narrowed into a line of discrete seamounts, only broadening again about 5 Myr ago when sufficiently young lithosphere drifted once again over the plume hotspot. Thus, Foundation hotspot volcanism can be prevented if the capping tectonic plate is too thick (≥ 6 Myr in the case of Foundation) for plume-hotspot melts to penetrate to the surface (O'Connor et al., 1998, 2001, 2002). The lack of a seamount chain connecting the Foundation and the Ngatamoto chains (McNutt et al., 1997) can be similarly explained, so supporting the notion that the Pacific plate has drifted a distance of at least 3400 km over a Foundation plume-hotspot during the last ~34 Myr.

Creation of broad zones of synchronous Foundation magmatism at regular ~1 Myr intervals leads us - in combination with recent numerical plume modeling (e.g., Larsen and Yuen, 1997; Larsen et al., 1999) - to propose that the Foundation Chain is the product of a stationary plume pulsing hot masses against the base of the Pacific plate from depth with an apparent periodicity of once per Myr (O'Connor et al., 2002). Assuming the validity of the hypothesis of deep mantle plumes (Morgan, 1971), our model for Foundation Chain development has implications for future investigations of Pacific midplate volcanism. We propose that plume-hotspots such as Foundation, spreading on impact with the lithosphere, influence very wide areas such that apparently unconnected hotspot volcanism can be produced simultaneously across wide swaths, often crosscutting seamount chains. Thus, variations in the age, structure and stress patterns of tectonic plates drifting over (pulsing) mantle plumes might control if, where and how hotspot volcanism develops on the Pacific plate. This modified plume-hotspot theory might also explain widespread scattered midplate volcanism (e.g., VERs) revealed by satellite altimetry mapping and also randomly distributed reheating events warming and raising Pacific lithosphere (Smith and Sandwell, 1997) - given that many other mantle plumes are similarly pulsing large masses of hot plume material (not necessarily with the same periodicity or mass) into broad regions impacting the base of the Pacific lithosphere.

Acknowledgements

We thank Captains H. Andresen and J.-C. Gourmelon and crews of the *F.S Sonne* and N/O *Atalante* and the '*SO100*' and '*Hotline*' scientific parties for unstinting efforts in making our dredge-sampling programs so successful. A. Koppers developed the freeware ArArCALC for blank handling and isochron and plateau calculations (Koppers, 2002). This work was supported by BMBF projects 03G0100A, 03G0100A0 and 03G0157A. The '*Hotline*' cruise was supported by INSU-CNRS. NSG contribution 2003xxxx.

References

- Brooks C, Hart SR, Wendt I (1972) Realistic use of two-error regression treatments as applied to rubidium–strontium data. *Rev. Geophys. Space Phys.* 10:551–557.
- Cande SC, Kent DV (1995) Revised calibration of the geomagnetic polarity time scale for the Late Cretaceous and Cenozoic. *J. Geophys. Res.* 100: 6093–6095.
- Clague DA, Dalrymple GB (1989) Tectonics, geochronology and origin of the Hawaiian–Emperor volcanic chain. In: Winterer EL, Hussong DM, Decker RW (Eds.), *The Geology of North America. Vol. N, The Eastern Pacific Ocean and Hawaii*. Geol. Soc. Am., Boulder 188–217.
- Dalrymple GB, Lanphere MA (1969) Potassium Argon Dating. W.H. Freeman Co., San Francisco.
- Dalrymple GB, Lanphere MA, Clague DA (1980) Conventional and $^{40}\text{Ar}/^{39}\text{Ar}$ ages of volcanic rocks from Ojin (Site 430), Nintoku (Site 432), and Suiko (Site 433) Seamounts and the chronology of volcanic propagation along the Hawaiian–Emperor chain. *Init. Rep. Deep Sea Drill. Proj.* 55:659–676.
- Dalrymple GB, Alexander Jr. EC, Lanphere MA, Kraker, GP (1981) Irradiation of samples for $^{40}\text{Ar}/^{39}\text{Ar}$ dating using the Geological Survey TRIGA reactor. *U.S. Geol. Surv. Prof. Pap.*, 1176.
- Devey CW and the SO100 scientific party (1995) The Foundation Seamount Chain. *Cruise Rep. 75*, Geol. Pal. Inst., University of Kiel, 123 pp.
- Devey CW, Hekinian R, Ackermant D, Binard N, Francke B, Hemond C, Kapsimalis V, Lorenc S, Maia M, Möller H, Perot, K, Pracht, J, Rogers T, Statterger K, Steinke, S, Victor, P (1997) The Foundation Seamount Chain: A first survey and sampling. *Mar. Geol.* 137:191–200.
- Faure G (1986) *Principles of Isotope Geology*. 2nd ed., Wiley, New York.
- Fleck RJ, Sutter JF, Elliot DH (1977) Interpretation of discordant $^{40}\text{Ar}/^{39}\text{Ar}$ age spectra of Mesozoic tholeiites from Antarctica. *Geochim. Cosmochim. Acta* 41:15–32.
- Hansen U, Yuen DA, Kroening SE, Larsen TB (1993) Dynamical consequences of depth-dependent thermal expansivity and viscosity on mantle circulation and thermal structure. *Phys. Earth Planet. Inter.* 77:205–223.
- Hekinian R, Stoffers P, Devey CW, Ackermant D, Hemond C, O'Connor JM, Binard N, Maia M (1997) Intraplate versus oceanic ridge volcanism on the Pacific Antarctic ridge near 37°S–111°W. *J. Geophys. Res.* 102:12265–12286.
- Hekinian R, Stoffers P, Ackermant D, Revillon S, Maia M, Bohn M (1999) Ridge-hotspot interaction: The Pacific-Antarctic Ridge and the Foundation Seamounts. *Mar. Geol.* 160:199–223.
- Hemond C, Devey CW (1996) The Foundation Seamount Chain, Southeastern Pacific: First isotopic evidence of a newly discovered hotspot track. *V.M. Goldschmidt Conf. J. Conf. Abstr.*, p. 255.
- Hemond C, Maia M, Gente P (1999) The Foundation Seamounts: Past and present ridge hotspot interactions? *EOS Trans. Am. Geophys. Union* 80:1056.
- Herron EM (1972) Sea-floor spreading and the Cenozoic history of the east–central Pacific. *Geol. Soc. Am. Bull.* 83:1671–1692.
- Hieronimus CF, Bercovici D (2000) Non-hotspot formation of volcanic chains: Control of tectonic and flexural stresses on magma transport. *Earth. Planet. Sci. Lett.* 181:539–554.
- Koppers AAP (1998) $^{40}\text{Ar}/^{39}\text{Ar}$ Geochronology and Isotope Geochemistry of the West Pacific Seamount Province: Implications for Absolute Pacific Plate Motions and the Motion of Hotspots. Ph.D thesis, Vrije Universiteit, Amsterdam.
- Koppers AAP, Phipps Morgan J, Morgan JW, Staudigel H (2001) Testing the fixed hotspot hypothesis using $^{40}\text{Ar}/^{39}\text{Ar}$ age progressions along seamount trails. *Earth Planet Sci. Lett.* 185:237–252.
- Kuiper K (2003) Ph.D thesis in prep, Vrije Universiteit, Amsterdam.
- Koppers AAP (2002) ArArCALC—software for $^{40}\text{Ar}/^{39}\text{Ar}$ age calculations. *Computers & Geosciences* 5:605–619.
- Kullerud L (1991) On the calculation of isochrons. *Chem. Geol.* 87:115–124.
- Lanphere MA, Dalrymple GB (1978) The use of $^{40}\text{Ar}/^{39}\text{Ar}$ data in evaluation of disturbed K–Ar systems. *Short Papers 4th Int. Conf. Geochronol. Cosmochronol. Isot. Geol.* 78-701:241–243.
- Larsen HC, Saunders AD (1998) Tectonism and volcanism at the southeast Greenland rifted margin: A record of plume impact and later continental rupture. *Proc. ODP Sci. Res.* 152:503–533.
- Larsen TB, Yuen DA (1997) Ultrafast upwelling bursting through the upper mantle. *Earth Planet. Sci. Lett.* 146:393–399.
- Larsen TB, Yuen DA, Storey M (1999) Ultrafast mantle plumes and implication for flood basalt volcanism in the Northern Atlantic Region. *Tectonophysics* 311:31–43.
- Lonsdale P (1988) Geography and history of the Louisville hotspot chain in the southwest Pacific. *J. Geophys. Res.* 93:3078–3104.
- Lonsdale P (1994) Geomorphology and structural segmentation of the crest of the southern (Pacific–Antarctic) East Pacific Rise. *J. Geophys. Res.* 99:4683–4702.
- Maia M, et al. (2000) The Pacific–Antarctic Ridge–Foundation hotspot interaction a case study of a ridge approaching a hotspot. *Mar. Geol.* 167:61–84.
- Maia M, Hemond C, Gente P (2001) Contrasted interactions between plume, upper mantle and lithosphere: Foundation chain case. *Geochem. Geophys. Geosyst.* 1:2000GC000117.
- Mammerickx J (1992) The Foundation seamounts: tectonic setting of a newly discovered seamount chain in the South Pacific. *Earth Planet. Sci. Lett.* 113:293–306.
- Mayes CL, Lawyer LA, Sandwell DT (1990) Tectonic history and new isochron chart of the South Pacific. *J. Geophys. Res.* 95:8543–8567.
- McDougall I, Harrison TM (1999) *Geochronology and Thermochronology by the $^{40}\text{Ar}/^{39}\text{Ar}$ Method*. University Press, Oxford.

- McIntyre GA, Brooks C, Compston W, Turek A (1966) The statistical assessment of Rb–Sr isochrons. *J. Geophys. Res.* 71:5459–5468.
- McNutt MK, Caress DW, Reynolds J, Jordahl KA, Duncan RA (1997) Failure of plume theory to explain the southern Austral Islands. *Nature* 389:479–482.
- Morgan WJ (1971) Convection plumes in the lower mantle. *Nature* 230:42–43.
- Morgan WJ (1978) Rodriguez, Darwin, Amsterdam, A second type of hotspot island. *J. Geophys. Res.* 83:5355–5360.
- O'Connor JM, Stoffers P, Wijbrans JR (1998) Migration rate of volcanism along the Foundation Chain, SE Pacific. *Earth Planet Sci. Lett.* 164:41–59.
- O'Connor JM, Stoffers P, Wijbrans JR (2000) Evidence from episodic seamount volcanism for pulsing of the Iceland plume in the past 70 Myr. *Nature* 408:954–958.
- O'Connor JM, Stoffers P, Wijbrans JR (2001) En Echelon volcanic elongate ridges connecting intraplate Foundation Chain volcanism to the Pacific–Antarctic spreading center. *Earth Planet Sci. Lett.* 192:633–648.
- O'Connor JM, Stoffers P, Wijbrans JR (2002) Pulsing of a focused mantle plume *Geophys. Res. Lett.* 29:10.1029/2002GL014681.
- Pringle MS (1993) Age progressive volcanism in the Musicians Seamounts: A test of the hot spot hypothesis for the Late Cretaceous. In: Pringle MS, Sager WW, Sliter WV, Stein S (Eds.), *The Mesozoic Pacific: Geology, Tectonics, and Volcanism*, *Geophys. Monogr. Series*, 77:187–215.
- Renne PR, Swisher CC, Kamber DB, Owens TL, de Paulo DJ (1998) Intercalibration of standards, absolute ages and uncertainties in $^{40}\text{Ar}/^{39}\text{Ar}$ dating. *Chem. Geol.* 145:117–152.
- Roddick JC (1978) The application of isochron diagrams in ^{40}Ar – ^{39}Ar dating: A discussion. *Earth Planet. Sci. Lett.* 41:233–244.
- Sandwell DT (1984) A detailed view of the South Pacific geoid from satellite altimetry. *J. Geophys. Res.* 89:1089–1104.
- Schilling J-G, Thompson G, Kingsley R, Humphris S (1985) Hotspot-migrating ridge interaction in the South Atlantic. *Nature* 313:187–191.
- Schilling J-G (1985) Upper mantle heterogeneities and dynamics. *Nature*, 314, 62–67, 1985.
- Schilling J-G (1991) Fluxes and excess temperatures of mantle plumes inferred from their interaction with migrating mid-ocean ridges. *Nature* 352:397–403.
- Sleep NH (1997) Lateral flow and ponding of starting plume material. *J. Geophys. Res.* 102:10,001–10,012.
- Smith WHF, Sandwell DT (1994) Bathymetric prediction from dense satellite altimetry and sparse shipboard bathymetry. *J. Geophys. Res.* 99:21803–21824.
- Smith WHF, Sandwell DT (1997) Global Sea Floor Topography from Satellite Altimetry and Ship Depth Soundings. *Science* 277:1956–1962.
- Tebbens SF, Cande SC (1997) Southeast Pacific tectonic evolution from early Oligocene to present. *J. Geophys. Res.* 102:12061–12084.
- Tebbens SF, Cande SC, Kovacs L, Parra JC, LaBrecque JL, Vergara H. (1997) The Chile Ridge: A tectonic framework. *J. Geophys. Res.* 102:12035–12059.
- Wijbrans JR, Pringle MS, Koppers AAP, Scheveers R (1995) Argon geochronology of small samples using the Vulkan argon laserprobe. *Proc. Kon. Ned. Akad. Wet.* 98:185–218.
- York D (1969) Least-squares fitting of a straight line with correlated errors. *Earth Planet. Sci. Lett.* 5:320–324.
- York D, Hall CM, Yanase Y, Hanes JA, Kenyon WJ (1981) Laser-probe $^{40}\text{Ar}/^{39}\text{Ar}$ dating of terrestrial minerals with a continuous laser. *Geophys. Res. Lett.* 8:1136–1136.
- York D (1984) Cooling histories from $^{40}\text{Ar}/^{39}\text{Ar}$ age spectra: Implications for Precambrian plate tectonics. *Annu. Rev. Earth Planet. Sci.* 12:383–409.

Figure Legends

Figure 1. Predicted topography (Smith and Sandwell, 1997) of SE Pacific seafloor showing the location of the Foundation Chain. MP = microplate; JF = Juan Fernandez; EPR = East Pacific Rise

Figure 2. Predicted topography of the Foundation Chain (Smith and Sandwell, 1997). *F. S. Sonne* and *N/O Atalante* dredge sites are indicated by black rimmed white dots. $^{40}\text{Ar}/^{39}\text{Ar}$ ages are summarized in Table 1, details of sample information and analytical date are in (O'Connor et al., 1998, 2001, 2002). IPF = inner pseudo fault and FR = failed rift of Selkirk microplate (Mammerickx, 1992).

Figure 3. (a) Sample age as a function of distance of dredge site from the present Pacific-Antarctic spreading center. The solid line is the York-2 linear regression to age data representing an average rate migration rate of volcanism along the Foundation chain of 91 ± 2 mm/yr (O'Connor et al., 1998). Ages reported in O'Connor et al., 1998 have been recalculated (O'Connor et al., 2001) using the new TCR monitor age (28.34 Ma; Renne et al., 1998). This recalculation leads to a small systematic increase in previously calculated ages leaving the calculated migration rate reported in O'Connor et al., 1998 unchanged. Analytical error bars ($\pm 2\sigma$) are shown.

(b) Seafloor age (Lonsdale, 1994) as a function of distance from the present day Pacific-Antarctic spreading center (dashed line). Gray shaded horizontal lines indicate individual episodes of coeval VER volcanism.

(c) Solid spheres show correlation between weighted averages of measured Foundation Chain $^{40}\text{Ar}/^{39}\text{Ar}$ ages (Table 1) and corresponding ages predicted on the basis of an assumed periodicity of once per Myr. A perfect correlation between measured and predicted ages assuming a periodicity of 1 Myr is shown as a regression line with individual episodes indicated by short cross-cutting lines. Cumulative probability plotting of Foundation ages (e.g., Table 1) further supports this inferred ~1 Myr periodicity.

Figure 4. Schematic reconstructions of the temporal and spatial relationship between the Foundation Chain and approaching Pacific-Antarctic spreading center (O'Connor et al., 2001). Bathymetry is interpolated from predicted topography of the Foundation Chain region (Smith and Sandwell, 1997). The enlargement of the spreading center region (e) incorporates Hydrosweep data collected during the SO100 cruise of the *F.S. Sonne* (Devey et al., 1997). Measured $^{40}\text{Ar}/^{39}\text{Ar}$ ages (Table 1) are in bold. Seafloor ages and interpolated FZs (solid dashed lines) are from (Lonsdale, 1994), following the timescale of (Cande and Kent, 1995). c=seafloor isochron; # =seamount number; X=dredge site.

Figure 5. (a) Predicted topography of the Foundation Chain region (Smith and Sandwell, 1997). Solid circles show locations of '*SO100*' (Devey et al., 1997) or '*Hotline*' (Maia et al., 2001) cruise dredge sites for which $^{40}\text{Ar}/^{39}\text{Ar}$ ages have been determined. 'North' and 'South' lines indicate the apparent bifurcation of the Foundation Chain. Box labeled 7.7 Ma shows a cluster of coeval seamounts (the most western seamount in this cluster is not shown) that might be linked to the development of the oldest Pacific-Antarctic Foundation VER (indicated by a question mark). PAC-ANT = Pacific-Antarctic spreading center.

(b) Shaded multibeam bathymetry of the Foundation Chain VERs (Maia et al., 2000, 2001). Dashed lines outline inferred *en echelon* NE-SW elongate 'zones' of coevally erupted VER volcanism. The weighted average of all ages measured for samples recovered from within each 'zone' (Table 2) is shown. Plus symbol denotes point on Pacific-Antarctic spreading center ($37^\circ 45' \text{ S}$; $111^\circ 7.5' \text{ W}$) from which sample site distances along the Foundation Chain (Figs. 3 & 7) have been calculated.

Figure 6. Dark red zone labeled '17 Ma hotspot zone' indicates the broad swath of scattered, structurally disconnected coeval Foundation hotspot magmatism produced during the ~17 Ma event/pulse of the Foundation mantle plume. Seafloor east of this ~17 Ma inferred hotspot zone/event/pulse labeled 'migrated' became significantly older at 20 Ma (Table 1) when the Selkirk Microplate was created by the transfer of a segment of the Nazca plate by an eastward spreading center jump (failure) and initiation of a 'new rift' (Mammerickx, 1992; Tebbens and Cande, 1997; O'Connor et al., 2002). The location of the hotspot during this 20 Ma event is indicated by light red zone. Seafloor labeled younger 'unmigrated' to the north of the Selkirk Microplate is significantly

younger than the Selkirk Microplate because it was produced by continuous uninterrupted spreading at an unmigrated segment of the spreading axis north of the 'Failed Rift' (Fig. 7). Variability in age of lithosphere drifting over, or close to, the Foundation plume resulting from microplate creation is shown in Fig. 7. Age data for dredge sites indicated by solid dots and open circles are in O'Connor et al., 2002 and 1998, respectively. Measured ages are shown below dredge sample numbers. FSC = Foundation Seamount Chain; IPF= Inner Pseudo Fault; FZ = Fracture Zone; bold blue lines = Failed Rift and IPF.

Figure 7. (a). $^{40}\text{Ar}/^{39}\text{Ar}$ and 'migrated' seafloor age as a function of distance from the present Pacific-Antarctic spreading center. The solid red line is the York-2 linear regression fit representing an average rate for the migration of volcanism along the chain of 91 ± 2 mm/yr (Fig. 3). As the Selkirk Microplate reached the active hotspot region at about 14 Ma, much older seafloor (≥ 6 Myr) began to cap the Foundation plume. This 'older'/'migrated' seafloor placed a sufficiently thick/strong lid over most of the region impacted by pulsed plume material to prevent the migration of plume melts to the seafloor during the interval ~14 Ma to ~11 Ma resulting in the transition from broad zones of hotspot volcanism to a narrow chain of seamounts. Blue solid lines denote 'older' seafloor, unbroken blue lines indicate known seafloor ages (Mammerickx, 1992; Lonsdale, 1994), and dashed blue line indicates extrapolated seafloor ages. The red swath indicates the broad zone of scattered coeval hotspot volcanism (open spheres) created by the proposed 17 Ma pulse of the Foundation plume crosscutting the narrow Foundation Chain - as revealed by predicted topography maps (Fig. 2). Analytical error bars are $\pm 2\sigma$.

(b) 'Migrated' seafloor age as a function of distance from the present Pacific-Antarctic spreading center – other details are the same as in (a). Long green dashed line indicates younger, 'unmigrated' seafloor created by the spreading center north of the 'Failed Rift' (extrapolation of known seafloor ages west of the Selkirk Microplate). The spreading center north of the 'Failed Rift' likely continued spreading normally such that 'younger' (≤ 6 Myr) seafloor was migrating over the northern flank of the Foundation plume. This younger, 'unmigrated' seafloor drifting by the northern flank of the Foundation plume was sufficiently thin to allow the passage of plume melts along a narrow strip leading to creation of a correspondingly narrow chain of Foundation seamounts.

Table 1. ^a Summary of Foundation Chain ⁴⁰Ar/³⁹Ar age data

Sample ID	^b Smt. number	^c Smt. name	Latitude °S	Longitude °W	Sample	Type	% ³⁹ Ar	Plateau (Ma)	2σ	Inverse Isochron (Ma)	2σ
<i>SO100 11DS-1</i>	<i>1a</i>	<i>Ampère</i>	32° 56.414' 32° 55.453'	130° 45.459' 130° 45.982'	wr	IH	64.4	21.6	0.2	21.7	1.1
<i>FH DR1-3</i>		<i>Aristotelis</i>	32° 30.33'	127° 30.09'	wr	IH	66.7	18.5	0.3	18.4	0.4
<i>SO100 18DS-1</i>	<i>5</i>	<i>Becquerel</i>	32° 28.871' 32° 28.870'	126° 00.456' 126° 00.981'	wr	IH	67.2	16.6	0.4	16.6	0.4
<i>SO100 17DS-1</i>	<i>5</i>	<i>Becquerel</i>	32° 28.474' 32° 28.403'	126° 04.069' 126° 04.086'	wr	IH	42.2	16.3	0.3		
Weighted Average								16.4	0.2		
<i>FH DR4-1</i>	<i>Del Cano</i>		33° 46.69'	126° 43.83'	wr	IH	44.5	16.1	0.4	16.3	0.7
<i>FH DR5-2</i>	<i>VER</i>	<i>Boltzmann</i>	34° 55.112'	126° 13.798'	wr	IH	99.7	16.8	0.3	16.6	1.0
<i>FH DR6-1</i>	<i>VER</i>	<i>Laplace</i>	34° 34.000'	125° 16.400'	wr	IH	32.3	16.6	0.2	16.1	0.6
<i>FH DR7-16</i>	<i>Failed Rift</i>		35° 20.849'	124° 45.723'	wr	SFs	100	20.4	0.4	19.5	3.7
<i>FH DR7-16</i>	<i>Failed Rift</i>		35° 20.849'	124° 45.723'	wr	IH	22.5	20.3	0.6	18.5	3.7
Weighted Average								20.4	0.3	19.0	2.6
<i>SO100 28GTV-2</i>	<i>8</i>	<i>Buffon</i>	33° 41.735' 33° 41.868'	124° 54.612' 124° 54.425'	plag	IH	88.1	9.0	0.1	9.0	0.1
<i>SO100 25DS-1</i>	<i>9</i>	<i>Celsius</i>	33° 20.764' 33° 20.891'	123° 52.525' 123° 52.752'	wr	IH	72.9	13.3	0.1	13.3	0.1
<i>SO100 26DS-1</i>	<i>9</i>	<i>Celsius</i>	33° 31.700' 33° 31.664'	124° 06.434' 124° 05.535'	plag	IH	93.3	13.1	0.6	13.2	1.2
Weighted Average								13.3	0.1	13.3	0.1
<i>SO100 33DS-1</i>	<i>10</i>	<i>Curie</i>	34° 07.384' 34° 08.396'	122° 22.038' 122° 21.610'	plag	IH	100	12.7	0.3	12.7	0.6
<i>SO100 38DS-1</i>	<i>11</i>	<i>Da Vinci</i>	34° 19.119' 34° 20.326'	121° 58.729' 121° 58.455'	plag	IH	99.6	11.8	0.2	11.6	0.9
<i>SO100 41DS-1</i>	<i>12b</i>	<i>Darwin b</i>	34° 52.352' 34° 51.896'	121° 33.309' 121° 33.353'	plag	IH	99.2	11.8	0.2	11.8	0.3
<i>SO100 45DS-1</i>	<i>13a</i>	<i>Einstein a</i>	35° 03.180' 35° 03.224'	120° 43.226' 120° 43.198'	plag	IH	89.2	13.6	0.2	13.2	0.8
<i>SO100 46DS-2</i>	<i>16</i>	<i>Fermi</i>	34° 57.336' 34° 57.508'	120° 24.490' 120° 23.455'	wr	IH	56.5	10.5	0.2	10.3	0.5
<i>SO100 50DS-1</i>	<i>18</i>	<i>Galilei</i>	34° 51.492' 34° 51.860'	119° 06.724' 119° 06.811'	plag	IH	99.9	9.5	0.2	9.2	1.1
<i>SO100 50DS-1</i>	<i>18</i>	<i>Galilei</i>			wr	IH	68.0	9.5	0.2	8.9	0.9
Weighted Average								9.5	0.1	9.0	0.7
<i>SO100 54DS-1</i>	<i>19b</i>	<i>Herschel b</i>	35° 06.976' 35° 06.200'	118° 33.132' 118° 33.329'	wr	IH	59.1	8.5	0.1	8.4	0.2
<i>SO100 56DS-1</i>	<i>21a</i>	<i>Hubble a</i>	35° 22.943' 35° 22.959'	118° 05.256' 118° 05.314'	plag	IH	99.6	7.8	0.1	7.8	0.2
<i>SO100 63DS-1</i>	<i>22</i>	<i>Hubboldt</i>	35° 48.000' 35° 47.663'	117° 26.305' 117° 26.303'	wr	IH	64.5	7.8	0.1	7.7	0.1
<i>SO100 60DS-1</i>	<i>23</i>	<i>Jenner</i>	35° 27.003' 35° 26.762'	117° 11.833' 117° 12.007'	plag	IH	92.0	7.6	0.1	7.8	3.8
<i>SO100 59DS-1</i>	<i>24b</i>	<i>Kepler</i>	35° 26.729' 35° 26.334'	116° 38.813' 116° 39.352'	plag	IH	99.9	7.3	0.2	7.3	0.2
<i>SO100 67DS-4</i>	<i>25</i>	<i>Kopernik</i>	36° 01.980' 36° 01.473'	115° 59.276' 115° 59.294'	plag	IH	98.4	6.3	0.2	6.3	0.4
<i>SO100 66DS-1</i>	<i>26</i>	<i>Lavoisier</i>	35° 47.484' 35° 47.454'	115° 39.335' 115° 38.124'	plag	IH	99.5	4.9	0.2	4.9	0.8

<i>SO100 66DS-1</i>	26	<i>Lavoisier</i>			plag	IH	95.4	4.8	0.2	3.9	1.5
<i>SO100 66DS-1</i>	26	<i>Lavoisier</i>			wr	IH	69.7	4.7	0.2	4.8	0.5
Weighted Average								4.8	0.1	4.8	0.4
<i>SO100 69DS-1</i>	27b	<i>Linné B</i>	36° 33.804'	115° 16.627'	wr	IH	100	5.1	0.1	5.1	0.1
			36° 33.524'	115° 16.230'							
<i>SO100 70DS-2</i>	28	<i>Mendel</i>	36° 20.907'	113° 55.696'	wr	IH	76.2	3.7	0.2	3.9	0.3
			36° 20.848'	113° 55.790'							
<i>FH DR13-1</i>	29	<i>Mendeleiev</i>	37° 01.600'	114° 02.56'	wr	IH	70.7	3.3	0.1	3.2	0.2
<i>FH DR13-1</i>	29				wr	IH	75.6	3.4	0.2	3.4	0.2
Weighted Average								3.3	0.1	3.3	0.1
<i>SO100 71DS-1</i>	30	<i>Mercator</i>	36° 40.812'	113° 28.350'	wr		100	2.1	0.1	2.1	0.1
			36° 41.770'	113° 26.926'							
<i>FH DR11-1</i>	31	<i>Newton</i>	36° 55.477'	113° 04.585'	wr	SFs	100	2.1	0.3	2.0	1.4
<i>FH DR11-1</i>	31				wr	IH	51.8	2.1	0.3	2.1	0.4
Weighted Average								2.1	0.2	2.1	0.4
<i>SO100 74DS-1</i>	32	<i>Ohm</i>	36° 56.987'	112° 12.875'	wr	SFs	100	2.0	0.4	2.3	1.2
			36° 57.427'	112° 13.765'							
<i>SO100 74DS-1</i>	32				wr	IH	100	1.6	0.5	2.0	0.6
Weighted Average								1.8	0.3	2.1	0.5
<i>SO100 76DS-1</i>	33	<i>Pascal</i>	37° 22.190'	112° 06.098'	wr	IH	77.4	1.1	0.1	1.1	0.2
			37° 22.377'	112° 06.003'							
<i>SO100 97DS-2</i>	33	<i>Pascal</i>	37° 25.016'	112° 03.419'	wr	SF		1.1	0.4		
			37° 24.662'	112° 03.882'							
<i>SO100 101GTV-2</i>	33	<i>Pascal</i>	37° 23.149'	112° 05.940'	wr	SF		1.1	0.3		
			37° 23.209'	112° 05.920'							
Weighted Average								1.1	0.1		
<i>SO100 99DS-5</i>	34	<i>Pasteur</i>	37° 15.768'	112° 03.044'	wr	IH	96.1	1.1	0.1	1.2	0.4
			37° 15.328'	112° 03.565'							
<i>SO100 77DS-1</i>	35	<i>Pauling</i>	37° 03.427'	111° 39.605'	wr	IH	100	1.1	0.2	1.1	0.3
			37° 04.094'	111° 39.662'							
<i>SO100 93DS-1</i>	36	<i>Planck</i>	38° 08.063'	111° 32.894'	wr	IH	100	0.5	0.1	0.5	0.3
			38° 07.515'	111° 33.403'							
<i>SO100 94DS-1</i>	37a	<i>Platon</i>	37° 53.367'	112° 53.847'	wr	IH	80	0.9	0.1	0.9	0.1
			37° 53.227'	112° 55.644'							
<i>SO100 95DS-1</i>	37b	<i>Richter</i>	37° 53.312'	112° 25.089'	wr	IH	100	0.9	0.1	0.9	0.1
			37° 53.787'	112° 25.912'							
<i>SO100 90DS-1</i>	38	<i>Rutherford</i>	38° 21.598'	110° 37.905'	wr	SFs	100	1.1	0.5	0.6	1.1
			38° 20.966'	110° 37.903'							
<i>SO100 90DS-1</i>	38				wr	IH	76.2	1.1	0.4	0.9	0.7
Weighted Average								1.1	0.3	0.8	0.6
<i>SO100 75DS-2</i>	39	<i>Schrödinger</i>	37° 16.680'	111° 51.521'	wr	IH	97.3	1.0	0.2	0.9	0.3
			37° 17.107'	111° 51.800'							
<i>SO100 82DS-1</i>	39	<i>North Ridge</i>	37° 27.530'	111° 12.654'	wr	SFs	100	0.4	0.1	0.5	0.4
			37° 27.134'	111° 12.059'							
<i>SO100 87DS-1</i>	39	<i>South Ridge</i>	37° 38.941'	111° 17.397'	wr	SFs	100	0.5	0.1	0.6	0.6
			37° 39.052'	111° 16.650'							
<i>SO100 87DS-1</i>	39	<i>South Ridge</i>			wr	IH	71.8	0.7	0.2	0.4	0.3
Weighted Average								0.5	0.1	0.4	0.3
<i>SO100 89DS-1</i>		<i>South Ridge</i>	37° 31.388'	111° 40.707'	wr	IH	94.5	0.7	0.1	0.7	0.2
			37° 31.897'	111° 41.332'							
<i>FH DR12-8</i>		<i>Wegener</i>	37° 55.935'	113° 42.372'	wr	IH	80.5	1.9	0.1	1.9	0.2
<i>FH DR14-14</i>		<i>Mohorovicic</i>	37° 27.78'	114° 34.773'	wr	IH	45.7	3.5	0.1	3.4	0.3
<i>FH DR14-16</i>		<i>Mohorovicic</i>	37° 27.78'	114° 34.773'	wr	IH	64.2	3.6	0.1	3.6	0.1
<i>FH DR14-17</i>		<i>Mohorovicic</i>	37° 27.78'	114° 34.773'	wr	IH	63.2	3.5	0.9	1.7	1.0
Weighted Average								3.5	0.1	3.6	0.1

<i>FH DR14-5</i>	<i>Mohorovicic</i>	37° 27.78'	114° 34.773'	wr	IH	59.1	2.8	0.1	2.8	0.4
<i>FH DR14-13</i>	<i>Mohorovicic</i>	37° 27.78'	114° 34.773'	wr	IH	86.4	0.7	0.03	0.7	0.1
<i>FH DR15-4</i>	<i>Linné Ridge</i>	35° 44.983'	114° 21.989'	wr	IH	49.3	5.0	0.2	4.6	0.5

^a Argon isotopic data, age calculation from argon isotopic data, plateau and isochron plots – together with detailed sample information – are in O'Connor et al., 1998, 2001, 2002. Ages in O'Connor et al., 1998 have been recalculated in O'Connor et al., 2001 using new TCR standard age of 28.34 Ma (Renne et al., 1998).

^b Seamount and ridge numbers assigned during 1995 F/S Sonne cruise (Devey et al., 1997).

^c Seamount/ridge names (Devey et al., 1997; Maia et al, 2001). Corresponding gravity anomaly in Mammerickx (1992) are in Devey et al., 1997 and O'Connor et al., 1998.

$\lambda_{\text{K}}^{40} = 5.543 \times 10^{-10}/\text{yr}$; Correction factors: $^{40}\text{Ar}/^{39}\text{Ar} (\text{K}) = 0.00086$; $^{36}\text{Ar}/^{37}\text{Ar} (\text{Ca}) = 0.00026$; $^{39}\text{Ar}/^{37}\text{Ar} (\text{Ca}) = 0.00067$

wr = whole rock; plag = plagioclase; IH = incremental heating; SFs = multiple single fusions; SF = single fusion

Table 2. Coeval Foundation Chain Volcanism

Seamount / Sample	Plateau (Ma)	$\pm 2\sigma$	Inverse Isochron (Ma)	$\pm 2\sigma$
<i>Del Cano</i>	16.1	0.4	16.3	0.7
<i>VER</i>	16.8	0.3	16.6	1.0
<i>VER</i>	16.6	0.2	16.1	0.6
5	16.6	0.4	16.6	0.4
Weighted Average	16.6	0.1	16.4	0.3
<i>21a</i>	7.8	0.1	7.8	0.2
22	7.8	0.1	7.7	0.1
23	7.6	0.1	7.8	3.8
Weighted Average	7.7	0.1	7.7	0.1
24	7.3	0.2	7.3	0.2
25	6.3	0.2	6.3	0.4
26	4.8	0.1	4.8	0.4
27b	5.1	0.1	5.1	0.1
<i>FH DR15-4</i>	5.0	0.2	4.6	0.5
Weighted Average	5.0	0.1	5.1	0.1
28	3.7	0.2	3.9	0.3
29	3.3	0.1	3.3	0.1
<i>FH DR14</i>	3.5	0.1	3.6	0.1
Weighted Average	3.5	0.1	3.5	0.1
<i>FH DR14</i>	2.8	0.1	2.8	0.4
30	2.1	0.1	2.1	0.1
31	2.1	0.2	2.1	0.4
32	1.9	0.3	2.2	0.5
<i>FH DR12-8</i>	1.9	0.1	1.9	0.2
Weighted Average	2.0	0.1	2.1	0.1
33	1.1	0.1	1.1	0.2
34	1.1	0.1	0.9	0.5
35	1.1	0.2	1.1	0.3
39	1.0	0.2	0.9	0.3
Weighted Average	1.1	0.1	1.0	0.1
37a	0.9	0.1	0.9	0.1
37b	0.9	0.1	0.9	0.1
Weighted Average	0.9	0.1	0.9	0.1
33	1.1	0.1	1.1	0.2
34	1.1	0.1	0.9	0.5
35	1.1	0.2	1.1	0.3
39	1.0	0.2	0.9	0.3
37a	0.9	0.1	0.9	0.1
37b	0.9	0.1	0.9	0.1
Weighted Average	1.0	0.1	0.9	0.1
<i>FH DR14 -13</i>	0.7	0.03	0.7	0.1
<i>SO100 89DS-1</i>	0.7	0.1	0.7	0.2
Weighted Average	0.7	0.03	0.7	0.1
<i>SO100 82DS-1</i>	0.4	0.1	0.5	0.4
<i>SO100 87DS-1</i>	0.5	0.1	0.4	0.3
36	0.5	0.1	0.5	0.3
Weighted Average	0.5	0.1	0.5	0.2

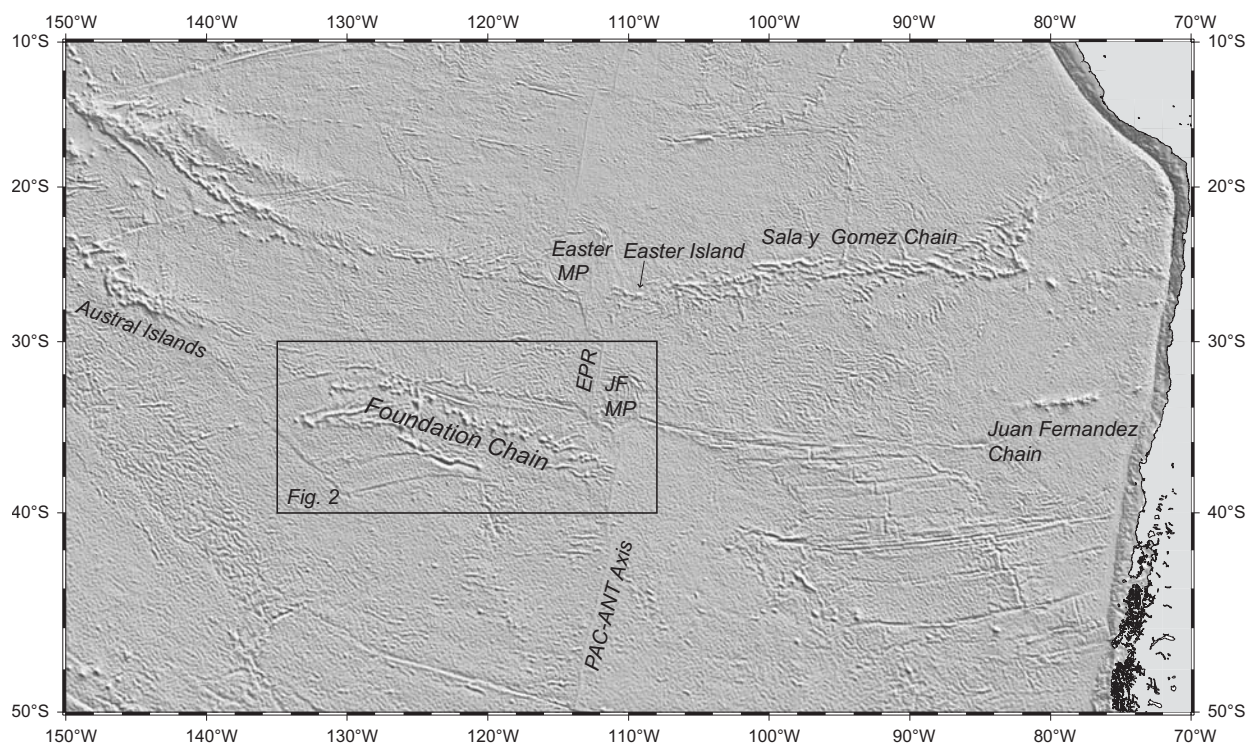


Figure 1

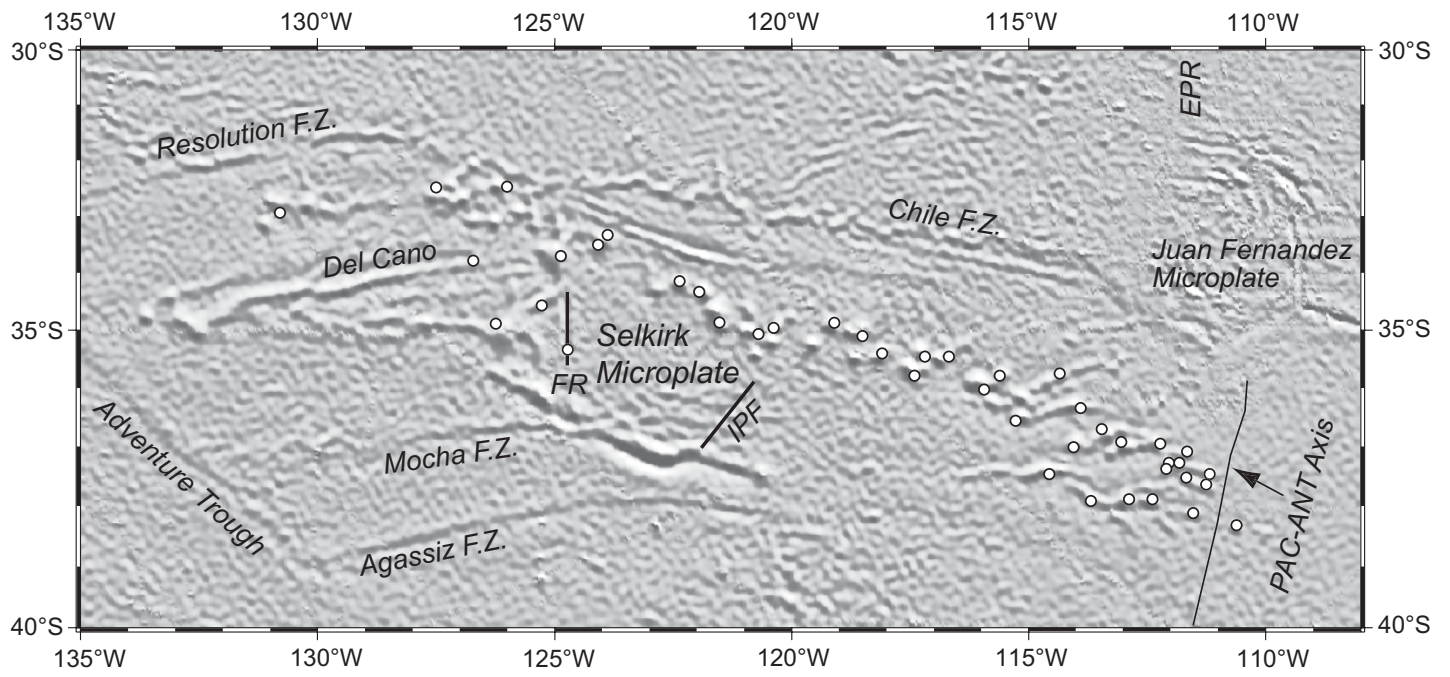


Figure 2

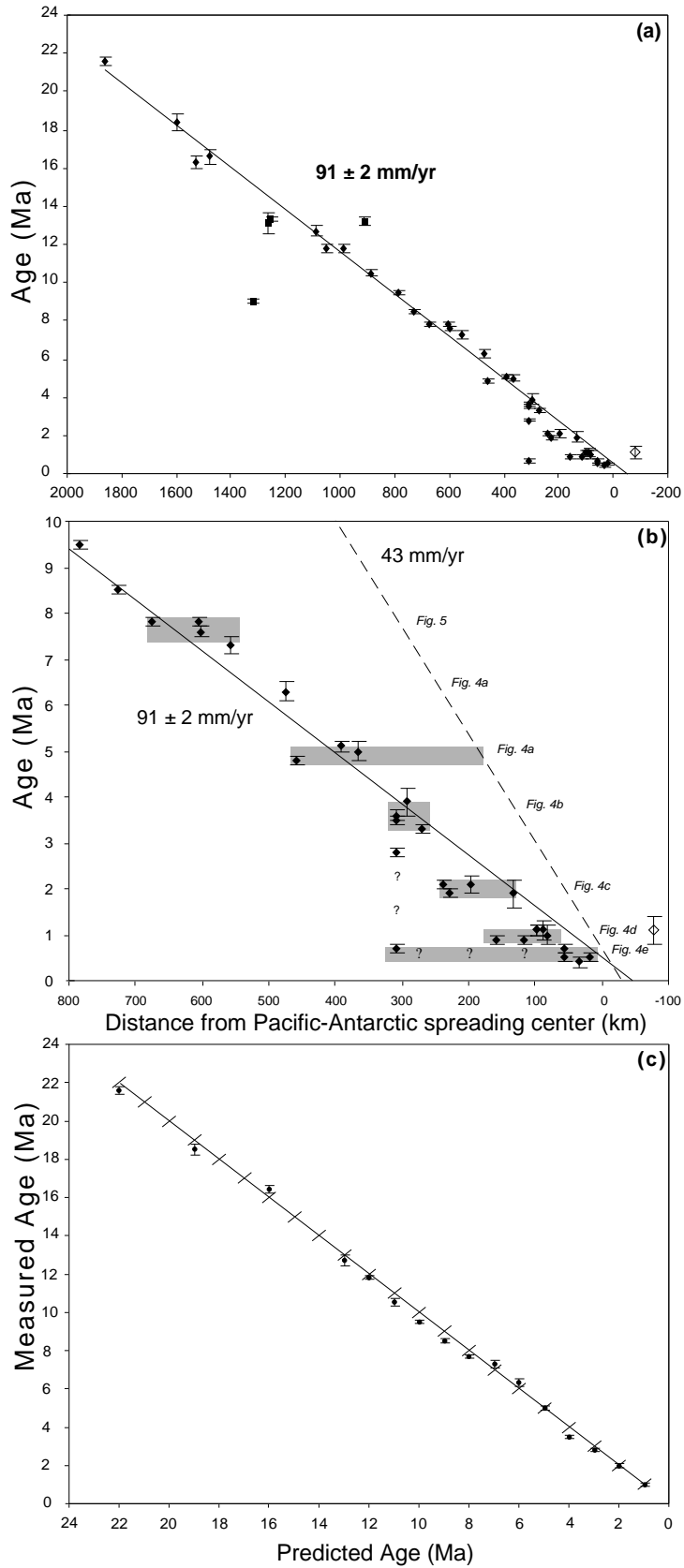


Figure 3

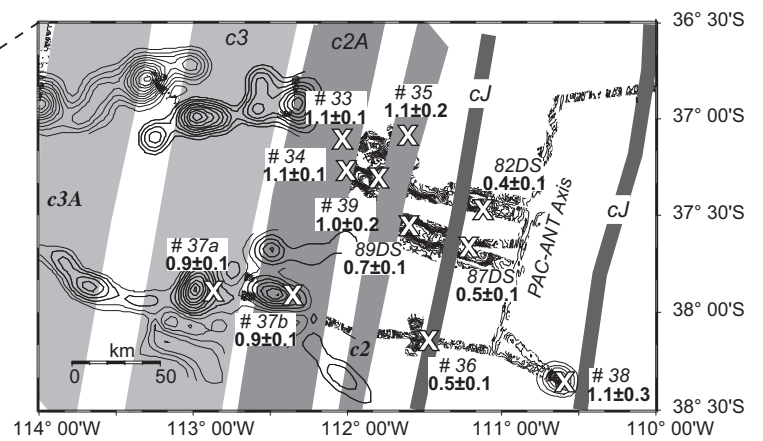
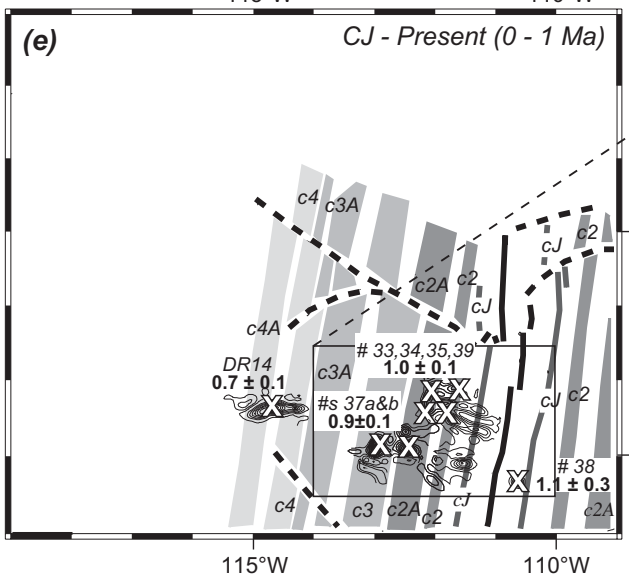
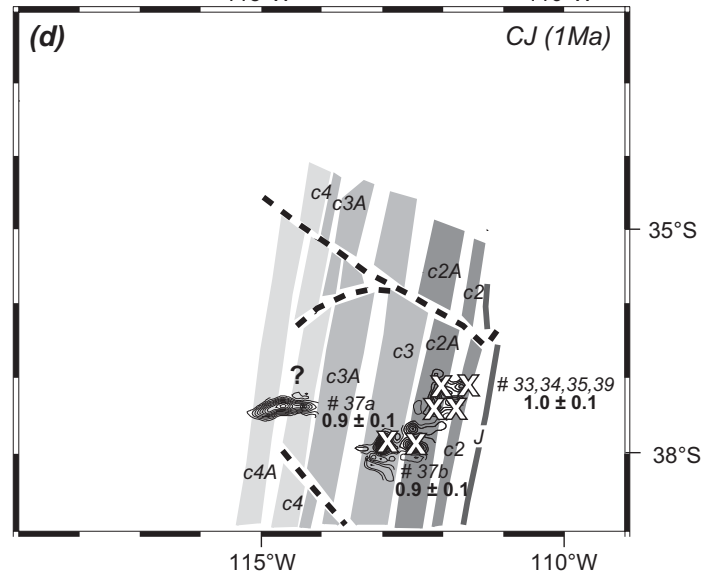
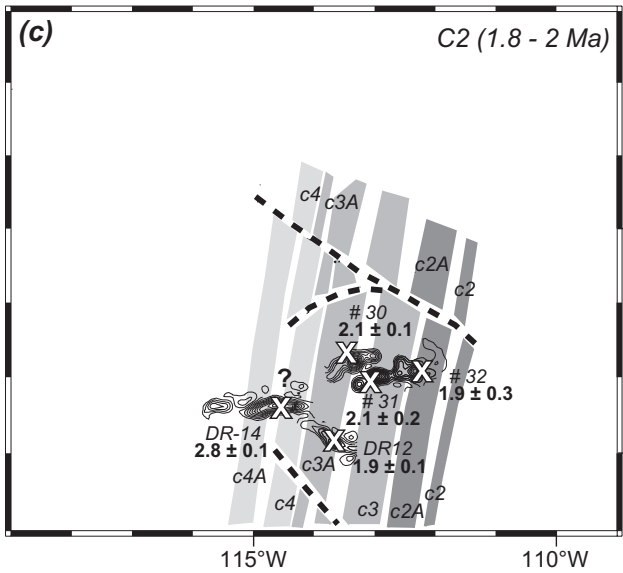
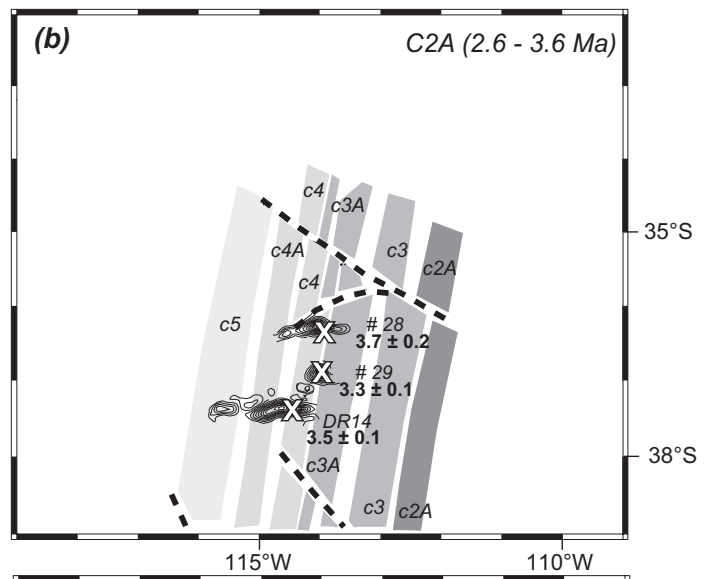
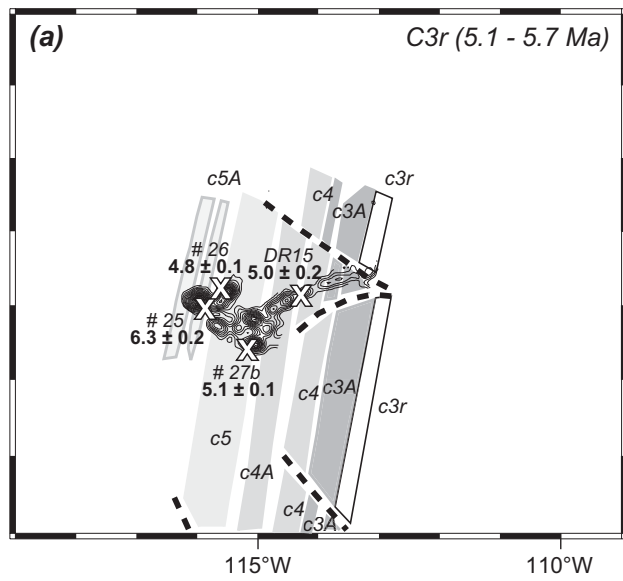


Figure 4

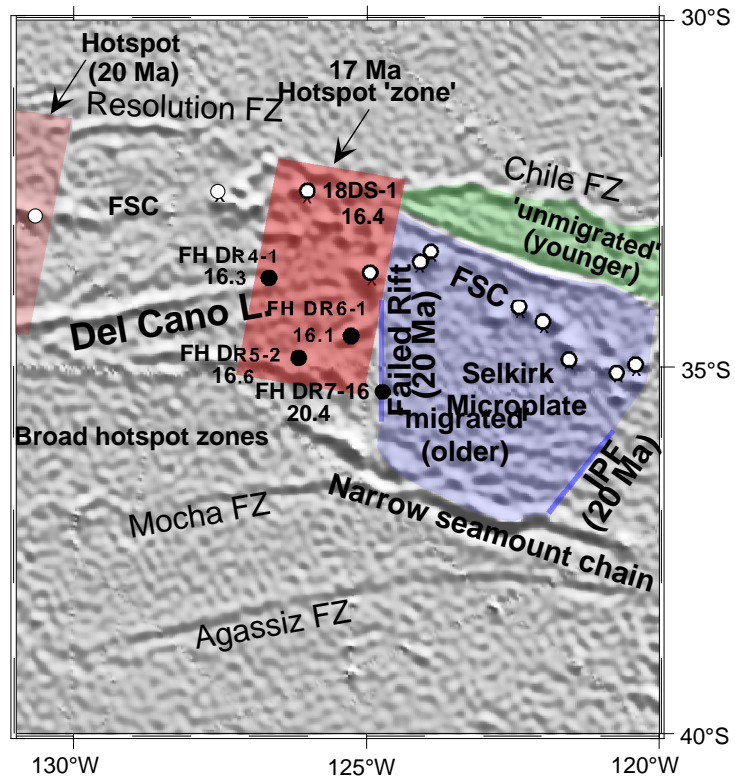


Figure 6

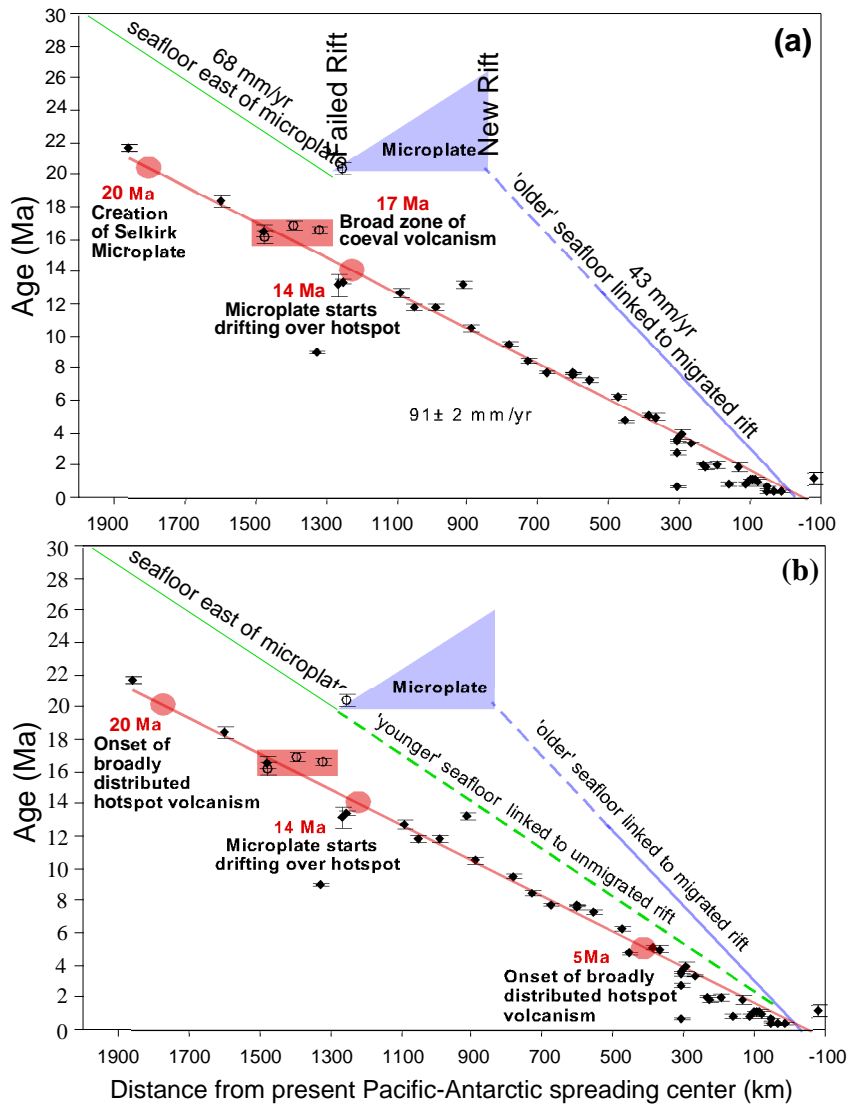


Figure 7

Monecke, T., Renno, A.D., and Herzig, P.M. (in press) Primary clinopyroxene spherulites in basaltic lavas from the Pacific-Antarctic Ridge. Journal of Volcanology and Geothermal Research.



ELSEVIER

Available online at www.sciencedirect.com

SCIENCE @ DIRECT®

Journal of volcanology
and geothermal research

Journal of Volcanology and Geothermal Research 2701 (2003) 1–9

www.elsevier.com/locate/jvolgeores

Primary clinopyroxene spherulites in basaltic lavas from the Pacific–Antarctic Ridge

Thomas Monecke*, Axel D. Renno, Peter M. Herzig

Department of Economic Geology and Leibniz Laboratory for Applied Marine Research, Institute of Mineralogy, Freiberg University of Mining and Technology, Brennhaugasse 14, 09596 Freiberg, Germany

Received 19 February 2003; accepted 14 July 2003

Abstract

Fresh glassy basaltic andesite samples recovered from the northern part of the Pacific–Antarctic Ridge contain abundant spherulites consisting of arrays of closely packed clinopyroxene fibers. The spherulites frequently enclose elongated vesicles that are tear drop-shaped or tailed. The long axes of the elongated vesicles were found to be always parallel to the orientation of the surrounding crystal fibers. In several cases, elongated vesicles having different orientations are hosted by a single spherulite. The existence of elongated vesicles provides unequivocal evidence that a significant proportion of the clinopyroxene fibers must have crystallized directly from a supercooled liquid at temperatures above the glass transition. Moreover, the absence of fractures within the spherulites and the surrounding glass as well as the observed nucleation of clinopyroxene fibers at vesicle walls are interpreted to be consistent with a primary origin of the clinopyroxene spherulites. Based on these textural observations it has to be concluded that spherulites do not represent a diagnostic texture for the devitrification of volcanic glass that occurs below the glass transition temperature.

© 2003 Published by Elsevier B.V.

Keywords: spherulites; volcanic glass; clinopyroxene; cooling history

1. Introduction

The volcanic eruption of silicate melts is frequently accompanied by rapid cooling where the melt is quenched to form volcanic glass. The glass is thermodynamically unstable and may be devitrified upon further cooling of the lava. The devitrification of quenched lava at temperatures below

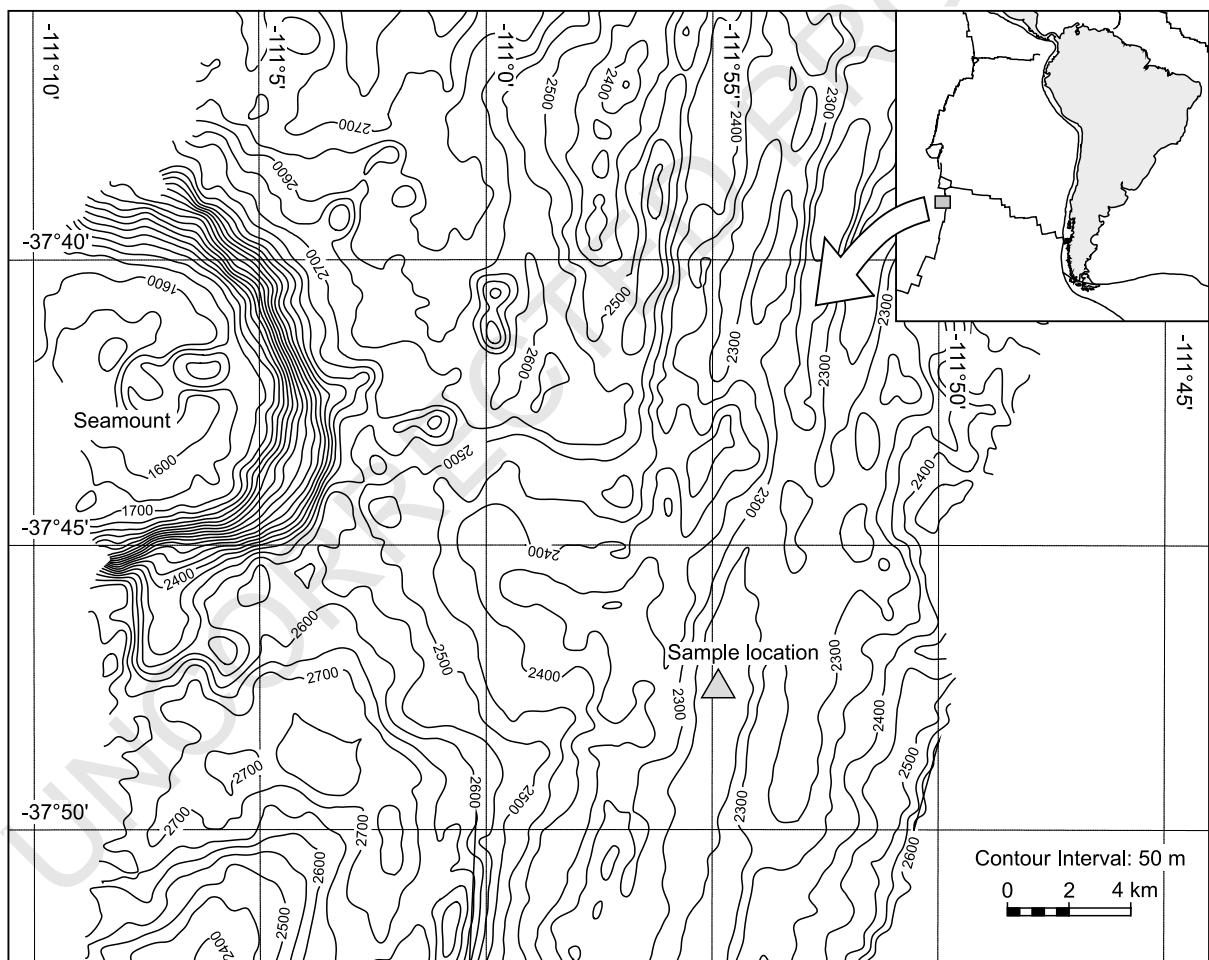
the glass transition is known to result in the formation of spherulites (Lofgren, 1971a). Spherulites are spherical, fan-shaped, bow-tie-shaped, plumose, or axiolitic aggregates of crystal fibers where each fiber represents a single crystal that has only a slightly different orientation from the adjacent crystal (Iddings, 1891; Lofgren, 1971b, 1974). Spherulites are typically well preserved in ancient volcanic sequences providing critical information on the cooling history of volcanic emplacement units that erupted millions to billions of years before the present (Swanson et al., 1989; Manley, 1992; Doyle, 2001). Spherulites have var-

* Corresponding author. Fax: +4-3731-39-2610.
E-mail address: tmoecke@mineral.tu-freiberg.de (T. Monecke).

44 iable sizes that typically range from millimeters to
 45 several centimeters although some as large as 3 m
 46 have recently been discovered (Smith et al., 2001).
 47 Spherulites have been observed in volcanic rocks
 48 of a broad compositional spectrum and are com-
 49 posed of clinopyroxene fibers in komatiites and
 50 basalts, plagioclase fibers in basalts and andesites,
 51 and alkali feldspar, quartz, or cristobalite fibers in
 52 dacites and rhyolites (Rogers, 1921; Kirkpatrick,
 53 1978; Natland, 1980; Davis and McPhie, 1996;
 54 Fowler et al., 2002).

55 During a research cruise of the German re-

search vessel R/V *Sonne* from June to July 2001, 56
 fresh lava containing abundant spherulites was 57
 recovered from the northern part of the Pacific– 58
 Antarctic Ridge. This paper describes the textures 59
 of the spherulites contained in this material as 60
 revealed by petrographic analyses of thin sections. 61
 It is shown that several textural characteristics 62
 constrain the timing of spherulite crystallization 63
 in the basaltic lava. The textural observations 64
 contradict the commonly held perception that all 65
 spherulites are devitrification products of volcanic 66
 glass. 67



1 Fig. 1. Bathymetric map of the Pacific–Antarctic Ridge near 37°47.5'S. The map shows that the northern end of the axial high
 2 of the central segment is located immediately opposite the youngest seamount of the central Foundation chain. The map also
 3 gives the sample location of the spherulitic lava investigated in the present study.

68 **2. Geological setting**

69 The northern part of the Pacific–Antarctic
70 Ridge is located near the eastern end of the Foun-
71 dation seamount chain that formed in response to
72 the passage of the Pacific Plate over a mantle
73 plume in recent geological times (O'Connor et
74 al., 1998). The spreading center of the Pacific–
75 Antarctic Ridge is currently located approxi-
76 mately 35 km to the east of the Foundation man-
77 tle plume (O'Connor et al., 1998; Maia et al.,
78 2000). Interaction with the hotspot resulted in sig-
79 nificant changes in the chemical compositions of
80 the lavas erupting at the northern Pacific–Antarc-
81 tic Ridge (Devey et al., 1997). One of the most
82 striking features is the occurrence of relatively
83 silicic volcanism at the spreading center (Hekinian
84 et al., 1999; Stoffers et al., 2002).

85 Rocks of intermediate compositions were
86 sampled near 37°47.5'S at the northern end of
87 an axial high of the central segment of the Pacif-
88 ic–Antarctic Ridge, immediately opposite the
89 youngest seamount of the central Foundation
90 chain (Fig. 1). The axial high is a prominent ap-
91 proximately 15 km long feature that rises to a
92 water depth of 2210 m. Intensive mapping by a
93 deep-towed camera vehicle revealed that the

94 northern part of the constructional high is built
95 up by two lava generations. The older lava typi-
96 cally comprises sediment-covered pillows whereas
97 the younger lava generation is distinctly glassy,
98 forming sheet flows with pillow or lobate lava at
99 the flow margins. The fresh glassy lava overlies
100 large parts of the older sediment-covered pillows
101 and locally infills collapse features in the older
102 lava. Deep fissures in one area dominated by the
103 younger lava were found to be associated with
104 diffuse hydrothermal venting giving rise to a slight
105 bottom temperature anomaly of 0.25°C. Areas of
106 upflowing hydrothermal fluids were typified by
107 the occurrence of abundant barnacles, mussels,
108 and clams. Sampling at this site was conducted
109 using a deep-sea TV-controlled grabbing device.
110 In addition to the vent fauna, very fresh glassy
111 dark blue to black aphyric lava containing abun-
112 dant spherulites was recovered.

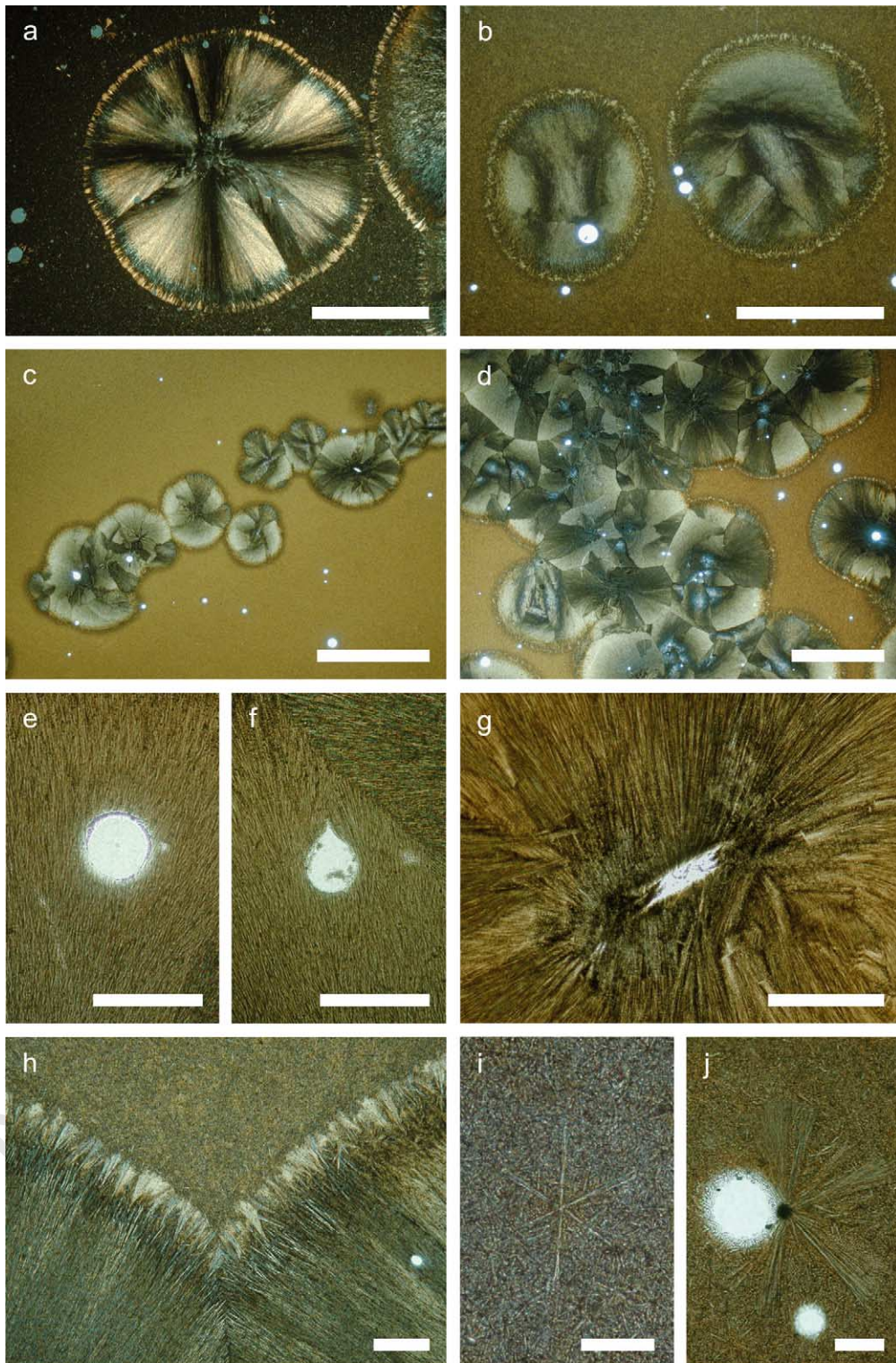
113 **3. Spherulites**

114 X-ray fluorescence (XRF) analysis of selected
115 lava samples was performed on standard fused
116 glass disks using a Philips PW 1400 X-ray spec-
117 trometer (Table 1). The chemical data revealed

Table 1
Geochemical and mineralogical composition of basaltic andesite recovered from the Pacific–Antarctic Ridge

	SO157-30GTV-2c	SO157-30GTV-2d	SO157-30GTV-2f
1			
2	Major elements (wt%; XRF):		
3	SiO ₂	52.12	52.06
4	TiO ₂	2.23	2.23
5	Al ₂ O ₃	13.11	13.13
6	Fe ₂ O ₃	14.61	14.72
7	MnO	0.24	0.24
8	MgO	3.87	3.78
9	CaO	8.27	8.25
10	Na ₂ O	3.76	3.66
11	K ₂ O	0.41	0.41
12	P ₂ O ₅	0.50	0.50
13	LOI	< 0.05	< 0.05
14	Total	99.12	98.98
15	Phase abundances (wt%; XRD):		
16	Am	54.5 ± 2.0	53.0 ± 2.2
17	Cpx	40.1 ± 1.9	43.3 ± 2.1
18	Mgt	5.4 ± 0.8	3.7 ± 0.4
19	Py	–	–
			0.5 ± 0.3

20 Notes: Am = amorphous component (volcanic glass), cpx = clinopyroxene, mgt = magnetite, py = pyrite, – = not detected.



118 that the black aphyric lava recovered at 37°47.5'S
 119 is a basaltic andesite. The mineralogical composi-
 120 tion of the samples was constrained by X-ray dif-
 121 fraction (XRD) using the Rietveld method (Mon-
 122 ecke et al., 2001). To quantify relative phase
 123 abundances, corundum was added to the pow-
 124 dered samples as an internal standard. Step scan
 125 data (5 to 80°2 θ Co tube, 0.03°2 θ step width,
 126 and 8 s/step counting time) were collected using
 127 a Seifert-FPM URD 6 diffractometer equipped
 128 with a diffracted-beam graphite monochromator
 129 and a variable divergence slit. The XRD patterns
 130 obtained are characterized by a broad amorphous
 131 scattering hump in addition to Bragg reflections
 132 corresponding to clinopyroxene. Refinement of
 133 the diffraction patterns revealed that the samples
 134 investigated consist of approximately equal
 135 amounts of glass and crystalline phases (Table
 136 1). Plagioclase was not detected by XRD suggest-
 137 ing that this phase is not present or, alternatively,
 138 represents only a minor constituent of the basaltic
 139 lava (< 1–2 wt%).

140 Petrographic analyses of thin sections showed
 141 that the spatial arrangement of spherulites varies
 142 substantially in the samples recovered from the
 143 surface of the lava flow. Composed of clinopyrox-
 144 ene, the spherulites occur as isolated spherical
 145 bodies dispersed throughout the glassy matrix
 146 (Figs. 2a,b) or form trails of impinging or coa-
 147 lesced spherulites (Fig. 2c). The spherical shape
 148 is typically lost when two or more spherulites

149 are in contact. Small groups of closely spaced
 150 spherulites are also present where adjacent spheru-
 151 lites impinge on one another or become coa-
 152 lesced to a considerable degree. Large clusters of
 153 coalesced spherulites consist of closely packed po-
 154 lygonal spherulite bodies surrounded by spheru-
 155 lites that are semicircular along contacts with the
 156 glassy matrix (Fig. 2d). Coalesced spherulites typ-
 157 ically exhibit triple point boundaries where the
 158 boundary lines separating adjacent spherulites
 159 range from perfectly planar to slightly curved.
 160 The clinopyroxene spherulites range in size from
 161 0.5 to 3.5 mm.

162 The internal organization of the clinopyroxene
 163 spherulites varies substantially in the basaltic an-
 164 desite. Many spherulites consist of arrays of
 165 closely packed clinopyroxene fibers arranged in
 166 a radial habit around a common center. These
 167 radial spherulites frequently display concentric
 168 zoning, probably due to variations in the packing
 169 density of the clinopyroxene fibers. Under crossed
 170 nicols, radial spherulites exhibit a cross-shaped
 171 extinction pattern. The extinction is centered at
 172 the origin of the radial spherulite, and the arms
 173 of the cross are oriented parallel to the transmis-
 174 sion directions of the microscopic polarizer and
 175 analyzer, respectively (Fig. 2a). More complicated
 176 arrangements of the clinopyroxene fibers are ob-
 177 served in sheaf spherulites. These spherulites con-
 178 sist of a central bow-tie sheaf clinopyroxene ag-
 179 gregate or tangled sheaves of clinopyroxene fibers

1
 2 Fig. 2. Thin section photomicrographs of clinopyroxene spherulites contained in the basaltic lava. (a) Radial spherulite displaying
 3 radial extinction. The spherulite is surrounded by volcanic glass containing abundant clinopyroxene microlites as well as several
 4 vesicles. Crossed polarized light. Scale bar: 1 mm. (b) Isolated sheaf spherulites. The left spherulite exhibits a central bow-tie
 5 sheaf clinopyroxene aggregate whereas the internal organization of the sheaves is more complex in the larger spherulite on the
 6 right side. The spherulites and the surrounding glassy matrix contain spherical vesicles. Plain polarized light. Scale bar: 1 mm.
 7 (c) Trail of impinging and partially coalesced, radial and sheaf spherulites. The coalesced spherulite at the lower left corner con-
 8 tains tear drop-shaped and spherical vesicles whereas the gas bubbles hosted by the glassy matrix are spherical. Plain polarized
 9 light. Scale bar: 1 mm. (d) Cluster of coalesced spherulites consisting of closely packed polygonal spherulite bodies surrounded
 10 by spherulites that are semicircular at the contact with the glassy matrix. Plain polarized light. Scale bar: 1 mm. (e) Spherical
 11 vesicle surrounded by clinopyroxene fibers. Plain polarized light. Scale bar: 100 μ m. (f) Tear drop-shaped vesicle hosted by a cli-
 12 nopyroxene spherulite. The long axis of the deformed vesicle is parallel to the orientation of the clinopyroxene fibers. Plain polar-
 13 ized light. Scale bar: 100 μ m. (g) Axialitic growth on a swallow-tailed crystal of intergrown plagioclase and clinopyroxene located
 14 in the center of a radial spherulite. Plain polarized light. Scale bar: 100 μ m. (h) Boundary zone of two coalesced radial spheru-
 15 lites. The boundary zone consists of an inner portion comprising relatively wide and apparently less closely packed fibers and an
 16 outer portion of fine, fanning clinopyroxene aggregates that are relatively widely separated. Plain polarized light. Scale bar: 100
 17 μ m. (i) Randomly oriented microlites and a stellate microlite grouping located in the glassy matrix of the basaltic lava. Plain po-
 18 larized light. Scale bar: 25 μ m. (j) Small open spherulite on a spherical pyrrhotite nucleus. The pyrrhotite nucleus is located at
 19 the wall of a vesicle contained in the glassy matrix of the basaltic lava. Plain polarized light. Scale bar: 25 μ m.

(Fig. 2b). The packing density of the crystal fibers in sheaf spherulites appears to be variable although neighboring clinopyroxene fibers are always separated by interfibrillar glass. Due to the bending and twisting of arrays of clinopyroxene fibers, sheaf spherulites exhibit relatively complex extinction patterns under crossed nicols.

The radial and sheaf spherulites frequently enclose vesicles. The shape of the vesicles ranges from spherical to slightly elongated (Fig. 2e,f). The elongated vesicles are tear drop-shaped or tailed where the long axis of the vesicle is always parallel to the orientation of the surrounding clinopyroxene fibers. The orientation of crystal fibers adjacent to the vesicles is commonly disturbed by newer fibers that nucleated at the vesicle walls, pointing away from the center of the spherulite. In some cases, the arrangement of arrays of clinopyroxene fibers enveloping small vesicles resembles strain caps and strain shadows occurring in deformed metamorphic rocks.

Some spherulites contained in the basaltic lava have a central nucleus. Nuclei identified include long, single clinopyroxene fibers, delicate swallow-tailed or skeletal crystals of intergrown plagioclase and clinopyroxene, and crosshatched arrays of clinopyroxene sheaves. The tiny nuclei commonly gave rise to an axiolitic growth of clinopyroxene fibers (Fig. 2g). A small xenolithic plagioclase cumulate was also observed in the center of one clinopyroxene spherulite.

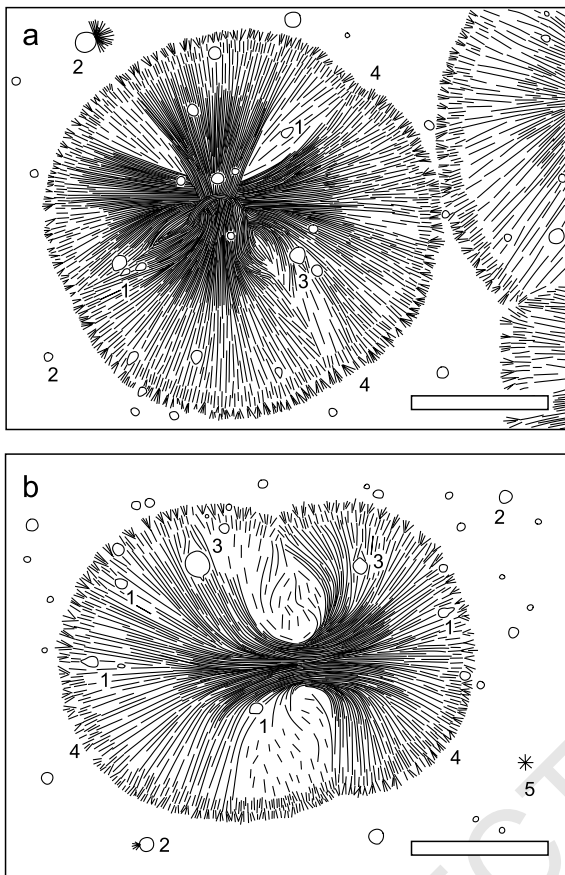
Most spherulites or spherulite clusters are surrounded by a distinct boundary zone that is 100–200 μm wide. The inner portion of the boundary zone consists of clinopyroxene fibers that are wider and apparently less closely packed than the fibers contained in the interior of the spherulites. The orientation of the crystal fibers is typically more or less constant across the contact (Fig. 2h). In some cases, the fibers of the inner boundary zone are almost perpendicularly arranged to the clinopyroxene crystals of the inner spherulite. The outer portion of the boundary zone is composed of fine, tenuous, matted clinopyroxene fibers forming small fanning aggregates that are relatively widely separated. Textural evidence suggests that the fan-shaped aggregates hosted by the glassy matrix surrounding the

spherulites have seeded on the tips of the larger clinopyroxene crystals of the inner boundary zone (Fig. 2h). The glassy matrix surrounding the spherulites is devoid of fractures and cracks visible under the microscope.

The glassy matrix contains a large number of clinopyroxene microlites. The microlites typically lack a preferred orientation although radially diverging, stellate microlite groupings are not uncommon (Fig. 2i). Spherical vesicles are common in the glassy matrix of the basaltic lava whereas tear drop-shaped or tailed vesicles were not observed. The spherical vesicles range in diameter from 5 to 250 μm . In addition to clinopyroxene microlites, pyrrhotite grains are dispersed throughout the glassy matrix. The pyrrhotite grains are spherical and frequently occur in spatial association with vesicles, possibly suggesting a coeval exsolution from the silicate melt. The vesicles and the pyrrhotite provided nuclei for the formation of small open spherulites consisting of arrays of clinopyroxene fibers. The orientation of the clinopyroxene arrays is commonly perpendicular to the interface between the spherical vesicle or pyrrhotite grain and the glass, respectively (Fig. 2j). Transmission electron microscopy revealed that the magnetite identified by XRD forms nanolites in the glassy matrix (Wirth, personal communication, 2003).

4. Timing of spherulite formation

Hitherto, reconstruction of the timing of spherulite formation has been considered to be extremely difficult because of the lack of unequivocal textural criteria allowing a distinction between spherulites grown from a melt and those resulting from the devitrification of volcanic glass (Lofgren, 1971a,b; Fowler et al., 2002). However, in the present case, the existence of deformed vesicles in the clinopyroxene spherulites proves that the matrix surrounding the growing crystal fibers behaved like a liquid at the time of crystal growth. The spherulite growth must have modified the bubble geometry because simple buoyancy of the exsolved gas through the liquid may not account for the observation that the orientation of elon-



1 Fig. 3. Schematic sketches of spherulites contained in the basaltic lava. (a) Radial spherulite containing abundant spherical and tear drop-shaped vesicles. (b) Sheaf spherulite that is typified by a central bow-tie sheaf clinopyroxene aggregate. The numbers denote textural features mentioned in the text. (1) Elongated vesicles contained in the spherulites. Note that the orientation of the vesicles is variable. (2) Spherical vesicles hosted by the glassy matrix surrounding the spherulites. (3) Disturbed orientation of crystal fibers adjacent to vesicle walls pointing away from the centers of the spherulites. (4) Boundary zone enclosing the spherulites. (5) Stellate microlite in the glassy matrix. The spherulites and the vesicles were directly drawn from photomicrographs. The vesicles were slightly enlarged to illustrate their geometries. Scale bar: 1 mm.

273 gated vesicles varies within a single spherulite
 274 (Fig. 3). Moreover, vesicles contained in the
 275 glassy matrix surrounding the spherulites were
 276 found to be always spherical. The absence of frac-
 277 tures within the spherulites as well as in the sur-
 278 rounding glassy matrix is apparently consistent

279 with a primary origin of the clinopyroxene spherulites because spherulites forming through the devitrification of glass are likely to be associated with cracks. Fractures may occur in and around spherulites forming through the devitrification of volcanic glass because the glass–crystal transition causes a more or less pronounced volume contraction (Pirsson, 1910). Moreover, axiolitic spherulites may be associated with fractures forming during the cooling of the glass because channeling of fluids along these cracks may trigger the devitrification of volcanic glass (Davis and McPhie, 1996). In contrast to the observed deformation of vesicles in the clinopyroxene spherulites, the absence of fractures alone does not provide unequivocal evidence for a primary magmatic origin of the spherulites because the stress building up during cooling or devitrification of the glass may have been below the critical stress required for brittle failure of the glassy matrix (Orowan, 1934). However, an additional textural observation pointing to a primary magmatic origin of the spherulites is the nucleation of clinopyroxene sheaves along the walls of vesicles. The crystal fibers may have nucleated at the vesicle walls because the energy required to open and maintain gas bubbles within the melt may have been lost in the form of heat causing cooling and nucleation at the bubble–melt interface (Phillips, 1973; Fowler et al., 2002). Nucleation of spherulites on bubble walls has been produced experimentally in supersaturated silicate melts (Davis and Ihinger, 1998) and has also been described for plagioclase spherulites in basalts (Fowler et al., 1987, 2002). However, care is needed when dealing with ancient volcanic rocks containing amygdala, because fluid circulation associated with the filling of the vesicles by secondary minerals may have initiated the formation of spherulites through devitrification of volcanic glass (Fowler et al., 2002).

320 In the case of the basaltic andesite investigated,
 321 it appears likely that the emplacement of the lava
 322 at the ocean floor was accompanied by very rapid
 323 cooling. The aphyric nature of the material indi-
 324 cates that the lava was initially free of crystals
 325 implying that crystallization at the liquidus tem-
 326 perature was inhibited. The supercooled basaltic

327 melt is interpreted to have remained in a liquid-
 328 like state after eruption until the glass transition
 329 temperature was reached, below which the mate-
 330 rial behaved like a glass (Scarfe, 1977; Ryan and
 331 Sammis, 1981; Moynihan, 1995). Because the
 332 presence of deformed vesicles proves that the cli-
 333 noproxene fibers crystallized from a matrix
 334 showing liquid-like behavior, the growth of the
 335 spherulites must have occurred, at least in part,
 336 above the glass transition temperature from the
 337 supercooled basaltic melt. However, the super-
 338 cooled melt must have attained a considerable
 339 degree of viscosity before crystallization of the
 340 spherulites was initiated because the matrix was
 341 able to support the delicate sheaves of crystal fi-
 342 bers and prevent denser spherulitic bodies from
 343 sinking to the bottom of the lava flow. Therefore,
 344 in many respects, spherulite formation in the ba-
 345 saltic lava can be compared to the crystallization
 346 of spherulites from supercooled melts in experi-
 347 mental systems (Lofgren, 1974; Baker and Freda,
 348 2001) as well as the formation of radiating arrays
 349 or lamellar ribbons of crystal fibers in technical
 350 products (Keith and Padden, 1963; Yan et al.,
 351 2000).

352 5. Conclusions

353 The present study reports several textural ob-
 354 servations that suggest that clinopyroxene spher-
 355 ulites contained in fresh glassy basaltic andesite
 356 samples recovered from the northern part of the
 357 Pacific–Antarctic Ridge crystallized from the lava
 358 shortly after effusive eruption at the seafloor while
 359 the lava was still in a liquid-like state. Based on
 360 the textural observations, it is proposed that
 361 spherulites in lavas may form from viscoelastic,
 362 supercooled melts above the glass transition tem-
 363 perature. Therefore, spherulites cannot be re-
 364 garded as a diagnostic texture for the devitrifica-
 365 tion of volcanic glass that takes place below the
 366 glass transition temperature unless textural evi-
 367 dence suggests that the matrix surrounding the
 368 spherulites was rigid at the time of crystal growth.

Acknowledgements

We thank Captain H. Papenhagen, his officers,
 and the crew onboard R/V *Sonne* cruise 157 for
 their expert help. The paper has benefited from
 discussions with P. Stoffers (Chief Scientist cruise
 SO-157) and S. Ioannou. We thank R. Kleeberg
 and S. Köhler for help provided during the XRD
 investigations. The XRF analyses were carried out
 by P. Appel. Suggestions by two anonymous re-
 viewers and B.D. Marsh helped to improve an
 earlier version of the manuscript. This work was
 supported by the German Federal Ministry of
 Education and Research (BMBF) and the Leibniz
 Program of the German Research Foundation
 (DFG).

References

- Baker, D.R., Freda, C., 2001. Eutectic crystallization in the undercooled orthoclase–quartz–H₂O system: experiments and simulations. *Eur. J. Mineral.* 13, 453–466.
- Davis, B.K., McPhie, J., 1996. Spherulites, quench fractures and relict perlite in a Late Devonian rhyolite dyke, Queensland, Australia. *J. Volcanol. Geotherm. Res.* 71, 1–11.
- Davis, M.J., Ihinger, P.D., 1998. Heterogeneous nucleation on bubbles in silicate melt. *Am. Mineral.* 83, 1008–1015.
- Devey, C.W., Hékinian, R., Ackermant, D., Binard, N., Francke, B., Hémond, C., Kapsimalis, V., Lorenc, S., Maia, M., Möller, H., Perrot, K., Pracht, J., Rogers, T., Statteger, K., Steinke, S., Victor, P., 1997. The Foundation Seamount Chain: a first survey and sampling. *Mar. Geol.* 137, 191–200.
- Doyle, M.G., 2001. Volcanic influences on hydrothermal and diagenetic alteration: Evidence from the Highway-Reward, Mount Windsor Subprovince, Australia. *Econ. Geol.* 96, 1133–1148.
- Fowler, A.D., Berger, B., Shore, M., Jones, M.I., Ropchan, J., 2002. Supercooled rocks: development and significance of varioles, spherulites, dendrites and spinifex in Archaean volcanic rocks, Abitibi Greenstone belt, Canada. *Precambrian Res.* 115, 311–328.
- Fowler, A.D., Jensen, L.S., Peloquin, S.A., 1987. Varioles in Archean basalts: products of spherulitic crystallization. *Can. Mineral.* 25, 275–289.
- Hékinian, R., Stoffers, P., Ackermant, D., Révillon, S., Maia, M., Bohn, M., 1999. Ridge-hotspot interaction: the Pacific–Antarctic Ridge and the Foundation seamounts. *Mar. Geol.* 160, 199–223.
- Iddings, J.P., 1891. Spherulitic crystallization. *Bull. Phil. Soc. Washington* 11, 445–463.
- Keith, H.D., Padden, F.J., Jr., 1963. A phenomenological

369

370
371
372
373
374
375
376
377
378
379
380
381
382
383

384

385
386
387
388
389
390
391
392
393
394
395
396
397
398
399
400
401
402
403
404
405
406
407
408
409
410
411
412
413
414
415
416
417

- 418 theory of spherulite crystallization. *J. Appl. Phys.* 34, 2409–
419 2421.
- 420 Kirkpatrick, R.J., 1978. Processes of crystallization in pillow
421 basalts, Hole 396B, DSDP Leg 46. In: Dmitriev, L., Heirt-
422 zler, J. et al. (Eds.), *Initial Reports of the Deep Sea Drilling*
423 *Project 46*, U.S. Government Printing Office, Washington,
424 DC, pp. 271–282.
- 425 Lofgren, G., 1971a. Experimentally produced devitrification
426 textures in natural rhyolitic glass. *Geol. Soc. Am. Bull.* 82,
427 111–124.
- 428 Lofgren, G., 1971b. Spherulitic textures in glassy and crystal-
429 line rocks. *J. Geophys. Res.* 76, 5635–5648.
- 430 Lofgren, G., 1974. An experimental study of plagioclase crys-
431 tal morphology: isothermal crystallization. *Am. J. Sci.* 274,
432 243–273.
- 433 Maia, M., Achemand, D., Dehghani, G.A., Gente, P., Hekin-
434 nian, R., Naar, D., O'Connor, J., Perrot, K., Morgan, J.P.,
435 Ramillien, G., Révillon, S., Sabetian, A., Sandwell, D.,
436 Stoffers, P., 2000. The Pacific–Antarctic Ridge–Foundation
437 hotspot interaction: a case study of a ridge approaching a
438 hotspot. *Mar. Geol.* 167, 61–84.
- 439 Manley, C.R., 1992. Extended cooling and viscous flow of
440 large, hot rhyolitic lavas: implications of numerical model-
441 ing results. *J. Volcanol. Geotherm. Res.* 53, 27–46.
- 442 Monecke, T., Köhler, S., Kleeberg, R., Herzig, P.M., Gem-
443 mell, J.B., 2001. Quantitative phase-analysis by the Rietveld
444 method using X-ray powder-diffraction data: application to
445 the study of alteration halos associated with volcanic-rock-
446 hosted massive sulfide deposits. *Can. Mineral.* 39, 1617–
447 1633.
- 448 Moynihan, C.T., 1995. Structural relaxation and the glass
449 transition. In: Stebbins, J.F., McMillan, P.F., Dingwell,
450 D.B. (Eds.), *Structure, Dynamics and Properties of Silicate*
451 *Melts*, *Reviews in Mineralogy* 32, Mineralogical Society of
452 America, Washington, DC, pp. 1–19.
- 453 Natland, J.H., 1980. Crystal morphologies in basalts dredged
and drilled from the East Pacific Rise near 9°N and the
Siqueiros fracture zone. In: Rosendahl, B.R., Hekinian, R.
et al. (Eds.), *Initial Reports of the Deep Sea Drilling Project*
54, U.S. Government Printing Office, Washington, DC, pp.
605–633.
- O'Connor, J.M., Stoffers, P., Wijbrans, J.R., 1998. Migration
rate of volcanism along the Foundation Chain, SE Pacific.
Earth Planet. Sci. Lett. 164, 41–59.
- Orowan, E., 1934. Die mechanischen Festigkeitseigenschaften
und die Realstruktur der Kristalle. *Z. Kristallogr. A* 89,
327–343.
- Phillips, W.J., 1973. Interpretation of crystalline spheroidal
structures in igneous rocks. *Lithos* 6, 235–244.
- Pirsson, L.V., 1910. On an artificial lava-flow and its spheru-
litic crystallization. *Am. J. Sci.* 30, 97–114.
- Rogers, A.F., 1921. Cristobalite in the spherulitic obsidian
from Yellowstone National Park. *Am. Mineral.* 6, 4–6.
- Ryan, M.P., Sammis, C.G., 1981. The glass transition in bas-
alt. *J. Geophys. Res.* 86, 9519–9535.
- Scarfe, C.M., 1977. Viscosity of some basaltic glasses at one
atmosphere. *Can. Mineral.* 15, 190–194.
- Smith, R.K., Tremallo, R.L., Lofgren, G.E., 2001. Growth of
megaspheulites in a rhyolitic vitrophyre. *Am. Mineral.* 86,
589–600.
- Stoffers, P., Worthington, T., Hekinian, R., Petersen, S., Han-
nington, M., Türkay, M., SO157 Shipboard Scientific Party,
2002. Silicic volcanism and hydrothermal activity docu-
mented at Pacific–Antarctic Ridge. *EOS Trans. Am. Geo-
phys. Union* 83, 301–304.
- Swanson, S.E., Naney, M.T., Westrich, H.R., Eichelberger,
J.C., 1989. Crystallization history of Obsidian Dome, Inyo
Domes, California. *Bull. Volcanol.* 51, 161–176.
- Yan, Y., Evetts, J.E., Zhang, J., Stobbs, W.M., 2000. Charac-
teristic spherulitic microstructure in partial-melt-processed
YBa₂Cu₃O_x/HfO₂. *J. Am. Ceram. Soc.* 83, 1266–1276.

**Haase, K. M., Stroncik, N. A.; and Stoffers, P.
Bimodal volcanism along the Pacific-Antarctic-East-
Pacific-Rise (PA-EPR) spreading axis. To be
submitted to Nature**

Bimodal volcanism along the Pacific-Antarctic-East-Pacific-Rise (PA-EPR) spreading axis

Karsten M. Haase, Nicole Stroncik, and Peter Stoffers

Institut für Geowissenschaften der Christian-Albrechts-Universität zu Kiel, D-24098 Kiel, Germany

Lavas erupting along oceanic spreading axes have relatively homogeneous compositions with the average composition of the oceanic crust thought to be represented by a „normal“ depleted mid-ocean ridge basalt with about 7% MgO and 50% SiO₂ [1]. Andesitic and dacitic lavas with SiO₂ contents >54% occur only very rarely on oceanic spreading centres and are believed to form by fractional crystallization processes or by melting of hydrothermally altered oceanic crust. The occurrence of andesitic and dacitic rocks on spreading axes may be analogues to the formation of the early continental crust on Earth. Our study of the southern PA-EPR reveals that silicic lavas erupt together with basalts on a 130 km long part of the spreading axis representing the largest known occurrence of andesites on a submarine portion of a spreading axis. The andesites and dacites occur on topographic highs of the axis and formed by fractional crystallization from basaltic parent magmas but also assimilated hydrothermally altered material. Importantly, the andesites show depletions of Nb contents relative to other incompatible elements, a signature typical of the continental crust. Silicic magmas generated at plume-influenced oceanic spreading axes could have contributed significantly to the generation of continental crust.

The oceanic and the continental crust are fundamentally different. The oceanic crust has a basaltic mean composition while the continental crust has an andesitic average composition. Furthermore, the oceanic crust is much more homogeneous than the continental crust and evolved rocks with SiO₂ contents above 52 wt.% (andesites, dacites and rhyolites) are very rare. SiO₂-rich magmas have been observed on oceanic spreading axes mostly close to hotspots and the best known region with abundant andesitic to rhyolitic lavas is Iceland, which is underlain by a deep mantle plume and a thick basaltic crust. The origin of silicic magmas in the oceans is not clear and they may form (1) by extreme fractional crystallization of basaltic magmas, (2) by re-melting of plagiogranites [2], or (3) by melting amphibolitized

parts of the oceanic lower crust [e.g. 3]. The formation of larger volumes of andesites to rhyolites in the oceans has also been suggested to be a possible precursor to the formation of parts of the early continental crust of the Earth in the Archean [e.g. 4].

The study region on the PA-EPR consists of a magmatically robust spreading segment bounded by two large overlapping spreading centres at latitudes 36°S and 41.5°S. The spreading axis is formed by a 2 to 5 km wide volcanically active axial ridge containing an up to 200 m wide axial summit trough with the youngest volcanism [5], typical for a fast-spreading axis with a full spreading rate of ~10 cm/yr. The water depth along the spreading axis varies from an average depth of 2200 m at 37.5°S towards a depth of 2500 m at 40°S. The shallow region of the PA-EPR, at 37.5°S, marks the point of intersection with the Foundation Seamount chain (Fig. 1a). The Foundation Seamount chain (FSC) probably formed above a deep mantle plume because the voluminous intraplate volcanoes build by it show an age-progression along the chain with the youngest volcanoes lying close to the PA-EPR [6, 7]. Geophysical studies suggest that the location of the plume is probably very close to the PA-EPR beneath the volcanic ridges [8]. Our new data of lavas from the axial summit trough show that the most enriched basalts ($^{206}\text{Pb}/^{204}\text{Pb}$ 19.4) occur at about 37.5°S on the PA-EPR, decreasing both to the north and to the south (Fig. 1b). The isotopic gradient reflects southward flow of enriched material from the Foundation plume along the spreading axis. This gradient is similar to the situation at other regions where mantle plumes flow into spreading axes, e.g. Galapagos or Iceland [9, 10] and reflects either mixing of the plume with depleted asthenospheric material [11] or increasing depletion by increasing melting of a heterogeneous plume [12]. Both the $^{206}\text{Pb}/^{204}\text{Pb}$ isotope gradient and the increasing water depths suggest an asymmetric and mainly southward directed material flow along the PA-EPR (Fig. 1). It has been shown previously that andesites occur in this region of plume inflow [13] but our new sampling indicates abundant andesitic and dacitic lavas between 37°S and 38.2°S (Fig. 1c) and again at 39.5°S, i.e. in an about 130 km long portion of the PA-EPR which is the largest occurrence of evolved rocks on the Earth's spreading system so far. The fact that basalts and andesites on the PA-EPR occur in the same narrow neovolcanic zone with a width of 100 to 200 m suggests that the changes in magma composition occur at time scales of perhaps 2,000 years because the fast spreading rate carries the crust rapidly away from the active zone. On the PA-EPR, the abundance of evolved lavas is not directly related to rift propagation because the andesites erupt in relatively stable regions of the segment distant from the ends of large overlapping spreading centres (Fig. 1). The evolved melts form beneath axis highs where the largest volumes of magma may rise into the shallow crust. The

occurrence of abundant hydrothermal activity in these regions implies an effective cooling at the these axial highs. This situation is similar to the central volcanoes observed in Iceland and in Afar where silicic lavas occur frequently at the sites of dike formation and rift propagation [14, 15]. We suggest that the volcanic cycle on the PA-EPR ends with the eruption of silicic lavas following the ascent of large volumes of basalts from the mantle and their eruption along several km long rifts. The occurrence of the silicic lavas of the PA-EPR differs from that of the submarine andesitic to rhyodacitic lavas from the Galapagos spreading centre which are restricted to the tips of two large propagating rifts [16, 17].

The origin of SiO₂-rich melts at oceanic spreading centres has been explained by two processes; (1) fractional crystallization of a basaltic melt [16, 18], and (2) melting of hydrothermally metamorphosed amphibolitic lower crust [3, 19]. Most andesites and dacites of the PA-EPR lie on a trend typical for fractional crystallization but the composition of the most evolved lavas could also be explained by melting of crustal amphibolite at low pressures (Fig. 2). For example, the TiO₂ contents in basaltic lavas increase to about 4% MgO whereas lavas with MgO contents below 4% have low Ti concentrations which could reflect the crystallization and fractionation of Ti-magnetite. Some andesites show low TiO₂ and SiO₂ contents at a given MgO concentration indicating that these magmas formed by mixing of an andesite with a basaltic liquid. The trends observed in the PA-EPR lavas generally resemble the variations found in magmas from the Galapagos spreading centre. Several evolved lavas on the PA-EPR have formed by magma mixing between an SiO₂-rich melt with about 2% MgO and a basaltic melt with about 6% MgO because their compositions lie along mixing trends rather than on a fractionation trend (Fig. 2a) and they contain abundant xenocrysts of olivine, clinopyroxene and plagioclase. Possibly the replenishment of an andesitic magma lens by basaltic melts leads to the eruption of well mixed hybrid lavas.

The andesites and dacites of the PA-EPR have higher Cl/K and ⁸⁷Sr/⁸⁶Sr than the basalts implying that they assimilated some seawater altered material. The andesites and dacites of the PA-EPR show increased Cl/K ratios compared to the basalts which generally have Cl/K similar to the estimated mantle value of about 0.1 (Table 1). The high Cl/K imply assimilation of hydrothermally altered crustal material which has also been observed in other lava suites from oceanic spreading axes [20, 21]. We also find a positive correlation between ⁸⁷Sr/⁸⁶Sr and ²⁰⁶Pb/²⁰⁴Pb (Fig. 3a) reflecting binary mixing between a radiogenic Foundation plume component and unradiogenic upper mantle material. Importantly, the andesitic and dacitic lavas have strongly increased ⁸⁷Sr/⁸⁶Sr for a given ²⁰⁶Pb/²⁰⁴Pb (Fig. 3a) in agreement with the assimilation of hydrothermally altered material with high ⁸⁷Sr/⁸⁶Sr. Assimilation-

fractional crystallization modelling using an altered crust composition with increased $^{87}\text{Sr}/^{86}\text{Sr}$ of 0.704 suggests that the andesites may have assimilated up to 25% of altered crust. The fact that not all andesites show the increased Sr isotope ratios implies that the reaction with altered crust is not a necessary prerequisite for andesite/dacite formation and that crystal fractionation must be more important than the assimilation process. Only the uppermost 1 to 1.5 km of the oceanic crust shows significantly raised Sr isotope compositions due to reaction with seawater [22] and thus the evolved melts must have assimilated at very shallow levels in the crust. A shallow magma lens at ~ 1.5 km beneath the highs at the PA-EPR is in agreement with predictions from the thermal structure of very fast spreading centres [23].

However, melting of amphibolite may cause significant fractionation of different incompatible element ratios, for example, Nb/Ta. The andesites have the same Nb/Ta as the basalts but much higher Hf/Sm (Fig. 4) requiring melting of 30 to 50% of amphibolite and/or that fractional crystallization fractionates Nb relative to the REE but not Nb/Ta. Consequently, a generation of the andesites from amphibolite melting appears unlikely unless most of the amphibole is molten which occurs by dehydration melting at temperatures up to 950°C . We conclude that the evolved magmas largely result from crystal fractionation processes. An interesting feature of the evolved lavas of the PA-EPR is their depletion of Nb relative to other incompatible elements like U, Th or La (Fig. 4b). The basalts have Nb/La of about 1 which is in the range of typical oceanic lavas [24]. In contrast, the SiO_2 -rich lavas have much lower Nb/La (and also Nb/U) indicating that these melts lost Nb preferentially relative to other incompatible elements. The lavas with less than 4% MgO have low Nb/La suggesting that the Nb depletion is probably due to the crystallization of Ti-magnetite at a late stage of fractional crystallization. Nb is compatible in Ti-magnetite while La is incompatible [25] and thus Ti-magnetite fractionation effectively reduces Nb/La (and Nb/Th) in the andesitic and dacitic melts. On the other hand, the Cr-Al spinels crystallizing from basaltic melts do not contain significant amounts of Nb so that the basalts show high Nb/La. The basaltic stage marks the time of crustal formation and the residual melts in the magma lenses beneath the PAR have time to fractionate and form andesites or even dacites.

The continental crust has an andesitic composition and low Nb relative to other incompatible elements like La or Th and it has been proposed that parts of the continental crust (especially in the Archean) may have formed from evolved lavas at oceanic plateaus [4]. Our data from the PA-EPR suggest that spreading centres with relatively thin crust may also be sites of formation of silica-rich magmas with relative Nb depletions and could have important implications for the generation of the earliest continental crust on Earth.

Importantly, the fact that evolved lavas with a deficit of Nb relative to other incompatible elements form at plume-influence spreading axes has significant influence on the mass balance of continental crust formed by subduction processes relative to plume-related crust formation [26]. The lower Nb/La of some plume-related magmas may indicate that the relative proportion of continental crust formed in oceanic plateau settings is higher than previously assumed. Furthermore, many large sulfide ore deposits of copper, zinc and other metals occur together with silicic volcanic rocks and it has been established that some, for example in the Canadian Abitibi province, may have formed at oceanic spreading axes [27, 28]. The abundant hydrothermal activity at the southern EPR together with the relatively large volume of silicic lavas may represent a recent example for the formation of such deposits.

Acknowledgments

We thank Captain Papenhagen and his crew for their help during the cruise and the BMBF for funding of this project through grant 03G0157A.

References

- 1 A.W. Hofmann, Chemical differentiation of the Earth: the relationship between mantle, continental crust, and oceanic crust, *Earth and Planetary Science Letters* 90, 297-314, 1988.
- 2 H. Sigurdsson, Generation of Icelandic rhyolites by melting of plagiogranites in the oceanic layer, *Nature* 269, 25-28, 1977.
- 3 R.K. O'Nions and K. Grönvold, Petrogenetic relationships of acid and basic rocks in Iceland: Sr-isotopes and rare-earth elements in late and postglacial volcanics, *Earth and Planetary Science Letters* 19, 397-409, 1973.
- 4 F. Albarède, The growth of continental crust, *Tectonophysics* 296, 1-14, 1998.
- 5 P. Lonsdale, Geomorphology and structural segmentation of the crest of the southern (Pacific-Antarctic) East Pacific Rise, *Journal of Geophysical Research* 99, 4683-4702, 1994.
- 6 J.M. O'Connor, P. Stoffers and J.R. Wijbrans, Migration rate of volcanism along the Foundation Chain, SE Pacific, *Earth and Planetary Science Letters* 164, 41-59, 1998.
- 7 C.W. Devey, R. Hékinian, D. Ackermann, N. Binard, B. Francke, C. Hémond, V. Kapsimalis, S. Lorenc, M. Maia, H. Möller, K. Perrot, J. Pracht, T. Rogers, K. Stattegger, S. Steinke and P. Victor, The Foundation Seamount Chain: a first survey and sampling, *Marine Geology* 137, 191-200, 1997.
- 8 M. Maia, C. Hémond and P. Gente, Contrasted interactions between plume, upper mantle, and lithosphere: Foundation chain case, *Geochemistry Geophysics Geosystems* 2, 10.1029/2000GC000117, 2001.
- 9 S.P. Verma, J.-G. Schilling and D.G. Wagoner, Neodymium isotopic evidence for Galapagos hotspot-spreading centre system evolution, *Nature* 306, 654-657, 1983.
- 10 S.-S. Sun, M. Tatsumoto and J.-G. Schilling, Mantle plume mixing along the Reykjanes Ridge axis: lead isotopic evidence, *Science* 190, 143-147, 1975.
- 11 J.-G. Schilling, Iceland mantle plume: geochemical study of Reykjanes Ridge, *Nature* 242, 565-571, 1973.
- 12 J. Phipps Morgan and W.J. Morgan, Two-stage melting and the geochemical evolution of the mantle: a recipe for mantle plum-pudding, *Earth and Planetary Science Letters* 170, 215-239, 1999.

- 13 R. Hékinian, P. Stoffers, D. Ackermann, S. Revilleon, M. Maia and M. Bohn, Ridge-Hotspot interaction: The Pacific-Antarctic Ridge and the Foundation seamounts, *Marine Geology* ?, 1999.
- 14 P. Lahitte, P.-Y. Gillot and V. Courtillot, Silicic central volcanoes as precursors to rift propagation: the Afar case, *Earth and Planetary Science Letters* 207, 103-116, 2003.
- 15 K. Saemundsson, Outline of the geology of Iceland, *Jökull* 29, 7-28, 1979.
- 16 G.R. Byerly, W.G. Melson and P.R. Vogt, Rhyodacites, andesites, ferro-basalts and ocean tholeiites from the Galapagos spreading center, *Earth and Planetary Science Letters* 30, 215-221, 1976.
- 17 D.M. Christie and J.M. Sinton, Evolution of abyssal lavas along propagating segments of the Galapagos spreading center, *Earth and Planetary Science Letters* 56, 321-335, 1981.
- 18 D.M. Christie and J.M. Sinton, Major element constraints on melting, differentiation and mixing of magmas from the Galapagos 95.5°W propagating rift system, *Contributions to Mineralogy and Petrology* 94, 274-288, 1986.
- 19 B.D. Marsh, B. Gunnarson, R. Congdon and R. Carmody, Hawaiian basalt and Icelandic rhyolite: indicators of differentiation and partial melting, *Geologische Rundschau* 80, 481-510, 1991.
- 20 P.J. Michael and J.-G. Schilling, Chlorine in mid-ocean ridge magmas: Evidence for assimilation of seawater-influenced components, *Geochimica et Cosmochimica Acta* 53, 3131-3143, 1989.
- 21 P.J. Michael and W.C. Cornell, Influence of spreading rate and magma supply on crystallization and assimilation beneath mid-ocean ridges: Evidence from chlorine and major element chemistry of mid-ocean ridge basalts, *Journal of Geophysical Research* 103, 18325-18356, 1998.
- 22 J.C. Alt, Hydrothermal alteration and mineralization of oceanic crust: Mineralogy, geochemistry, and processes, in: *Volcanic-associated massive sulfide deposits: Processes and examples in modern and ancient settings*, C.T. Barrie and M.D. Hannington, eds., pp. 133-155, Soc. Econ. Geol., Ottawa, 1999.
- 23 G.M. Purdy, L.S.L. Kong, G.L. Christeson and S.C. Solomon, Relationship between spreading rate and the seismic structure of mid-ocean ridges, *Nature* 355, 815-817, 1992.

- 24 A.W. Hofmann, K.P. Jochum, M. Seufert and W.M. White, Nb and Pb in oceanic basalts: new constraints on mantle evolution, *Earth and Planetary Science Letters* 79, 33-45, 1986.
- 25 R.L. Nielsen, L.M. Forsythe, W.E. Gallahan and M.R. Fisk, Major- and trace-element magnetite-melt equilibria, *Chemical Geology* 117, 167-191, 1994.
- 26 R.L. Rudnick, Making continental crust, *Nature* 378, 571-578, 1995.
- 27 C.T. Barrie, J.N. Ludden and T.H. Green, Geochemistry of volcanic rocks associated with Cu-Zn and Ni-Cu deposits in the Abitibi subprovince, *Economic Geology* 88, 1341-1358, 1993.
- 28 S.J. Piercey, S. Paradis, D.C. Murphy and J.K. Mortensen, Geochemistry and peteotectonic setting of felsic volcanic rocks in the Finlayson Lake volcanic-hosted massive sulfide district, Yukon, Canada, *Economic Geology* 96, 1877-1905, 2001.
- 29 T.C. Juster, T.L. Grove and M.R. Perfit, Experimental constraints on the generation of FeTi basalts, andesites, and rhyodacites at the Galapagos spreading center, 85°W and 95°W, *Journal of Geophysical Research* 94, 9251-9274, 1989.
- 30 J.S. Beard and G.E. Lofgren, Dehydration melting and water-saturated melting of basaltic and andesitic greenstones and amphibolites at 1, 3, and 6.9 kb, *Journal of Petrology* 32, 365-401, 1991.
- 31 F.J. Spera and W.A. Bohrson, Energy-constrained open-system magmatic processes; I, General model and energy-constrained assimilation and fractional crystallization (EC-AFC) formulation, *Journal of Petrology* 42(5), 999-1018, 2001.

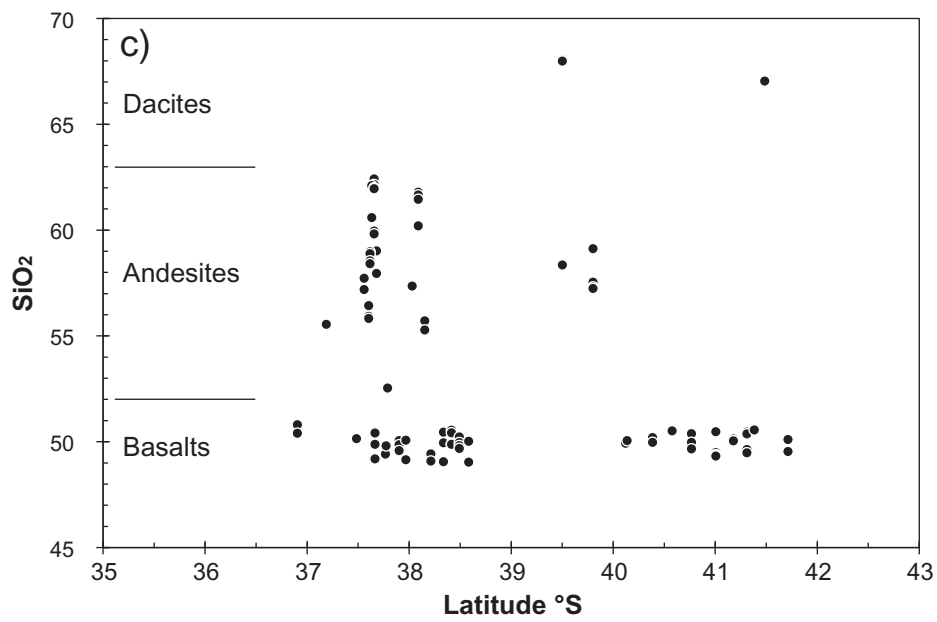
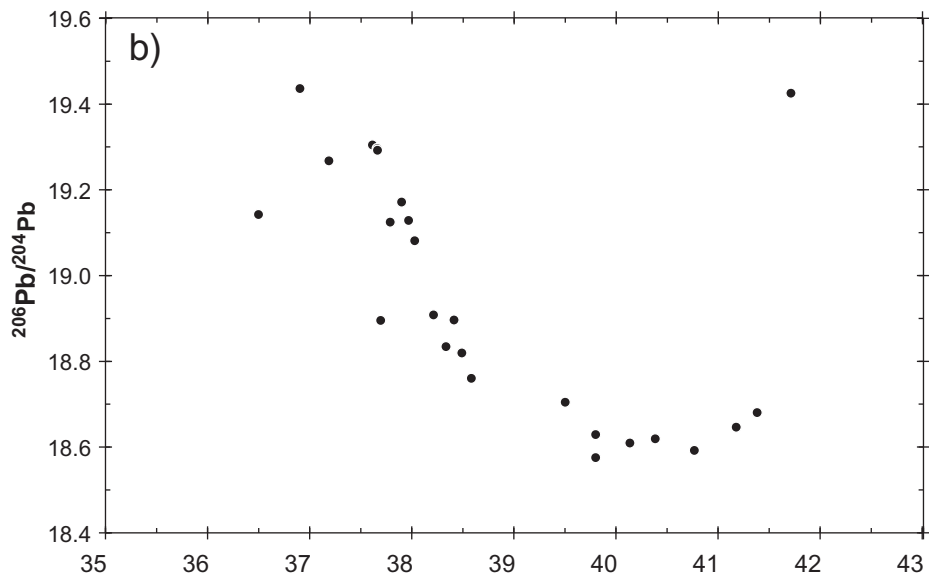
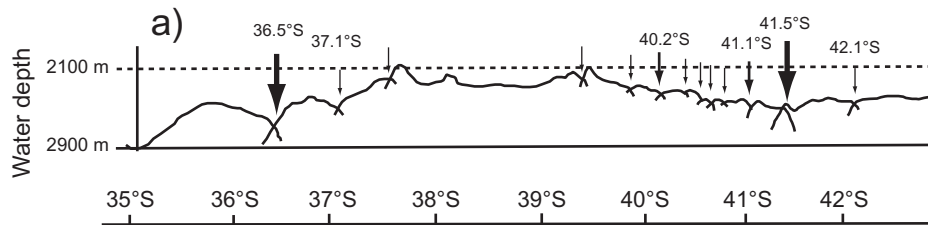
Figure captions

Figure 1: (a) Variation of water depth along the Pacific Antarctic Ridge (PAR) and the locations of major offsets in the volcanically active zone after Lonsdale [5]. (b) Variation of the SiO₂ contents in volcanic glasses dredged along the PAR showing a large region with bimodal volcanism, i.e. erupting both basaltic and andesitic lavas. (c) Variation of the ²⁰⁶Pb/²⁰⁴Pb isotope ratios of the recovered lavas indicating the inflow of plume material with high Pb isotopes into the spreading axis near the Foundation Hotspot and mixing along the axis.

Figure 2: Variation of (a) SiO₂ and (b) TiO₂ versus MgO of the PAR lavas together with an experimentally determined trend of fractional crystallization [29] and the compositions of melts formed at low pressures from amphibolite [30]. While basaltic lavas lie on the fractionation trend, most of the andesites may be formed either by fractional crystallization or partial melting of the crust. Several andesites lie along a mixing trend between a basaltic and an andesitic magma.

Figure 3: Strontium isotopes versus (a) ²⁰⁶Pb/²⁰⁴Pb and (b) versus Sr concentrations suggesting binary mixing between the Foundation Hotspot source and an unradiogenic source for the basalts. Several andesites and dacites have significantly higher ⁸⁷Sr/⁸⁶Sr for a given Pb isotope ratio compared to the basalts indicating assimilation of altered oceanic crust with an ⁸⁷Sr/⁸⁶Sr of 0.704. Lines show results of the EC-AFC model [31] indicating up to 25% assimilation and 40% fractional crystallization to explain the observed variation.

Figure 4: (a) Nb/Ta versus Zr/Sm and (b) Nb/La versus (La/Sm)_N showing that andesites and dacite have similar Nb/Ta as the basalts but higher Zr/Sm. Lines shows melting path of amphibolite suggesting that amphibolite cannot explain the increased Zr/Sm. The PAR andesites and dacites have similar Nb/La and La/Sm as some Archean volcanic rocks from the Abitibi Belt, Canada, associated with large sulfide deposits.



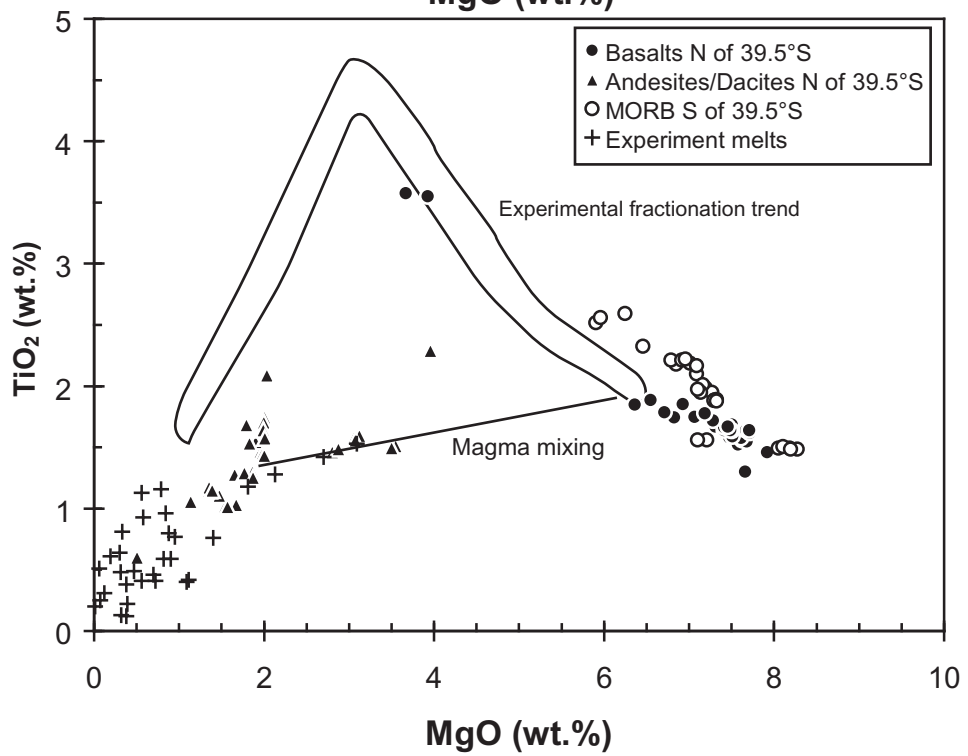
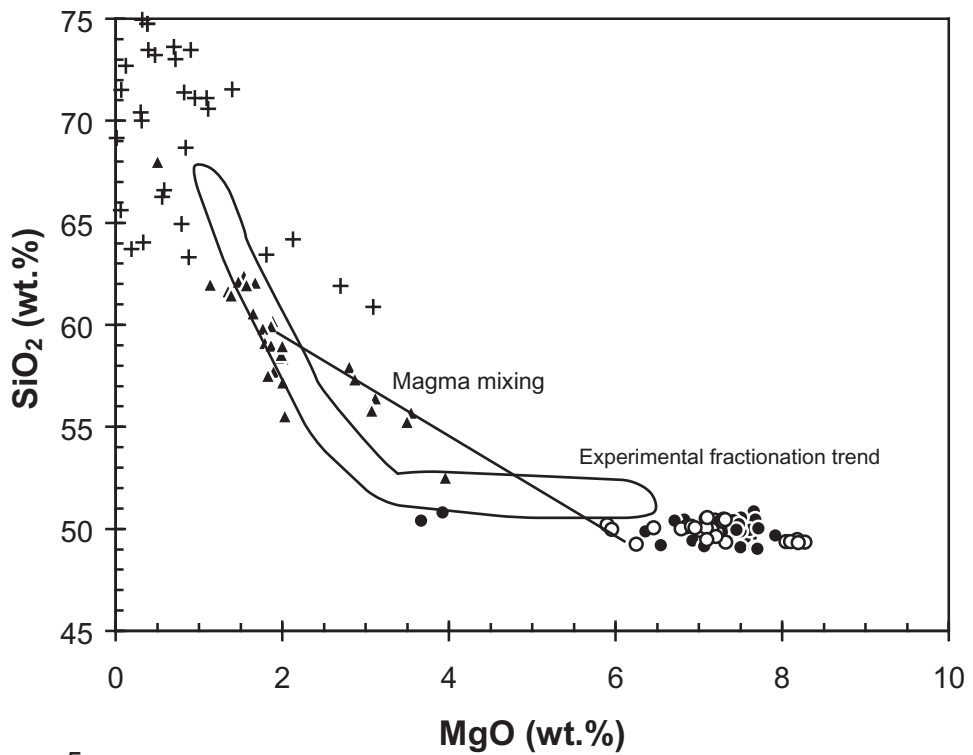


Figure 2

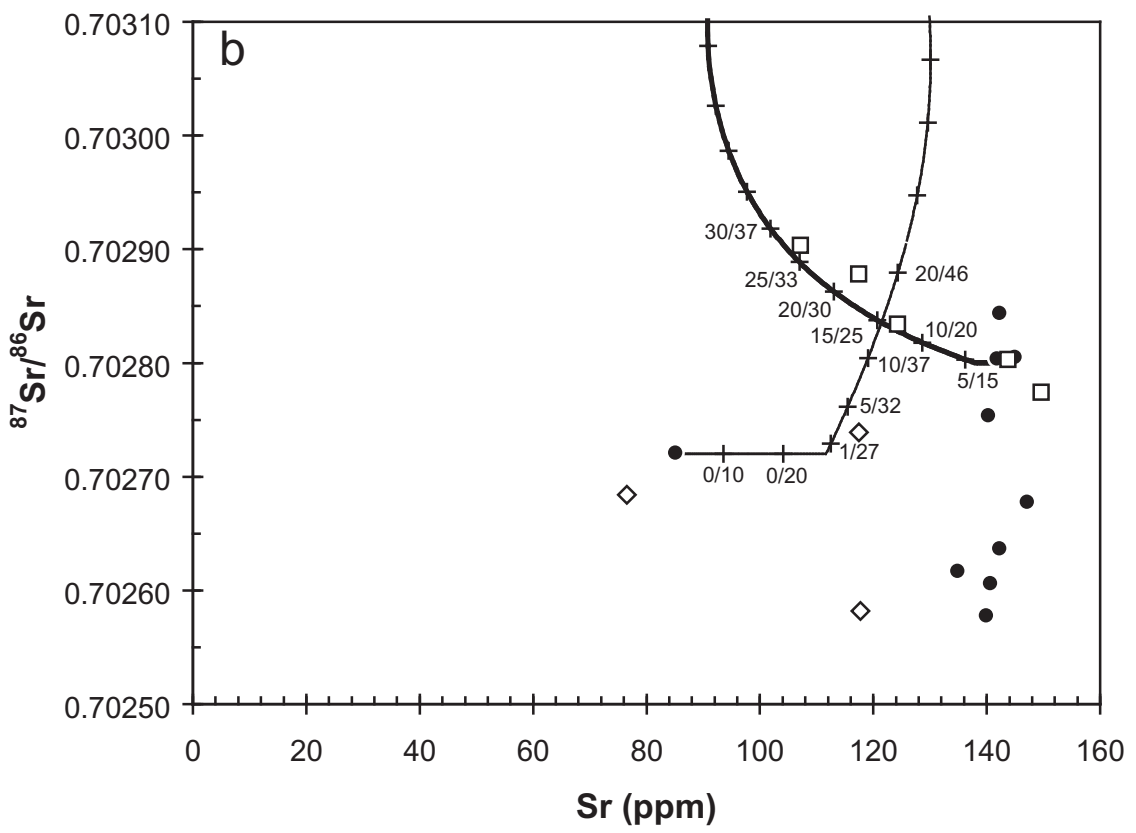
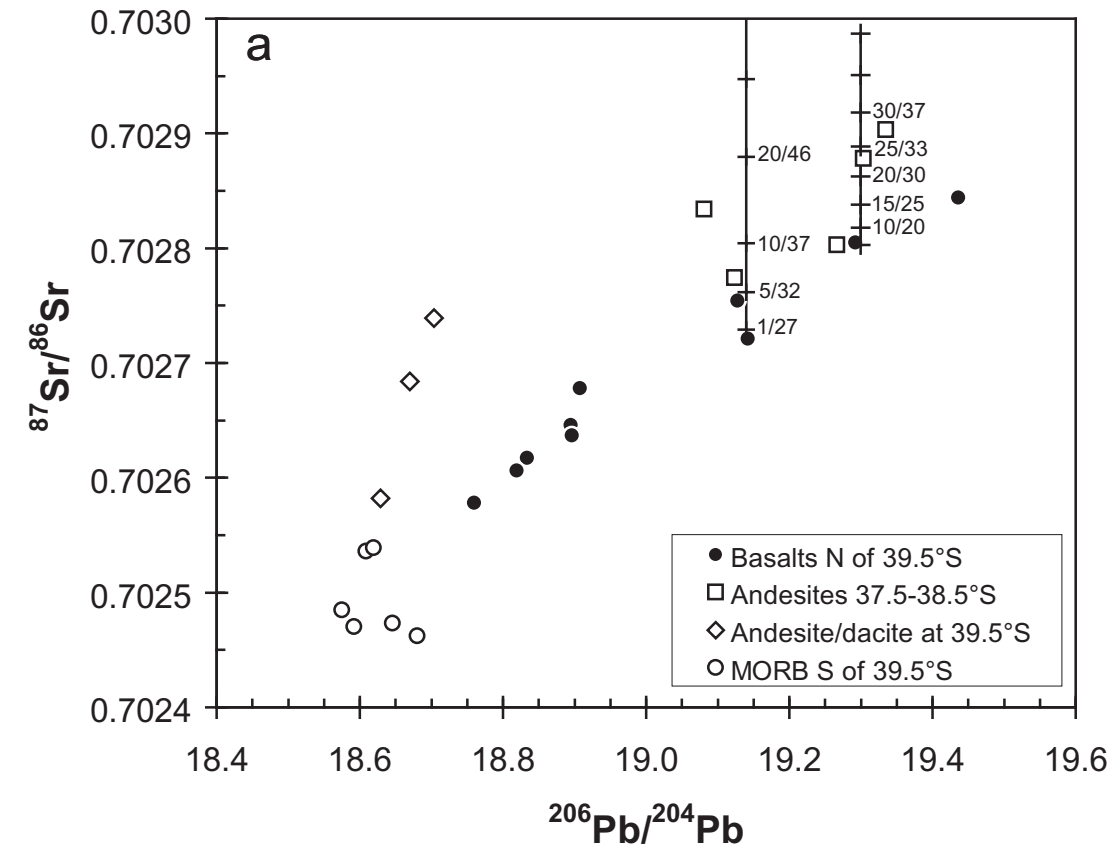


Figure 3

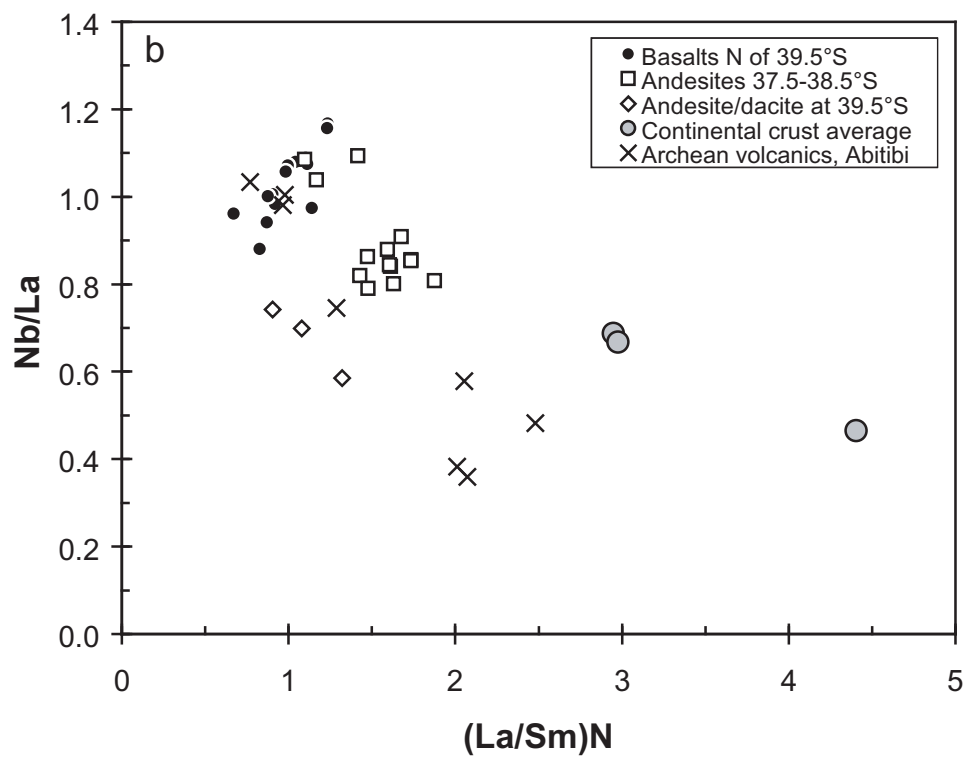
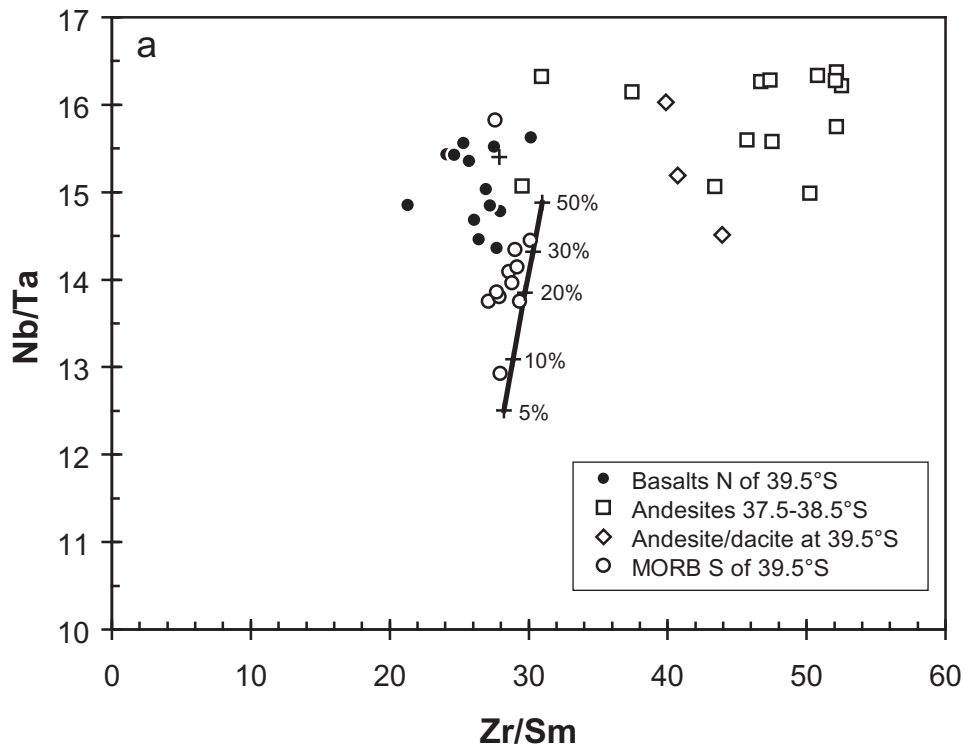


Figure 4

**Stroncik, N. A., Haase, K. M., and Stoffers, P.
Geochemical Case Study of a Ridge Approaching a
Plume – Plume-Ridge Interaction between the
Foundation Plume and the Pacific-Antarctic-East-
Pacific Rise (PA-EPR). To be submitted to Earth and
Planetary Sciences Letters.**

Geochemical Case Study of a Ridge Approaching a Plume – Plume-Ridge Interaction between the Foundation Plume and the Pacific-Antarctic-East-Pacific Rise (PA-EPR)

Nicole A Stroncik, Karsten M. Haase, and Peter Stoffers

Institut für Geowissenschaften der Christian-Albrechts-Universität zu Kiel, D-24118 Kiel, Germany

Abstract

Glassy to phyric submarine lavas were dredged from 36 sites along the PA-EPR at its intersection with the Foundation Seamount Chain between latitudes 36.5°S and 41.5°S. The Foundation plume creates an about 350 km wide geochemical anomaly, between latitudes 36.5 and 39.8°S, along the PA-EPR. Even though this geochemical anomaly roughly coincides with the extension of the bathymetric anomaly generated by the plume no increased degree of melting is observed at the loci of maximum plume influx at the ridge, indicating a low mantle excess temperature. The relatively small size of the anomaly, compared to plume-ridge interaction settings such as Galapagos and Easter, implies a relatively low plume flux for the Foundation plume. In general, mid-ocean ridge basalt (MORB) along the anomaly is variably enriched in incompatible elements and radiogenic isotopes derived from the Foundation plume, with the borders between plume influenced and non influenced MORB, to the north and to the south, coinciding with two, large overlap spreading centres (OSCs). Strong southerly isotopic gradients extending from the point of maximum plume influx suggest a mainly southward directed plume flow along this southward propagating ridge. Mixing between the enriched plume material and the MORB material probably takes place during this horizontal flow of molten plume material in the partially molten asthenosphere. In general, it can be stated that the chemistry of the investigated mid-ocean ridge lavas is a direct consequence of the magmatic domain prevailing along a mid-ocean ridge in close proximity to a mantle plume and two ridge offset.

Introduction

Mantle plumes and mid-ocean ridges are common features all around our globe and represent the main loci, in addition to subduction zones, at which mass- and thermal-fluxing between the Earth's interior and surface takes place. In areas where mantle plumes are located in the vicinity of mid-ocean ridges those flows, which under "normal" circumstances are working independently, interact, and it has been established in the last years that the dispersal of plume flows within the upper mantle can be strongly altered by mid-ocean ridges [1-7]. In this context three types of plume-ridge interaction have been recognised: (1) ridges approaching plumes (e.g. Louisville, Foundation), (2) plumes being situated directly beneath ridges (e.g.

Iceland, Azores) and (3) ridges drifting away from plumes (e.g. Ascension, Reunion, Galapagos). Whereas the last two types of plume-ridge interaction have been studied intensively, studies on the first type, of a ridge approaching a plume, are scarce. A number of geophysical and geochemical information have been obtained by those studies: (1) bathymetric, gravitational and thermal anomalies are found at ridges influenced by plumes, (2) crustal thickening has been observed, (3) age-progression of the hot-spot track is obscured near the ridge, (4) gaps in the hot-spot track can occur, (5) ridge lavas show enrichment by plume material, (6) off-axis seamounts exhibit compositional mixtures between both magma sources and (7) along-axis chemical, thermal and bathymetric gradients can be observed. Based on these observations a variety of models concerning the mode of flow between plumes and mid-ocean ridge have been developed [1, 2, 8-12].

Basically, the foundation of all of these models is the cognisance that some sort of asthenospheric flow is generated between the plume and the ridge. The most prominent of those models is the so-called mantle-plume source / migrating-ridge sink model (MPS/MRS) developed by Schilling and co-workers [5, 13, 14], in which the mid-ocean ridge acts as a sink, draining the buoyant plume material along a sublithospheric channel into the ridge. When the plume is centred beneath the ridge the preferential flow direction is along axis, roughly symmetrical about the plume. As the plume moves away from the ridge the plume develops a preferential non-radial flow towards the migrating ridge which continues to act as a sink, using the channel progressively “carved” by the plume itself from the time it was ridge centred. Based on these model Schilling postulated that the along-axis extension of the plume introduced anomaly is directly related to the distance between the plume and the ridge [5, 13] and that the width of the anomaly is directly related to the size of the plume and thus can be a measure for the plume flux [5, 6, 13, 15]. Both inferences can only be adequately proofed by the study of different plume-ridge interaction settings in nature. The main driving force for plume flow to the ridge is the natural buoyancy of the plume material together with the magnitude of plume flux in conjunction with the basal structure of the lithosphere [2, 4, 5, 14]. Experiments in conjunction with numerical modelling largely support the MPS/MRS model and put further constrains on the different parameters influencing the plume flow to the ridge, such as viscosity of the plume material, ridge spreading rate or ridge migration velocity [1, 2, 8, 11, 15-17]. Nonetheless one of the major aspects in the study of plume-ridge interaction, namely the physical state of the plume material (solid, highly viscous material, melt) flowing to the ridge, still remains a highly debated matter, which can only beyond doubt be resolve by extensive geochemical studies of MORBs influenced by plumes.

In this context the Foundation-PA-EPR region not only provides the opportunity to study another case of plume-ridge interaction but to study the case of a ridge approaching a plume. Previous surveys of the region have established that the Foundation plume influences the PA-EPR, creating a bathymetrical and thermal anomaly of about 350 km length [18, 19]. The size of the geochemical anomaly is, up to now, not really known, since previous projects were determined on the investigation of the Foundation Seamount Chain (FSC). Anyway a width of the along axis geochemical anomaly ranging between 100 and 200 km has been proposed [18, 20-22]. In this paper we will focus on the spatial distribution of Sr-, Nd- and Pb-isotopes in conjunction with trace elements in order to establish the magnitude of plume-influence on the

ridge and to model the nature of plume-ridge interaction along the PA-EPR to put further constraints on the mode of material flow in plume-ridge interaction settings. For this reason we are not going to discuss the results of the entire sample suite obtained, but are going to focus on the volcanics sampled between 36.5°S and 40.5°S along the ridge axis.

Geologic Setting

The PA-EPR is the roughly NNE-SSW trending, 2500 km long southward continuation of the tropical East-Pacific-Rise (EPR) separating the relatively fast moving Pacific Plate and the near stationary Antarctic Plate. To the north, at latitude 35°S, the PA-EPR is bounded by the Juan Fernandez Triple junction and to the south, at latitude 56°S, by the Heezen transform fault, which is the northern most member of the large Eltanin fault system. In general, the PA-EPR consists of six, variably long (between 150 and 560 km), first and second order segments separated by transform and non-transform offsets. The northern three segments, having a total length of 1650 km, are separated by two large, left stepping overlap spreading centres with lateral displacements of 27 and 45 km respectively. The southern segments, having a total length of 850 km, are separated by one left-lateral and two right-lateral transform fault systems with lateral displacements ranging between 60 and 200 km. This contrast in segmentation style is mainly thought to be caused by the increase in spreading rate from the south to the north, which raises the minimum threshold for the minimum length of stable transform fault systems [23, 24]. The spreading rate along the PA-EPR increases northward from about 8.4 cm/a at 56°S to 10 cm/a at 35°S. The northern three segments are further subdivided, by medium and small overlap spreading centres, into several third order segments, with lateral displacements of 12 to 5 and 5 to 2 km respectively. The length of the structurally defined spreading segments separated by those non-transform offsets varies between 15 and 250 km. In addition to these overlap centres of variable dimensions there are many smaller (< 2 km) lateral shifts distributed along the axes resulting in small bends of parts of the axial ridge system, defining fourth order segments.

Considering spreading axes geomorphology the PA-EPR is a typical fast spreading ridge system dominated by axial ridges oriented perpendicular to the spreading direction and volcanic rift zones situated along their crests. At special tectonic settings spreading axes geomorphologies typical for medium to slow spreading mid ocean ridges, such as axial ridges with crests lower than adjacent fault blocks or well-developed axial rift valleys, are occurring. The prominently above the abyssal hill terrain rising axial ridges are generally up to 20 km wide and mostly of triangular cross section. Ridge depth increases from the north to the south. Along axis profiles are mainly characterised by low bathymetrical gradients producing axial ridges with rather flat instead of humped along axis morphologies. An exception to this is segment 2 along which the majority of samples presented here have been obtained.

The entire sampling area, which is situated between latitudes 36°50'S and 41°50'S, not only comprises segment 2 but also the northern most tip of segment 3 and the large overlap basin separating these two second order segments of the PA-EPR (Fig.: 1). Yet segment 2 is, caused

by its close proximity to the Foundation hotspot, particularly attention-grabbing and many of the geomorphological features observed along this segment have their origin in this proximity. The Foundation hotspot is thought to be situated 35 km west of the northern part of segment 2, at latitude $\sim 37.5^\circ$ [18, 19]. Segment 2 is with its 2300 m average depth anomalously shallow compared to the 2800 m average depth normal for the EPR. Its axial ridge is riddled with small volcanic cones resulting in a rather hummocky geomorphology with steep along axes bathymetrical gradients compared to the mainly smooth geomorphology being typical for “normal” sections of the PA-EPR and the EPR. The 460 km long segment 2 is further partitioned by 7 third order and a larger number of fourth order discontinuities into several segments ranging in length between 5 and 78 km (Fig.: 1). The third order discontinuities, which consist of six left stepping and one right stepping OSC, are located between latitudes $37^\circ 22'S$ and $41^\circ 20'S$. The majority of those OSCs is located between latitudes $39^\circ 85'S$ and $41^\circ 20'S$ thus leaving about 50 % of the entire segment 2 rather undisturbed of major ridge break ups (Fig.: 1). The ridge axis displacement at these OSCs varies between 0.85 and 9 km, with overlap lengths being between 9.5 and 34.5 km. The size of the depth anomalies created at those OSCs varies between 15 and 460 m (Fig.: 1). Fourth order discontinuities in the form of devils are located along the entire ridge segment. Even though these devils are associated with ridge bends resulting in changes of strike direction of the ridge between 3 and 10° they are not associated with depth anomalies or ridge break ups and axes displacements.

A detailed discussion of the geomorphology and structural segmentation of the PA-EPR along with the tectonic processes being responsible for their formation has been conducted by Lonsdale in 1994 [24].

Sampling and Analytical methods

The samples investigated in this study have been obtained in June and July 2001 during the cruise SO157 of the German research vessel FS Sonne. The recovered samples range from aphyric to sparsely phyrlic lavas and pillows of basaltic, andesitic and dacitic composition (Table 1), with the majority of samples containing fresh glass. Glass particles of 120 different samples have been analysed by means of electron microprobe (EMP) at the Institut für Geowissenschaften of the Christian-Albrechts-Universität Kiel, using a JEOL Superprobe 8900 and standard wavelength dispersive techniques. The instrument has been operated at an accelerating voltage of 15 kV and beam currents of 20 nA. The beam diameter during standardisation and measurement has been set at 12 μm . Counting times on peaks and background varied depending on the element analysed, having been set to 20 seconds for all major elements except Na_2O , S and Cl, which have been analysed with peak counting times of 10 and 180 seconds respectively. Background counting times have always been set to half of peak counting times. The quality of the data has been checked by repeated measurement of a set of glass standards for which the results are presented in Table 1. For trace element analysis glass shards have been hand picked under a binocular and washed with deionised water in an ultrasonic bath. The trace element concentrations of cleaned glasses have been

obtained using a Agilent 7500 ICP-MS at the Institut für Geowissenschaften of the Christian-Albrechts-Universität Kiel using methods described previously [25]. The data are shown in Table ? together with the average values determined for the international standards BHVO-1 and BIR-1. The reproducibility is found to be better than 2% whereas the accuracy ranges from < 5% for the rare earth elements (REE), Rb, Sr, Ba and Nb, to < 10% for the other elements. The analysis of isotopes has been conducted on rock powders of hand picked glass shards which have been leached for one hour in hot ultra pure 6N HCl before dissolution. The ion exchange techniques used to produce Sr, Nd, and Pb separates has been described by [26]. Sr and Pb isotope ratios have been analysed using a Finnigan MAT 262 mass spectrometer in static mode at GEOMAR, Kiel. The Nd isotope compositions have been analysed in dynamic mode on the same machine. Applied isotope fractionation corrections for Sr have been $^{86}\text{Sr}/^{88}\text{Sr} = 0.1194$ and $^{146}\text{Nd}/^{144}\text{Nd} = 0.7219$, with repeated measurements of NBS 987 (n = 12) yielding $^{87}\text{Sr}/^{86}\text{Sr} = 0.710218$ ($2\sigma = 0.000024$). Repeat measurements of the Nd Spex standard (n = 10) and of the La Jolla standard (n = 3) gave an average of 0.511710 (15) $^{143}\text{Nd}/^{144}\text{Nd} = 0.511827$ ($2\sigma = 0.000007$). Our reported Sr and Nd analyses (Table 1) are normalised to values of NBS 987 and La Jolla of 0.71025 and 0.511855, respectively. Pb data have been fractionation-corrected using repeated measurements of NBS 981 (n = 13; errors are 2σ values; $^{206}\text{Pb}/^{204}\text{Pb} = 16.909 \pm 0.017$, $^{207}\text{Pb}/^{204}\text{Pb} = 15.455 \pm 0.022$, $^{208}\text{Pb}/^{204}\text{Pb} = 36.584 \pm 0.069$) normalised to its accepted values [27]. The relative precision per mass unit of the NBS 981 runs was <1 ‰ (2σ), and Pb blanks were negligible (<50 pg).

Results

The geochemical characteristics of magmas erupted along the PA-EPR between latitudes 36.5°S and 41.5°S are displayed in Fig. 2a-d. Those magmas can be, based on their isotope and trace element patterns, subdivided into two different magmatic suites: (1) a northern magmatic suite (NMS), extending from latitude 36.5°S to 39.8°S and (2) a southern magmatic suite (SMS), being positioned between latitudes 39.8°S and 41.5°S. The NMS consists of basalts and andesites (Table 1) exhibiting relatively large arrays in $^{87}\text{Sr}/^{86}\text{Sr}$ - (0.7025-0.7029), $^{206}\text{Pb}/^{204}\text{Pb}$ - (18.76-19.43) and $^{143}\text{Nd}/^{144}\text{Nd}$ -ratios (0.512987-0.513101) (Fig. 2a-d), being relatively enriched in incompatible elements (Fig. 2d). The lavas of this suite nearly span the same range in isotopic composition as those of the Foundation Seamount Chain (FSC). The degree of incompatible element enrichment of the NMS as well as their $^{87}\text{Sr}/^{86}\text{Sr}$ - and $^{206}\text{Pb}/^{204}\text{Pb}$ -ratios decrease along axes north and south of around 36.8° (Fig. 2a-d), whereas $^{143}\text{Nd}/^{144}\text{Nd}$ -ratios increase. As shown in Fig. 2a-d the southward decreasing gradient to low $^{87}\text{Sr}/^{86}\text{Sr}$ - and $^{206}\text{Pb}/^{204}\text{Pb}$ -ratios and high $^{143}\text{Nd}/^{144}\text{Nd}$ -ratios is rather smooth, whereas the boundary to lower $^{87}\text{Sr}/^{86}\text{Sr}$ - and $^{206}\text{Pb}/^{204}\text{Pb}$ -ratios and higher $^{143}\text{Nd}/^{144}\text{Nd}$ -ratios to the north seems to be rather sharp. Interestingly the transition zone from radiogenic to less radiogenic isotope compositions, and from incompatible element enrichment to “none”, coincides in both cases with major tectonic disturbances of the ridge axes, namely two large left-lateral overlap spreading centres (OSC) which are situated at about 36.5 and 39.5°S. In contrast to the NSM the SMS is mainly composed of basaltic rocks with relatively constant $^{87}\text{Sr}/^{86}\text{Sr}$ -ratios of around 0.7025 and with only mildly varying $^{206}\text{Pb}/^{204}\text{Pb}$ - and $^{143}\text{Nd}/^{144}\text{Nd}$ -ratios ranging

between 18.57 and 18.68 and 0.513094 and 0.513111 respectively, showing no distinct enrichment in incompatible elements. The larger scatter observed in the Sr-isotopic data of both suites compared e.g. to the Pb-isotopic data are caused by contamination processes of the primary magmas, as shown by the covariation of $^{87}\text{Sr}/^{86}\text{Sr}$ - with Cl/K-ratios (Fig. 3).

In general covariations in Sr, Pb and Nd isotope ratios as well as in incompatible element ratios can be observed in both magmatic suites, but with no overlaps occurring between the suites. The NMS exhibits negative trends between $^{143}\text{Nd}/^{144}\text{Nd}$ and both Sr and Pb isotopes and positive trends between $^{87}\text{Sr}/^{86}\text{Sr}$ and $^{206}\text{Pb}/^{204}\text{Pb}$, whereas the SMS shows negative trends between $^{143}\text{Nd}/^{144}\text{Nd}$ and $^{206}\text{Pb}/^{204}\text{Pb}$ and $^{87}\text{Sr}/^{86}\text{Sr}$ and $^{206}\text{Pb}/^{204}\text{Pb}$, but positive trends between $^{143}\text{Nd}/^{144}\text{Nd}$ and $^{87}\text{Sr}/^{86}\text{Sr}$ (Fig. 4a-c). Volcanics of the NMS generally show positive covariations between incompatible element ratios (e.g. Rb/Zr or $(\text{La}/\text{Ce})_{\text{N}}$), lying in elongation of the trend defined by lavas from the FSC, with $^{87}\text{Sr}/^{86}\text{Sr}$ and $^{206}\text{Pb}/^{204}\text{Pb}$, but correlate negatively with $^{143}\text{Nd}/^{144}\text{Nd}$ (Fig. 5a-c). Lavas of the SMS, on the other hand, show negative covariations between incompatible element ratios and $^{206}\text{Pb}/^{204}\text{Pb}$, but correlate positively with $^{87}\text{Sr}/^{86}\text{Sr}$ and $^{143}\text{Nd}/^{144}\text{Nd}$ (Fig. 5a-c). In general volcanics from the SMS reveal higher incompatible element ratios than those from the SMS (Fig. 5a-c).

All of the investigated MORBs from the PA-EPR show similar variations of Na10.0 versus $(\text{La}/\text{Sm})_{\text{N}}$ with MORBs from the NMS being more incompatible element enriched than those from the SMS, whereas the basalts from the FSC tend to higher Na10.0 and are even more incompatible element enriched (Fig. 6a). No correlation between Si10.0 and $(\text{Dy}/\text{Yb})_{\text{N}}$ can be observed in PA-EPR MORBs, in contrast to this the FSC lavas exhibit negative correlations between Si10.0 and $(\text{Dy}/\text{Yb})_{\text{N}}$ (Fig. 6b). In general the compositional and isotopic range observed in the NMS of the PA-EPR is comparable to this found in Easter Microplate MORBs or MORBs from the Galapagos spreading centre, even though the tectonic situation of the FSC-PA-EPR system is completely different from that of the other two.

Discussion

Constraints on the mantle sources generating the PA-EPR lavas – homogeneous versus heterogeneous plume source and asthenospheric mantle

As shown by the data presented above, variably incompatible element enriched MORB, compared to average EPR MORB [28], with relatively radiogenic Sr and Pb isotopes occurs on a roughly 350 km long section of the PA-EPR, between latitudes 36.5°S and 39.8°S (Fig. 2a-d), a geochemical anomaly being about 150 to 250 km wider than suggested in previous studies [18-20, 22]. As the degree of incompatible element enrichment of the investigated samples corresponds with changes in $^{87}\text{Sr}/^{86}\text{Sr}$, $^{206}\text{Pb}/^{204}\text{Pb}$ and $^{143}\text{Nd}/^{144}\text{Nd}$ isotope ratios (Fig. 5a-c) the observed variability in incompatible elements of the NMS can not be caused by partial melting processes, because radiogenic isotopes are not fractionated during such processes. Thus this variability must have its origin in the source region of the PA-EPR lavas. Devey et al. (1997) as well as Hekinian et al. (1997, 1999) and Maia et al. (2001) suggested, based on trace element and Pb isotope data that magmatism on the PA-EPR, at its intersection

with the FSC, is influenced by enriched, radiogenic mantle material derived from the Foundation plume. Indeed, the coincidence of the peak of incompatible element enrichment and Sr- and Pb-radiogenicity of the NMS with the by Maia et al. (2000) proposed present position of the Foundation plume, as well as the fact that the NMS exhibits nearly the same range in incompatible element and isotopic composition as FSC lavas, clearly indicate that the source of this enrichment is the Foundation plume. On the other hand, the PA-EPR MORB trend indicates a depleted end-member similar to the average EPR MORB of White et al. (1987) with $^{87}\text{Sr}/^{86}\text{Sr}$ and $^{206}\text{Pb}/^{204}\text{Pb}$ ratios of around 0.7025 and 18.4 respectively (Fig. 4c).

Even though it can be easily agreed upon the fact that the influence of the Foundation plume is the prime reason for the incompatible element enrichment and radiogenic composition of some of the NMS, considerable debate can break out concerning the actual appearance of the mantle plume influencing the ridge. In this context e.g. Hekinian et al. (1997) and Niu and Hekinian (2003) proposed, based on the heterogeneous incompatible element and isotopic composition of lavas occurring on the seamounts of the FSC situated between longitudes 114°W and 111°W around latitude 37°S that the PA-EPR volcanics are derived from successive partial melting and melt extraction from a heterogeneous plume source, being mixed with alkali-rich and alkali-depleted components. This model displays some similarities to the “two-stage melting plume-pudding mantle model” of Phipps Morgan and Morgan (1999) [12]. In this model the depleted MORB melts are derived from the partial melting of the restite leftover from melt extraction of a first, low degree (about 1-4%) melting event of the original mantle plume, creating enriched ocean island basalts. Since this restite is, according to Phipps Morgan and Morgan (1999), hot and buoyant it ponds beneath the lithosphere as an asthenosphere layer, which will rise and melt a second time as a mid-ocean ridge is reached. However, what kind of trace element and isotope patterns could be expected if the PA-EPR volcanics would be derived from successive partial melting and melt extraction from a heterogeneous plume source? As partial melting events are going to significantly change the incompatible element composition of the source while leaving its isotopic composition untouched, the result of such successive partial melting events would be a restite being more and more stripped of its incompatible elements (e.g. La, Ce, Nd) while still inheriting the radiogenic Sr and Pb isotope signature of the plume. The sampling of such a plume by a mid-ocean ridge would result, even after mixture with the depleted matrix of the plume, in the generation of volcanics along the ridge being variably depleted in incompatible elements with quite radiogenic isotope compositions. Thus one would find a number of mixing lines with different depleted but still quite radiogenic end-members, which is not the case considering the trace element data of the NMS (Fig. 8a and b). Instead the volcanics of the NMS are nearly as enriched as samples 70DS1SO100 and 70DS2SO100 (Table 1), proposed by Hekinian et al. (1997, 1999) to represent the “original”, undepleted plume material.

The inconsistency of the “successively depleted heterogeneous plume model” with the geochemical situation observed along the PA-EPR is also supported by the results of modal batch melt modelling displayed in Figs. 7a and b. The isotopic composition of the enriched end-member, used in the model, is based on the highest $^{87}\text{Sr}/^{86}\text{Sr}$ and lowest $^{143}\text{Nd}/^{144}\text{Nd}$ values measured on samples from the FSC. The trace element concentrations of the enriched

mantle source were taken from McDonough and Sun (1995) [29]. The distribution coefficients for trace elements between minerals and melt were taken from Kelemen et al. (1993) [30] and Johnson (1998) [31]. The phase proportions for the garnet lherzolite used in the model have been modified after Kelemen (1993). The isotopic composition of the MORB source is based on the most depleted PA-EPR MORB. Its trace element composition was taken from Hoffman (1988) [32], whereas the phase proportions for the spinel-lherzolite are from Kelemen (1993). As shown in Fig. 9 the most depleted MORB observed along the PA-EPR can be generated by around 20% of partial melting of the assumed MORB source. The successive depletion of the plume material has been simulated by sequential melting using a partial melting degree of 2%. In a second step the MORB source and the evolving plume source have been mixed. The results of this modelling are exemplified using Sm/Nd, Ce/Yb, Sr and Nd isotopes (Fig. 7a and b). In general the volcanics of the NMS show a positive trend of increasing Ce/Yb and Sm/Nd with increasing $^{87}\text{Sr}/^{86}\text{Sr}$ and $^{143}\text{Nd}/^{144}\text{Nd}$ respectively. As shown in Figs. 7a and b the incompatible element depletion of the enriched source by sequential partial melting is quite quick, resulting in ever changing end-member compositions of the still radiogenic source, which can not produce the geochemical trends observed along the PA-EPR. On the other hand, the geochemical patterns of the NMS can be easily modelled as resulting from binary mixtures of 80 to 95% MORB melt and 5 to 20% melts formed by about 6% partial melting of an enriched mantle source (Fig. 8a and b).

Conclusions

- (1) The Foundation plume creates a roughly 350 km long geochemical anomaly, between latitudes 36.5°S and 39.8°S, along the PA-EPR, roughly coinciding with the length of the bathymetric anomaly produced by the plume.
- (2) The PA-EPR magmas generated along the geochemical anomaly contain variable volumes of enriched plume material, whereby the boundaries between plume influenced and non-influenced MORB, to the north and the south, correspond to the position of two large OSCs.
- (3) The pronounced isotopic gradient towards the south indicates a mainly southward directed plume flow along this southward propagating rift.
- (4) The relatively small size of the anomaly created by the Foundation plume, compared to plume ridge interaction settings such as Galapagos or Easter, suggests that the plume flux emanating from the Foundation plume is relatively low.
- (5) No significant increase in the degree of melting is observed at the loci of maximum plume influx into the ridge, indicating that the excess temperature of the Foundation plume material must be relatively low.

- (6) The mixing process between the MORB and the Foundation plume material takes place by mixing of melts in the shallow, asthenospheric mantle during mainly lateral flow of the plume.

Acknowledgments

We thank Captain Papenhagen and his crew for their help during the cruise and the BMBF for funding of this project through grant 03G0157A.

References

- 1 N.M. Ribe, U.R. Christensen and J. Theissing, The dynamics of plume-ridge interaction; 1, Ridge-centered plumes, *Earth and Planetary Science Letters* 134(1-2), 155-168, 1995.
- 2 N.H. Sleep, Lateral flow of hot plume material ponded at sublithospheric depths, *Journal of Geophysical Research, B, Solid Earth and Planets* 101(12), 28,065-28,083, 1996.
- 3 C. Small and L.V. Danyushevsky, A plate-kinematic explanation for mid-ocean-ridge depth discontinuities, in press.
- 4 C. Small, Observations of ridge-hotspot interactions in the Southern Ocean, *Jour Geophys Res* 100(B9), 17.931-17.946, 1995.
- 5 J.-G. Schilling, G. Thompson, R. Kingsley and S. Humphris, Hotspot-migrating ridge interaction in the South Atlantic, *Nature* 313, 187-191, 1985.
- 6 J.G. Schilling, R. Kingsley, D. Fontignie, R. Poreda and S. Xue, Dispersion of the Jan Mayen and Iceland mantle plumes in the Arctic; a He-Pb-Nd-Sr isotope tracer study of basalt from the Kolbeinsey, Mohns, and Knipovich ridges, *Journal of Geophysical Research, B, Solid Earth and Planets* 104(5), 10,543-10,569, 1999.
- 7 J.P. Morgan, The thermodynamics of pressure-release melting a plum-pudding mantle, in: AGU 1999 fall meeting., Anonymous, ed., *Eos, Transactions, American Geophysical Union* 80; 46 Suppl., pp. 1172, American Geophysical Union, Washington, DC, United States, 1999.
- 8 M.G. Braun and R.A. Sohn, Melt migration in plume-ridge systems, *Earth and Planetary Science Letters* 213, 417-430, 2003.
- 9 K.M. Haase, C.W. Devey and S.L. Goldstein, Two-way exchange between the Easter mantle plume and the Easter microplate spreading axis, *Nature* 382, 344-346, 1996.
- 10 S.M. Jones, Test of a ridge-plume interaction model using oceanic crustal structure around Iceland, *Earth and Planetary Science Letters* 208(3-4), 205-218, 2003.
- 11 C. Kincaid, J.G. Schilling and C. Gable, The dynamics of off-axis plume-ridge interaction in the uppermost mantle, *Earth and Planetary Science Letters* 137(1-4), 29-43, 1996.
- 12 M.J. Phipps and W.J. Morgan, Two-stage melting and the geochemical evolution of the mantle; a recipe for mantle plum-pudding, *Earth and Planetary Science Letters* 170(3), 215-239, 1999.
- 13 J.-G. Schilling, Upper mantle heterogeneities and dynamics, *Nature* 314, 62-67, 1985.
- 14 J.-G. Schilling, Fluxes and excess temperatures of mantle plumes inferred from their interaction with migrating mid-ocean ridges, *Nature* 352, 397-403, 1991.

- 15 N.H. Sleep, Ridge-crossing mantle plumes and gaps in tracks, *G3* 3, 33, 2002.
- 16 N.H. Sleep, Hotspots and mantle plumes: some phenomenology, *Journal of Geophysical Research* 95, 6715-6736, 1990.
- 17 M. Albers and U.R. Christensen, Channeling of plume flow beneath mid-ocean ridges, *Earth and Planetary Science Letters* 187(1-2), 207-220, 2001.
- 18 M. Maia, D. Ackermann, G.A. Dehghani, P. Gente, R. Hékinian, D. Naar, J.O. Connor, K. Perrot, J.P. Morgan, G. Ramillien, S. Révillon, A. Sabetian, D. Sandwell and P. Stoffers, The Pacific-Antarctic Ridge-Foundation hotspot interaction: a case study of a ridge approaching a hotspot, *Marine Geology* 167, 61-84, 2000.
- 19 M. Maia, C. Hémond and P. Gente, Contrasted interactions between plume, upper mantle, and lithosphere: Foundation chain case, *G³* 2, 2000GC000117, 2001.
- 20 C.W. Devey, R. Hékinian, D. Ackermann, N. Binard, B. Francke, C. Hémond, V. Kapsimalis, S. Lorenc, M. Maia, H. Möller, K. Perrot, J. Pracht, T. Rogers, K. Statterger, S. Steinke and P. Victor, The Foundation Seamount Chain: a first survey and sampling, *Marine Geology* 137, 191-200, 1997.
- 21 R. Hékinian, P. Stoffers, D. Achermann, S. Révillon, M. Maia and M. Bohn, Ridge-hotspot interaction: the Pacific-Antarctic Ridge and the foundation seamounts, *Marine Geology* 160, 199-223, 1999.
- 22 R. Hékinian, P. Stoffers, C. Devey, D. Achermann, C. Hémond, J. O'Conner, N. Binard and M. Maia, Intraplate versus ridge volcanism on the Pacific-Antarctic Ridge near 37°S - 111°W, *Jour. Geophys. Res.* 102(B6), 12,265-12,286, 1997.
- 23 K.C. MacDonald, D.S. Scheirer and S.M. Carbotte, Mid-ocean ridges; discontinuities, segments and giant cracks, *Science* 253(5023), 986-994, 1991.
- 24 P. Lonsdale, Geomorphology and structural segmentation of the crest of the southern (Pacific-Antarctic) East Pacific Rise, *Journal of Geophysical Research*, B, *Solid Earth and Planets* 99(3), 4683-4702, 1994.
- 25 C.-D. Garbe-Schönberg, Simultaneous determination of thirty-seven trace elements in twenty-eight international rock standards by ICP-MS, *Geostandards Newsletters* 17, 81-97, 1993.
- 26 K.A. Hoernle and G.R. Tilton, Sr-Nd-Pb isotope data for Fuerteventura (Canary Islands) basal complex and subaerial volcanics: applications to magma genesis and evolution, *Schweizerische Mineralogische und Petrographische Mitteilungen* 71, 3-18, 1991.
- 27 W. Todt, R.A. Cliff, A. Hanser and A.W. Hofmann, Evaluation of a ²⁰²Pb-²⁰⁵Pb double spike for high-precision lead isotope analysis, *Am. Geophys. Un. Geophys. Monograph* 95, 429-437, 1996.
- 28 W.M. White, A.W. Hofmann and H. Puchelt, Isotope geochemistry of Pacific mid-ocean ridge basalt, *Journal of Geophysical Research* 92, 4881-4893, 1987.
- 29 W.F. McDonough and S.S. Sun, The composition of the Earth, in: *Chemical evolution of the mantle* 120; 3-4, pp. 223-253, Elsevier, Amsterdam, Netherlands, 1995.
- 30 P.B. Kelemen, N. Shimizu and T. Dunn, Relative depletion of niobium in some arc magmas and the continental crust: partitioning of K, Nb, La and Ce during melt/rock reaction in the upper mantle, *Earth and Planetary Science Letters* 120, 111-134, 1993.
- 31 K.T.M. Johnson, Experimental determination of partition coefficients for rare earth and high-field-strength elements between clinopyroxene, garnet, and basaltic melt at high pressures, *Contributions to Mineralogy and Petrology* 133, 60-68, 1998.
- 32 A.W. Hofmann, Chemical differentiation of the Earth: the relationship between mantle, continental crust, and oceanic crust, *Earth and Planetary Science Letters* 90, 297-314, 1988.

Figure and Table Captions

- Fig. 1:** Bathymetric map of the PA-EPR. Red lines outline the axis trends and the position of major ridge break-ups (overlap spreading centres). The position of the Foundation mantle plume is taken from Maia et al. (2000).
- Fig. 2:** Distribution and geochemical composition of samples along the spreading axis of the PA-EPR. The stippled field denotes the location and compositional variation of Foundation seamount chain (FSC) lavas. Data source of FSC lavas: Devey et al. (1997) and Maia et al. (2000), and this paper.
- Fig. 3:** Positive covariations of $^{87}\text{Sr}/^{86}\text{Sr}$ with Cl/K-ratios, being a tracer for alteration of oceanic crust, indicate that the scatter observed in the Sr isotopic composition of PA-EPR lavas, compared to their Pb and Nd isotopic compositions, is caused by assimilation of altered oceanic crust during late stage magma development.
- Fig. 4:** Isotopic composition of the PA-EPR lavas compared to incompatible element enriched FSC lavas. Data source as in Fig. 2.
- Fig. 5:** Incompatible element ratios Rb/Zr and (La/Ce)_N versus $^{87}\text{Sr}/^{86}\text{Sr}$, $^{206}\text{Pb}/^{204}\text{Pb}$ and $^{143}\text{Nd}/^{144}\text{Nd}$ showing the different linear trends of lavas from the NMS and SMS. See text for further explanation. Data source same as in Fig. 2.
- Fig. 6:** Variation of (a) fractionation-corrected Na₂O (Na₉) versus (La/Sm)_N and (b) fractionation corrected SiO₂ (Si₉) versus (Dy/Yb)_N in PA-EPR MORB compared to FSC basalts. See text for further explanation. Data source same as in Fig. 2.
- Fig. 7:** (Sm/Nd)_N versus $^{143}\text{Nd}/^{144}\text{Nd}$ ratios (a) and (Ce/Yb)_N versus $^{87}\text{Sr}/^{86}\text{Sr}$ ratios (b). The trace element composition of the enriched mantle source was taken from McDonough and Sun (1995), whereas this for the MORB source was taken from Hofman (1988). The phase proportions for the garnet lherzolite and spinel-lherzolite used in the modal batch melting model are from Kelemen (1993). In this case stepwise melting, using steps of 2% melting degree, has been modelled. The black dots denote the changing composition of the restite, serving as starting composition for the next melting event. The black lines, in each case, represent mixing lines between the MORB source (degree of melting (F): 20%) and the successively molten plume source (F: 5%). The marks along the mixing lines represent the ratios of the end-member components (10% steps). Data source: this paper.

Fig. 8: (Sm/Nd)_N versus ¹⁴³Nd/¹⁴⁴Nd ratios (a) and (Ce/Yb)_N versus ⁸⁷Sr/⁸⁶Sr ratios (b). The trace element composition of the enriched mantle source was taken from McDonough and Sun (1995), whereas this for the MORB source was taken from Hofman (1988). The phase proportions for the garnet lherzolite and spinel-lherzolite used in the modal batch melting model are from Kelemen (1993). Lines connecting the sources are mixing lines for mixtures of MORB source (F: 20%) with melts formed by varying degrees (F: 1-20%) of the enriched mantle source. Data source same as in Fig. 7.

Fig. 9: REE pattern of the most depleted MORB sample compared to the REE pattern produced by 20% melting of the Hofman MORB source (1988) in the spinel lherzolite field. Used phase proportions are the same as in Fig. 7. See text for further explanations. Data source same as in Fig. 7.

Table 1 Location and major element, trace element and isotopic composition of PA-EPR lavas

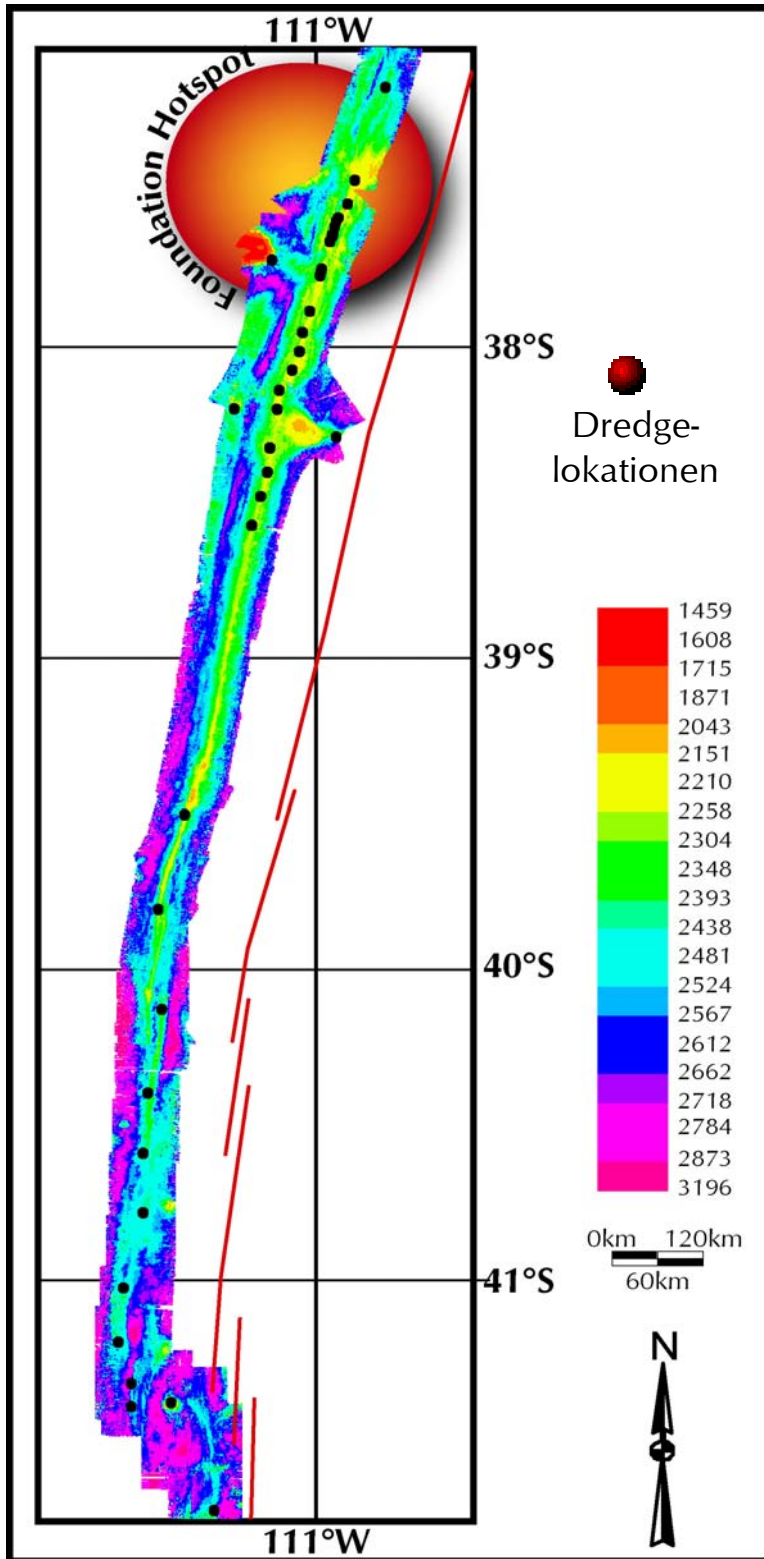


Fig. 1

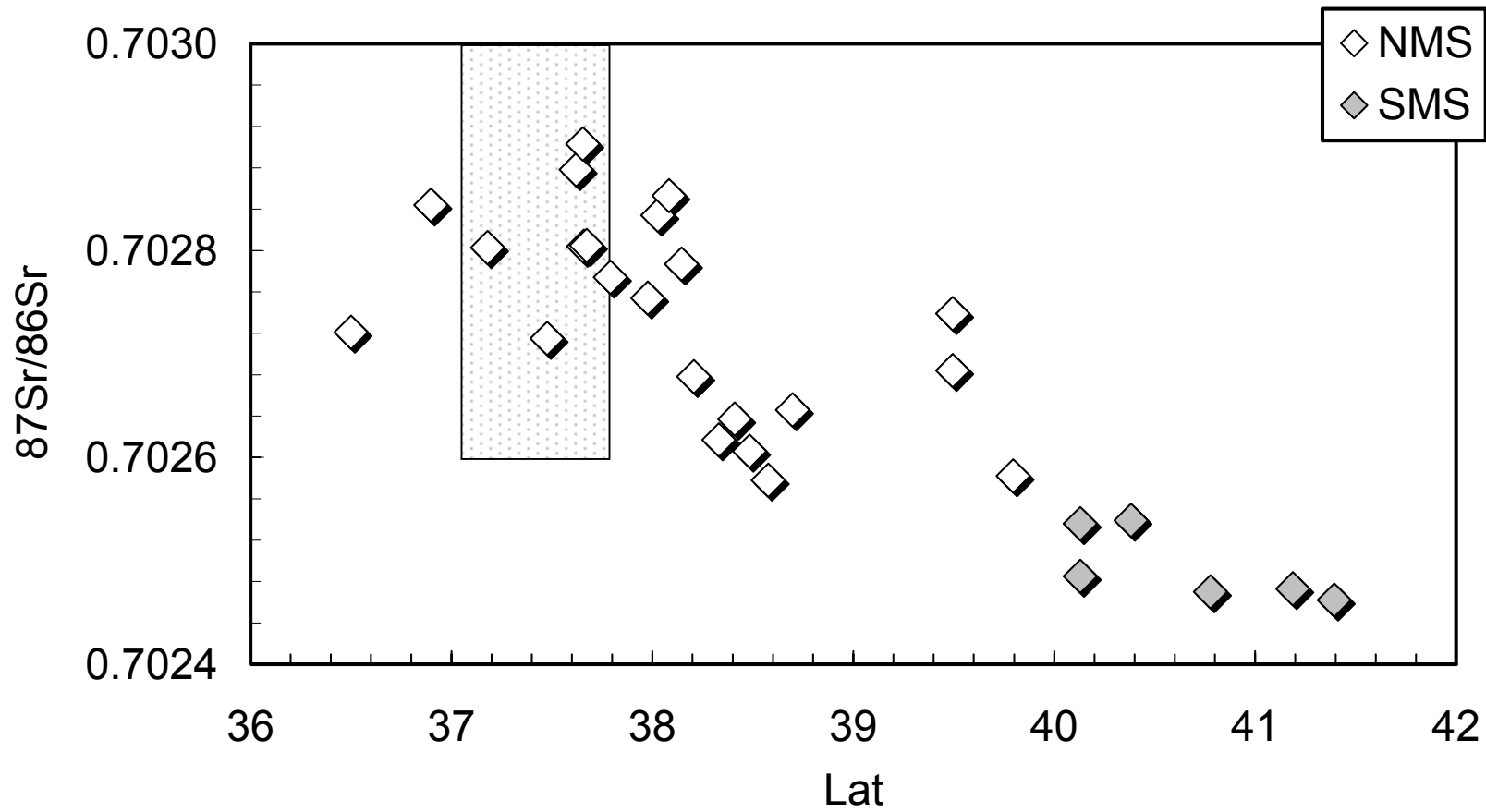


Fig. 2a

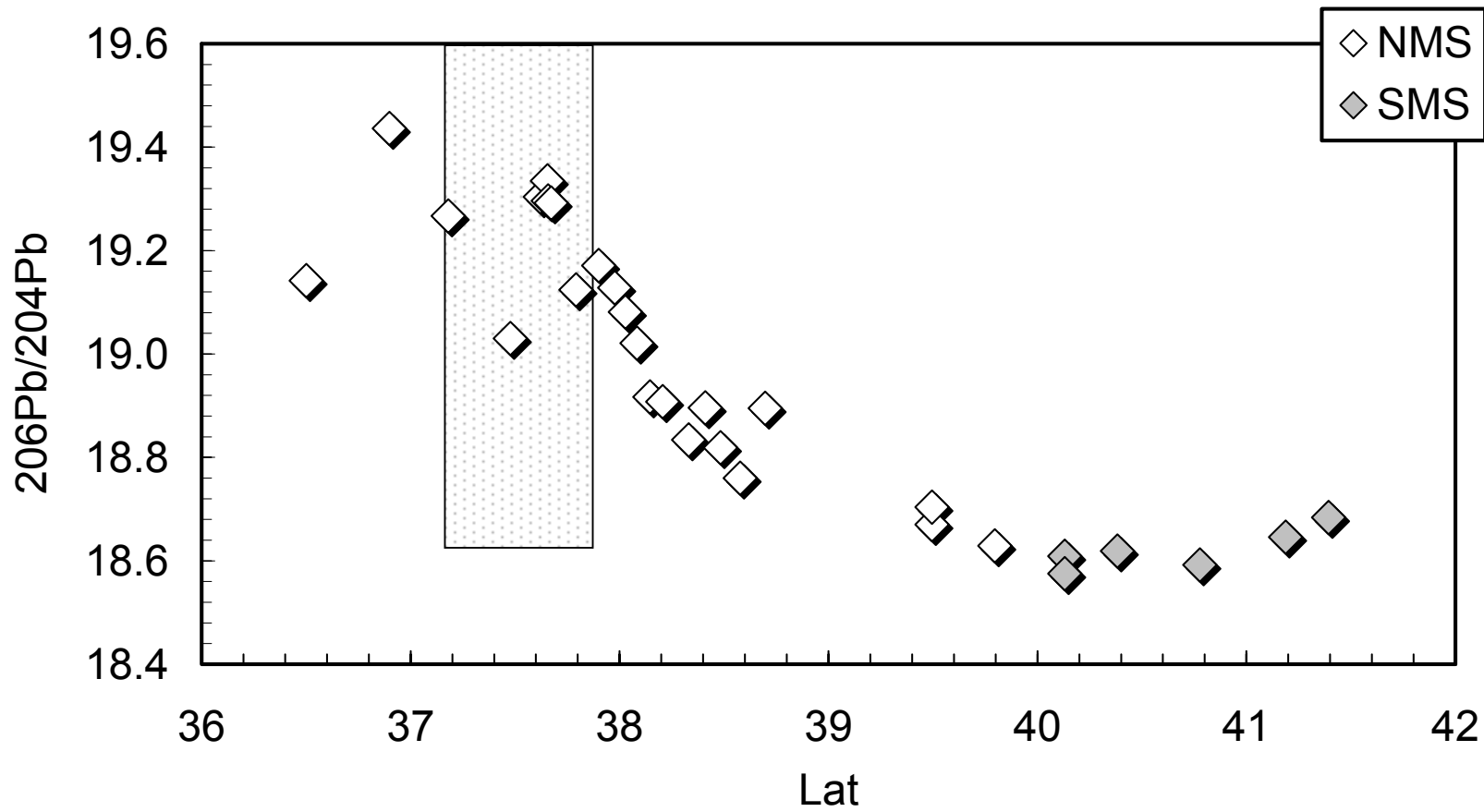


Fig. 2b

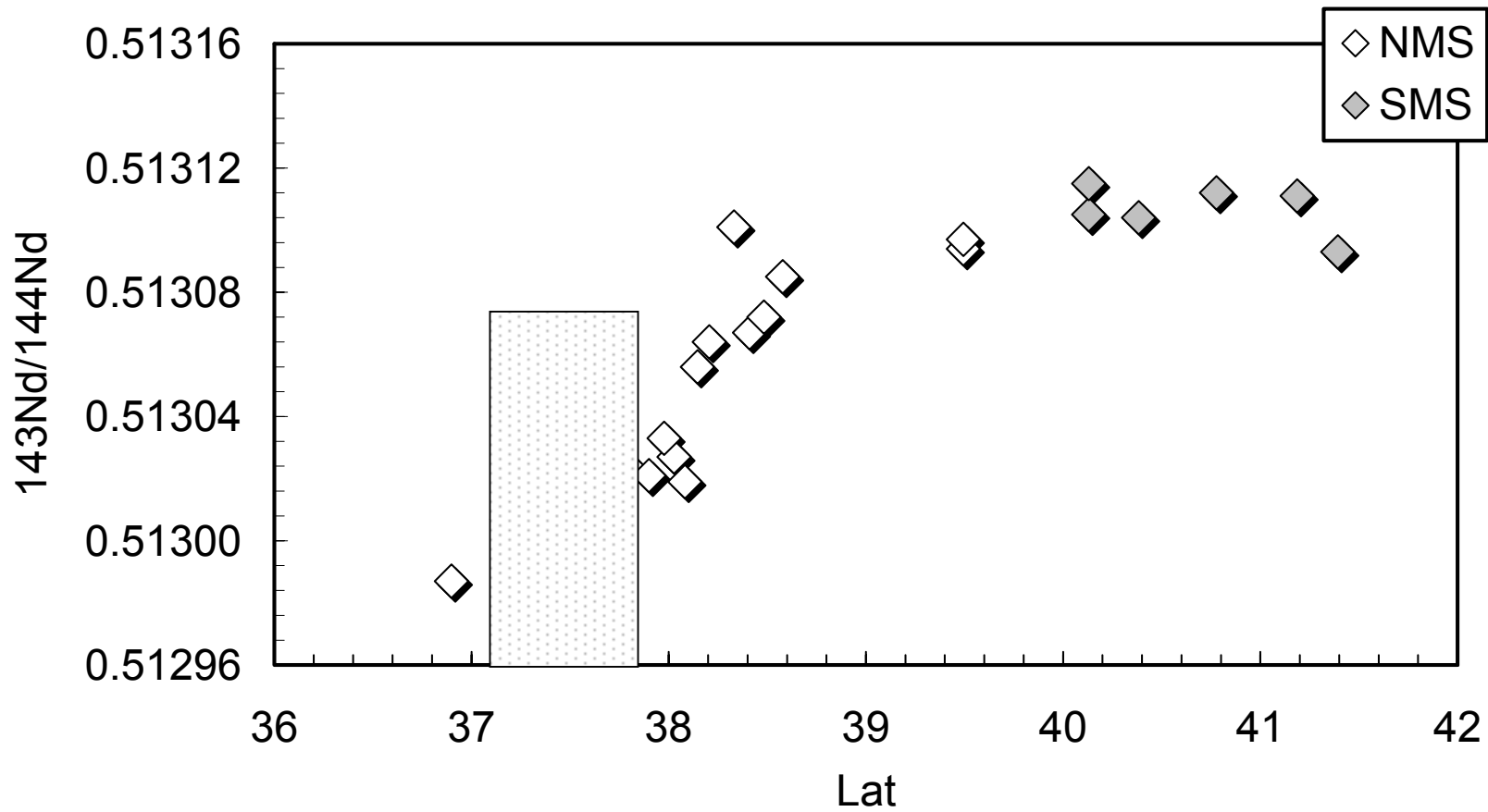


Fig. 2c

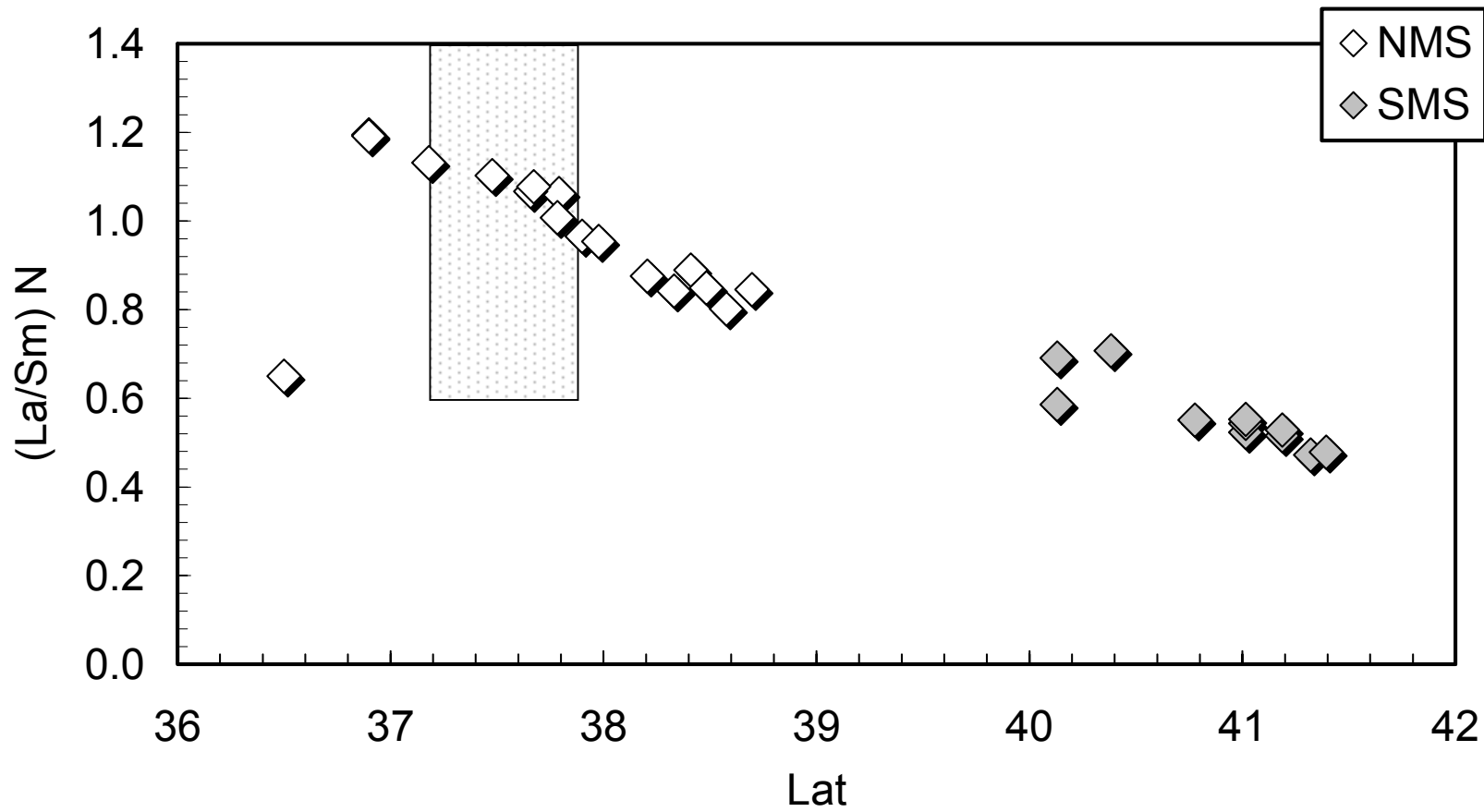


Fig. 2d

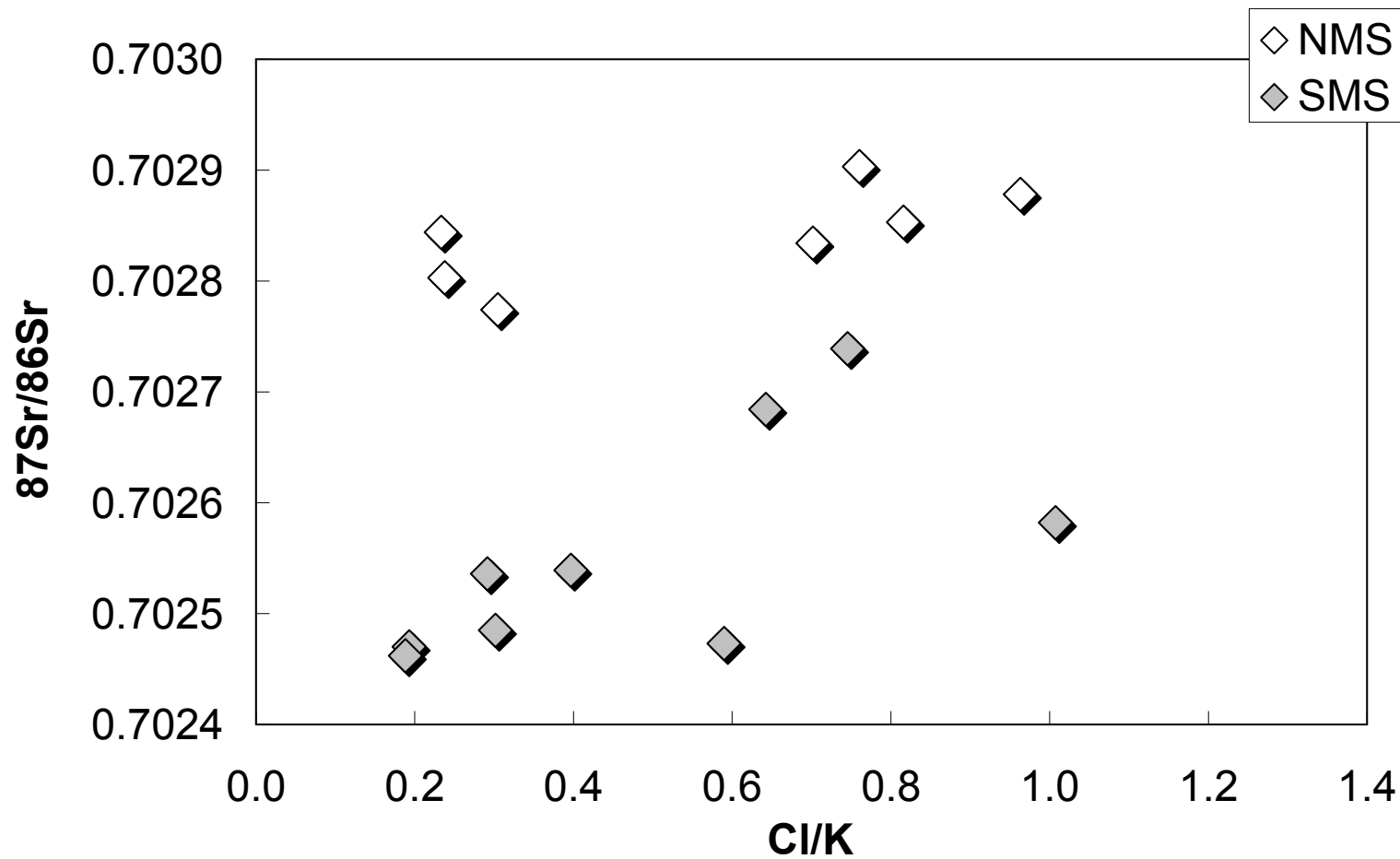


Fig. 3

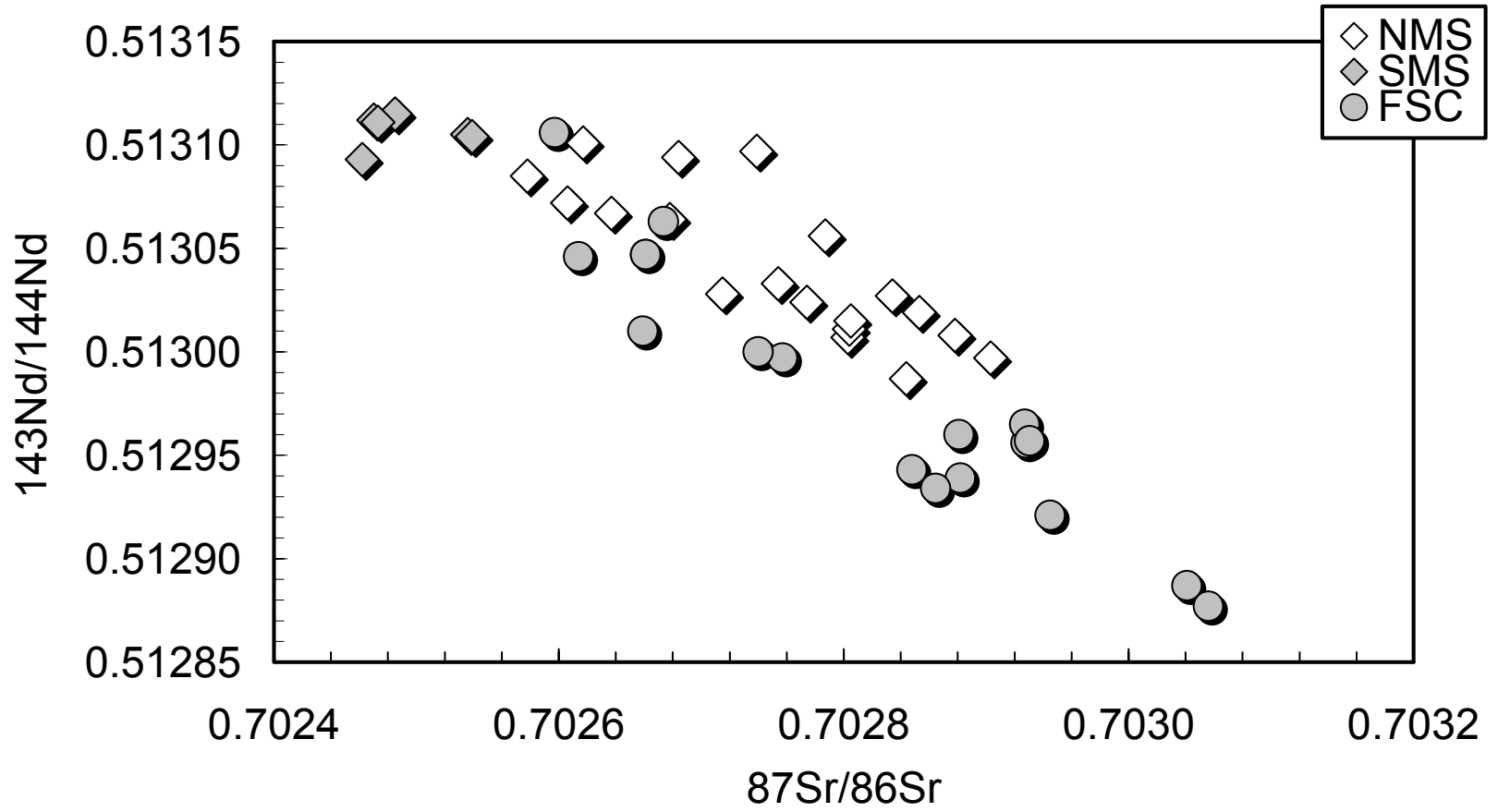


Fig. 4a

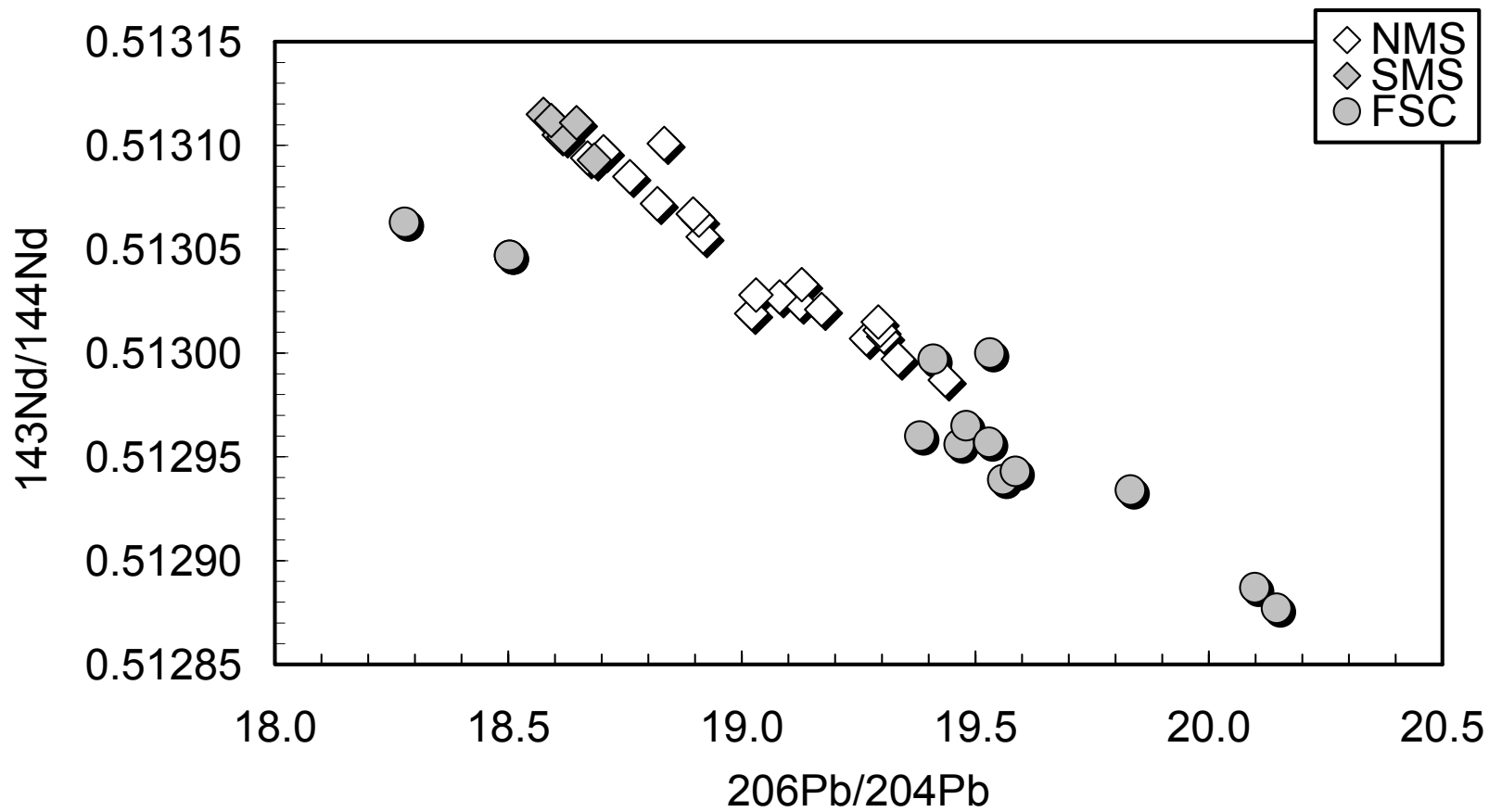


Fig. 4b

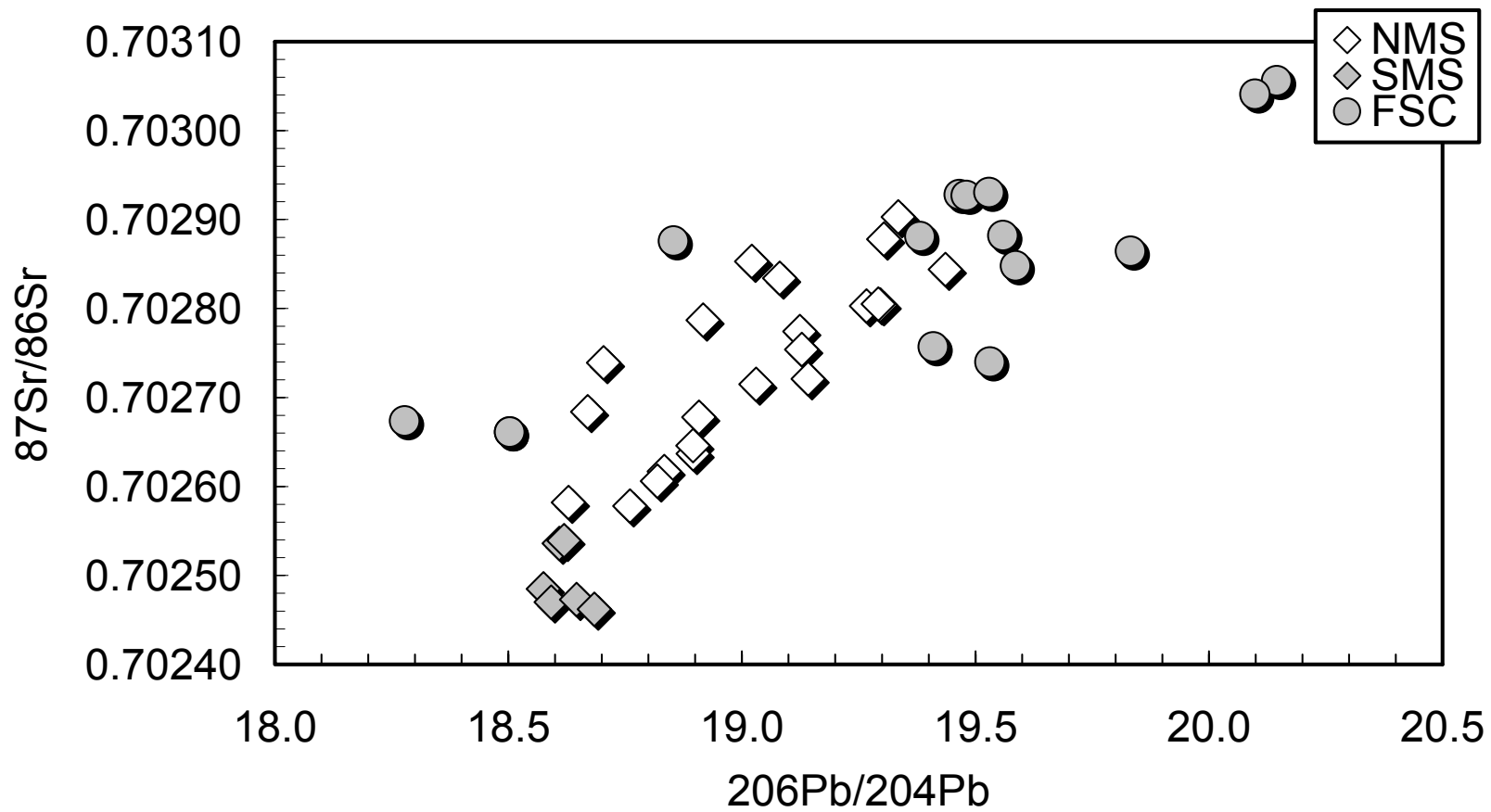


Fig. 4c

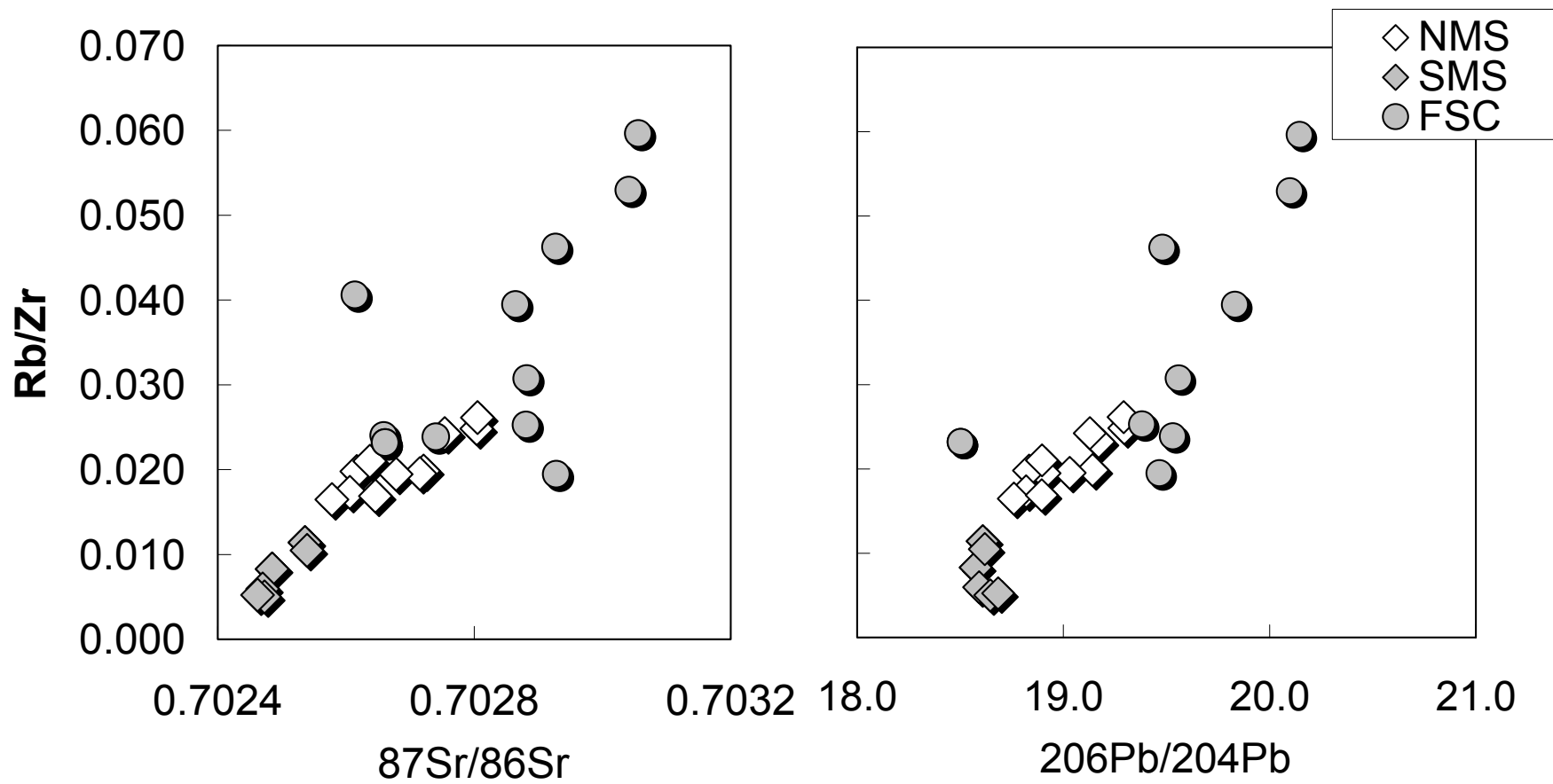
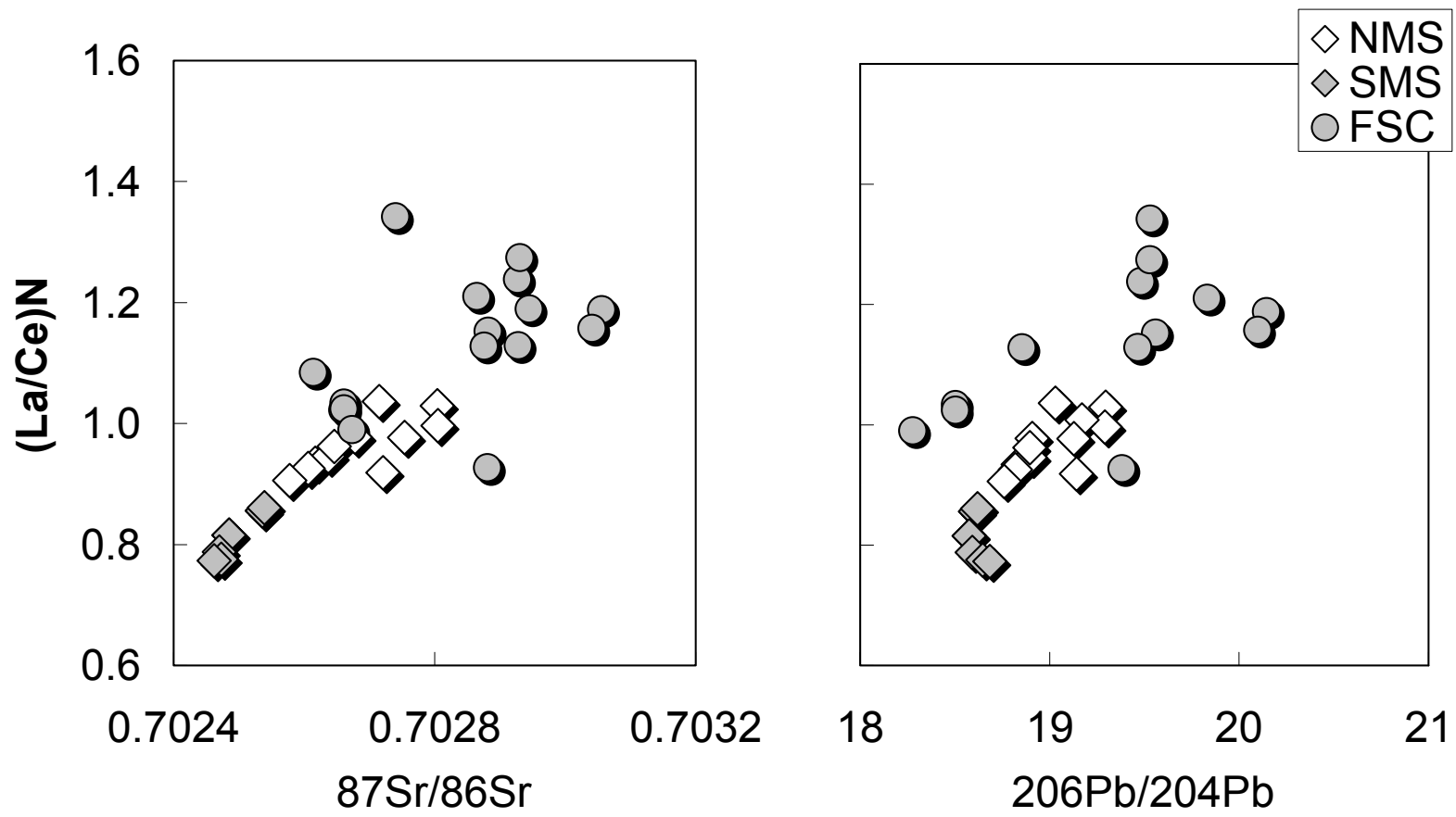


Fig. 5a



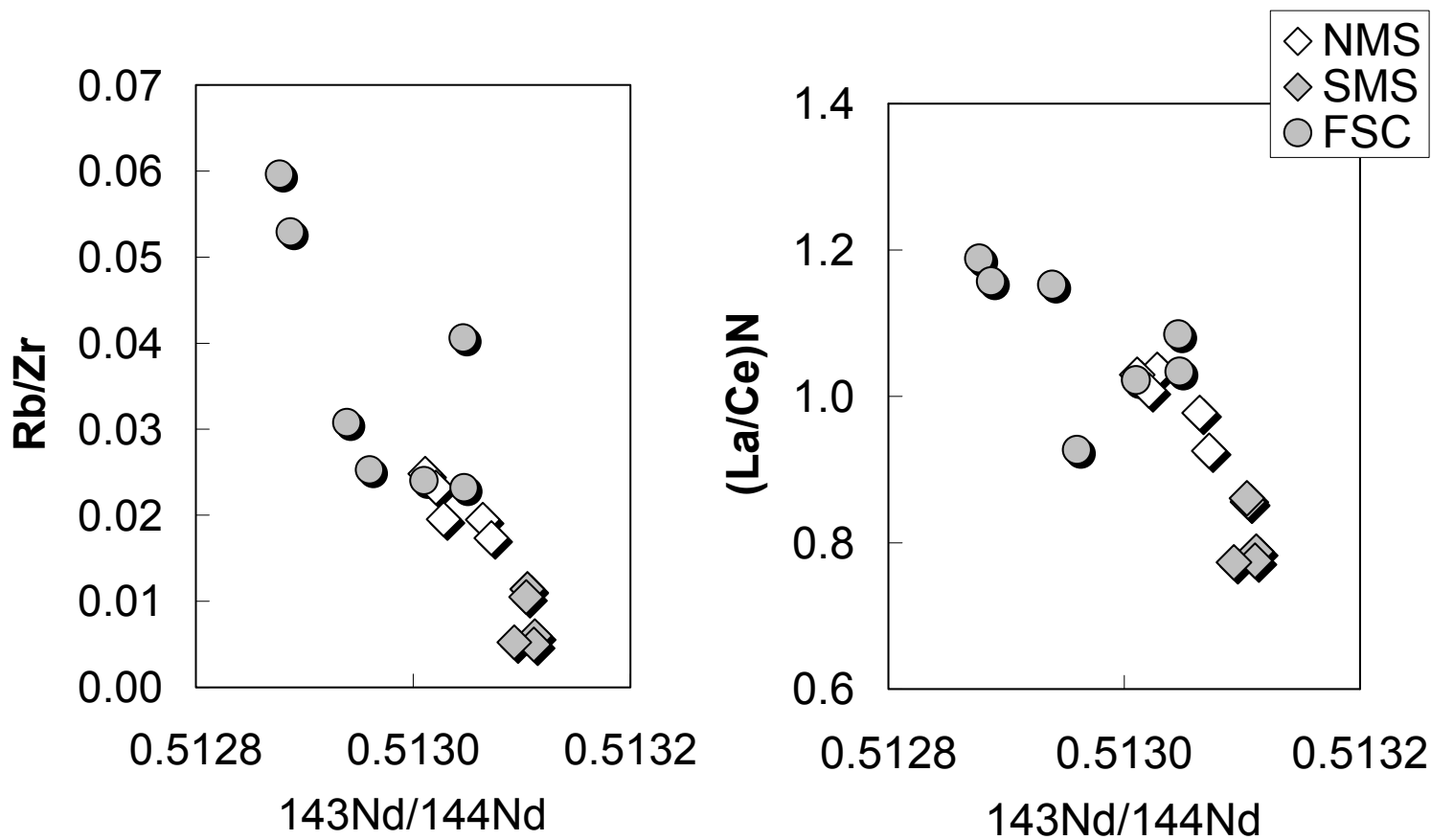


Fig. 5c

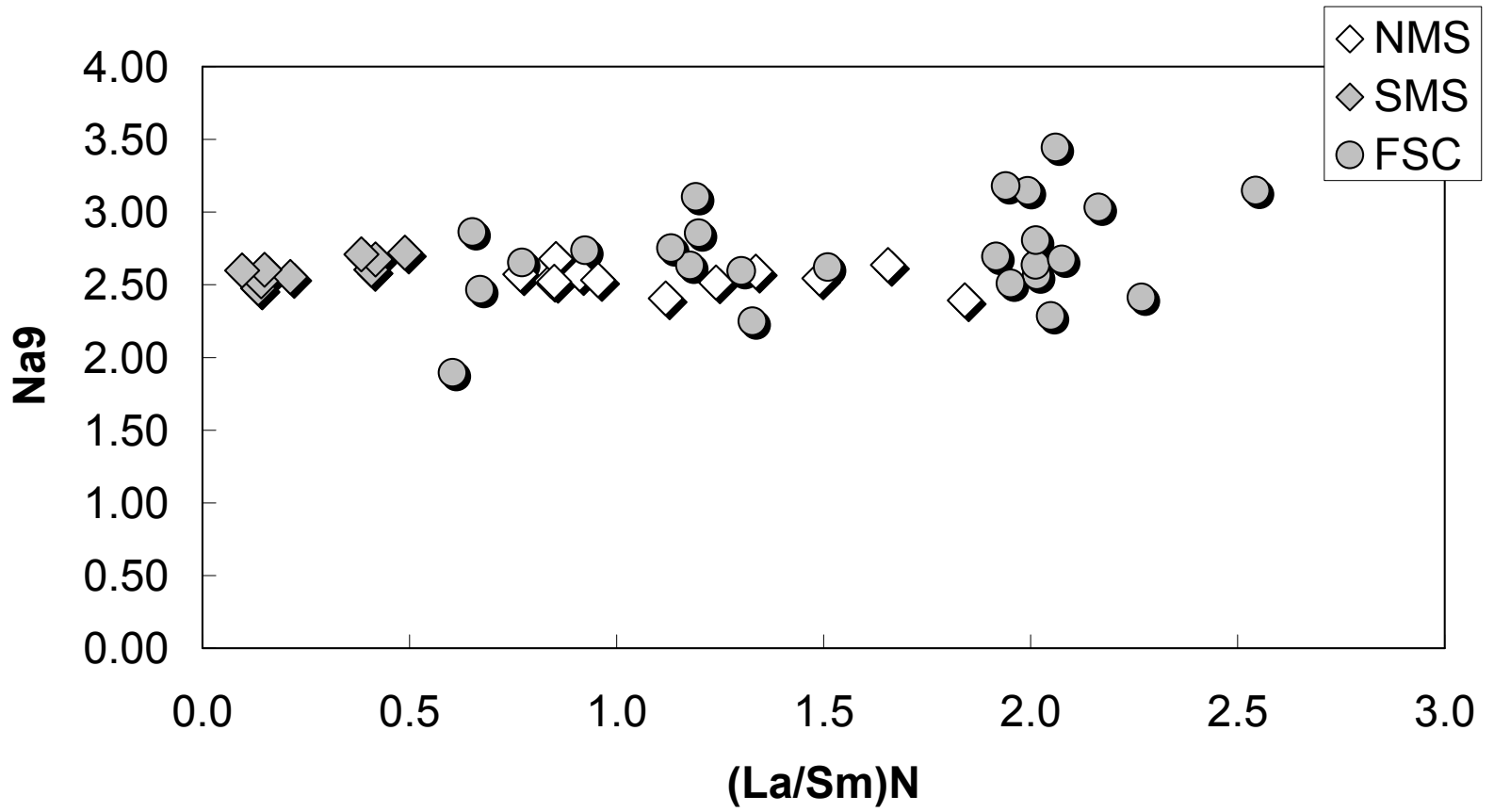


Fig. 6a

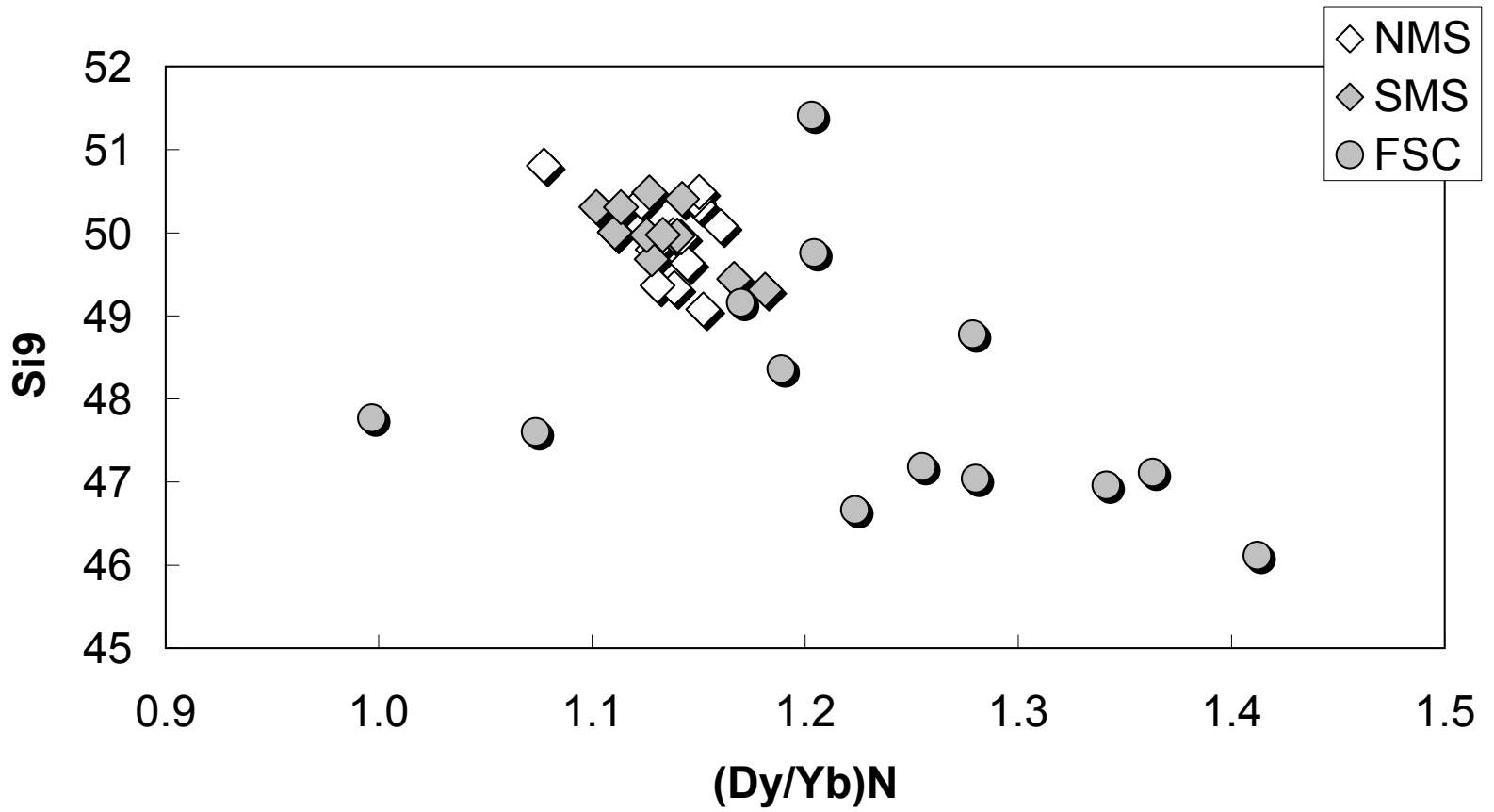


Fig. 6b

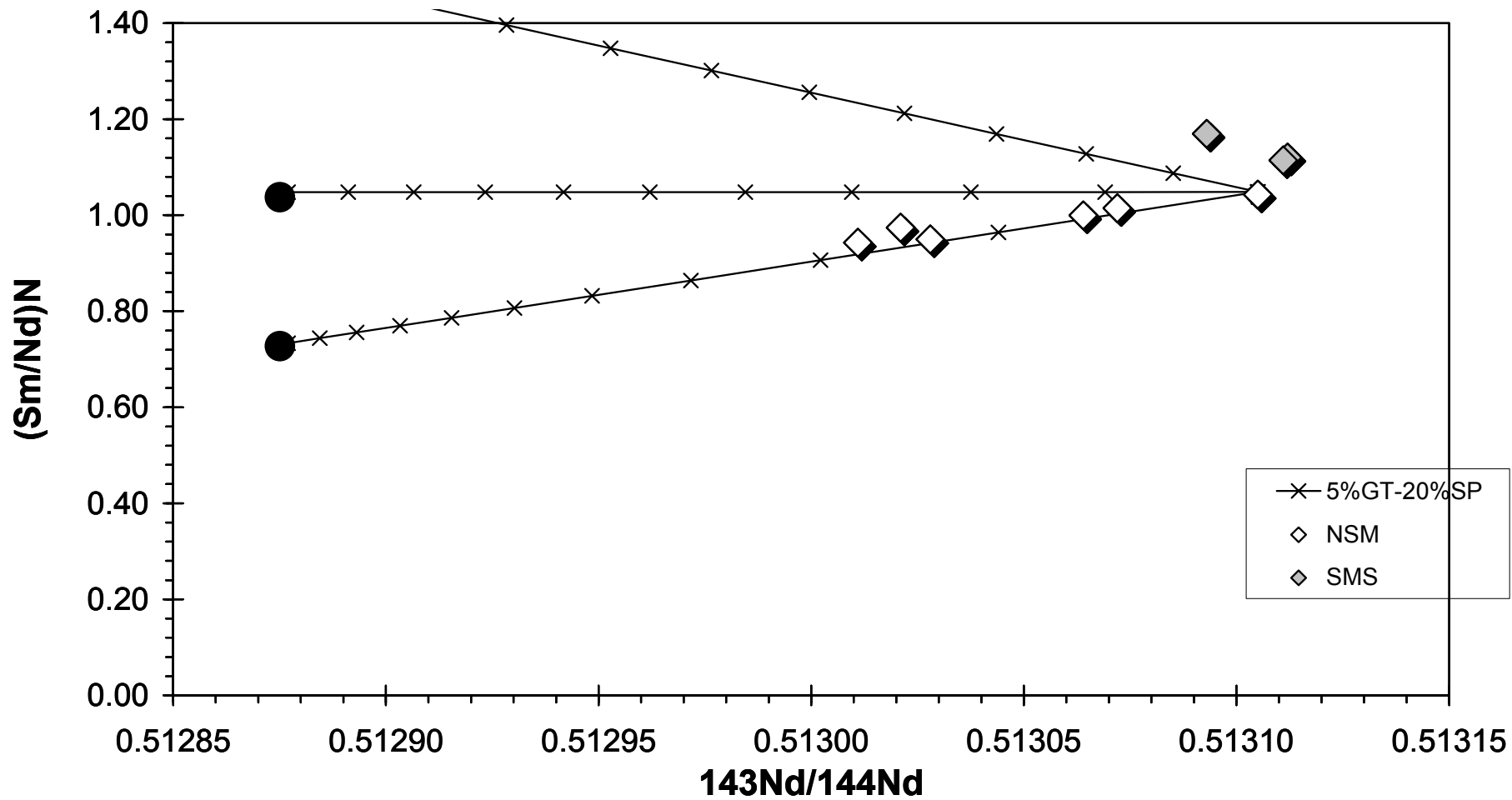


Fig. 7a

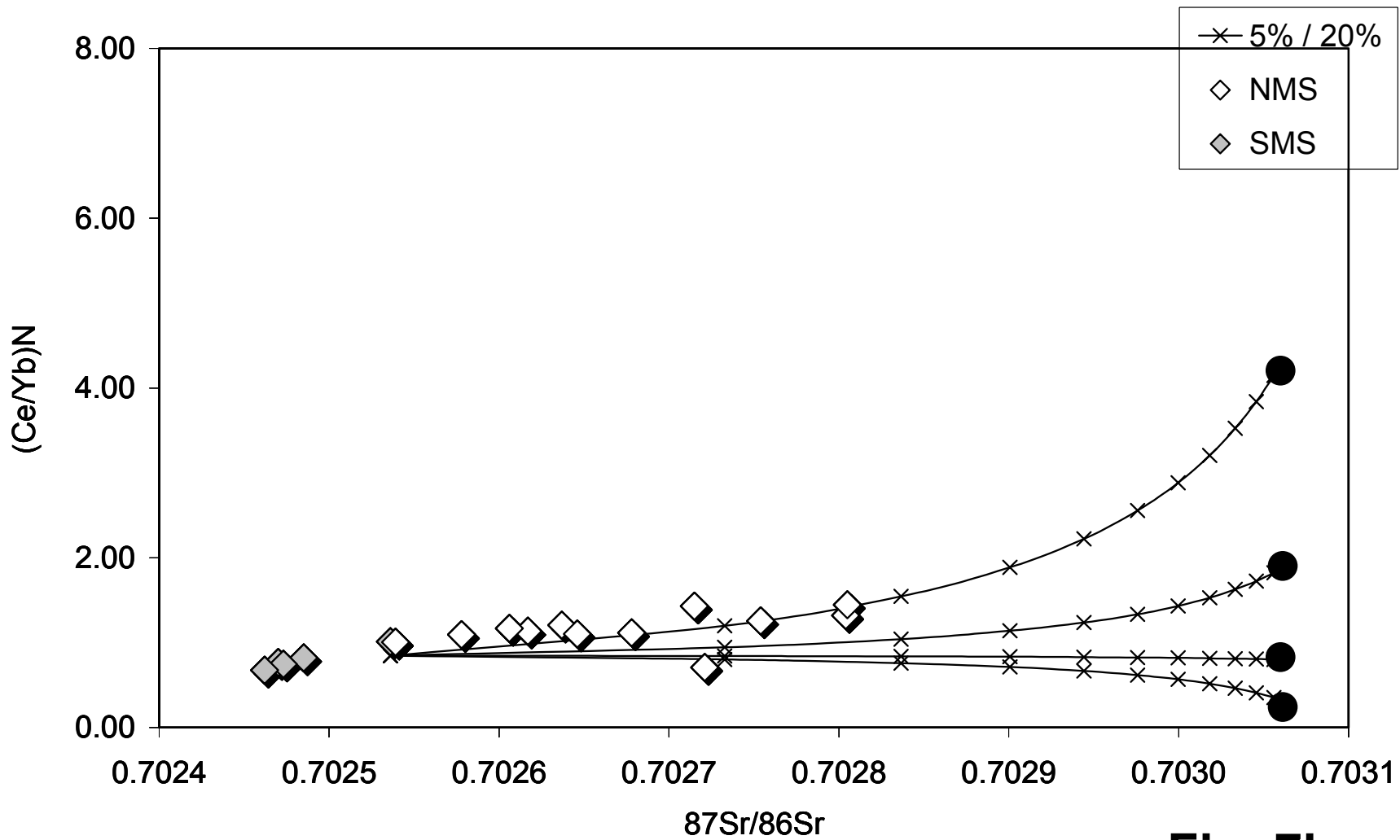


Fig. 7b

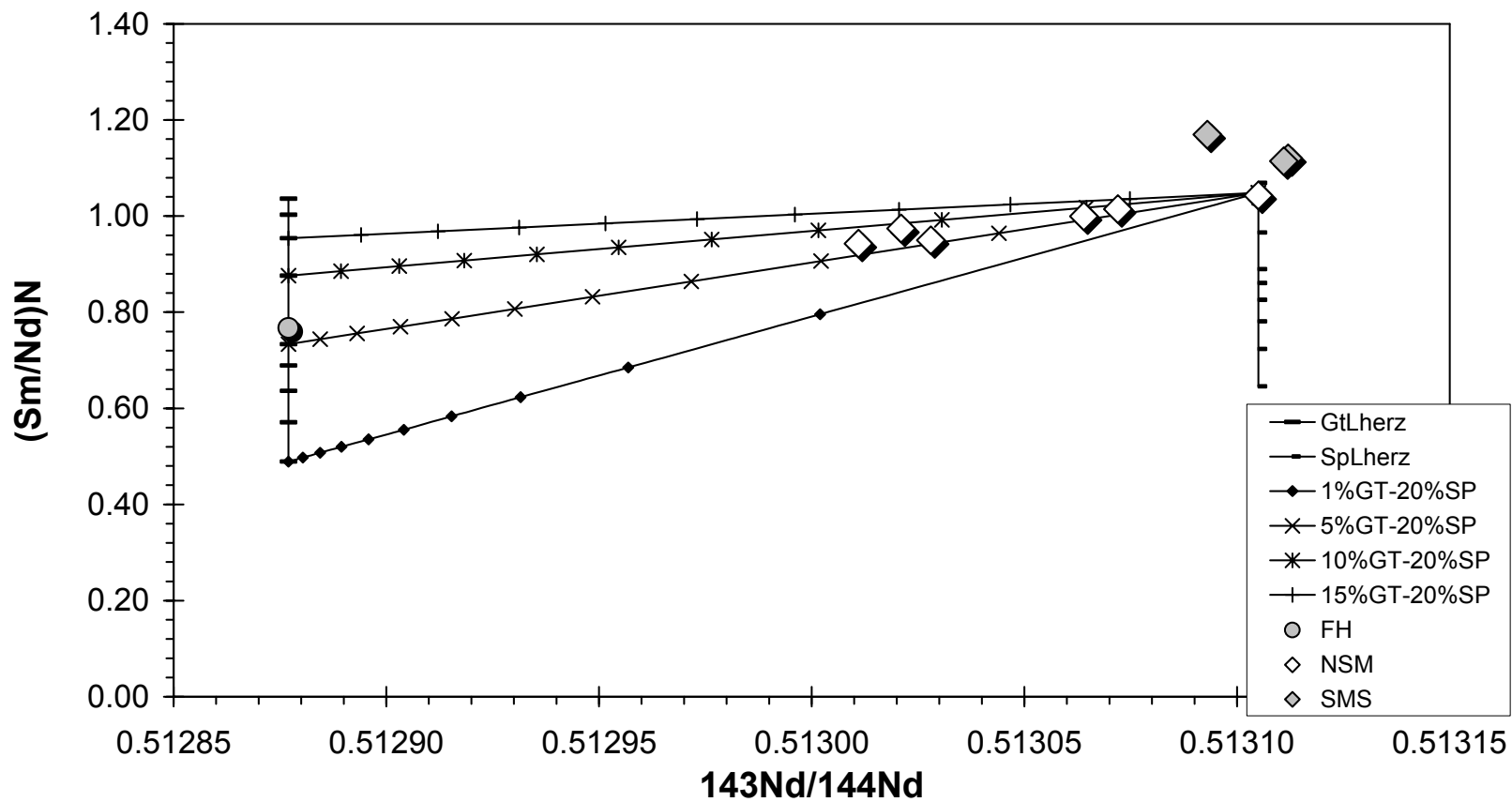


Fig. 8a

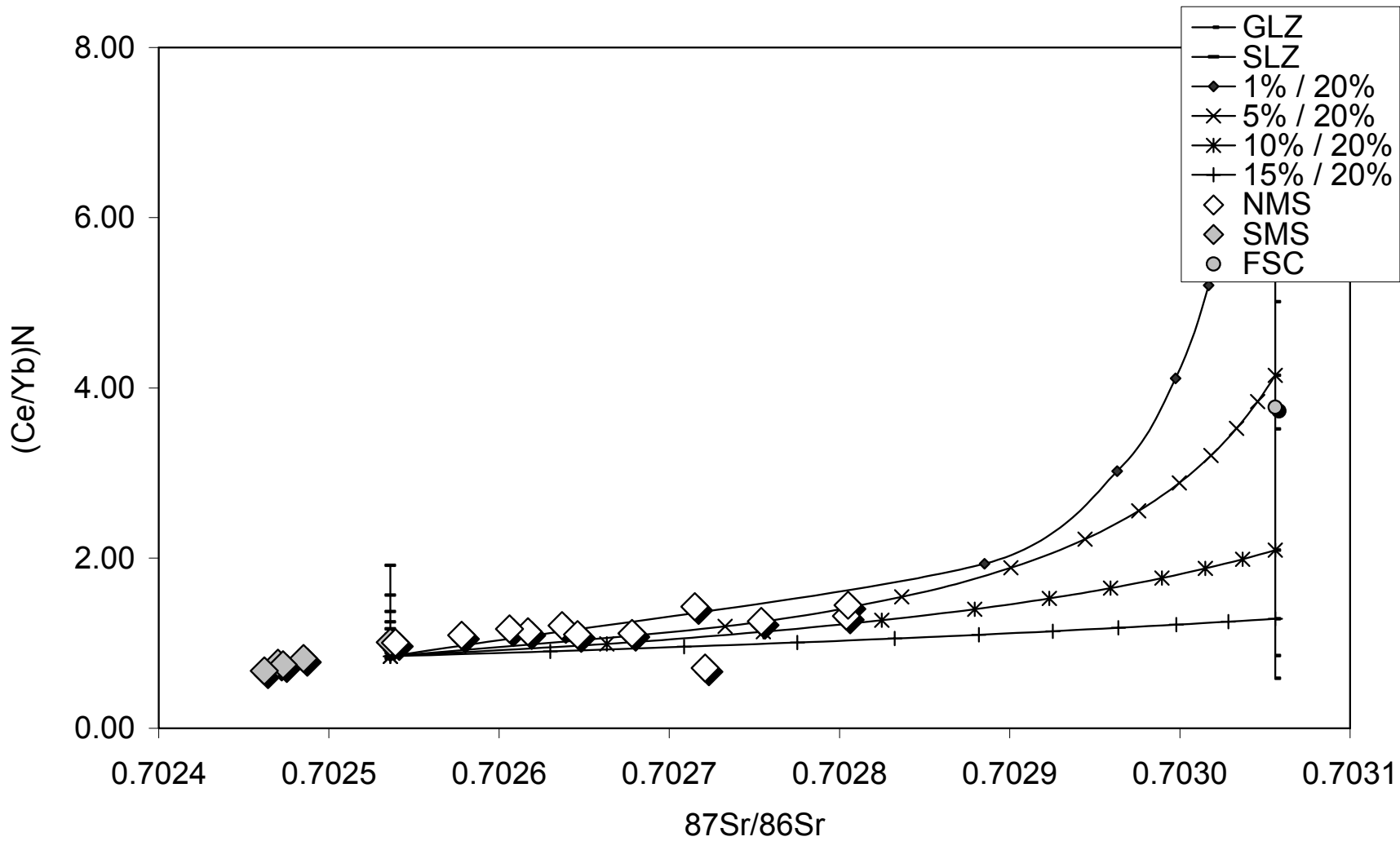


Fig. 8b

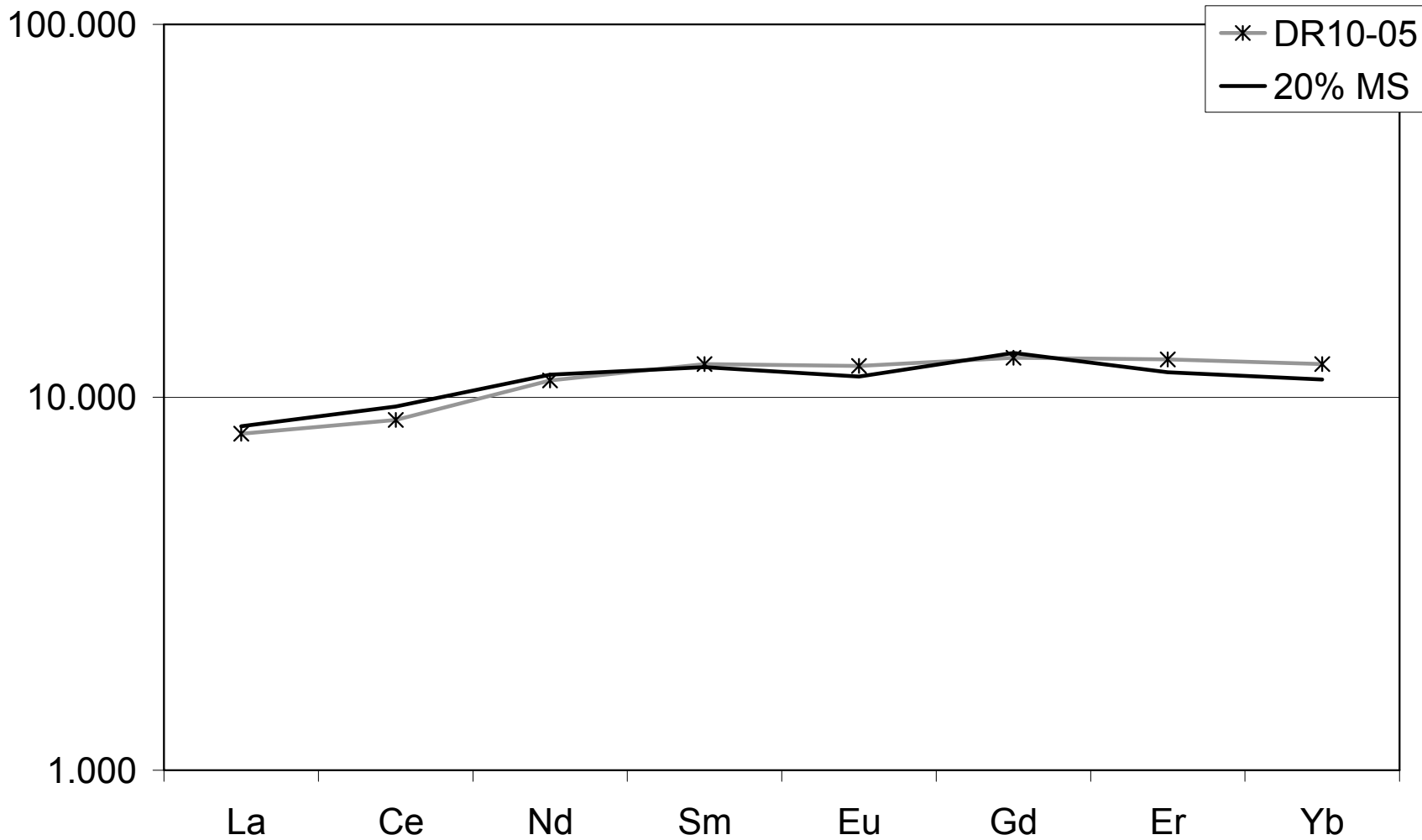


Fig. 9

Studienarbeit

Characterisation of the hydrothermal potential along the Pacific-Antarctic Ridge between 37°33'S and 41°43'S with Fe-Mn oxyhydroxides

Kerstin Schreiber

Betreuer: Prof. Dr. Peter Herzig
Dr. Thomas Kuhn

TU Bergakademie Freiberg
Lehrstuhl für Lagerstättenlehre und Petrologie
und Leibniz-Labor für Angewandte Meeresforschung
Brennhausgasse 14, D-09596 Freiberg

Content

Abstract 1

1. INTRODUCTION..... 2

2. STUDY SITE 2

3. SAMPLE DESCRIPTION 3

4. ANALYTICAL TECHNIQUES 5

 4.1. DESCRIPTION OF THE METHODS 5

 4.2. DISCUSSION OF THE LEACHING METHOD 6

5. RESULTS 10

6. DISCUSSION 13

 6.1. GENETIC INTERPRETATION OF THE PAR SAMPLES 13

 6.2. REGIONAL COMPARISON OF THE HYDROTHERMAL POTENTIAL BETWEEN PAR AND FOUNDATION 22

7. CONCLUSIONS 24

ACKNOWLEDGEMENTS..... 24

REFERENCES..... 25

APPENDIX..... 28

Abstract

Fe-Mn oxyhydroxides from the Pacific-Antarctic Ridge (PAR) have been geochemically studied. The precipitates occur on hard rocks as thin coatings with a thickness up to 1 mm and as crusts which are up to 4 mm thick. Because of the high amount of country rock in the samples they were selectively leached with a mixture of ammonia oxalate and oxalic acid.

The studied ferromanganese coatings and crusts from the PAR are characterized by negative Ce_{SN} -anomalies and low Co and REE concentrations indicating a hydrothermal origin. According to the Mn/Fe ratios between 0.37 and 1.02, the low Ba contents and the missing positive Eu_{SN} -anomalies most of the samples have been classified as hydrothermal plume fallout. One sample seems to be directly precipitated from a hydrothermal fluid since it shows very high Ba-concentrations, a positive Eu-anomaly and very low REE contents. But in marked contrast to typical hydrothermal crusts which were directly precipitated from a hydrothermal fluid and that have high Mn/Fe ratios, the PAR crust has a Mn/Fe ratio of 0.34 pointing to a precipitation from an iron rich fluid. Three crusts which were sampled from the surrounding of a hydrothermal field have exceptional high Cu and Zn concentrations with up to 2.77 wt.% Cu and 0.45 wt.% Zn. Mineralogical investigations and leaching experiments show that Cu and Zn do not form own mineral phases (such as sulfides) but are bound to the Mn and Fe oxyhydroxides by scavenging.

Since all investigated PAR samples show hydrothermal signatures a high hydrothermal potential is suggested for the PAR. For comparison chemical data of Fe-Mn crusts from the Foundation Seamount Chain were investigated. In contrast to PAR the Foundation Seamount Chain shows a much lower hydrothermal activity.

1. Introduction

Ferromanganese crusts can be formed by hydrogenetic, hydrothermal or diagenetic processes. Hydrothermal crusts often occur at mid-ocean ridges, back arc spreading centres and sometimes at active seamounts since the preconditions for the development of a hydrothermal system are often given in such tectonic environments.

From the superfast spreading East Pacific Rise (EPR) a high hydrothermal activity in the form of many small hydrothermal vents is known. But there is almost nothing known about the hydrothermal activity of the Pacific-Antarctic Ridge (PAR) which is the southern prolongation of the East Pacific Rise.

During cruise SO-157 of the German R/V Sonne in 2001, the PAR was sampled with dredges and the TV-grab between 37°33'S and 41°43'S. Fe-Mn oxyhydroxide coatings and crusts were collected from recovered rocks (Stoffers et al., 2001).

In this study the formation of these coatings and crusts is investigated by geochemical and mineralogical methods and based on the results an estimation of the hydrothermal potential of the PAR shall be given.

Typical hydrothermal signatures of Mn crusts are pronounced negative Ce_{SN} -anomalies (suffix SN = shale normalized), low Co and rare-earth-element (REE) concentrations and a fractionation of Fe and Mn (Usui and Someya, 1997). Additionally the signatures differ due to the precipitation from a hydrothermal fluid or from a hydrothermal plume (Kuhn, 1999).

For comparison and for an extension of the considered area geochemical data of ferromanganese crusts from the Foundation Seamount Chain which intersects the PAR between 37°11'S and 38°20'S, are included in the discussion (chapter 6).

2. Study site

Fe-Mn coatings were collected from the Pacific-Antarctic Ridge between 37°33'S - 41°43'S during cruise SO-157 of the German R/V Sonne.

The superfast SE Pacific spreading centres form a complex tectonic environment which includes the active Easter and Juan Fernandez Microplates and two major mantle plumes, Foundation and Easter (Stoffers et al., 2001). The Pacific-Antarctic Ridge is the southern prolongation of the superfast spreading East-Pacific-Rise (125-152 mm/yr; Cormier, 1999).

The spreading axis itself shows a regional topographic anomaly (36°30'S - 41°30'S) in the area where it is intersected by the Foundation Seamount Chain (between

37°11'S and 38°20'S; Fig. 10). In marked contrast to slow spreading MOR the mapped area of the fast spreading PAR is not characterized by a distinctive rift valley but in general by a central doming.

According to the interaction between the Foundation mantle plume and the spreading axis a great volcanic rock variation with enriched basalts and silica-rich volcanic rocks like andesites were produced in this area (Stoffers et al., 2001).

The Foundation Seamount Chain consists of seamounts and short volcanic ridges in a 180 km wide and 2000 km long area between 33°S, 131°W (Resolution Fracture Zone) and 37°S, 111°W (PAR).

It reflects the progressive drift of the Pacific Plate over an active mantle plume whereas the truly intraplate volcanism changes to a near ridge volcanism with time. This change is characterized by a morphological development from large isolated edifices in the west to elongated ridges of associated volcanoes at the eastern end of the chain near the Pacific-Antarctic spreading axis. Immediately adjacent to the Pacific-Antarctic spreading axis, the Foundation chain is characterised by three east-west trending, flat topped ridges associated with seamounts (Devey et al., 1995). These are the Northern, Central and Southern Foundation Chain. But only the Southern Foundation Chain seems to cross to the eastern side of the PAR. At present the Foundation plume is located ~ 35 km to the west of the PAR crest near 37°25'S (Stoffers et al., 2001).

Further south, between 39°20'S - 41°25'S the PAR is characterized by a series of short ridge segments separated by left-stepping overlapping spreading centres. At the most southern overlapping spreading centre (41°22'S) of the investigated area a large isolated conical seamount which is 450 m high and 6 km in diameter has been built within the overlap basin (Stoffers et al., 2001; Fig. 10 B).

3. Sample description

Within this study 13 Fe-Mn oxyhydroxide coatings and crusts from 9 different sampling stations of the PAR (in a longitudinal transect from 37°33'S - 41°23'S) were examined.

Samples 06DS, 24DS, 31GTV-7, 31GTV-8, 31GTV-9, 50DS and 52DS come from the axial PAR crest (Fig. 10 A and B). Worth mentioning are the 31GTV-samples that were collected from the surroundings of a hydrothermal field (~ 37°46.5'S) at the Central Axial High. 12DS, 34DS and 38DS were dredged from off-axis seamounts which are situated at the intersection area between the PAR and the Central (12DS) as well as the Southern (34DS, 38DS) Foundation Chain, respectively (Fig. 10 A).

The Samples 49DS-6, 49DS-7 and 49DS-10 were sampled at the summit area of a large off-axis seamount which is situated in a basin between two overlapping spreading centres at 41°22.5'S and 111°23.0'W (Fig. 10 B).

Most of the Fe-Mn precipitates from the PAR occur as thin coatings with a thickness up to 1 mm and often with a powder-like appearance. Samples 31GTV-7, 31GTV-8, 31GTV-9 and 49DS-6, 49DS-7, 49DS-10 only consist of slightly thicker crusts up to 4 mm (Table 1).

The Fe-Mn oxyhydroxides descend from water depths between 2157 and 2537 m and occur on different rock types and generations, even on very young volcanic rocks which may be only tens of years old (Stoffers et al., 2001).

Table 1. Sample description

Station	Coordinates of tracks	Sample description
06DS	From 37°33.710'S 110°49.560'W, 2228m To 37°33.502'S 110°49.341'W, 2264m	Continuous Mn oxide rind up to 1 mm thick on aphyric andesite.
12DS	From 37°44.488'S 111°04.020'W, 2316m To 37°44.282'S 111°03.860'W, 2331m	Patchy Mn oxide coatings (partly up to 1 mm), velvet-like, partly intergrown with Fe oxyhydroxides on plagioclase basalt.
24DS	From 37°54.201'S 110°56.845'W, 2260m To 37°54.008'S 110°56.850'W, 2266m	Local minor Mn oxides (< 1mm) on aphyric basalt glass.
31GTV-7 31GTV-8 31GTV-9	Ship 37°46.5379'S 110° 54.6379'W 2225 m	Mn oxides up to 3-4 mm thick on aphyric andesite. 31GTV-7: a crust that comes loose by itself after drying; 31GTV-8 and 31GTV-9: velvet-like crusts which are similar to Mn crusts known from other hydrothermal sites, containing some clay and Fe oxides.
34DS	From 38°12.86'S 111°11.17'W, 2308m To 38°12.68'S 111°11.09'W, 2157m	Mixture of minor orange Mn oxides (<< 1 mm) on basically fresh aphyric andesite glass and of a Mn oxide coating consistently 1 mm thick over entire plagioclase basalt boulder.
38DS	From 38°18.282'S 110°51.776'W, 2501m To 38°17.653'S 110°51.487'W, 2351m	Mixture of a Mn oxide crust up to 1 mm thick on relatively old plagioclase basalt, orange Mn oxides up to 1mm thick on aphyric basalt and of a Mn oxide coating up to 1 mm thick over grey aphyric basalt glass.
49DS-6 49DS-7 49DS-10	From 41°22.379S 111°23.226W, 2210m To.....41°22.862S 111°22.910W, 2225m	Rather thick Mn coatings on different rocks: 49DS-6: coating on altered black aphyric basalt glass. 49DS-7: 1 mm coating on black aphyric basalt glass. 49DS-10: 2-3 mm thick cauliflower-like on grey aphyric basalt.
50DS-2	From 41°23.153'S 111°30.798'W, 2464m To 41°23.608'S 111°30.464'W, 2507m	Mn oxides as coating in fractures on plagioclase basalt glass.
52DS	From 41°10.846'S 111°33.201'W, 2525m To 41°11.23'S 111°33.375'W, 2537m	Mixture of thin Mn oxide coating (1 mm) on more weathered olivine-plagioclase basalt glass and Mn oxides on fresher glassy olivine-plagioclase basalt.

4. Analytical techniques

4.1. Description of the methods

To sample the Fe-Mn precipitates, the thin coatings and crusts were brushed off the rocks and oven-dried at 60 °C. Afterwards the samples were studied microscopically for possible contaminations, for example vessel lacquer. They were then grinded to < 200 µm.

For chemical analysis the samples were selectively leached to get only the Fe-Mn oxyhydroxide phase and not the country rock which could not be separated properly. The country rock consists mainly of volcanic glass and rock and perhaps of crystalline Fe oxides.

In order to leach ions bound to easily reducible Mn oxides and moderately reducible amorphous Fe oxyhydroxides the samples were treated according to leaching step 3 of a sequential leaching method developed by Koschinsky and Halbach (1995). This leaching step was modified with respect to the solid/solution ratio.

70 mg (original weight) of sample material were mixed with 50 ml 0.2 M ammonia oxalate and adjusted to pH 3-3.5 with about 35-42 ml oxalic acid. After stirring the mixture for 12-14 hours the insoluble rest was removed by filtration with a 45 µm membrane filter. In order to get the leaching weight that means the amount of the solved material the insoluble rest was dried, weighed and the value was deducted from the original weight.

All leachates were finally made up to 100 ml with 1 M HNO₃ (1ml).

The samples were analysed for the major elements Mn, Fe, Al, and for the trace elements Cu, Co, Zn, Ba, Y, and the REE. The chemical analysis were performed at the geochemical laboratory of the TU Bergakademie Freiberg by Inductively-Coupled Plasma Mass-Spectrometry (ICP-MS) and Inductively-Coupled Plasma Atomic-Emission Spectrometry (ICP-AES) and for some samples at the geochemical laboratory of the FU Berlin (ICP-MS and Atomic-Absorption Spectrometry (AAS); Appendix: Table 1 and 4).

All reagents used were at least analytical grade. Precision and accuracy were checked against in-house and international standards (USGS NOD-A-1; Flanagan and Gottfried, 1980). Analytical data for the standard NOD-A-1 in comparison with published data are presented in the Appendix (Table 1 and 3).

Nearly pure Fe-Mn crusts with different genetic origin (hydrogenetic / hydrothermal) were used to check if the leaching step completely dissolves the Fe-Mn oxyhydroxides. This was done by comparing element concentrations of the leachates and the bulk samples (chapter 4.2: Fig. 1, 2, 4; Appendix: Table 2, 5). The hydrogenetic crust SO 167 were formed at the Osbourn Trough (sample: SO167

121DR 15-30 mm; T. Kuhn, unpublished data). M33/2 comes from the surroundings of the Central Indian Ridge and was formed as hydrothermal plume fallout (sample: M33/2 31GTV 0-1; Kuhn et al., 1998; Kuhn, 1999).

To check the accuracy of the method three sample leachates were performed in duplicate and measured for the major (Mn, Fe, Al) and trace elements (Cu, Co, Zn, Ba). The leachates were analysed by the same laboratories as described before (chapter 4.2: Fig. 1, 2; Appendix: Table 2, 5).

In addition digestions of some bulk samples were made. The samples (100 mg) were digested at 50°C for 1 h and at 100°C for 1 h in carbon vessels using a mixture of concentrated HF/HCl/HNO₃ in a ratio of 1:3:1. After evaporation the rest was twice dissolved in H₂O/HCl in a ratio of 1:1, boiled and evaporated. Final solutions were made up in 0.5 M HCl in polyethylene bottles.

Bulk chemical analysis were again analysed by ICP-MS, ICP-AES and AAS techniques at the geochemical laboratories of the TU Bergakademie Freiberg (ICP-MS; AES) and at the FU Berlin (ICP-MS; AAS); Appendix: Table 2 and 5).

4.2. Discussion of the leaching method

Accuracy of the used leaching method is generally good (Fig. 1 and Fig. 2). The performed duplicates 31GTV-a leachate, 31GTV-b leachate, M33/2-a leachate, M33/2-b leachate have almost identical major and trace element concentrations (maximum error is 7.00 %). Indeed, the concentrations can differ but the proportions are almost similar.

Larger errors occur for sample 06DS-a leachate and 06DS-b leachate. For instance the Ba concentrations between the leachates a and b differ for 33.49 %. This may be ascribed to the high percentage of volcanic glass in this sample which remains on the filter as fine particles. During drying and weighing these particles can easily be lost wherefore the weighing error increases. This circumstance especially takes effect on elements with minor concentrations (Mn: 10.46 %, Fe: 5.22 % but Zn: 20.18 % and Ba 33.49 % differences).

The effect of the weighing error can also be seen on the systematic higher major and trace element concentrations of the leachate 06DS-a compared to 06DS-b.

Nevertheless, the element proportions keep similar which suffices to qualitatively characterize the Fe-Mn oxyhydroxides.

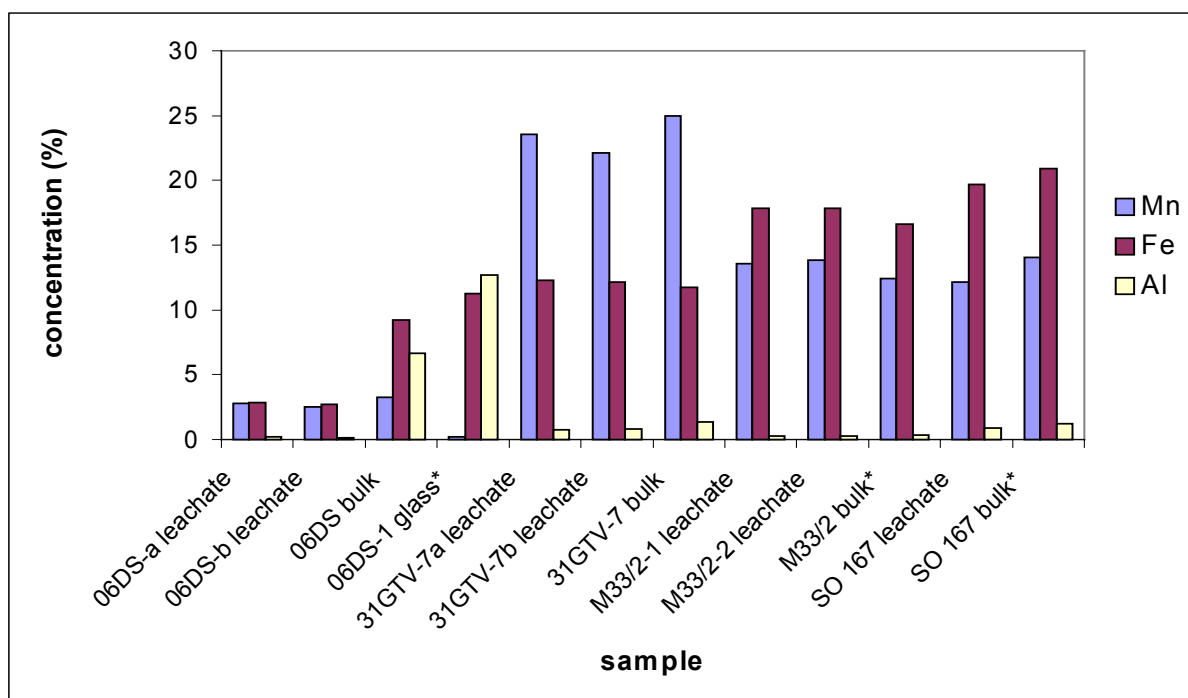


Fig. 1. Comparison of the major element concentrations between leachates and bulk samples. Samples 06DS, 31GTV-7 and M33/2 are in duplicates. All leachate concentrations refer to the original weight to make a comparison with the bulk samples possible. 06DS represents a thin Fe-Mn oxyhydroxide coating on glassy volcanic rock. M33/2 is a Fe-Mn crust formed by hydrothermal plume fallout (M33/2 bulk* = sample M33/2 31GTV 0-1; Kuhn et al., 1998) and SO 167 is a hydrogenetic crust (SO167 bulk* = sample SO167 121DR 15-30 mm; T. Kuhn, unpublished data). In addition the Mn, Fe and Al element concentrations of a volcanic glass from the dredge location 06DS (06DS-1 glass*; K. Haase, unpublished data) are presented. The duplicates give evidence of the good accuracy of the selective leaching method

The differences of the major, trace and REY (REE + Y) element concentrations between the leachates and the bulk samples depend on the country rock content. Especially sample 06DS (Fig. 1 and 2) has a high amount of volcanic glass and thereby big differences in the element concentrations. For comparison the element concentration for fresh volcanic glass of the same dredge location 06DS are given (K. Haase, unpublished data). As one can see in Fig. 1, the glass has higher Fe and Al contents than the leached Mn-Fe-oxihydroxides (referred to original weight). Therefore the bulk sample as a mixture of the Fe-Mn crust and the volcanic glass has also higher Fe and Al concentrations than the leachate.

On the contrary, the concentrations of the samples 31GTV-7, M33/2 and SO167 are similar between leachates and bulk samples. This is due to smaller amounts of country rock in the bulk sample.

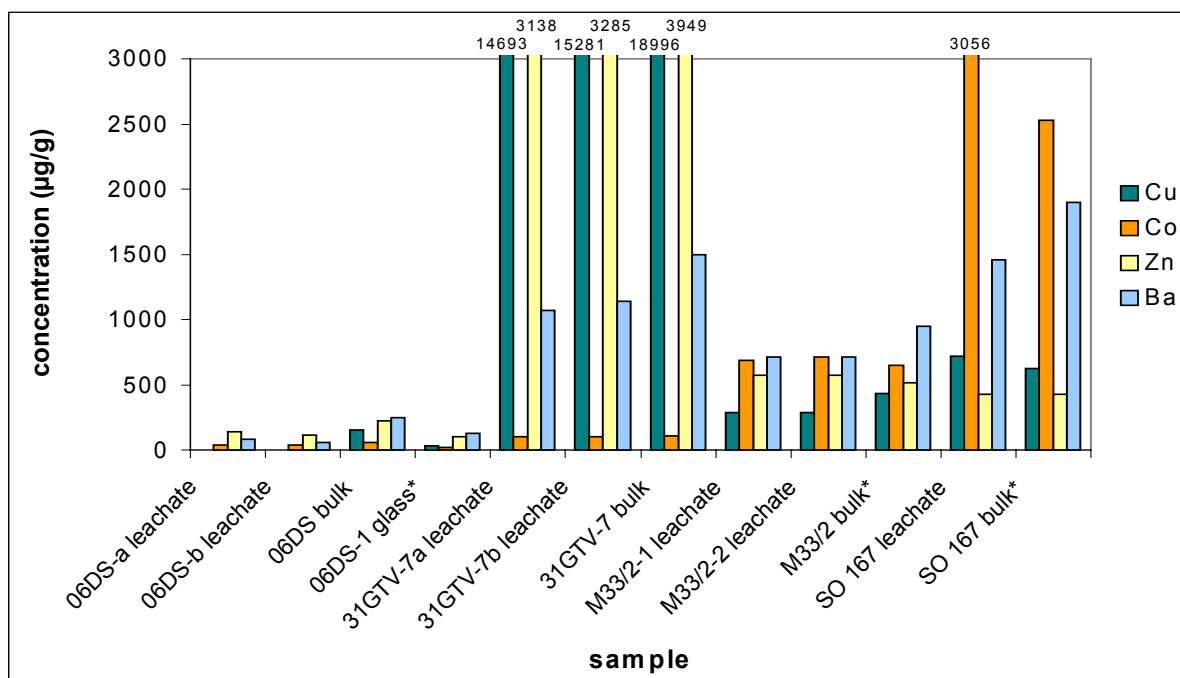


Fig. 2. Comparison of the trace element concentrations of Cu, Co, Zn and Ba between leachates and the samples. Samples 06DS, 31GTV-7 and M33/2 are in duplicates. All leachate concentrations refer to the original weight to make a comparison with the bulk samples possible. For sample identification refer to Fig.1. Accuracy of the leaching method is good as shown by duplicates.

Since most of the investigated samples have country rock/Fe-Mn oxyhydroxide ratios similar to sample 06DS a selective leaching procedure is necessary in order to extract and analyse the Fe-Mn oxyhydroxides only. This is especially true for trace elements and even more for REY. For instance comparing the leachate of 06DS with its bulk sample composition and with the volcanic glass it is obvious that the bulk sample composition is considerably controlled by the volcanic glass and not by the Fe-Mn oxides (Fig.3).

In this case a bulk sample analysis would not represent the Fe-Mn precipitates. And this may be true for most of the samples.

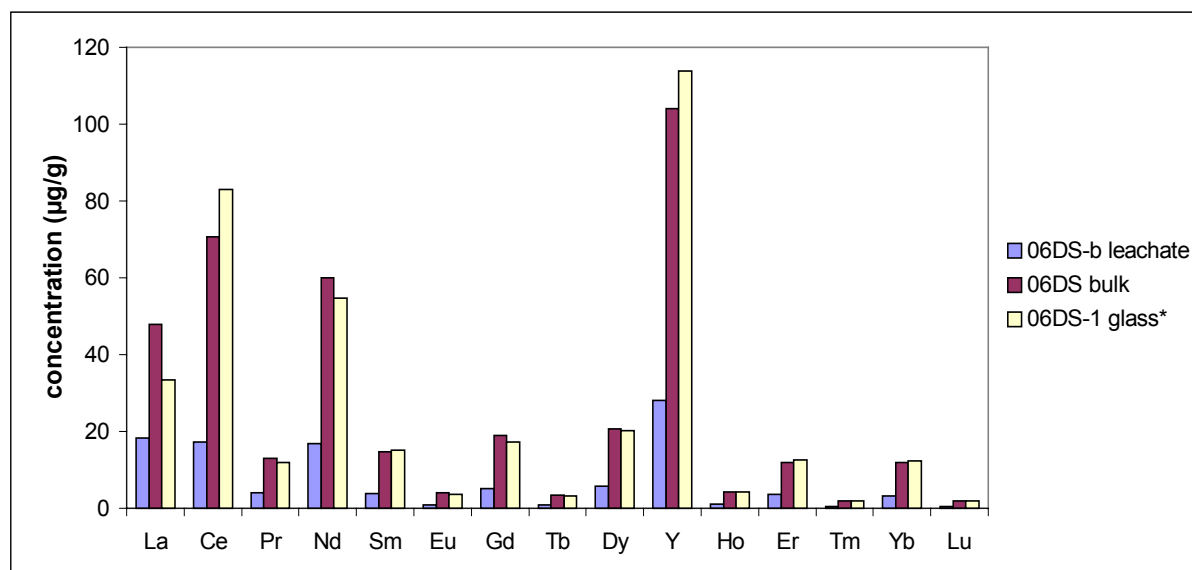


Fig. 3. Comparison of the REE and Y concentrations (Y inserted between Dy and Ho) between leachate 06DS-b, bulk sample 06DS and a volcanic glass (sample 06DS-1; K. Haase, unpublished data). The leachate concentrations refer to the original weight to make a comparison with the bulk samples possible. The high REY contents in the volcanic glass considerably control the bulk sample concentrations.

Investigating the shale normalized (suffix SN, shale is Post-Archean Australian Shale after McLennan, 1989) REY patterns the leachates show a depletion of the MREE and LREE compared to the bulk samples (Fig. 4). This fractionation may be caused by re-adsorption of the MREE and LREE during leaching onto particles, colloids or onto the bottle walls. However, Ce_{SN} seems to be less depleted compared to other REE. The reducing agent used for leaching may cause the reduction of Ce^{4+} to Ce^{3+} which maybe the reason for Ce_{SN} being less depleted in the leachate compared to other REE. A negative Ce_{SN} -anomaly in the bulk sample therefore, results in a less pronounced negative Ce_{SN} -anomaly in the leachate. But if there is a negative Ce_{SN} -anomaly in the leachate there also should be a negative one in the bulk sample. A positive Ce_{SN} -anomaly in the bulk sample will lead to an even more positive one in the leachate (Fig. 4). In general, the direction of the Ce_{SN} -anomaly is preserved during leaching, thus it can be used for genetic interpretation.

A general rule may be that the higher the REY concentrations in the bulk sample the higher the REY depletion during leaching. Since the investigated samples have rather low REY concentrations with distinct negative Ce_{SN} -anomalies the used selective leachate is thought to represent the true REY pattern of the Fe-Mn oxyhydroxides (see chapter 5).

The positive Eu_{SN} -anomaly typical for hydrothermal crusts like sample 31GTV seems to be preserved during leaching, too.

The phenomenon of the re-adsorption of REE during chemical leaching has also been described by Sholkovitz (1989). Sholkovitz discovered this re-adsorption of REE onto sediments by many different leaching solutions even at low pH. Unfortunately there were no experiments with the leaching solution NH_4 -oxalate and oxalic acid which were used in this study.

Because of the MREE and LREE depletion a quantitative description of the REE from leached samples is not useful but the pattern of the Ce_{SN} -anomaly can be used for characterization of the Fe-Mn oxyhydroxides.

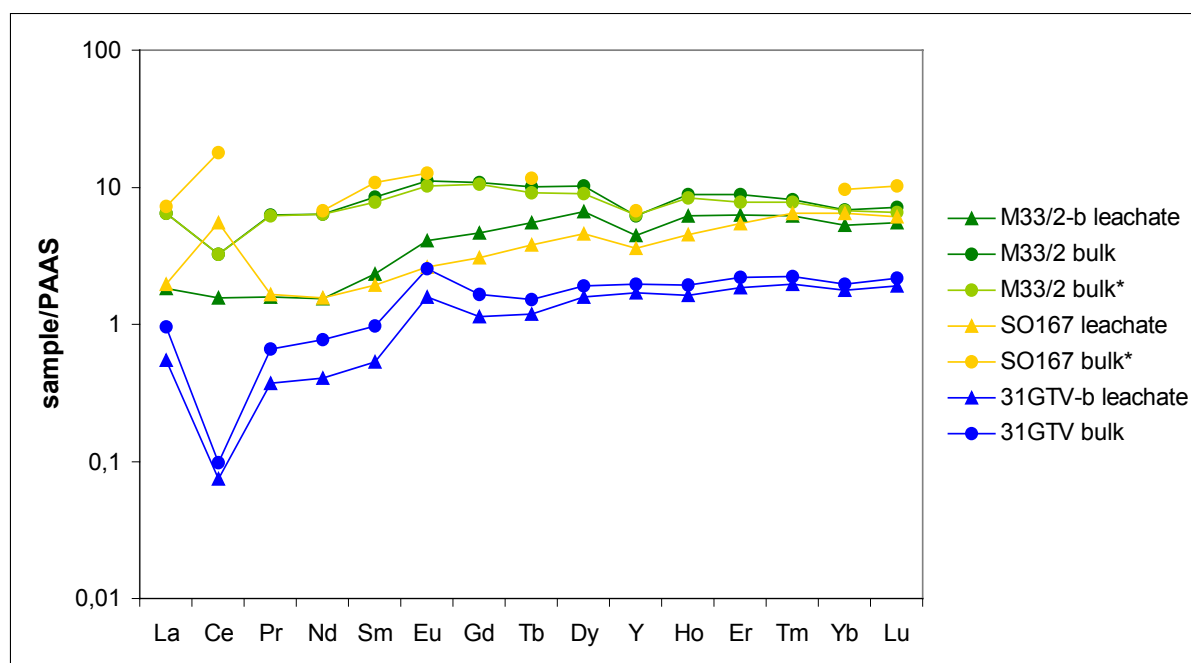


Fig. 4. Shale-normalized (PAAS refers to Post-Archean Australian Shale after McLennan, 1989) REE and Y patterns (Y inserted between Dy and Ho). The leachate concentrations refer to the original weight to make a comparison with the bulk samples possible. Sample 31GTV is a hydrothermal crust. For sample identification refer to Fig.1. The selective leaching produces a depletion of the MREE and LREE but the Ce_{SN} - and Eu_{SN} -anomaly seem to be preserved.

5. Results

Table 2 and 5 (Appendix) present the leachates compositional data. The Fe-Mn coatings are characterized by different major element concentrations which are compiled and compared with literature data in Fig. 5. Mn has contents ranging from 5.2 to 28.9 wt.% and Fe concentrations vary between 8.7 and 20.5 wt.%. In general the Al contents are lower than 2 wt.%. Only samples 12DS (2.5 wt.%), 24DS (10.4 wt.%) and 38DS (4.1 wt.%) have higher Al contents.

According to the Mn and Fe abundances the Mn/Fe ratios are varying over a wide range. Samples 06DS-a, -b, 34DS, 50DS-2 show Mn/Fe ratios close to unity. Samples 12DS, 24DS, 38DS, 49DS-6, 49DS-7, 49DS-10, 52DS have lower Mn/Fe ratios between 0.34 (24DS) and 0.86 (52DS). An enrichment of Mn compared to Fe show the samples 31GTV-7a, -b, 31GTV-8 and 31GTV-9 with Mn/Fe ratios ranging from 1.47 to 1.92.

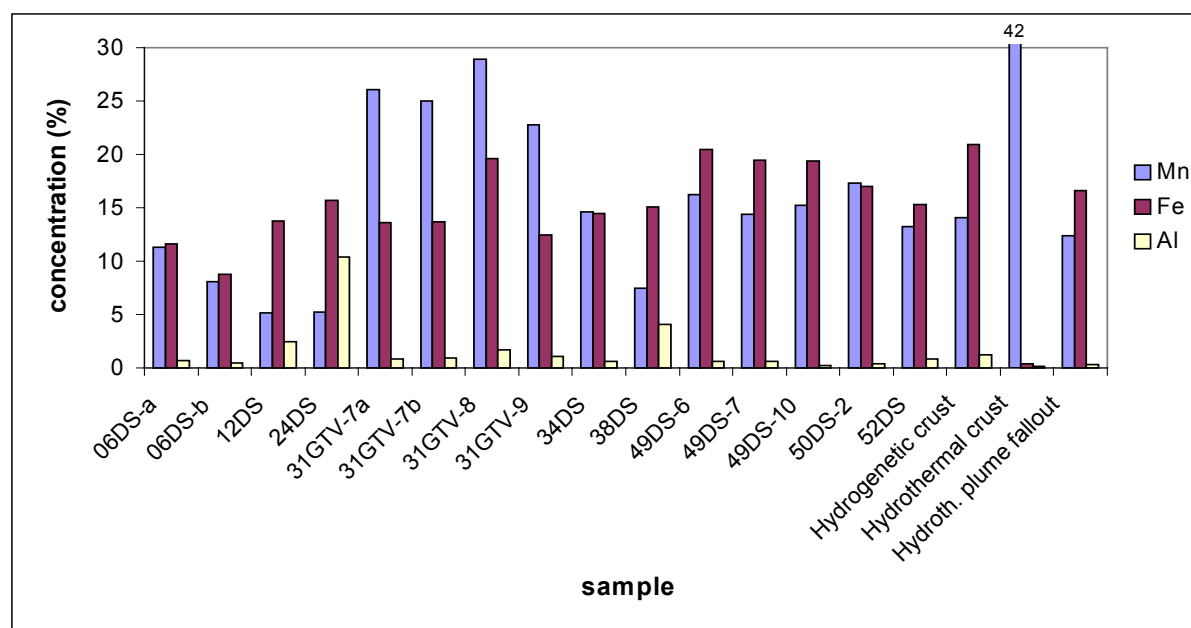


Fig. 5. Comparison of the major element concentrations between the PAR samples and literature data. Literature data: Hydrogenetic crust = sample SO167 121DR 15-30 mm (T. Kuhn, unpublished data); Hydrothermal crust = sample SO99 85DK-3 (Kuhn et al., 2003). Note, the hydrothermal crust was sampled at the periphery of a hydrothermal system explaining the high Mn/Fe ratio. Hydrothermal plume fallout = sample M33/2 31GTV 0-1 (Kuhn et al., 1998). All PAR samples are leachate concentrations and refer to leachate weight. The Fe-Mn precipitates are characterized by different major element concentrations.

Trace element concentrations of Cu, Co, Zn and Ba also vary considerably in the sample set (Fig. 6). Samples 31GTV-7, 31GTV-8 and 31GTV-9 are separated from all other samples because of very high concentrations of Cu (3400-27700 $\mu\text{g/g}$), Zn (1330-4490 $\mu\text{g/g}$) and Ba (1090-1760 $\mu\text{g/g}$). Even hydrothermal crusts from other locations show much lower Cu and Zn concentrations (Fig. 6).

All other PAR samples have low Cu and Zn contents ranging for Cu between b.d.l. (below detection limit) and 787 $\mu\text{g/g}$ and for Zn from contents below detection limit to 579 $\mu\text{g/g}$. Compared with three reference samples (Fig. 6) the Ba contents are relative low and most similar to hydrothermal plume fallout (Kuhn et al., 1998; Kuhn, 1999). Only sample 24DS differs by having extreme high Ba concentrations (6190

$\mu\text{g/g}$), the highest of all PAR samples. Co is present in low concentrations between 111 and 448 $\mu\text{g/g}$.

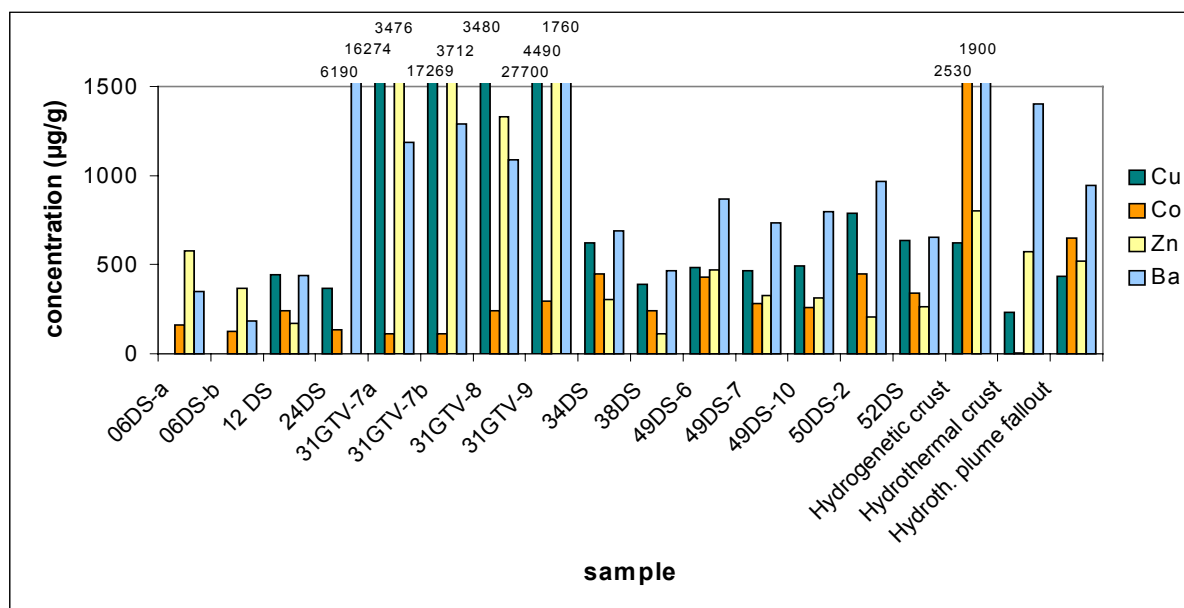


Fig. 6. Comparison of the trace element concentrations between the PAR samples and literature data. Literature data: Hydrogenetic crust = sample SO167 121DR 15-30 mm (T. Kuhn, unpublished data). Hydrothermal crust = sample SO99 85DK-3 (Kuhn et al., 2003). Note, the hydrothermal crust was sampled at the periphery of a hydrothermal system, explaining the low Co, Zn, Ba concentrations. Hydrothermal plume fallout = sample M33/2 31GTV 0-1 (Kuhn et al., 1998; Kuhn, 1999). All PAR samples are leachate concentrations refer to leachate weight. The Fe-Mn precipitates are characterized by different trace element concentrations.

On the basis of the shale-normalized REY patterns the PAR samples can be divided into two groups (Fig. 7). Group 1 is characterized by higher ΣREE contents (not shale-normalized) ranging from 85.7 $\mu\text{g/g}$ to 309 $\mu\text{g/g}$ and comprises the samples: 06DS-b, 31GTV-7b, 31GTV-8, 31GTV-9, 34DS, 49DS-6, 49DS-7, 48DS-10, 50DS-2 and 52DS. The REY_{SN} patterns of Group 1 display different strong negative Ce_{SN} -anomalies ranging from very strong negative Ce_{SN} -anomalies (31GTV-7b, 31GTV-8, 49DS-7, 49DS-10 with $(\text{Ce}/\text{Pr})_{\text{SN}}$ ratios between 0.14-0.22) to smaller Ce_{SN} -anomalies (06DS-b, 31GTV-9, 34DS, 49DS-6, 50DS-2, 52DS with $(\text{Ce}/\text{Pr})_{\text{SN}}$ ratios between 0.26-0.48). Samples 31GTV-7b and 31GTV-9 also show a positive Eu_{SN} -anomaly.

In contrast to Group 1, Group 2 has lower ΣREE contents of 27.4 $\mu\text{g/g}$ and 44.7 $\mu\text{g/g}$. Group 2 is made up of the samples 12DS and 24DS. Another characteristic feature of this group is the small negative Ce-anomaly, being reflected by the $(\text{Ce}/\text{Pr})_{\text{SN}}$ ratios, of 0.36 for sample 24DS and 0.34 for sample 12DS. Both samples of this group show positive Eu_{SN} -anomalies.

Note, that the values of the ΣREE and the $(\text{Ce}/\text{Pr})_{\text{SN}}$ ratios are only approximate values since the REE get fractionated during leaching (discussed in chapter 4.2). Therefore, a more detailed discussion of the REY patterns is not possible.

Due to the problems being connected with the used leaching method, a more detailed classification based on the REY patterns is not possible.

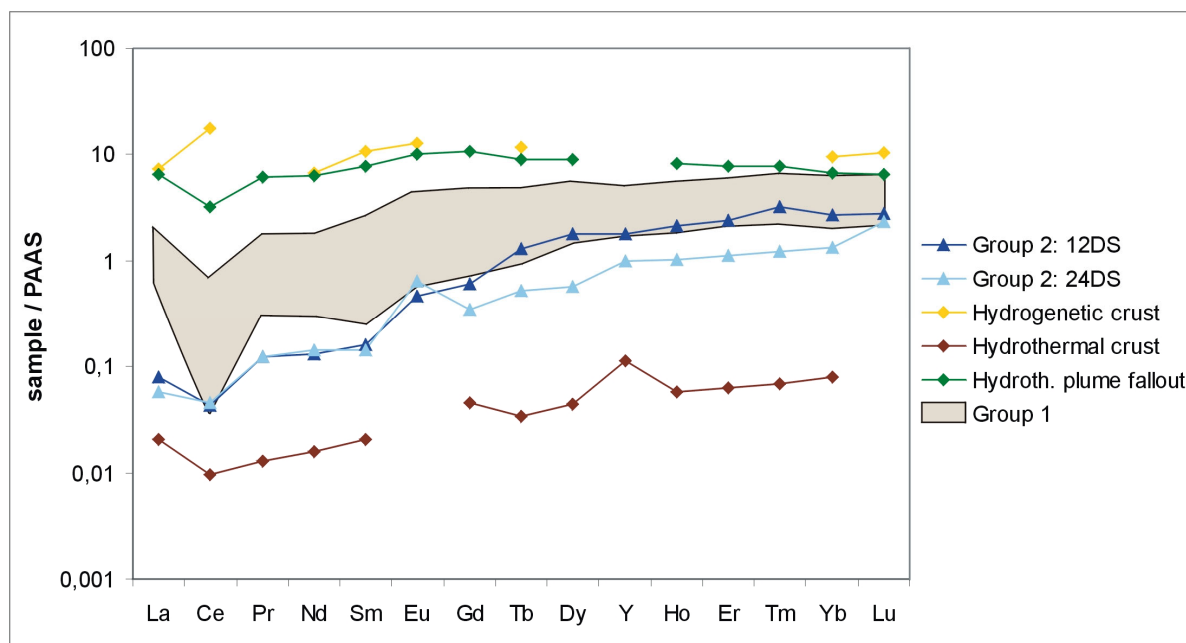


Fig. 7. Comparison of the REY patterns (SN-normalized) between the PAR-samples and literature data. Based on the sum of the REE concentrations and the Ce_{SN} -anomaly the PAR samples can be divided into two groups. Group 1 comprises the samples: 06DS-b, 31GTV-7b, 31GTV-8, 31GTV-9, 34DS, 38DS, 49DS-6, 49DS-7, 49DS-10, 50DS-2, 52DS and group 2 is made up of 12DS and 24DS. For identification of literature data refer to Fig.6. All PAR samples are leachate concentrations referring to leachate weight.

6. Discussion

6.1. Genetic interpretation of the PAR samples

A diagenetic growth of all investigated PAR samples can be excluded since they all were formed on more or less fresh volcanic rocks. Therefore, the PAR Fe-Mn oxyhydroxides got their element content from the surrounding water body which might either be seawater, hydrothermal plumes or hydrothermal fluids.

The low Co concentrations and the negative Ce_{SN} -anomaly point to a fast growth of the PAR-samples, otherwise the Fe-Mn precipitates would have enriched Co and Ce

by oxidative scavenging from seawater. Also the low ΣREE contents between 27 and 309 $\mu\text{g/g}$ confirm this since slow growing hydrogenetic crusts have high average REE contents (for example about 1400 $\mu\text{g/g}$ for samples from the northwest Pacific; Usui and Someya, 1997). REE are sorptively scavenged from seawater by settling Fe-Mn oxyhydroxides (Usui and Someya, 1997).

A fast precipitation rate of Fe-Mn oxyhydroxides requires an increased supply of Mn and Fe. Therefore, apart from seawater there must be an additional and more important Mn and Fe source. On a mid-ocean ridge this can only be hydrothermal activity.

The ternary plot of Co to Mn and Fe (Fig. 8) shows interpreted hydrothermal and hydrogenous fields. PAR samples data plot in the hydrothermal field which is bordered by a dotted line because of the gradually transition from hydrothermal crusts formed by hydrothermal fluids, crusts which were formed by plume fallout as well as hydrogenetic crusts formed by precipitation from normal seawater (Kuhn, 1999). Thus, the Co concentrations of the PAR samples are higher than the average content of hydrothermal crusts from the northwest Pacific which were formed by hydrothermal fluids (72.3 $\mu\text{g/g}$; Usui and Someya, 1997) but they are lower than the Co contents of hydrothermal plume fallout crusts from the Central Indian Ocean (Kuhn et al., 1998).

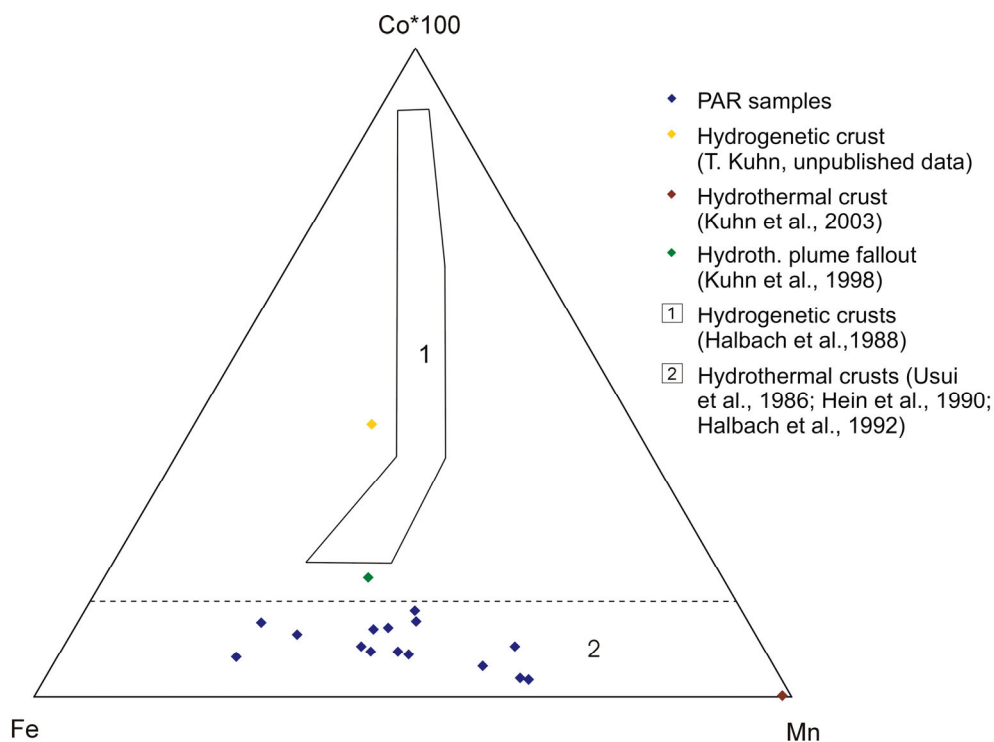


Fig. 8. Ternary plot of Co, Mn, and Fe of PAR samples compared to literature data. PAR samples data plot in the hydrothermal field. The leachate concentrations of the PAR samples refer to the leachate weight.

Another fool of separating hydrothermal from hydrogenetic Fe-Mn deposits is the comparison of La with Ce (Fig. 9) All PAR samples have low La and Ce concentrations and high La/Ce ratios similar to other hydrothermal crusts and seawater. As a result of the high growth rates of hydrothermal crusts, there is almost no enrichment of Ce by oxidative scavenging. This is caused by the slow reaction kinetics of the Ce(III) oxidation (Kuhn et al., 1998).

In contrast to hydrothermal crusts, Ce enrichments are evident for hydrogenetic crusts by their low La/Ce values (generally < 1 ; Nath et al., 1997). However, the position of the samples in the La-Ce plot largely depends on the time (during and after the deposition) the Fe-Mn precipitates have been in contact with seawater. Thus, some PAR samples divert from the seawater line the higher their La and Ce concentrations are (Fig. 9 A). Probably this results from a higher influence of seawater as a REE source and a slower deposition or longer contact to seawater after the formation of the precipitates. These processes increase the decoupling of Ce from the REE(III) which is typical for crusts formed by hydrothermal plume fallout. The gradual transition between crusts formed by hydrothermal fluids and by hydrothermal plume fallout is also reflected by the Fe-Mn oxyhydroxide coatings and crusts of the Pacific-Antarctic Ridge.

For example sample 24DS show typical hydrothermal signatures suggesting a formation from a hydrothermal fluid. That is provable by the extreme high Ba content (6190 $\mu\text{g/g}$), the low Co concentration, the positive Eu_{SN} -anomaly, the low Cu and Zn concentrations as well as the low ΣREE content. As crystalline baryte is not soluble in the used leaching solution, the Ba should be bound to the Fe-Mn phases. According to the low La and Ce contents in the La-Ce plot the sample is situated close to the hydrothermal crust of the North Fiji Basin (Kuhn et al., 2003; Fig. 9 A).

In contrast to normal hydrothermal crusts which were formed by a fluid, 24DS has a very low Mn/Fe ratio of 0.34 pointing to a precipitation from an iron rich hydrothermal fluid. Up to now iron rich hydrothermal fluids have not been considered as an origin of hydrothermal Fe-Mn crusts. Crusts with a similar Mn/Fe ratios for example from the Central Indian Ocean were described by Nath et al. (1997) as distal hydrothermal deposits. But these crusts have higher Co, Cu, Zn and ΣREE contents than the PAR sample 24DS, in consequence of a increased hydrogenetic input. Such distal hydrothermal crusts were probably formed by hydrothermal plume fallout. Except the weak negative Ce_{SN} -anomaly that can also be produced by the leaching method a hydrogenetic input can not be recognized for 24DS.

Fe and Mn are fractionated in a hydrothermal system due to its slightly different behaviour according to pH, Eh and temperature conditions. Fe is precipitated proximal to a hydrothermal vent site either as sulfide from the hydrothermal fluid or as oxide from the hydrothermal plume. Mn is precipitated distal to a hydrothermal vent

either from a hydrothermal plume or from a low-temperature hydrothermal fluid. The latter is often dramatically enriched in Mn compared to Fe ($Mn/Fe > 1000$; Kuhn et al., 2003). From this reasoning sample 24DS seems to be precipitated close to an active high-temperature vent site. Because of the small thickness of the coating the fluids are proposed to emanate for a short period in this area.

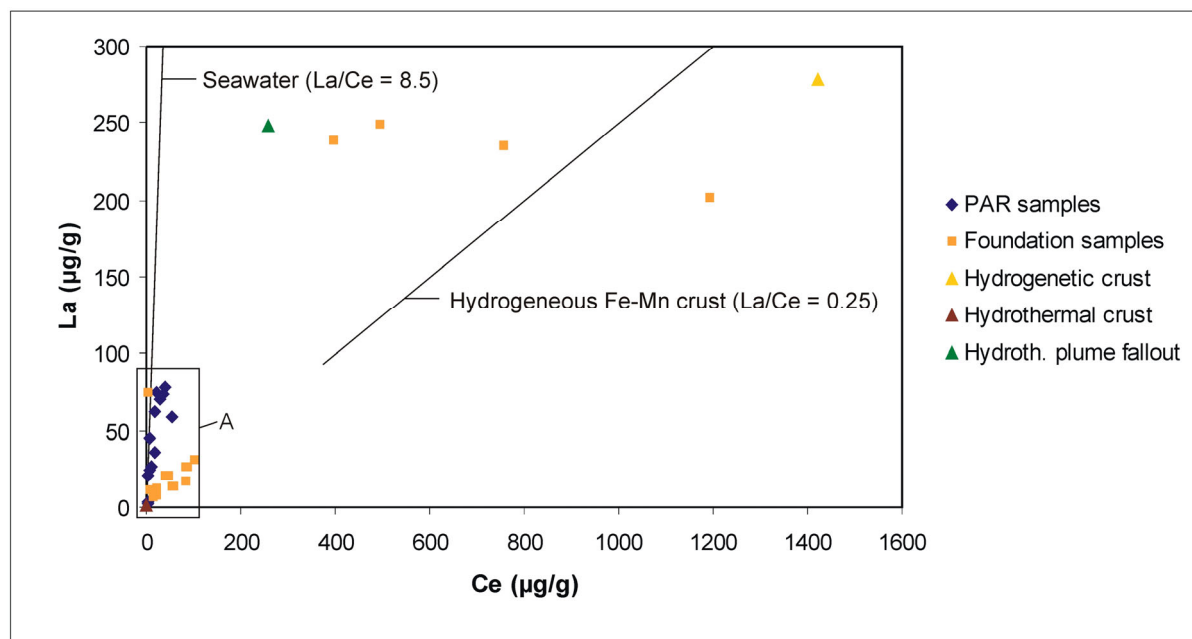
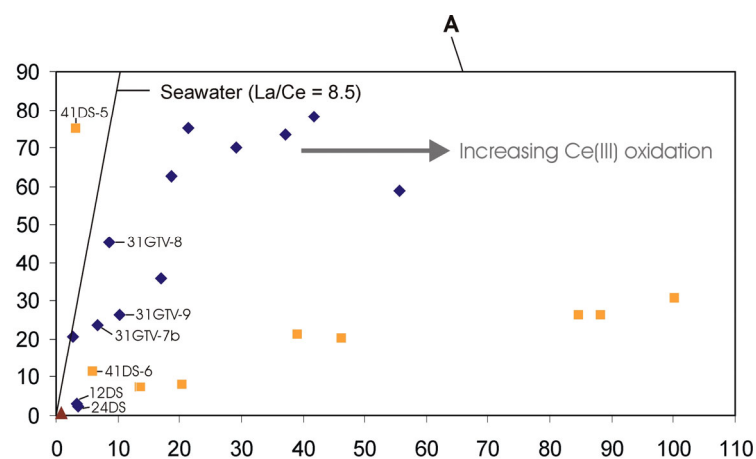


Fig. 9 The plot of La versus Ce shows several different sample sets: the PAR samples (leachate weight); crusts from the Foundation Seamount Chain (P. Stoffers, unpublished data) as well as crusts precipitated from hydrothermal fluids (hydrothermal crust) and from hydrothermal plumes (hydrothermal plume fallout). The Foundation crusts are discussed in chapter. 6.2.

Hydrothermal crusts have low La and Ce concentrations and are similar to seawater ($La/Ce = 8.5$ for seawater from the SE Pacific; water depth: 2500m; Klinkhammer et al., 1983). In comparison, hydrogenetic crusts have higher La and Ce contents but lower La/Ce -ratios (similar to 0.25 hydrogenet. crust from the Central Indian Basin, Nath et al., 1997).

Samples 31GTV-7, -8 and -9 which have been collected from the surroundings of a hydrothermal field also show strong hydrothermal signatures. The chemical data of



these crusts, for example the high Mn/Fe ratios, the high Ba and low Co concentrations, the negative Ce_{SN}-anomalies, and the positive Eu_{SN}-anomalies point to a formation of these crusts by precipitating from a diffuse emanating hydrothermal fluid. The appearance of the crusts which differ from all other samples by a greater thickness (3-4 mm) further supports the hydrothermal origin from a fluid.

But in marked contrast, the XRD analysis of the samples 31GTV-7 and 31GTV-9 (personal communication R. Kleeberg) indicate that in both crusts crypto-crystalline δ -MnO₂ (vernadite) is the only manganese phase present. The X-ray diffractograms show broad peaks at 2.4 Å and 1.4 Å. This poorly crystalline structure is generally formed by a precipitation from the water column (Usui and Someya 1997; Kuhn, 1999). Therefore, in comparison to the chemistry, the mineralogy of the crusts points to a precipitation from a hydrothermal plume.

No matter whether the crusts have been formed from a fluid or as plume fallout, they were sampled close to an active hydrothermal system with exposed sulphide talus, diffuse low-temperature discharge, and white smoke in the water column (Stoffers et al., 2001). Additionally the fluids have to be enriched in manganese to cause the high Mn/Fe ratios of the crusts. It is unlikely that a black smoker fluid is strongly enriched in manganese compared to Fe and therefore, the crusts should not have precipitated from a high-temperature fluid.

A possible conclusion is that the 31GTV crusts were precipitated from a plume of a medium-temperature fluid, for example a white smoker plume which was enriched in Mn compared to Fe. Fe-Mn precipitates from a plume fallout with such a high Mn/Fe ratio have not been described yet in literature.

The La-Ce plot of 31GTV (Fig. 9 A) displays a similar La/Ce ratio like other crusts of hydrothermal origin which is similar to seawater. But 31GTV samples differ from typical hydrothermal crusts formed from a fluid by containing more La and Ce. This implies a higher seawater influence probably by uptake of lanthanides from seawater during and after the hydrothermal formation of the crusts.

The very high Cu and Zn concentrations of the 31GTV samples with up to 27700 µg/g Cu and 4490 µg/g Zn, are also very special. Generally, hydrothermal crusts contain less Cu and Zn than hydrogenous crusts (Usui and Someya, 1997). Usui and Someya (1997) calculated average contents of 228 µg/g Cu (max. value: 1700 µg/g) and 238 µg/g Zn (max. value: 1427 µg/g) for hydrothermal crusts from the northwest Pacific.

In a distance of about 30-50 m from station 31GTV sulfides were recovered during 33GTV which have a composition of about 90 wt.% pyrite and < 10 wt.% chalcopyrite and sphalerite (S. Petersen, unpublished data). Therefore, Cu and Zn is proposed to be of hydrothermal origin. Since sulfides are not soluble in the reducing oxalate leaching solution and the XRD analysis did not show crystalline phases such as sulfides (personal communication R. Kleeberg), Cu and Zn seems to be bound to the Fe-Mn phases in the crusts. The solubility of Cu does not allow for high Cu

concentrations in white smoker fluids or in Mn-enriched, low-T diffuse fluids (von Damm, 1995). Therefore, Cu and Zn probably derive from oxic alteration of sulfides from nearby sulfide chimneys and sulfide talus. During the sulfide oxidation Cu and Zn is released and got enriched in the bottom water which influences the crusts. Copper dissolution and transport by seawater would probably occur as chlorides species as CuCl_2^- and CuCl_3^{2-} for the Cu(I) oxidation state and CuCl_3^- for Cu(II) state (Stouff and Boulègue, 1989). Dissolved Cu may also occur as carbonate complex in seawater (Li, 1991).

A sulfide alteration would also explain the different high amounts of these two elements in the three crusts since the sulfide talus is not distributed homogeneously in the area and currents influence the distribution of the element-enriched bottom water. Although all the crusts have high Cu and Zn values the samples 31GTV-7 and 31GTV-9 have Cu contents which are one order of magnitude higher than the concentrations of 31GTV-8 and also the Zn contents are more than twice as high. Hydrothermal Fe-Mn crusts with similar high Cu concentrations even up to 5.6 wt.% have been described from the EPR ($\sim 7^\circ\text{N}$) by Stouff and Boulègue (1989). They presume that Cu is adsorbed as Cu(I) atoms and partly as Cu(II) atoms mainly within the MnO_2 structure. But in contrast to the PAR crusts, these crusts consist of a 10-7 Å phyllosulfate which might be related to todorokite or busserite (10 Å) and birnesite (7 Å). The authors do not provide the hypothesis that the copper originates from oxidation of hydrothermal sulfides since the crusts only show a limited role of seawater in their precipitation. Rather they presume the direct precipitation of Mn-Cu oxide or oxyhydroxide from a hydrothermal fluid, probably from the remaining dense fluid after phase separation (Stouff and Boulègue, 1989).

However, for the three PAR crusts an influence of seawater is obvious according to their mineralogy and to the higher REE concentrations (Fig. 7 and 9 A) compared to 24DS and to typical hydrothermal crusts supporting the hypothesis that Cu and Zn was derived from the alteration of sulfides.

The rest of the PAR samples (06DS-a, -b, 12DS, 34DS, 38DS, 49DS-6, -7, -10, 50DS-2, 52DS) can be classified as hydrothermal plume fallout. They are characterized by negative Ce_{SN} -anomalies, missing positive Eu_{SN} -anomalies, and Mn/Fe ratios between 0.37 and 1.02. This is further supported by Cu concentrations similar to those of plume fallout samples from the Central Indian Ocean (Kuhn et al., 1998). Ba is generally low, lower than in typical hydrogenetic crusts where the Ba comes from seawater and lower than in hydrothermal crusts where the Ba comes from hydrothermal fluids (Usui and Someya, 1997). Compared to the plume fallout samples from the Indian Ocean (Kuhn et al., 1998) many PAR samples have lower Ba contents.

Although sample 12DS has similar to 24DS a Mn/Fe ratio of 0.38 and a low ΣREE content, the higher Co, Cu and Zn contents, the low Ba concentration, and the missing positive Eu_{SN} -anomaly point to a formation from a hydrothermal plume.

For samples 34DS and 50DS-2 a significant input from normal seawater is suggested due to the Mn/Fe ratios close to unity and higher Co and Cu values compared to other PAR samples.

Compared to 31GTV most of the PAR samples occur as thin coatings on the hard rock substrate. The only exception is sample 49DS-10 which forms 2-3 mm thick crusts. But there is no deviation of the chemical signature compared to the other plume fallout crusts. The greater thickness suggests either the crusts grew faster or for a longer period.

Given the formation of all crusts (except 24DS) as plume fallout, samples 31GTV precipitated close to a hydrothermal vent site all other samples formed distal (far away) from vent sites.

Since all PAR samples show a hydrothermal signature, a similar high hydrothermal potential as the EPR can be assumed at least for the investigated area of the PAR. It is not clear how many hydrothermal sites along the PAR are necessary to produce hydrothermal signals in all crust. However, the morphology of the PAR is similar to the EPR suggesting a rather high spreading rate. Mid-ocean ridges with high spreading rates are characterized by many but small and short-lived hydrothermal systems. This is probably also the case for the PAR.

Due to the doming of the central spreading axis and the missing distinctive rift valley of the PAR the hydrothermal plumes will not be limited to propagate along the rift valley over great distances but will drift according to local currents in almost all directions over the ridge flanks. Samples 34DS and 38DS recovered at off-axis seamounts could be formed by plumes deriving from hydrothermal vents at the spreading axis since no information of a possible hydrothermal activity at these two seamounts was found (Fig. 10 A).

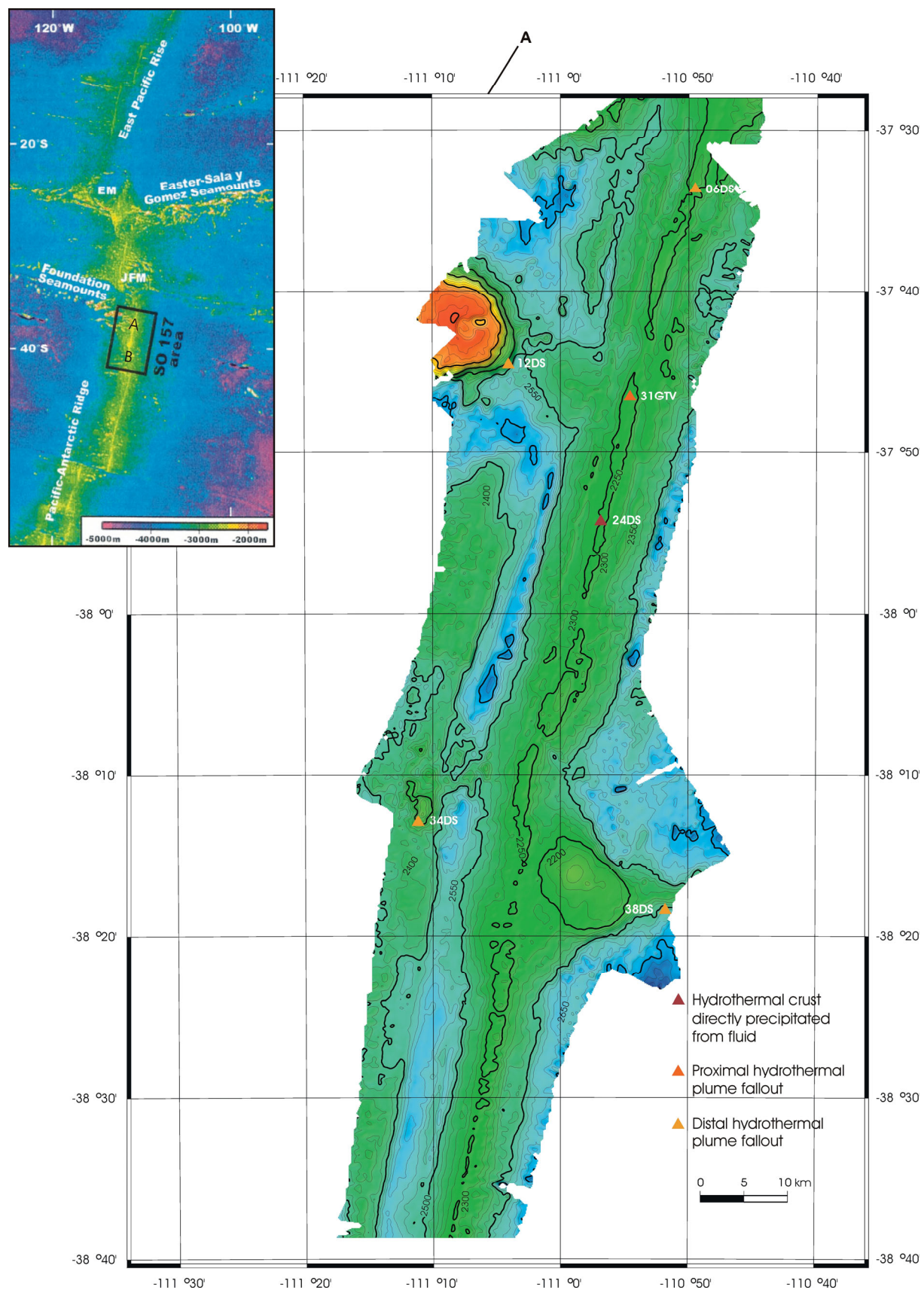
An extinct low temperature and short-lived hydrothermal activity is supposed for the off-axis seamount (37°42'S, 111°08'W) where sample 12DS derives from. This is supported by Fe-oxide chimneys observed during TV-grab operation (Stoffers et al., 2001). The hydrothermalism probably led to the formation of 12DS which were collected at the SE-flank of the seamount (Fig. 10 A).

Also the hydrothermal vent those plume produced the Mn-Fe-oxhydroxides 49DS-6, -7, -10 is probably situated at the same seamount from which the samples descends. This is supported by the tectonic setting of the off-axis seamount which is situated in a tectonic active area between two overlapping spreading centres (Fig 10 B) and by traces of disseminated pyrite which were found in volcanic rocks from the same location 49DS (Stoffers et al., 2001).

The rest of the analysed samples were collected from the central rift valley (Fig. 10 A and B) where most of the hydrothermal systems are situated.

Because of the small thickness of the PAR samples and the fact that the Mn coatings and crusts occur on very young volcanic rocks which may only be some tens of years

old, the influence of hydrothermal plumes is supposed to exist only for a short and a recent period.



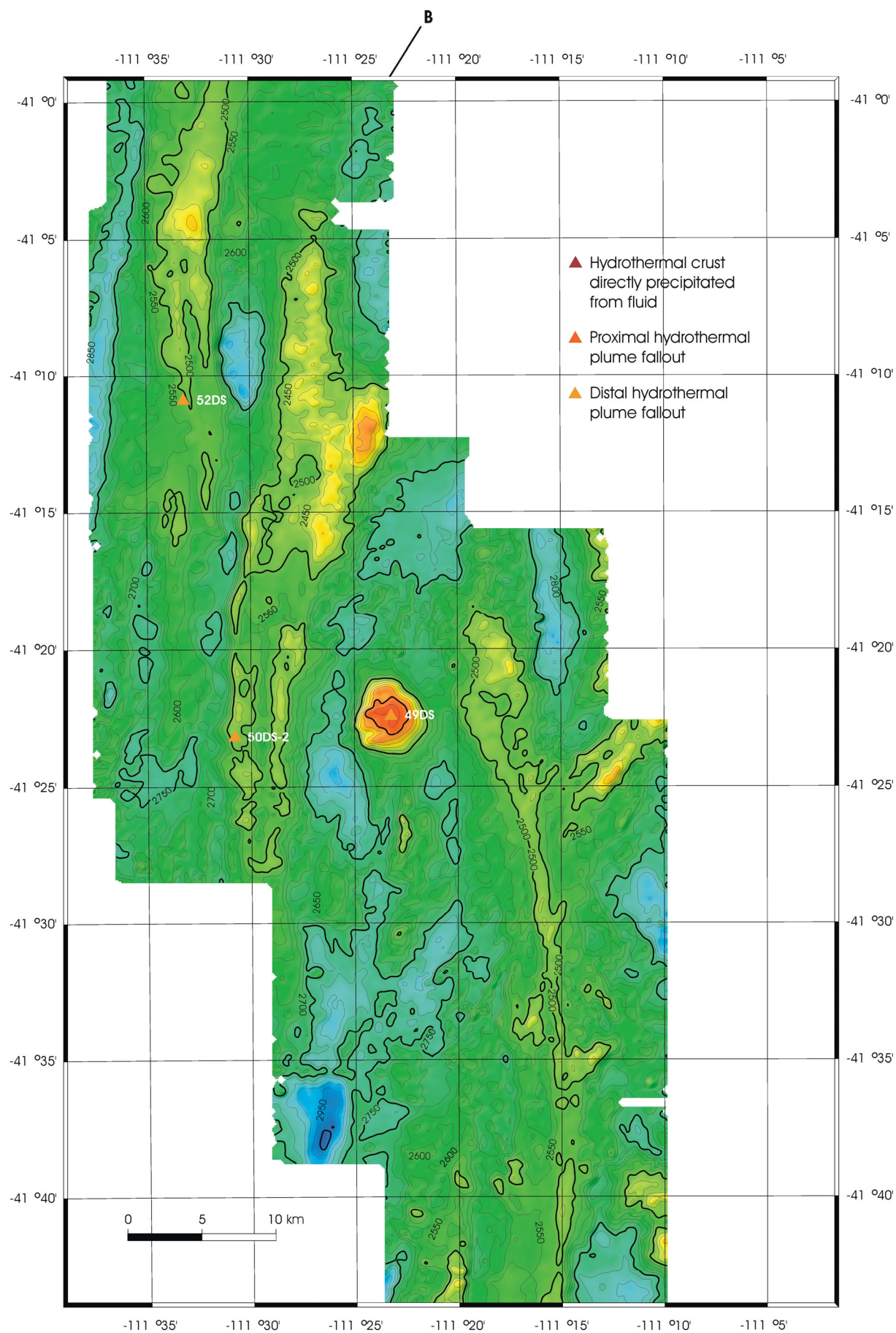


Fig. 10. Bathymetry and sample locations of the investigated area of the PAR. **A** comprises the area between 37°27'S and 38°40'S and **B** the area between 40°58'S and 41°47'S. The insert of A shows the general region with the working area as marked box. Maps were produced during cruise SO-157.

6.2. Regional comparison of the hydrothermal potential between PAR and Foundation

For a regional study the PAR crusts were compared with ferromanganese crusts from the Foundation Seamount Chain (FSC) taken during cruise SO-100 (Devey et al., 1995). The comparison is based on trace element concentrations like Cu, Co, Zn, Ba and REY-contents (P. Stoffers, unpublished data).

The shale normalized REY patterns of the FSC samples display a certain variety what can be attributed to different types of formation (Fig. 11).

Based on the high REE-concentrations the positive Ce_{SN} -anomalies and the high Co and Ba contents samples 11DS-7top and 31DS-2 are classified as hydrogenetic crusts. 11DS-7bottom and 18DS-6 were also formed by hydrogenetic precipitation since they show high REE, Co, Ba and Cu contents. But because of the missing positive Ce_{SN} -anomalies these crusts were probably diagenetically superimposed (Fig. 11). This is supported by the fact that of 11DS-7 and 18DS-6 precipitated on sediment substrate, whereas 31DS-2 grew on basalt.

Samples 41DS-5 and 41DS-6 probably are of hydrothermal origin. They show pronounced negative Ce_{SN} -anomalies (Fig.11), very low Co, and high Ba concentrations. If these crusts were precipitated from a hydrothermal fluid or a hydrothermal plume can not be concluded for sure since on the one hand they have low Co and high Ba contents but on the other hand sample 41DS-6 has relative high ΣREE concentrations. Additionally both samples have high Cu (1903 $\mu\text{g/g}$; 3279 $\mu\text{g/g}$) and Zn (759 $\mu\text{g/g}$; 871 $\mu\text{g/g}$) contents (P. Stoffers, unpublished data). In literature hydrothermal crusts generally have low Cu and Zn values (Hodkinson et al., 1994) since Cu and Zn generally precipitate as sulfides. But some hydrothermal crusts with high concentrations were described from the Hawaiian Archipelago, the Johnston Island Ridge, and from the Yap Arc (Cu: 2403 $\mu\text{g/g}$; Zn: 1477 $\mu\text{g/g}$; Hodkinson et al., 1994). As mentioned before extreme high Cu contents are known from hydrothermal crusts of the EPR (7°N; Stouff and Boulègue, 1989).

The rest of the considered FSC samples (26DS-9, 26DS-11, 36DS-1, 37DS-2, 41DS-6/2, 58DS-11, 80GTV, 89DS-5, 94DS-6) show strange signatures like weak positive, negative or no Ce_{SN} -anomalies, lower REE contents compared to hydrogenetic crusts (Fig.11), a strong variation of Cu und Ba concentrations, relative low Co contents and were classified as diagenetically influenced crusts. Since the intensity of the diagenetic overprint can not be estimated it is not possible to say if the signatures are primary or secondary. Except the samples 36DS-1 and 37DS-2 which grew on strongly altered basalt all diagenetic crusts have a sediment substrate (Devey et al., 1995) which enables such diagenetic fluid flows.

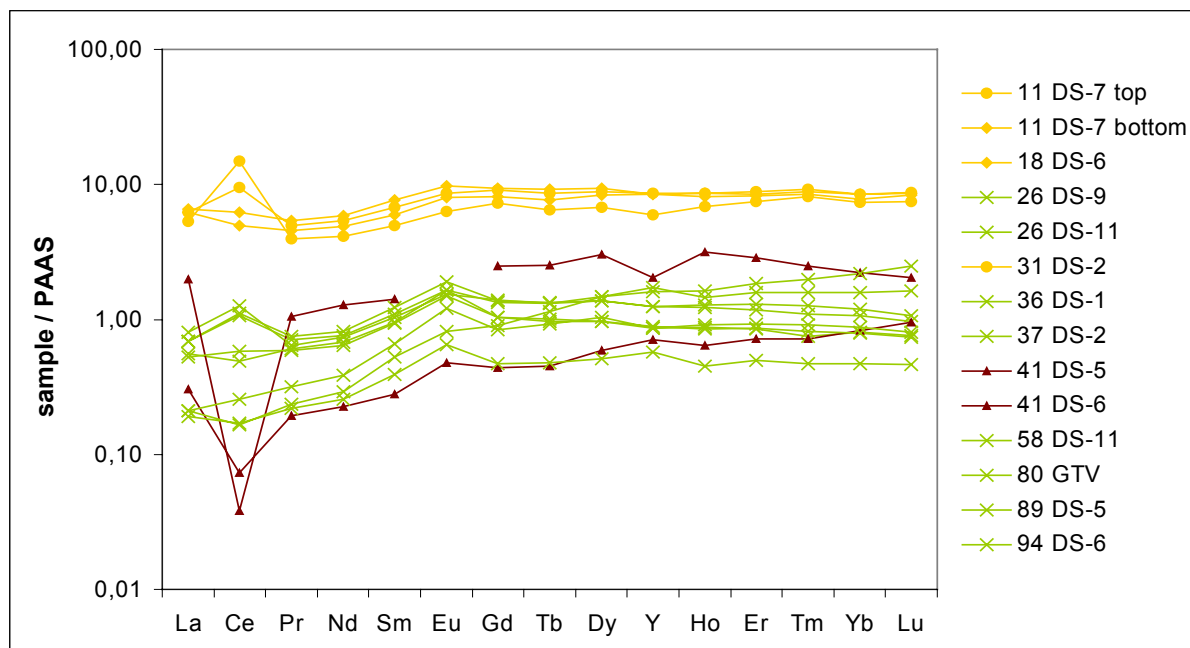


Fig. 11. Shale-normalized REY patterns of Fe-Mn crusts from the Foundation Seamount Chain. Based on the sum of the REE concentrations and the Ce_{SN} -anomaly the crusts can be divided into 3 different groups of formation. The yellow drawn samples are hydrogenetic crusts and the samples with the yellow diamonds probably were diagenetically influenced after its formation. Hydrothermal crusts are displayed in dark red and the green samples are interpreted as diagenetically influenced crusts.

The classification of the Foundation crusts is also proved by the La/Ce plot (Fig. 9). In this diagram four hydrogenetic crusts scatter around the 0.28 line as hydrogenetic crusts do. But obviously the two diagenetically influenced hydrogenetic crusts (11DS-7bottom, 18DS-6) were according to their higher La/Ce-ratios shifted towards the seawater line.

According to their high La/Ce ratios the two hydrothermal crusts (41DS-5, 41DS-6) also contrast with the other Foundation crusts by plotting near the seawater line which also represents hydrothermal crusts.

The diagenetic superimposed crusts show only a low variation of the La content but a higher one of the Ce content. Therefore, they group around a imaginary line with a La/Ce ratio of about 0.34 which differ significantly from the seawater line (Fig. 9 A).

Compared with the PAR, the Foundation Seamount Chain has a much lower hydrothermal potential. Along the FSC there are hydrogenetic, hydrothermal and diagenetically superimposed crusts. Most of the FSC crusts are diagenetically superimposed. Hydrothermal activity can only be demonstrated at one sample location (Seamount 12B, dredge track: from 34°52.352'S/121°33.309'W to 34°51.896'S/121°33.353'W, 2050-1726 m water depth; Devey et al., 1995). Nevertheless, some of the diagenetic crusts could also have a hydrothermal origin but due to the diagenetic overprint this is not provable. Hydrogenetic crusts were sampled from 3 seamounts .

7. Conclusions

The selective leaching is a suitable analytical method for a qualitative characterization of Fe-Mn precipitates that are contaminated by country rock. However, the REE show a re-adsorption during the leaching leading to a depletion of the MREE and LREE. The reason of the fractionation remains speculative.

In principle, the shale normalized patterns of the Ce_{SN} -anomaly and the Eu_{SN} -anomaly are preserved during leaching but a small weakening for negative Ce_{SN} -anomalies is possible. This is caused by the minor depletion of Ce compared to the other LREE. A general rule may be that samples with high REE contents fractionate more than samples with low REE contents.

The studied Fe-Mn-precipitates from the PAR are characterized by negative Ce_{SN} -anomalies, low Co and REE concentrations indicating a hydrothermal origin. Strictly speaking, most of the samples are suggested to be formed by precipitating from a hydrothermal plume. According to its chemical composition sample 24DS seems to be originated from a low-temperature, Fe-rich hydrothermal fluid.

The formation of three crusts from the sample location 31GTV can not be explained exactly as geochemical and mineralogical data point to different types of formation. In any case the samples show strong hydrothermal signatures. They have exceptional high Cu and Zn concentrations with up to 2.77 wt.% Cu and 0.45 wt.% Zn. Based on the XRD analysis and the character of the leaching solution Cu and Zn are bound to the Fe-Mn phases by adsorptive scavenging and are not incorporated as sulfides in the crusts.

Since all samples have hydrothermal signatures the PAR has a high hydrothermal potential at least between 37°33'S and 41°43'S. Also two off-axis seamounts are supposed to show hydrothermal activity.

In comparison to the PAR the Foundation Seamount Chain shows a much lower hydrothermal activity. Apart from two hydrothermal crusts collected from one seamount most of these crusts are diagenetically superimposed or of hydrogenetic formation.

Acknowledgements

The study was performed within the Foundation project funded by BMBF/BEO under the grant 03G0157B. Special thanks to T. Kuhn for the PAR and reference samples and the helpful discussions. I'm also grateful to those at the TU Bergakademie Freiberg and FU Berlin who supported the leaching experiments and analyses presented here. I thank P. Stoffers and K. Haase for the provision of chemical data

from the Foundation Seamount Chain and PAR and R. Kleeberg for the XRD analyses.

References

- Cormier, M.H., 1999. The ultrafast East Pacific Rise: instability of the plate boundary and implications for accretionary processes. In: Cann, J.R., Elderfield, H., Laughton, A. (Eds.), *Mid-Ocean Ridges: Dynamics of processes associated with creation of new ocean crust*. Cambridge University Press, Cambridge. 301 pp.
- DeCarlo, E.H. and McMurtry, G.M., 1992. Rare-earth element geochemistry of ferromanganese crusts from the Hawaiian Archipelago, central Pacific. *Chem. Geol.* 95, 235-250.
- Devey, C., Scientific Party of the Foundation Seamount Chain cruise, 1995. Sonne 100: The Foundation Seamount Chain. Technical Cruise Report R/V Sonne cruise SO-100, Geol.-Paläont. Inst. Univ. Kiel, Nr.75. 123 pp.
- Flanagan, F.J., Gottfried, D., 1980. US Geol. Surv. Rock Standards: III. Manganese-nodule reference samples USGS-NOD-A-1 and USGS-NOD-P-1. *USGS Prof. Pap.*, 1155.
- Halbach, P., Puteanus, D., Giovanoli, A., 1988. Transport and Accumulation Processes. In: Halbach, P., Friedrich, G., von Stackelberg, U. (Eds.), *The Manganese Nodule Belt of the Pacific Ocean*. Enke Verlag, Stuttgart, pp. 151-158.
- Halbach, P., Wahsner, M., Schwanold, G., Pracejus, B., Halbach, M., Koschinsky, A., 1992. Geowissenschaftliche Untersuchungen des Hydrothermalismus und der Lagerstättenbildung im intrakontinentalen Backarc-Becken des Okinawa-Troges. Abschlußbericht des Forschungsprojektes 03R 404A an das BMFT, Hydromin 2, SO71. Zentrum für Rohstofforientierte Meeresforschung, Technische Universität Clausthal, 188 pp.
- Hein, J.R., Scientific Party of the Farnella cruise F10-89-CP, 1990. Geological, geochemical, geophysical and oceanographic data and interpretations of seamounts and Co-rich ferromanganese crusts from the Marshall Islands, KORDI-USGS R.V. Farnella cruise F10-89-CP, U.S. Geological Survey, Washington, D.C.
- Hodkinson, R.A., Stoffers, P., Scholten, J., Cronan, D.S., Jeschke, G., Rogers, T.D.S., 1994. Geochemistry of hydrothermal manganese deposits from the Pitcairn Island hotspot, southeastern Pacific. *Geochim. Cosmochim. Acta* 58, 5011-5029.

- Klinkhammer, G., Elderfield, H., Hudson, A., 1983. Rare earth elements in seawater near hydrothermal vents. *Nature* 305, 185-188.
- Koschinsky, A., Halbach, P., 1995. Sequential leaching of marine ferromanganese precipitates: genetic implications. *Geochim. Cosmochim. Acta* 59, 5113-5132.
- Kuhn, T., Bau, M., Blum, N., Halbach, P., 1998. Origin of negative Ce anomalies in mixed hydrothermal-hydrogenetic Fe-Mn crusts from the Central Indian Ridge. *Earth Planet. Sci. Lett.* 163, 207-220.
- Kuhn, T., 1999. Geochemische und mineralogische Charakterisierung von Fe-Mn-Präzipitaten und Sedimenten aus der Umgebung der Rodrigues Triple Junction (zentraler Indischer Ozean) unter besonderer Berücksichtigung hydrothermalen Einflüsse. Shaker Verlag, Aachen. 169 pp.
- Kuhn, T., Bostick, B.C., Koschinsky, A., Halbach, P., Fendorf, S., 2003. Enrichment of Mo in hydrothermal Mn precipitates: possible Mo sources, formation process and phase associations. *Chem. Geol.* 199, 29-43.
- Li, Y.H., 1991. Distribution patterns of the elements in the ocean: A synthesis. *Geochim. Cosmochim. Acta* 55, 3223-3240.
- McLennan, S.M., 1989. Rare earth elements in sedimentary rocks: influence of provenance and processes. In: Lipin, B.R., McKay, G.A. (Eds.), *Geochemistry and Mineralogy of Rare Earth Elements. Reviews in Mineralogy*, vol. 21, pp. 169-200.
- Nath, B.N., Plüger, W.L., Roelandts, I., 1997. Geochemical constraints on the hydrothermal origin of ferromanganese encrustations from the Rodriguez Triple Junction, Indian Ocean. In: Nicholson, K., Hein, J. R., Bühn, B., Dasgupta, S. (Eds.), *Manganese Mineralization: Geochemistry and Mineralogy of Terrestrial and Marine Deposits. Geol. Soc. Spec. Publ.*, No. 119, The Geological Society, London, pp. 199-211.
- Roelandts, I., 1992. Comparison of inductively coupled plasma and neutron activation analysis for precise and accurate determination of nine rare-earth elements in geological materials. *Chem. Geol.* 67, 171-180.
- Sholkovitz, E.R., 1989. Artifacts associated with the chemical leaching of sediments for rare-earth elements. *Chem. Geol.* 77, 47-51.
- Sholkovitz, E.R., Landing, W.M., Lewis, B.L., 1994. Ocean particle chemistry: The fractionation of rare earth elements between suspended particles and seawater. *Geochim. Cosmochim. Acta* 58, 1567-1579.
- Stoffers, P., Scientific Party of the Foundation 3 cruise, 2001. Sonne 157 Foundation 3 cruise to the Foundation Seamount Chain: Magmatic and Hydrothermal Processes at a Spreading Axis influenced by a Hotspot: the Pacific – Antarctic Ridge and off-Axis Seamounts near 37° S. Technical Cruise Report R/V Sonne cruise SO-157, Inst. für Geowiss., Universität Kiel, Nr. 17. 132 pp.

- Stouff, P., Boulègue, J., 1989. Geochemistry and crystallochemistry of oceanic hydrothermal manganese oxyhydroxides showing Mn-Cu association. *Geochim. Cosmochim. Acta* 53, 833-843.
- Usui, A., Yuasa, M., Yokota, S., Nohara, M., Nishimura, A., Murakami, F., 1986. Submarine hydrothermal manganese deposits from the Ogasawara (Bonin) Arc, off the Japan islands. *Marine Geology*, 73, 311-322.
- Usui, A. and Someya, M., 1997. Distribution and composition of marine hydrogenetic and hydrothermal manganese deposits in the northwest Pacific. In: Nicholson, K., Hein, J. R., Bühn, B., Dasgupta, S. (Eds.), *Manganese Mineralization: Geochemistry and Mineralogy of Terrestrial and Marine Deposits*. Geol. Soc. Spec. Publ., No. 119, The Geological Society, London, pp. 177-198.
- Von Damm, K.L., 1995. Controls on the Chemistry and Temporal Variability of Seafloor Hydrothermal Fluids. In: S.E. Humphris, R.A. Zierenberg, L.S. Mullineaux and R.E. Thomson (Eds.), *Seafloor Hydrothermal Systems*. American Geophysical Union, Washington, D.C., pp. 222-247.

Appendix

Table 1. Major and trace element concentrations of the selective leachates investigated in this study and the USGS Fe-Mn nodule standard NOD-A-1. Leachate concentrations refer to leaching weight.

	Mn (wt.%)	Fe (wt.%)	Al (wt.%)	Cu (µg/g)	Co (µg/g)	Zn (µg/g)	Ba (µg/g)
PAR-samples							
DS06-a ²	11.30	11.59	0.70	b.d.l.	162	580	348
DS06-b ²	8.05	8.74	0.46	0.00	124	368	184
12DS ¹	5.19	13.8	2.45	445	244	170	439
24DS ¹	5.26	15.7	10.4	368	136	b.d.l.	6190
31GTV-7a ²	26.07	13.59	0.85	16274	111	3476	1185
31GTV-7b ²	25.02	13.72	0.94	17269	113	3712	1291
31GTV-8 ¹	28.9	19.6	1.72	3480	240	1330	1090
31 GTV-9 ¹	22.8	12.5	1.09	27700	295	4490	1760
34DS ¹	14.6	14.5	0.60	623	448	306	689
38DS ¹	7.45	15.1	4.07	389	242	112	467
49DS-6 ¹	16.2	20.5	0.58	482	429	469	868
49DS-7 ¹	14.4	19.5	0.61	466	282	329	736
49DS-10 ¹	15.2	19.4	0.22	491	261	312	798
50DS-2 ¹	17.3	17.0	0.38	787	448	204	967
52DS ¹	13.2	15.3	0.83	637	341	265	655
NOD-A-1 (a) ¹	17.2	8.75	1.30	1055	2820	1070	1570
NOD-A-1 (b)	18.54	10.93	2.05	1300	3100	687	1670

1: measured at the TU Bergakademie Freiberg (Mn, Fe, Al, Zn: ICP-AES; Co, Cu, Ba: ICP-MS)

2: measured at the FU Berlin (Mn, Fe: AAS; Al, Cu, Co, Zn, Ba: ICP-MS)

(a): bulk sample measured within this study at the TU Bergakademie Freiberg

(b): „Best value“ of the USGS Fe-Mn Nodule standard NOD-A-1 (Flanagan and Gottfried, 1980)

b.d.l.: below detection limit

Table 2. Major and trace element concentrations of some selective leachates and accompanying bulk samples investigated in this study. Leachate concentrations refer to original weight.

	Mn (wt.%)	Fe (wt.%)	Al (wt.%)	Cu (µg/g)	Co (µg/g)	Zn (µg/g)	Ba (µg/g)
PAR-samples							
06DS-a leachate ²	2.79	2.86	0.17	b.d.l.	40.0	143	85.7
06DS-b leachate ²	2.49	2.71	0.14	b.d.l.	38.5	114	57.0
06DS bulk ²	3.25	9.25	6.65	150	54.9	224	250
31GTV-7a leachate ²	23.54	12.27	0.77	14693	99.9	3138	1070
31GTV-7b leachate ²	22.14	12.14	0.83	15281	100	3285	1143
31GTV-7 bulk ²	25.00	11.75	1.35	18996	110	3949	1500
Reference samples							
M33/2-1 leachate ²	13.57	17.85	0.29	286	686	571	714
M33/2-2 leachate ²	13.85	17.85	0.29	286	714	571	714
M33/2 bulk ²	17.98	20.48	0.44	550	749	649	1199
SO167 leachate ¹	12.12	19.71	0.91	723	3056	428	1457

1: measured at the TU Bergakademie Freiberg (Mn, Fe, Al, Zn: ICP-AES; Co, Cu, Ba: ICP-MS)

2: measured at the FU Berlin (Mn, Fe: AAS; Al, Cu, Co, Zn, Ba: ICP-MS)

b.d.l.: below detection limit

Reference sample: M33/2 is formed by hydrothermal plume fallout (sample M33/2 31GTV 0-1; Kuhn et al., 1998) and SO 167 is a hydrogenetic crust (sample SO167 121DR 15-30mm; T. Kuhn, unpublished data).

Table 3. Comparison of Y and REE concentrations of the USGS Fe-Mn nodule standard NOD-A-1 between this study and literature data.

ID	Y (µg/g)	La (µg/g)	Ce (µg/g)	Pr (µg/g)	Nd (µg/g)	Sm (µg/g)	Eu (µg/g)	Gd (µg/g)	Tb (µg/g)	Dy (µg/g)	Ho (µg/g)	Er (µg/g)	Tm (µg/g)	Yb (µg/g)	Lu (µg/g)
This Study ¹	112	109	780	24.6	108	23.4	6.10	28.2	4.30	25.8	5.15	15.7	2.35	15.1	2.40
Kuhn et al., 1999	114	112	745	24.5	100	21.5	5.34	26.1	3.95	22.7	4.72	14.2	2.15	13.7	2.16
Flanagan and Gottfried, 1980		133	563		85	20.9	4.45	20.5	4.87				1.72	16.3	2.16
DeCarlo and McMurtry, 1992		111	654	22.0	101	21.6	4.77	27.2		21.0		11.2		11.9	2.18
Roelandts, 1992		105	701		93	21.0	5.24	22.3		21.6				13.4	2.00
Nath et al., 1992		115	656	21.7	94	20.4	5.81	34.3	4.2	25.8	5.09	15.6	2.19	15.4	2.21

1: bulk sample measured at the TU Bergakademie Freiberg (ICP-MS)

Table 4. Y and REE concentrations of the selective leachates investigated in this study. Leachate concentrations refer to leaching weight.

PAR samples	Y (µg/g)	La (µg/g)	Ce (µg/g)	Pr (µg/g)	Nd (µg/g)	Sm (µg/g)	Eu (µg/g)	Gd (µg/g)	Tb (µg/g)	Dy (µg/g)	Ho (µg/g)	Er (µg/g)	Tm (µg/g)	Yb (µg/g)	Lu (µg/g)
DS06-b ¹	90.7	58.9	55.7	13.0	54.3	12.10	2.87	16.80	2.71	18.70	3.70	11.60	1.61	10.3	1.45
12DS ¹	48.5	3.00	3.40	1.10	4.50	0.90	0.50	2.80	1.00	8.40	2.10	6.90	1.30	7.60	1.20
24DS ¹	27.1	2.20	3.60	1.10	4.80	0.80	0.70	1.60	0.40	2.70	1.00	3.20	0.50	3.80	1.00
31GTV-7b ¹	52.0	23.7	6.68	3.71	15.6	3.36	1.94	6.01	1.04	8.37	1.83	5.94	0.90	5.69	0.93
31GTV-8 ¹	141	45.5	8.60	6.80	29.8	6.50	2.90	15.1	3.10	22.3	5.50	16.9	2.70	17.8	2.80
31 GTV-9 ¹	66.5	26.5	10.2	4.20	18.9	3.90	2.00	8.00	1.30	9.60	2.40	7.40	1.00	6.80	1.20
34DS ¹	96.8	69.9	29.2	12.7	50.3	10.5	3.80	17.9	3.00	20.7	4.30	12.5	1.90	12.3	1.90
38DS ¹	45.4	20.6	2.80	2.60	10.1	1.40	0.60	3.40	0.70	6.80	1.80	6.00	1.00	6.10	1.10
49DS-6 ¹	113	36.0	16.9	5.60	22.2	4.90	2.20	12.9	2.80	20.4	4.70	15.4	2.50	14.0	2.30
49DS-7 ¹	113	62.6	18.6	9.40	38.5	8.20	2.60	15.0	2.90	20.9	4.70	14.5	2.30	14.2	2.20
49DS-10 ¹	123	75.1	21.4	11.1	44.9	9.90	2.90	16.9	3.00	21.5	5.00	15.7	2.30	15.2	2.30
50DS-2 ¹	115	78.0	41.7	15.6	60.2	15.0	4.40	22.5	3.80	26.0	5.60	16.8	2.50	14.6	2.20
52DS ¹	101	73.5	37.2	14.5	58.7	12.4	3.80	19.6	3.60	22.7	4.60	13.6	2.10	13.5	2.10

1: measured at the TU Bergakademie Freiberg (ICP-MS)

Table 5. Y and REE concentrations of some selective leachates and accompanying bulk samples investigated in this study. Leachate concentrations refer to original weight.

	Y ($\mu\text{g/g}$)	La ($\mu\text{g/g}$)	Ce ($\mu\text{g/g}$)	Pr ($\mu\text{g/g}$)	Nd ($\mu\text{g/g}$)	Sm ($\mu\text{g/g}$)	Eu ($\mu\text{g/g}$)	Gd ($\mu\text{g/g}$)	Tb ($\mu\text{g/g}$)	Dy ($\mu\text{g/g}$)	Ho ($\mu\text{g/g}$)	Er ($\mu\text{g/g}$)	Tm ($\mu\text{g/g}$)	Yb ($\mu\text{g/g}$)	Lu ($\mu\text{g/g}$)	
PAR-samples																
06DS-b leachate ¹	28.8	18.3	17.3	4.03	16.8	3.75	0.89	5.21	0.84	5.80	1.15	3.60	0.50	3.19	0.45	
06DS bulk ¹	104	47.9	70.7	13.0	60.1	14.6	4.00	19.0	3.30	20.6	4.20	12.0	1.90	12.0	1.90	
31GTV-7b leachate ¹	46.0	21.0	5.91	3.28	13.8	2.97	1.72	5.32	0.92	7.41	1.62	5.26	0.80	5.04	0.82	
31GTV-7 bulk ¹	52.8	36.8	7.78	5.81	26.1	5.39	2.74	7.68	1.18	8.91	1.93	6.31	0.90	5.57	0.94	
Reference samples																
M33/2-2 leachate ¹	121	70.0	125	14.0	52.3	13.0	4.43	21.6	4.27	31.2	6.08	17.8	2.52	14.9	2.38	
M33/2 bulk ¹	167	246	257	55.7	216	47.1	12.1	50.4	7.77	48.0	8.75	25.2	3.31	19.4	3.09	
SO167 leachate ¹	97.4	74.7	441	14.6	53.0	10.8	2.84	14.2	2.93	21.4	4.50	15.6	2.60	18.1	2.63	

1: measured at the TU Bergakademie Freiberg (ICP-MS)

Reference sample: M33/2 is formed by hydrothermal plume fallout (sample M33/2 31GTV 0-1; Kuhn et al., 1998) and SO 167 is a hydrogenetic crust (sample SO167 121DR 15-30mm; T. Kuhn, unpublished data).

Kurzfassungen

**Hekinian, R., Worthington, T., and Stoffers, P.
(2002) Explosive and Silicic Magmatism in the
Deep Ocean. Chapman Conference on Explosive
Subaqueous Volcanism, 21th – 25th Jan. 2002, New
Zealand**

Explosive and Silicic Magmatism in the Deep Ocean

[*R. Hekinian*] (Institute for Geoscience, University of Kiel, Olshausenstr. 40, D-24118 Kiel, Germany; ph: +49-431-8802085; fax: +49-431-8804376; e-mail: hekinian@wanadoo.fr); T. Worthington (Institute for Geoscience, University of Kiel; ph: +49-431-8802854; e-mail: tw@gpi.uni-kiel.de); P. Stoffers (Institute for Geoscience, University of Kiel; ph: +49-431-8802850; e-mail: pst@gpi.uni-kiel.de)

Volcanism in the deep ocean is dominated by sheet and pillow basalt flows. Nevertheless, pyroclastic rocks and hyaloclastite outcrop at 2 km-depth on the Mid-Atlantic Ridge near 34°50'N and testify to deep-water explosive eruptions of E-MORB and alkali basalt. Both the water and total carbon contents of these lavas increase with incompatible element concentrations. Their high vesicularity reflects early exsolution of CO₂, whereas H₂O will remain in the melt to water-depths of several hundred metres. Elsewhere, explosive volcanism and silicic lavas (>55 wt.% SiO₂) are found along parts of mid-ocean spreading centres affected by mantle plumes, in backarc basins, and on intraplate seamounts at depths in excess of 3 km. Tabular and lobate sheet flows of vesicular andesite–dacite form domal structures ~200 m-high overlying pillow basalt on segments of the 2.2 km-deep Pacific–Antarctic Ridge near the Foundation seamount chain (37–39°S). Similar flows outcrop on high-standing parts of the backarc Valu Fa Ridge (Lau Basin). In the intraplate setting (e.g., Pitcairn- SE Pacific), silicic magmatism occurs at small (<0.5 km-high) volcanic edifices where alkali- and volatile-rich trachyte is associated with pyroclastic rocks and hyaloclastite. The silicic magmas in each of these ocean floor settings reflect fractional crystallisation of basaltic melts, during which volatiles behave as strongly incompatible elements. Explosive volcanism is generally restricted to small volcanic cones or off-axis seamounts, where the repose interval between eruptions is longer than at axial ridges. The additional time may allow gas bubbles to accumulate at the top of the magmatic column and reach sufficient size and concentration for bubble walls to burst.

1. Chapman Conference on Explosive Subaqueous Volcanism
2. Invited
3. (a) R. Hekinian, Institute for Geoscience, University of Kiel, Olshausenstr. 40, D-24118 Kiel, Germany; (b) ph: +49-431-8802085; (c) fax: +49-431-8804376; (d) e-mail: hekinian@wanadoo.fr
4. No

**Stroncik, N. A., Haase, K. M., and Stoffers P. (2002)
Petrogenesis of lavas from the Pacific-Antarctic-
Ridge (PAR) – insights into magma generation
processes at fast spreading ridges in proximity to
hotspots. Beihefte zum European Journal of
Mineralogy, 14: 163**

Petrogenesis of lavas from the Pacific-Antarctic Ridge (PAR) – insights into magma generation processes at fast spreading ridges in proximity to hotspots

Stroncik, N. A¹, Haase, K.¹ and Stoffers, P.¹

¹ Institut für Geowissenschaften, Universität Kiel,
Olshausenstr. 40, 24098 Kiel
(nst@gpi.uni-kiel.de, kh@gpi.uni-kiel.de,
pst@gpi.uni-kiel.de)

Glassy to phyrlic submarine lavas were dredged from 36 sites along the Pacific-Antarctic Ridge (PAR) at its intersection with the Foundation Seamount Chain between latitudes 36°50'S and 41°50'S. The project pursues the following aims: (1) to establish the nature of plume-ridge interaction and (2) to pin-point the petrogenetic processes being responsible for the formation of high-Si lavas (up to 68 wt.% SiO₂) outcropping along the ridge crest.

The samples recovered comprise a suite of rocks ranging from basalts via basaltic andesites and andesites to dacites. The spreading axes close to the Foundation Hotspot shows bimodal volcanism, with basalts and andesites sampled at the same sites. This implies frequent changes of the composition of erupting lava and the presence of a stable magma system beneath the spreading axes. The chemistry of the rocks is largely controlled by fractional crystallisation of olivine ±feldspar ±clinopyroxene ±Ti-magnetite ±apatite. Increased Cl/K ratios in andesites relative to basalts calls for assimilation of hydrothermally altered material during the generation of the higher differentiated lavas.

Lead isotope and La/Yb ratios correlate positively with ⁸⁷Sr/⁸⁶Sr ratios indicating variable degrees of binary mixing between an enriched, more radiogenic plume and a depleted, less radiogenic upper mantle source. A southward directed compositional gradient exists along the ridge crest with the most enriched and radiogenic samples occurring around 37°50'S (position of the Foundation Hotspot) and the most depleted ones around 40°S. No such gradient can be found north of 37°50'S. This suggest that the Foundation Hotspot creates an asymmetric anomaly which largely controls the petrogenesis of magmas along this segment of the PAR (between latitudes 37°50'S and 39°50'S).

**Stroncik, N. A., Haase, K. M., and Stoffers P. (2002)
Generation of highly silicic lavas along the Pacific-
Antarctic-Ridge (PAR): Insights into magma
chamber processes along a hotspot influenced
ridge section. Eos. Trans. AGU, 83 (47), Fall Meet.
Suppl., Abstract**

V52A-1273 1330h POSTER

Geochemical and Pb and Nd Isotopic Characteristics of the Tethyan Asthenosphere: Implications for the Origin of the Indian MORB-type Mantle

Ji-Feng Xu¹ (jifengxu@gig.ac.cn)

Paterno R. Castillo² ((858) 534-0383; pcastillo@ucsd.edu)

¹Guangzhou Institute of Geochemistry, Chinese Academy of Sciences, Wushan, Guangzhou 510640, China

²Scripps Institution of Oceanography, University of California, San Diego, La Jolla, CA 92093-0212, United States

It is unclear why the Pb, Nd, and Sr isotopic composition of the modern mid-ocean ridge basalts (MORB) from the Indian Ocean is different from that of the North Atlantic and Pacific Oceans. A possible explanation for this is that the Indian MORB-type isotopic signature is a long-lived regional feature of the mantle, as evidently shown by the isotopic composition of the 350 Ma MORB-like crust of the Tethys Ocean, which existed in the same region presently occupied by the Indian Ocean (Xu et al., *Earth Planet. Sci. Lett.* 198, 2002). However, this hypothesis is in conflict with the lack of Indian MORB-type isotopic signature in a number of 150 Ma Tethyan and Indian Ocean crusts (Mahoney et al., *J. Petrol.* 39, 1998; Weis and Frey, *J. Geophys. Res.* 101, 1996). To further constrain the origin of the Indian MORB-type isotopic signature, we analyze the chemical and Pb, Nd, and Sr isotopic composition of representative mafic rocks from four Tethyan ophiolites ranging in age from 90 to 360 Ma. The Sr isotopic composition of the samples is unreliable due to alteration, but the alteration resistant trace element and age-corrected Nd and Pb isotopic results indicate that these Tethyan rocks were derived from a geochemically depleted asthenospheric source that had a clear Indian MORB-type isotopic signature. We therefore conclude that the bulk of the Indian suboceanic mantle was most probably inherited from the Tethyan asthenosphere. A few regions in both the Tethyan and Indian Oceans, however, are most probably underlain by North Atlantic and Pacific MORB-type mantle (and vice-versa) because of the flow of the asthenosphere in response tectonic plate reorganizations that lead to openings and closings of ocean basins (e.g., Flower et al., *Tectonophysics*. 333, 2001).

V52A-1274 1330h POSTER

Testing Binary Mixing Models for Lavas Erupted Along the Reykjanes Ridge: Insights From C-He Relationships

Goverdina A.M. de Leeuw¹ ((858) 822 2426; gdeleeuw@ucsd.edu)

David R Hilton¹ (drhilton@ucsd.edu)

Alison M Shaw¹ (amshaw@ucsd.edu)

Bamley J Murton² (bjm@soc.soton.ac.uk)

Rex N Taylor² (rex@soton.ac.uk)

¹Geosciences Research Division, Scripps Inst. Oceanography, La Jolla, CA 92093-0244, United States

²University of Southampton, Southampton Oceanography Centre, Empress Dock, European Way, Southampton SO14 3ZH, United Kingdom

We report new CO₂ abundance and isotope data for 36 basalt glasses erupted along the Reykjanes Ridge between latitudes 57.5 and 63°N. Lavas can be divided into (a) water-rich samples (~0.4 wt.%), erupted at depths < 775m north of 61.5°N, and (b) samples with water ~ 0.2 wt.%, erupted at depths of 620 - 2060 m and located between 57.5 and 61.5°N. Based upon He-Pb isotope systematics (Hilton et al., *EPSL*, 2000), deeper samples (category b) lie along binary mixing trajectories between plume-like (³He/⁴He ~ 30R_A; ²⁰⁶Pb/²⁰⁴Pb ~ 18.7) and MORB-like endmembers (³He/⁴He ~ 8R_A; ²⁰⁶Pb/²⁰⁴Pb ~ 18.0). Shallow samples (category a) do not fall on mixing trajectories: consistent with volatile loss followed by addition of a crustal contaminant, resulting in lower ³He/⁴He ratios. The aim of this study is to test whether binary mixing trends are observed using C-He relationships.

All samples were analyzed using incremental heating techniques which allows for resolution of vesicled CO₂ from CO₂ dissolved within the glass matrix. Results show that samples north of 61.5°N (category a) have low CO₂ contents in both the vesicle (2-37 ppm) and dissolved (15-61 ppm) phases. The isotopic composition of the CO₂ varies between -8 and -34‰ (vesicle) and -6 and -10‰ (glass). The combined effect of low CO₂ concentrations and low δ¹³C values are consistent with extensive gas loss ± contamination of

volatile-poor magmas with an isotopically-light C component. In contrast, samples in category b have significantly higher CO₂ abundances (vesicles: 7-318 ppm; glass: 9-200 ppm) and higher and less variable δ¹³C values (vesicles: -5 to -26‰; glass: -4 to -11‰). This suggests that category b samples have not been subjected to the same degree of degassing and/or contamination as samples in category a.

By combining the vesicle-sited CO₂ abundances with He-contents determined by crushing (Hilton, op. cit), CO₂/³He ratios for the vesicle phase can be derived. We observe high ratios (3×10⁹ to 2×10¹⁰) in the more degassed category a samples. Category b CO₂/³He ratios show a trend from low CO₂/³He values (3×10⁸) and MORB-like ²⁰⁶Pb/²⁰⁴Pb to high CO₂/³He values (up to 2×10¹⁰) and more radiogenic ²⁰⁶Pb/²⁰⁴Pb. There are two possible explanations for the observed trends: 1) degassing followed by contamination with a high CO₂/³He crustal component. This process controls C-He relationships in low concentration (highly degassed) samples close to Iceland. 2) mixing between a MORB-like source (CO₂/³He ~ 2×10⁹) and an enriched source with a higher initial CO₂/³He value. This process controls samples in category b.

V52A-1275 1330h POSTER

Binary Mixing Processes at a Ridge Segment as Shown by Historic Reykjanes Peninsula Lavas, Iceland

David W Peate¹ (dwp@dlc.ku.dk)

Louise E Thomas² (l.e.thomas@open.ac.uk)

Adam J R Kent³ (ajrk@dlc.ku.dk)

Sveinn P Jacobsson⁴ (sjak@ni.is)

Joel A Baker¹ (jab@dlc.ku.dk)

¹Danish Lithosphere Centre, Oester Voldgade 10-L, Copenhagen K DK-1350, Denmark

²Dept of Earth Sciences, The Open University, Milton Keynes MK7 6AA, United Kingdom

³Dept of Geosciences, Oregon State University, Corvallis, OR 97331, United States

⁴Icelandic Institute of Natural History, Hlemmur 3, Reykjavik 125, Iceland

Binary mixing between compositionally distinct melts has been recognised as an important process in generating the compositional diversity of oceanic magmatism at several length scales, and it has been argued that local variations in ²³⁸U/²³⁰Th of MORB lavas are controlled by such a process. Additional information about the melting behaviour of the mixing end-members that might potentially be provided by ²²⁶Ra is limited by the lack of precise age control for most MORB samples. The Reykjanes Peninsula (SW Iceland) is essentially an onshore, 80 km long, plume-influenced 'mid-ocean' ridge segment, but with a well-dated record of historic basaltic lavas (MgO 6.5-9.2 wt%) erupted between c. 940 AD and 1340 AD. Sr-Nd isotope data indicate minimal shallow-level crustal assimilation. Coherent linear trends shown by high-precision (double-spike) Pb isotope data and correlations with incompatible element ratios (e.g. La/Yb) provide evidence for binary mixing between a 'depleted' end-member with ²⁰⁶Pb/²⁰⁴Pb < 18.7 and La/Yb_N < 1.3 and an 'enriched' end-member with ²⁰⁶Pb/²⁰⁴Pb > 18.9 and La/Yb_N > 2.7. The historic lavas are dominated by the 'enriched' end-member (~50-90%), and the 'depleted' end-member is only found in a relatively undiluted form in picrites erupted during the last deglaciation. Work is in progress to obtain U-Th-Ra disequilibria data on these historic lavas to see if they preserve systematic correlations with Pb isotope and trace element data and thus place critical constraints on the melt generation processes.

V52A-1276 1330h POSTER

Generation of Highly Silicic Lavas Along the Pacific-Antarctic Ridge (PAR): Insights into Magma Chamber Processes Along a Hotspot Influenced Ridge Section

Nicole A Stronck¹ (+49 431 880 3694; nst@gpi.uni-kiel.de)

Karsten Haase¹ (+49 431 880 2865; kh@gpi.uni-kiel.de)

Peter Stoffers¹ (+49 431 880 2850; pst@gpi.uni-kiel.de)

¹Nicole A. Stronck, Institute of Geosciences Christian-Albrechts-University Olshausenstr. 40, Kiel 24118, Germany

A sample suite comprising rocks ranging from basalt via basaltic andesite and andesite to dacite has been dredged along the fast spreading (10 cm/a) N'PAR at its intersection with the Foundation Seamount chain, denoting the current position of the Foundation Hotspot, between latitudes 36.5 and 41.5°S. Andesites and dacites occur along the section of the N'PAR being mainly influenced by the hotspot (36.5° to 39.8°) and are not related to propagating rifts. Major and trace element data as well as Sr-, Nd- and Pb-isotope composition reveal that the magmas generated along the PAR are (1) derived from a heterogeneous source and (2) are related by multiple differentiation trends.

Fractional crystallization modeling shows that the basaltic rocks are controlled by low-pressure fractionation of olivine, plagioclase, clinopyroxene and Titanomagnetite. Two differentiation trends can be defined: (1) basalts erupted between 37 and 39.50°S are controlled by crystallization of olivine -> olivine + plagioclase -> olivine + plagioclase + clinopyroxene and (2) basalts erupted between 40 and 41°S are controlled by the crystallization sequence plagioclase -> plagioclase + olivine -> plagioclase + olivine + clinopyroxene. This difference in differentiation trends is caused by higher crystallization pressures of the melts along the PAR section between 37 and 39.50°S. The H₂O content does not vary significantly along axis, thus a higher H₂O content, which would delay plagioclase crystallization, can be ruled out as a cause for the development of these different differentiation trends.

The andesites and dacites are not related to their basaltic parents by simple low-pressure fractional crystallization. The existence of clinopyroxene xenocrysts, ranging in Mg# from 40 to 87, and plagioclase xenocrysts, ranging in An from 22 to 87, in the andesites shows that they have been generated by mixing between basaltic and dacitic melts. Although the andesites and dacites are dominated by low-pressure mineral assemblages, their TiO₂-, FeO_{tot}- and Cl-content cannot be achieved by normal low-pressure fractional crystallization. Elevated Cl/K and ⁸⁷Sr/⁸⁶Sr ratios indicate that assimilation of altered oceanic crust has been involved in andesite and dacite generation.

The thicker crust associated with the hotspot leads to polybaric crystal fractionation. A complex plumbing and magma storage system is active beneath the PAR. Abundant hydrothermal activity in the area of andesite volcanism suggests a relation to the formation of evolved melts and results in an effective alteration of the crust.

V52A-1277 1330h POSTER

Late Stage MORB Volcanism at the Cuesta Ridge Ophiolite Remnant: Evidence for Ridge Collision or Back-arc Basin Spreading?

Cameron A Snow¹ (casnow@stanford.edu)

John W Shervais² (shervais@cc.usu.edu)

¹Stanford University, Dept. of Geological and Environmental Sciences, Stanford, CA 94305, United States

²Utah State University, Dept. of Geology, Logan, UT 84322, United States

The origin and significance of ophiolites has been a major focus of research over the past three decades, with most attention focusing on whether they form at mid-ocean ridges or above subduction zones. The termination of igneous activity in ophiolites has received far less attention, since it is assumed that igneous activity ends when the ophiolite is obducted. The middle Jurassic Coast Range Ophiolite (CRO) of California provides an excellent opportunity to study not only the origin of ophiolites, but also the termination of igneous activity related to ophiolite formation.

Geologic mapping of the Cuesta Ridge ophiolite remnant of the CRO reveals an ophiolite sequence in thrust contact with the underlying Franciscan assemblage. The section consists of a 1.5 km thick mantle section of serpentinized harzburgite and a MTZ consisting of dunite, wehrlite, and pyroxenite. The mantle section is overlain by isotropic gabbro, with sills of wehrlite and pyroxenite, a sheeted sill complex of quartz-hornblende diorite, and a 1.3 km thick volcanic section comprising massive flows, pillow lava, and volcanic breccias with calc-alkaline and boninitic affinities, all capped by tuffaceous radiolarian chert. Late stage dikes of tholeiitic basalt cross-cut the quartz diorite sheeted sill complex, and similar basalts occur as flows at the top of the volcanic section, below the tuffaceous cherts.

The majority of the volcanic rocks at Cuesta Ridge have low Ti/V ratios (11-21) and other trace element characteristics (e.g., low HFSE, low Zr/Y) that are atypical of MORB and suggest formation in an SSZ setting. High MgO and SiO₂-Cr plots show that about 40 percent of the volcanics have strong boninitic affinities, consistent with formation in the fore arc region of an island arc. The quartz-hornblende diorites, which cut the lower volcanics, have SiO₂ ranged of 52-75 percent, much too high for rocks formed at mid-ocean spreading centers. In contrast, the late stage dikes and uppermost flows, which cut the sheeted sill complex and overlie the main volcanic section, have a MORB-like affinity with

**O`Connor, J. A., Stoffers, P., and Wijbrans (2003)
Distinguishing local from deep sources using high-
resolution age-mapping of oceanic hotspot
volcanism. Penrose Conference, 25th -29th Aug.
2003, Iceland**

Distinguishing local from deep sources using high-resolution age-mapping of oceanic-hotspot volcanism?

J.M. O'Connor¹, P. Stoffers¹, J.R. Wijbrans²

¹*Institute for Geosciences, Christian-Albrechts University, D-24118 Kiel, Germany*

email: joconnor@gpi.uni-kiel.de

²*Department of Isotope Geochemistry, Vrije Universiteit, 1081 HV Amsterdam, The Netherlands*

Introduction

The temporal, spatial and geochemical distribution of hotspot volcanism has long been a key to investigating the processes controlling hotspot-lithosphere interaction and the hypothesis of deep mantle plumes. High-precision dating is therefore of first-order importance when seeking to understand the long-term processes controlling the history and distribution of hotspot volcanism. Our aim here is to draw attention to the issue of plume theory developing much faster than the accumulation of real data due to the prohibitive cost of ship time and post-cruise analyses. Recent studies indicate that data remain far too scarce to provide robust ocean-wide understanding of histories and distributions of hotspot provinces. We support this proposition with the example of recent ⁴⁰Ar/³⁹Ar data for rocks from the Foundation Seamount Chain (O'Connor et al. 1998, 2001, 2002) (Figs. 1 & 2). Our results show how a detailed understanding of the long-term history of time progressive volcanism along seamount chains and their surrounding structures can begin the process of distinguishing long term (i.e., deep?) plume-hotspot behavior from local lithospheric control.

Short-lived (local) versus long-lived (deep?) control of Foundation hotspot volcanism

The main trend in the Foundation age data is one of linear migration of midplate – often geochemically enriched – volcanism at a rate of 91 ± 2 mm/yr along the Foundation Chain for at least the past 22 Myr. Such time progressive volcanism supports the conventional model of the Pacific plate drifting over a narrow, stationary plume of hot mantle material upwelling from depth. Furthermore, similarity between rates of migration of volcanism along the Hawaiian and Foundation chains supports a stationary Foundation versus Hawaiian mantle plume, at least for the past 22 Myr.

However, our dredge-sampling covered volcanic elongated ridges (VER) flanking the Foundation Chain at different stages of development (Fig. 2). The transition from a narrow line of seamounts to a broad region of volcanic elongate ridges (VERs) about 5 Myr ago was assumed initially to be the result of interaction between the Foundation plume and the encroaching Pacific-Antarctic spreading-center. Some of our data support this notion by showing that volcanism along morphologically distinct VERs can develop occasionally as rapidly formed continuous lines of coeval volcanism extending from a region of intraplate volcanism to the Pacific-Antarctic spreading center. However, a significantly more dominant trend is for coeval, yet structurally disconnected, segments of Foundation Chain VERs to develop in a series of *en echelon*, NE-SW elongate ‘zones’ of coeval hotspot volcanism. These elongate zones developed at intervals of approximately 1 Myr while maintaining a basically steady-state orientation and size as the Pacific-Antarctic spreading center migrated continually closer to the Foundation plume hotspot. Although such VER development was controlled in part by local factors (e.g. location of nearest spreading center segment, lithospheric stress), long-lived attributes of the Foundation plume hotspot (e.g. size, orientation, periodicity) appear to have played a significant role.

The key to testing this notion is the fact that the Foundation Chain represents a rare, possibly unique, case of a hotspot trail crossing a fossil microplate. Prior to encountering the Selkirk Microplate the Foundation Chain formed as broad zones of scattered, synchronous Foundation volcanism – similar to those identified west of the present Pacific-Antarctic spreading center (Fig. 2). However, once the significantly older microplate lithosphere began capping the plume hotspot about 14 Myr ago, the chain narrowed abruptly into a line of discrete seamounts, only broadening again about 5 Myr ago when sufficiently young lithosphere once again drifted over the plume hotspot. Foundation hotspot volcanism can therefore be prevented across elongate hotspot zones if the capping tectonic plate is too thick for plume melts to penetrate to the surface. (O'Connor et al., 1998, 2001, 2002). The lack of a seamount chain connecting the Foundation and the Ngatemato chains (McNutt et al., 1997) can be similarly explained, so supporting the notion that the Pacific plate has drifted a distance of at least 3400 km over a Foundation plume-hotspot during the last ~34 Myr. We infer from this information that Foundation Chain development was controlled primarily by tectonic plate migration over broad zones of hot plume material of fundamentally constant size and orientation created with an apparent periodicity of about once per Myr (O'Connor et al., 2002).

Creation of broad zones of synchronous Foundation magmatism at regular ~1 Myr intervals leads us – in combination with recent numerical plume modeling (e.g., Larsen and Yuen, 1997; Larsen et al., 1999) – to propose that the Foundation Chain is the product of a stationary plume pulsing hot masses against the base of the Pacific plate from depth with an apparent periodicity of once per Myr (O'Connor et al., 2002). Assuming the validity of the hypothesis of deep mantle plumes (Morgan, 1971), our model for Foundation Chain development has implications for future investigations of Pacific midplate volcanism. We propose that plume-hotspots such as Foundation, spreading on impact with the lithosphere, influence very wide areas such that apparently unconnected hotspot volcanism can be produced simultaneously across wide swaths, often crosscutting seamount chains. Thus, variations in the age, structure and stress patterns of tectonic plates drifting over (pulsing?) mantle plumes might control if, where and how hotspot volcanism develops on the Pacific plate. This modified plume-hotspot theory might also explain widespread scattered midplate volcanism (e.g., VERs) revealed by satellite altimetry mapping as well as randomly distributed reheating events warming and raising Pacific lithosphere (Smith and Sandwell, 1997) – given that many other mantle plumes are similarly pulsing large masses of hot plume material (not necessarily with the same periodicity or mass) into broad regions impacting the base of the Pacific lithosphere.

Conclusion

While we find evidence for a link between local plate tectonic processes (lithospheric architecture, stress, rifting) and the distribution of hotspot volcanism we also see evidence for long-term underlying episodic/periodic 'plume-hotspot' control. Thus, in the case of the Foundation hotspot we believe that we can distinguish between second-order lithospheric and first-order 'plume-hotspot' processes controlling the history and distribution of volcanism. This insight would not have been possible without an unusually extensive dredge-sampling and post-cruise analytical program. For example, the conventional wisdom that the broad region of volcanic elongate ridges near the Pacific-Antarctic spreading axis are primarily the product of plume-ridge interaction would still prevail – especially considering the focus of so many resources on active spreading-ridge research.

Inferring plume behavior from localized studies of oceanic volcanism inevitably produces a 'snap-shot' of what could well be a long-term dynamic mantle process. We believe therefore that the possibility of distinguishing local from long-lived (deep?) processes controlling the history

and distribution of hotspot provinces provides the opportunity of 1) better testing current plume-hotspot theory and 2) merging new multidisciplinary thinking with the acquisition of real data from selected volcanic provinces. In short, developing and testing old – and especially new ideas and models – requires significantly more detailed sampling and age/geochemical analyses.

References

- Larsen TB, Yuen DA (1997) Ultrafast upwelling bursting through the upper mantle. *Earth Planet. Sci. Lett.* 146:393–399.
- Larsen TB, Yuen DA, Storey M (1999) Ultrafast mantle plumes and implication for flood basalt volcanism in the Northern Atlantic Region. *Tectonophysics* 311:31–43.
- Mammerickx J (1992) The Foundation seamounts: tectonic setting of a newly discovered seamount chain in the South Pacific. *Earth Planet. Sci. Lett.* 113:293–306.
- McNutt MK, Caress DW, Reynolds J, Jordahl KA, Duncan RA (1997) Failure of plume theory to explain the southern Austral Islands. *Nature* 389:479–482.
- Morgan WJ (1971) Convection plumes in the lower mantle. *Nature* 230:42–43.
- O'Connor JM, Stoffers P, Wijbrans, JR (1998) Migration rate of volcanism along the Foundation Chain, SE Pacific. *Earth Planet Sci. Lett.* 164:41- 59.
- O'Connor JM, Stoffers P, Wijbrans JR (2001) En Echelon volcanic elongate ridges connecting intraplate Foundation Chain volcanism to the Pacific-Antarctic spreading center. *Earth Planet Sci. Lett.* 192:633-648.
- O'Connor JM, Stoffers P, Wijbrans JR (2002) Pulsing of a focused mantle plume *Geophys. Res. Lett.* 29:10.1029/2002GL014681.
- Smith WHF, Sandwell DT (1997) Global Sea Floor Topography from Satellite Altimetry and Ship Depth Soundings. *Science* 277:1956-1962.

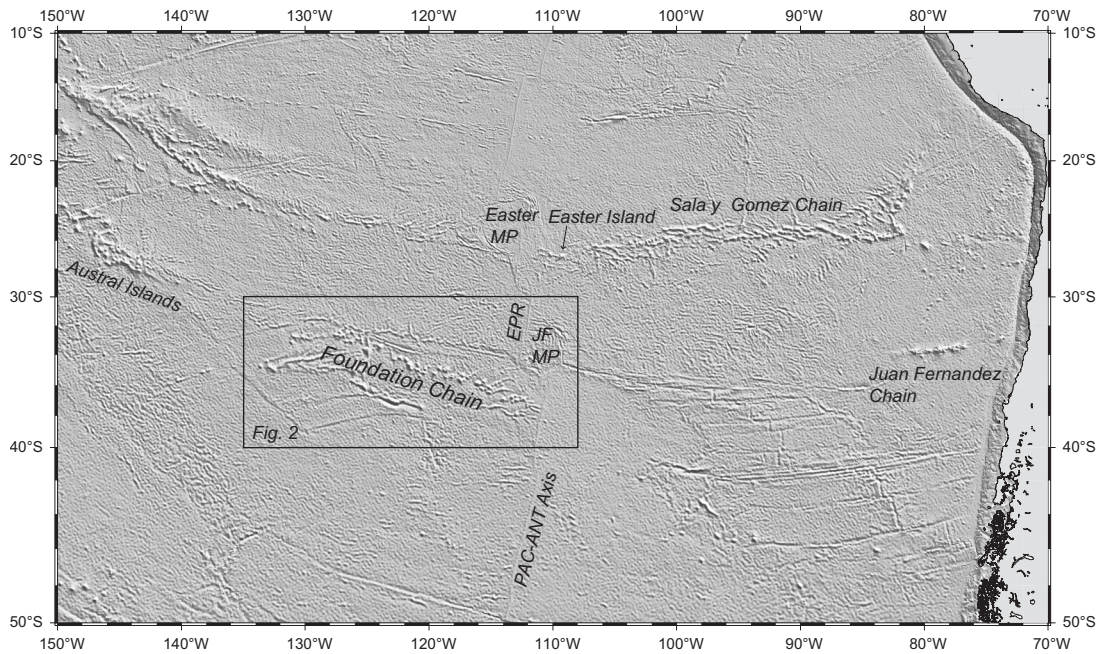


Figure 1. Predicted topography (Smith and Sandwell, 1997) of SE Pacific seafloor showing the location of the Foundation Chain. MP = microplate; JF = Juan Fernandez; EPR = East Pacific Rise. Figure modified after O'Connor et al., 1998

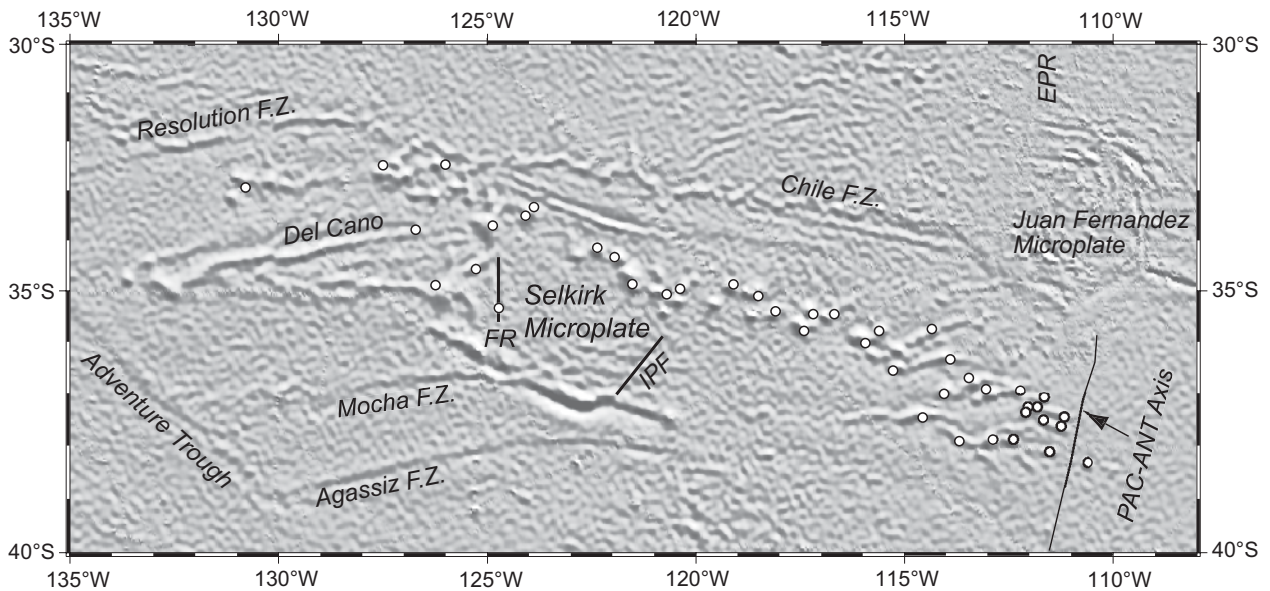


Figure 2. Predicted topography of the Foundation Chain (Smith and Sandwell, 1997). *F. S. Sonne* and *N/O Atalante* dredge sites are indicated by black rimmed white dots. $^{40}\text{Ar}/^{39}\text{Ar}$ ages, details of sample information and analytical date are in (O'Connor et al., 1998, 2001, 2002). IPF = inner pseudo fault and FR = failed rift of Selkirk microplate (Mammerickx, 1992). Figure modified after O'Connor et al., 1998

**O`Connor, J. A., and Wijbrans (2003) Lithospheric
and Melt Anomaly Control of Foundation Chain
Volcanism. Eos. Trans. AGU, 84 (46), Fall Meet.
Suppl., Abstract**

¹Scripps Institution of Oceanography, IGPP, La Jolla, CA 92093-0225, United States

²Vrije Universiteit, De Boelelaan 1085, Amsterdam 1081 HV, Netherlands

³SURCC, Rankine Avenue, East Kilbride G75 0QF, United Kingdom

By far the largest number of secondary hotspots (cf. Courtillot et al., 2003) can be found in the "South Pacific Thermal and Isotopic Anomaly" (SOPITA) or "Superswell" region. Its Cretaceous counterpart is preserved in a large range of seamounts and guyots found in the "West Pacific Seamount Province" (WPSF). The seamounts in these regions display very distinct and long-lived isotopic signatures (Staudigel et al., 1991; Koppers et al., 2003) that can be used to combine source region chemistry and seamount geochronology to map out mantle melting anomalies over geological time. These mappings may resolve many important questions regarding the stationary character, continuity and longevity of the melting anomalies in the South Pacific mantle and its secondary hotspots. Of all secondary hotspots that are currently active in the SOPITA we could identify only two hotspots that appear to be long-lived and that have Cretaceous counterparts in the WPSF. Plate reconstructions show that the "HIMU-type" Southern Wake seamounts may have originated from the Mangaia-Rurutu "hotline" in the Cook-Austral Islands, whereas the "EMI-type" Magellan seamounts may have originated from the Rarotonga hotspot. All other hotspots in the SOPITA and WPSF are short-lived (or intermittently active) as evidenced by the presence of numerous seamount trail "segments" representing no more than 10-40 Myr of volcanism. Our observations violate one or more assumptions of the classical Wilson-Morgan hotspot hypothesis: (1) none of the South Pacific hotspots are continuously active, (2) most are short-lived, (3) some show evidence of hotspot motion, and (4) most of them have poor linear age progressions, if any at all. On top of this we have evidence for volcanism along "hotlines" and the "superposition" of hotspots. The simple and elegant "hotspot" model, therefore, seems insufficient to explain the age distribution and source region characteristics of intra-plate volcanoes in the South Pacific. This has led to new models that retain the concept of mantle plumes, but these lack both simplicity and predictive power. New models that call on "extension" are indeed simple and they may explain most characteristics of Earth's intra-plate volcanism, but they also have limited predictive power, making it more difficult to test for their validity. We argue that we require a combination of processes: one that forces regional magmatism from a large-scale source of buoyancy from below (like the rise of plumelets shooting off the top of a superplume) and one process that acts from above, as intra-plate extension opens up pathways that allow the lithosphere to be penetrated by magma.

V21B-05 0905h

Geochemical constraints on melting process in the GLIMPSE region

Kathleen E Donnelly¹ ((845) 365-8660; donnelly@ldeo.columbia.edu)

Charles H Langmuir² (langmuir@eps.harvard.edu)

Steven L Goldstein¹ ((845) 365-8787; steveg@ldeo.columbia.edu)

¹LDEO, 61 Rt. 9W, Palisades, NY 10964, United States

²Harvard University - Dept of Earth and Planetary Sciences, 20 Oxford St., Cambridge, MA 02138, United States

The GLIMPSE region, where there are cross grain gravity lineaments, has abundant volcanism that permits tests of melting conditions and mantle sources associated with these important off-axis features. The Sojourn and Brown Ridges are extensive linear features, subparallel to one another and perpendicular to the East Pacific Rise (EPR), which lies to the east. The Brown Ridge lies further to the east of Sojourn, ending ~60 km or less from the EPR. South of the two ridges, Hotu and Matua are central complexes punctuated by dozens of smaller cones. Fresh lava flows with no topographic expression also cover portions of the sea floor in the general area. The recent flows on flat lying terrain include a flow northwest of the Sojourn Ridge, arguing for recent volcanism in the west as well as in the east. Samples from two cruises show that compositions range from highly depleted to strongly enriched. Sojourn Ridge samples show a general increase in enrichment with increasing distance from the EPR. On the Brown Ridge sporadic spikes of enrichment with no systematic geographic distribution occur and are associated with limited isotopic variations that are similar to those observed on the EPR, suggesting very recent enrichment and depletion events near the spreading axis. In contrast Hotu and Matua samples largely consist of incompatible element enriched lavas with isotopic compositions similar to Easter Island. Evidence for recent volcanism is found throughout the region. In the west, SiO₂ contents are significantly lower, reflecting higher pressures of formation and therefore little lithospheric thinning in the west. On the Brown Ridge

in the east, recent volcanism also is apparent, but low SiO₂ contents are not observed reflecting younger and thinner lithosphere.

V21B-06 0920h

Origin of Cross-Grain Gravity Lineations and Intraplate Volcanic Ridges: Constraints and Ideas From the GLIMPSE Experiment

Donald W. Forsyth¹ (4018631699; Donald.Forsyth@brown.edu)

GLIMPSE Science Team (Donald.Forsyth@brown.edu)

¹Brown University, Dept. of Geological Sciences, Brown University, Providence, RI 02912, United States

Three hypotheses have been advanced in the literature for the origin of cross-grain gravity lineations and associated volcanic ridges in the Pacific: small-scale convective rolls aligned by asthenospheric shear in the direction of absolute plate motion; lithospheric bowing or cracking by remotely applied stresses; and mini-plumes or hotspots. Inspired by the compositional anomalies and age progression along the Pukapuka ridge, we have suggested a fourth possibility; that the volcanic ridge and seamount chains are associated with rapid transport of volatile-rich, low viscosity mantle in the asthenosphere back toward the East Pacific Rise. The GLIMPSE experiment was designed to provide constraints on these conceptual models by measuring crustal thickness variations, seismic velocity anomalies in the underlying mantle, density anomalies as revealed through bathymetry and gravity, variations in mantle composition and the depth and degree of melting as indicated by major and trace elements and isotopic composition of the melt products, thickness of the brittle lithosphere shown by depth extent of microearthquakes, and age progression of volcanism. The study area west of the East Pacific Rise and just south of the Garrett fracture zone includes the Hotu-Matua volcanic complex, which has recent volcanic activity distributed over a region about 60 km across and 200 km long, and the Sojourn/Brown ridges, which are the largest and most continuous of these intraplate volcanic ridges. A year-long deployment of ocean-bottom seismometers, extensive underway geophysical surveying and dredging and geochemical analysis of basalts indicates that there are distinct differences between the processes of formation of the Hotu/Matua and Sojourn/Brown chains. Our current interpretation is that, rather than the gravity lineations beginning to form in seafloor 4-5 Ma old, they die out as the East Pacific Rise spreading center is approached.

V21B-07 0940h

Lithospheric and Melt Anomaly Control of Foundation Chain Volcanism

John M O'Connor^{1,2} (jocconnor@gpi.uni-kiel.de)

Peter Stoffers² (pst@gpi.uni-kiel.de)

Jan R Wijbrans¹ (Jan.Wijbrans@falw.vu.nl)

¹Department of Isotope Geochemistry, Vrije Universiteit, Amsterdam 1081 HV, Netherlands

²Institute for Geosciences, Christian-Albrechts Universität, Kiel D-24118, Germany

The Foundation Chain is a small chain of seamounts and volcanic ridges extending northwestward from the Pacific-Antarctic spreading ridge. ⁴⁰Ar/³⁹Ar age data show linear migration of volcanism along-chain at a rate of 91±2mm/yr for the past 22 Myr (O'Connor et al., 1998). The case history of the Foundation Chain is notable because it is a rare example of a hotspot melting anomaly that has been traversed by a fossil microplate and is now being encroached by the active Pacific-Antarctic spreading ridge. Prior to the Selkirk Microplate encountering the melt anomaly the Foundation Chain formed as broad elongate zones of scattered, synchronous volcanism cross-cutting the overall NW-SE trend of the chain (O'Connor et al., 2002). But once the significantly older microplate began capping the melt anomaly about 14 Myr ago, the chain narrowed abruptly into a single line of discrete seamounts, only broadening again about 5 Myr ago when sufficiently young lithosphere again started drifting over the melting anomaly. Measured ages show a dominant trend of coeval, yet structurally disconnected, segments of Foundation Chain VERs developing in a series of en echelon, elongate 'zones' of coeval volcanism cross-cutting the overall NW-SE seamount trend (O'Connor et al., 2001). These elongate zones developed at intervals of approximately 1 Myr while maintaining a basically steady-state orientation and size as the Pacific-Antarctic spreading ridge migrated closer to the melt anomaly. Although VER development was controlled in part by local factors (e.g. location of nearest spreading ridge segment, lithospheric thickness and stress), long-lived attributes of the Foundation melt anomaly

(e.g. size, orientation, periodicity) must have played a pivotal role. Foundation volcanism can be suppressed across elongate melt 'zones' if the capping tectonic plate is too tight for melts to penetrate to the surface (O'Connor et al., 2001, 2002). The lack of a seamount chain connecting the Foundation and the Austral volcanoes can be similarly explained, thus extending the age of the Foundation melting anomaly back to at least 34 Myr ago (McNutt et al., 1997). While lithospheric architecture controls if and where Foundation volcanism occurs (e.g., chain broadening and narrowing), it cannot explain the origin of the underlying long-lived melting anomaly. The timing and distribution of Foundation Chain volcanism requires a long-lived process that creates broad melting anomalies of fundamentally constant size and orientation under a moving Pacific lithosphere with an apparent periodicity of about once per Myr (O'Connor et al., 2001, 2002). Thus, the Foundation Chain is a product of lithospheric architecture and a first-order mantle process controlling the existence and behavior of an underlying long-lived melt anomaly.

V21C MCC: Level 1 Tuesday 0830h

Volcanic Emissions to the Troposphere: Posters II (joint with A, B)

Presiding: F M Schwandner, Institute of Mineralogy and Petrography; D L Lopez, Ohio University

V21C-0522 0830h POSTER

Acid Loading of Soils by Magmatic CO₂ at Mammoth Mountain, California

Kenneth A McGee¹ (1-360-993-8931; kenmcgee@usgs.gov)

Terrence M Gerlach¹ (tgerlach@usgs.gov)

Michael P Doukas¹ (mdoukas@usgs.gov)

¹U.S. Geological Survey, Cascades Volcano Observatory, 1300 SE Cardinal Court 100, Vancouver, WA 98683, United States

Areas of tree kill appeared in the early 1990's after a shallow intrusion of magma under the south flank of Mammoth Mountain, California. Subsequent field measurements have revealed high concentrations of soil CO₂ in these areas, the locations of which are controlled by faults and fractures that serve as conduits for magmatic CO₂ streaming to the surface from depth. Detailed surveys at the largest of these tree-kill areas, Horseshoe Lake, about 14 ha in size, have consistently shown soil CO₂ concentrations that range up to 90% or greater in the shallow soil layers. Continuous soil CO₂ monitoring stations established in 1995 at Horseshoe Lake reveal a pattern of both short-term and seasonal variations in magmatic CO₂. Because the pressure of CO₂ is externally fixed by CO₂ streaming to the surface, carbonic acid activity is constrained by open-system buffering of magmatic CO₂. Eight years of intensive soil CO₂ monitoring have documented a consistent pattern whereby pH values as low as 4 can be achieved in the soil solution during spring melting of the winter snow pack. Coupled with the seasonal drop in pH, aluminum, which can also be toxic to forest ecosystems, is released from soils in those areas with the highest CO₂ concentrations. After more than a decade of exposure to elevated levels of CO₂ and repeated cycles of acid loading, along with nearly complete tree and vegetation mortality and the release of Al³⁺, the soils at Horseshoe Lake and the other areas of tree kill may not recover their ability to sustain any significant level of forest production for several years, even if the CO₂ degassing should stop immediately. The level of in-situ acid loading by magmatic CO₂ in the tree kill areas around Mammoth Mountain rivals that of the better known process of rain-out of acid gases from volcanic plumes in the troposphere.

V21C-0523 0830h POSTER

Two Decades of Degassing at Kilauea Volcano, Hawaii: Perspectives on Island Impacts

Tamar Elias¹ (808-967-8826; telias@usgs.gov)

A. Jeff Sutton¹ (808-967-8805; ajsutton@usgs.gov)

¹USGS, Hawaiian Volcano Observatory POB 51, Hawaii Ntl Park, HI 96718, United States

The ongoing eruption of Kilauea provides an opportunity to examine how volcanic emissions impact the natural and human environment of the island of

**Stroncik, N. A., Haase, K. M., and Stoffers (2003)
Mantelplume-Einfluß und die Bildung von
andesitischen Laven am Pazifisch-Antarktischen
Rücken: Ergebnisse der Ausfahrt SO157. BMBF
Statusseminar 2003, Hamburg**



Projektträger des BMBF und BMWi
Forschungszentrum Jülich GmbH

Statusseminar 2003

Meeresforschung mit FS Sonne



12. – 14. März 2003 in Hamburg

Tagungsband

Meeres- und Polarforschung

 **bmb+f** Bundesministerium für
Bildung und Forschung

Mantelplume-Einfluß und die Bildung von andesitischen Laven am Pazifisch-Antarktischen Rücken: Ergebnisse der Ausfahrt SO157

Nicole A. Stroncik, Karsten M. Haase und Peter Stoffers
Institut für Geowissenschaften der Universität Kiel, Olshausenstr. 40, D-24098 Kiel

Die Ausfahrt „SO157“ hatte eine detaillierte Beprobung des Pazifisch-Antarktischen-Rückens (PAR) zwischen 36.5°S und 41.5°S zur Aufgabe. Das 2500 km lange, schnell spreizende (84-100 mm/a) Rückensystem des PAR, wird im Norden durch die Juan Fernandez Triple Junction und im Süden durch die Heezen Transformstörung begrenzt und bildet die südliche Fortsetzung des East-Pacific-Rise (EPR). Der PAR kann anhand von Transformstörungen und Overlapping Spreading Centers in sechs verschieden lange und verschieden differenzierte Segmente unterteilt werden, wobei das nördlichste Segment durch seine Lage in unmittelbarer Nähe des Foundation Hotspots von besonderem Interesse ist. Erste Untersuchungen dieses Segments während der Ausfahrten „SO100“ und „Atalante“ haben eine ausgeprägte bathymetrische Anomalie sowie das für ozeanische Spreizungsachse ungewöhnliche Vorkommen von hochdifferenzierten Laven in diesem Bereich gezeigt.

Im Pazifik wurden bisher nur wenige Plume-Rücken-Systeme beobachtet. Untersuchungen haben jedoch gezeigt, daß geochemische Anomalien von Spreizungsachsen in der Nähe von Hotspots oft komplexer sind, als es in geophysikalischen Anomalien (z.B. Bathymetrie) zum Ausdruck kommt. Dies läßt vermuten, daß das Plumematerial komplexen Verteilungsmustern unterliegt. In diesem Zusammenhang stellt das System „Foundation Hotspots – PAR“ eine weitere Besonderheit dar, da es sich um ein Gebiet handelt, in dem ein Rücken auf einen Hotspot zuwandert. Aus diesen Zusammenhängen haben sich folgende Projektzielsetzungen ergeben: (1) Charakterisierung der Plume-Rücken Interaktionen und der ihnen zu Grunde liegenden Manteldynamik sowie (2) Charakterisierung der petrogenetischen Prozesse, die zur Bildung der hochdifferenzierten Magmen in diesem Bereich führen.

Während der Ausfahrt wurden an 60 verschiedenen Dredge- und TV-Greifer-Stationen insgesamt 230 Gesteinsproben genommen. Das Probenmaterial umfaßt glasige bis kristalline Proben, deren Zusammensetzung von Basalt über basaltischen Andesit und Andesit bis zu Dazit variiert, wobei Basalte, basaltische Andesite und Andesite innerhalb einer Probenlokation auftreten können. Dies legt den Schluß nahe, daß der Chemismus der eruptierten Laven öfter wechselt und ein Magmenkammersystem unter dem Rücken vorhanden sein muß. Andesite und Dazite treten hauptsächlich in dem Gebiet des PAR auf, der am stärksten vom Hotspot beeinflusst ist (36.5° bis 39.8°S). Diese differenzierten Laven stehen nicht im Zusammenhang mit propagierenden Riftsystemen. Haupt- und Spurenelementdaten sowie die Sr-, Nd-, und Pb-Isotopenzusammensetzung der Proben zeigen, daß die Magmen des nördlichen PAR (1) aus einer heterogenen Quelle stammen und (2) über verschiedene Differentiationstrends miteinander in Beziehung stehen.

Modellierungen der fraktionierenden Kristallisation zeigen, daß der Chemismus der Basalte durch die Fraktionierung von Olivin, Plagioklas, Klinopyroxen und Ti-Magnetit bei niedrigen Drücken kontrolliert wird, wobei zwei verschiedene Trends definiert werden können: (1) Basalte, die zwischen 37°S und 39.5°S eruptierten, sind durch die Kristallisation von Olivin → Olivin + Plagioklas → Olivin + Plagioklas + Klinopyroxen kontrolliert und Basalte, die zwischen 40°S und 41°S eruptierten, werden durch die Kristallisationssequenz Plagioklas → Plagioklas + Olivin → Plagioklas + Olivin + Klinopyroxen kontrolliert. Diese unterschiedlichen Differentiationstrends kommen durch einen höheren Kristallisationsdruck der Magmen im nördlicheren Bereich zustande. Eine Erhöhung des Wassergehalts in den Magmen würde zur Verzögerung der Plagioklaskristallisation führen, kann aber als Ursache der Entwicklung verschiedener Differentiationstrends ausgeschlossen werden, da die H₂O – Konzentration in den Proben entlang des Rückens nur wenig variiert.

Die Andesite und Dazite sind nicht durch simple fraktionierte Kristallisation bei niedrigen Drücken aus den Basalten entstanden. Klinopyroxenphänokristalle mit Mg# zwischen 40 und 87 und Plagioklasphänokristalle mit An-Gehalten zwischen 22 und 87 in den Andesiten legen den Schluß nahe, daß diese aus der Mischung basaltischer und dazitischer Schmelzen entstanden sind. Hohe Cl/K und ⁸⁷Sr/⁸⁶Sr Verhältnisse sind weiterhin ein Indiz dafür, daß die Assimilation alterierter ozeanischer Kruste eine Rolle bei der Bildung der Andesite und Dazite gespielt hat.

Pb-Isotope und La/Yb Verhältnisse korrelieren positiv mit ⁸⁷Sr/⁸⁶Sr Verhältnissen und zeigen, daß eine binäre Mischung zwischen einer angereicherten, radiogeneren Quelle (Plume-Quelle) und einer verarmten, weniger radiogenen Quelle (MORB Mantel) bei der Bildung der Magmen vorliegt. Ein südwärts gerichteter geochemischer Gradient ist in den Proben zu beobachten, wobei die am stärksten angereicherten und radiogensten Proben um 37.5°S (Position des Foundation Hotspot) zu finden sind und die verarmtesten bei 40°S. Ein nördlich gerichteter geochemischer Gradient tritt nicht auf.

Zusammenfassend läßt sich sagen, daß der Foundation Hotspot eine asymmetrische geochemische Anomalie verursacht, die die Entwicklung der Magmen dieses Segments des PAR (zwischen 37.5°S und 39.5°S) nachhaltig beeinflusst. Die durch den Hotspot verursachte Krustenverdickung führt zu einer polybarischen fraktionierten Kristallisation der Schmelzen in einem komplexen Magmenkammersystem unter dem PAR.

Öffentlichkeitsarbeit

Silikatreiche Lava unter dem Meer

Anreicherung von Quarz in erstarrter Schmelze

Es ist geradezu ein Dogma in den Geowissenschaften, daß die Gesteine der ozeanischen Erdkruste aus Basalten bestehen. Daß es aber auch einige submarine Feuerberge gibt, aus denen sich silikatreiche Lava ergießt, wird häufig vergessen. Nach einer Expedition mit dem Forschungsschiff „Sonne“ in den Südostpazifik haben Kieler Forscher nun ein wenig Licht auf diese außergewöhnliche Form des untermeerischen Vulkanismus geworfen.

Eines der wichtigsten Kriterien für die Klassifizierung von vulkanischen Gesteinen ist ihr Gehalt an Quarz. Er kann zwischen etwa 40 und ungefähr 70 Prozent schwanken. Gesteine mit hohem Quarzgehalt werden als „felsisch“ bezeichnet. Die meisten Vulkane an Land produzieren solche silikatreichen, felsischen Ergußgesteine. Aus den untermeerischen Vulkanen, vor allem aber aus den Spreizungszonen der mittelozeanischen Rücken, strömt dagegen „mafische“ Lava, die nur geringe Mengen an Quarz enthält und zu Basalt erstarrt. Daher sind für jene Gesteine, aus denen die Erdkruste unter den Ozeanen aufgebaut ist, Konzentrationen an Siliziumdioxid zwischen 47 und 50 Prozent typisch.

Schon seit längerem ist aber bekannt, daß an mindestens drei Stellen in untermeerischen Spreizungszonen silikatreiche Lava mit einem Quarzgehalt von mehr als 55 Prozent austritt. Dazu gehört der nördliche Teil des ostpazifischen Rückens bei etwa 10,5 Grad nördlicher Breite sowie ein Ableger des Galápagos-Rückens. Vor einigen Jahren fanden deutsche und französische Meeresgeologen frische silikatreiche Laven auch in einem Seegebiet etwa 1200 Kilometer südlich der Osterinsel. Die submarinen

Vulkane dort gehören zum nördlichen Ausläufer des pazifisch-antarktischen Rückens. Auf der 157. Expedition mit dem Forschungsschiff „Sonne“ haben Forscher unter Leitung von Peter Stoffers vom Institut für Geowissenschaften der Universität Kiel im vergangenen Jahr diese Vulkane zum erstenmal genauer untersucht.

Mit Greifern, die von Bord des Schiffes ferngesteuert wurden, sammelten die Meeresgeologen an insgesamt 65 Stellen Proben der Ergußgesteine. An diesen Stellen lag der Meeresboden jeweils in weit über 2000 Meter Wassertiefe. Der Quarzanteil der gesammelten Ergußgesteine betrug zwischen 55 und 64 Prozent. Diese waren damit den vulkanischen Gesteinen an Land viel ähnlicher als den typischen ozeanischen Basalten. Außerdem variierte der Anteil an Magnesium in den Gesteinsproben sehr stark.

Wie die Forscher nun in „Eos“ (Bd. 83, S. 301) schreiben, kommt es unterhalb der untersuchten Vulkane offenbar zu einer „fraktionierten“ Kristallisation des Magmas. Dabei erstarrt sie zum Teil, und es reichert sich eine silikatreiche Schmelze an, die dann an einigen Stellen austritt. Offen bleibt bislang aber noch die Frage, was südlich der Osterinsel zu dieser Fraktionierung führt, während es in den meisten anderen submarinen Spreizungszonen nicht dazu kommt. Die Kieler Forscher vermuten, daß im nördlichen Teil des pazifisch-antarktischen Rückens Gesteinsschmelze aus dem tiefen Erdmantel in die Nähe der Erdkruste gelangt. Dadurch stünde südlich der Osterinsel ein größeres Magmareservoir als in anderen Spreizungszonen zur Verfügung, was wiederum zur Fraktionierung führte.

hra